Acta morphologica et anthropologica (23)

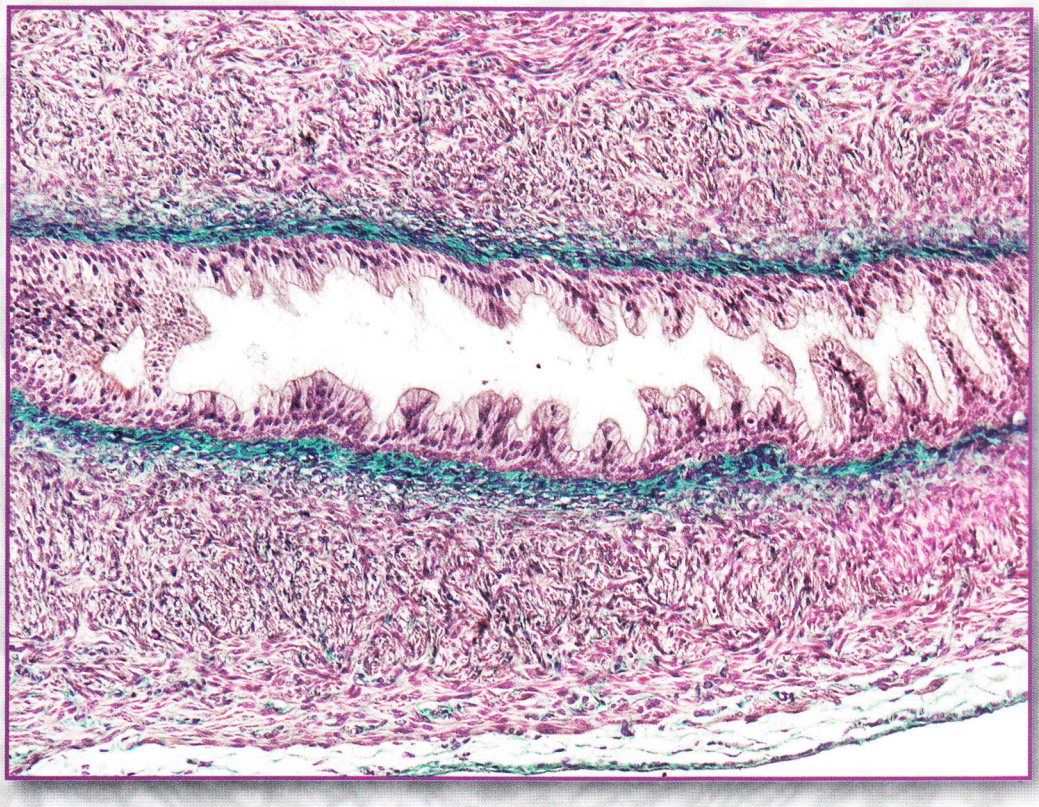

Prof. Marin Drinov Publishing House
of Bulgarian Academy of Sciences

ISSN 1311-8773

Acta morphologica et anthropologica (23)

23 • Sofia • 2016
Institute of Experimental Morphology, Pathology and Anthropology with Museum
Bulgarian Anatomical Society

Contents

ISSN 1311-8773

Acta morphologica et anthropologica (23)

23 ● Sofia ● 2016
Institute of Experimental Morphology, Pathology and Anthropology with Museum
Bulgarian Anatomical Society

Contents

Morphology

Anthropology and Anatomy

Institute of Experimental Morphology, Pathology and Anthropology with Museum
Bulgarian Anatomical Society

Acta morphologica et anthropologica, 23
Sofia ● 2016

Morphology

The Importance and Application of Testicular Angiotensin Converting Enzyme (tACE) as a Marker for Evaluation of Mammalian Spermiogenesis and Fertility

N. Atanassova[1], E. Lakova[2], E. Pavlova[1], D. Dimova[1], Y. Koeva[3], M. Davidoff[4]

[1]Dept. Experimental Morphology, Institute of Experimental Morphology, Pathology and Anthropology with Museum, Bulgarian Academy of Sciences, 1113 Sofia, Bulgaria
[2]Dept. Physiology and Pathophysiology, Medical University – Pleven
[3]Dept. Anatomy, Histology and Embryology, Medical University, Plovdiv
[4]Institute of Anatomy 1, UKE, University of Hamburg, Germany

Two isoforms – somatic (sACE) and testicular (tACE) are known. The aim of the present study is to reveal the role of tACE as a marker for germ cell differentiation, in particular for spermatid development. The specific pattern of tACE protein expression was studied in normal and experimental condition (spontaneous hypertension, androgen withdrawal, hyperglycaemia). Normally, tACE could serve as a marker for developmental stage of germ cell differentiation. In experimental pathological conditions that lead to male infertility, tACE was proven as a useful marker for evaluation of spermiogenesis. Testicular ACE provides precise evaluation for retention of the first spermatogenesis and spermatid depletion in adulthood. The summary of our data obtained so far characterized tACE as a proper cellular marker for elongating spermatids and mature spermatozoa. Our review provides new vision for tACE as unique tool for evaluation for stage-specific changes in spermiogenesis and in particular stage in spermatid elongation.

Key words: angiotensin converting enzyme (ACE), testis, spermatogenesis, spermatids, germ cells.

Introduction

Angiotensin I-converting enzyme (ACE, kininase II, CD 134) is well-known component of renin-angiotensin system (RAS) and kallikrein-kinin system (KKS), both playing an important role in male reproduction [25, 29]. ACE is membrane bound zink metallopro-

teinase dipeptidase that removes 2 residues from C terminus of certain peptides. ACE is responsible for the conversion of angiotensin (Ang) I to the potent vasoconstrictor Ang II and for inactivation of vasodilator peptide bradykinin. Therefore, ACE has been implicated in the control of blood pressure and fluid-electrolyte balance [23]. ACE acts through two G protein coupled receptors, AT I and AT II. Activation of AT I receptors is responsible for vasoconstriction and aldosterone release while AT II receptors are proposed to mediate antagonizing effects and apoptosis [11].

There is another form of ACE named ACE 2 in humans and mammals. This enzyme is Zink metalloproteinase with carboxypeptidase activity that shares approximately 42% identity with the catalytic site of somatic ACE [34]. ACE 2 is involved in the generation of alternative angiotensin peptides in particular in the conversation of Ang II to Ang (1-7), which is vasodilatator and Ang (1-9) [35]. This data suggested that ACE2 can be viewed as a counterbalancing tissue-specific mechanism within the activated RAS.

ACE exists in two isoforms – somatic and testis-specific (germinal) and both are encoded by one and the same gene having 26 exons. Somatic ACE (sACE) is the longer variant having MW of 170 kDa. This isoform generates Ang II and it is blocked by ACE inhibitors [12, 13]. In contrast, the shorter variant – testicular ACE (tACE), having MW 110 kDa, does not generate Ang II and the substrate is unknown. The isoform is not blocked by ACE inhibitors. Testicular ACE is transcribed by alternative promoter in intron 12 only during spermatogenesis being localized in developing post meiotic germ cells (spermatids) [18]. As a result N-domain is unique in this isoform due to translated exon 13. The C-domain is identical in both, sACE and tACE.

Somatic ACE is produced by endothelium and several other somatic tissues [22]. The same enzyme is localized in male reproductive system mostly in endothelia cells and Leydig cells of the testis as well as in epithelial cells of the epididymis and prostate. The sACE is expressed in human germ cells during fetal life and is constant feature of germ cell cancer, analyzed by monoclonal antibodies.

Studies on human males revealed time-related changes in the cell specific expression of sACE. Switch of both ACE isoforms in human germ cells was reported: sACE occurred in foetal gonocytes but only tACE is exclusively expressed in spermatids and spermatozoa. Sertoli cells show generally only a weak and markedly diffuse immunoreactivity for sACE. This labelling disappears towards the end of gestation but may be maintained in some seminiferous tubules for months after birth. Both of Leydig cell populations – fetal and adult expressed sACE [26].

Both of ACE isoenzymes play an essential role in male reproduction system. Main function of sACE is local production of Ang II that modulates Leydig cell steroidogenesis and regulates tubular contractility in the prostate. Somatic ACE and generated AngII may contribute to sperm motility, capacitation and acrosome reaction via the angiotensin II type (AT II) receptor [14]. Furthermore the ACE product - angiotensin II is supposed to be involved in the regulation of fluid- and electrolyte transport in the epididymis. Ang II secreted from the basal cells in the epididymis may exert its effect on electrolyte transport by acting on Ang II receptors on the basolateral membrane of the principal cells [36]. Somatic ACE is localized on apical portion of epididymal epithelial cells. Acting as peptidase, ACE was suggested to participate in remodeling of seminal fluid as well as in detoxification. In addition, sACE cleaves and inactivates LHRH (Luteinizing hormone-releasing hormone) and substance P, both neuropeptide hormones involved in testosterone production by Leydig cells. Somatic ACE is expressed mainly in human germ cell during fetal development and it is constant feature of intratubular germ cell neoplasia (CIS), being oncofoetal marker [12]. Served as peptidase, the sACE cleaves and inactivates the tetra peptide

goralatide (N-acetyl-seryl-aspartyl-lysil-proline – AcSDKP), which is a natural and circulating inhibitor of proliferation of hematopoietic stem cell and other progenitor cells. AcSDKP blocks the S phase entry of normal but not of neoplastic cells and thus promotes survival and resistance of stem cells to chemotherapy and radiation. Therefore, inhibition of sACE may open new strategies in the prevention of side-effect during cancer therapy [13]. In KKS, sACE is responsible for degradation of bradykinin which stimulates germ cell proliferation [2] suggesting negative role of sACE for germ cell mitotic division.

Recent studies by Akman et al. [1] indicated that treatment with an ACE inhibitor (Ramipril) play protective role against the toxic effect of doxorubicin, used as chemotherapy agent for cancer therapy. However, combined application of Ramipri and Erythropoietin hormone (Darbepoetin) provided remarkable protective effects for testicular macro-parameters (area of seminiferous tubules, lumen and seminiferous epithelium) and sperm parameters (sperm count, motility, live-dead sperm rate and total abnormal sperm rate).

The peptidase ACE2 was localized primary into Leydig cells of the rat testis and in both Leydig and Sertoli cells of the human testis demonstrated by immunohistochemistry. ACE2 was not present in germ cells or endothelial cells, thereby showing a different cellular distribution to the homologous peptidase tACE, but overlapping with the distribution sACE [15].

Testicular ACE is germ cell specific isoform that is essential for male fertility. This isoform is expressed in germ cells during spermiogenesis and tACE is localized only in elongating spermatids and spermatozoa. In contrast to sACE, tACE does not generate vasoconstrictor peptide AngII and substrate for tACE has not been identified. Acting as dipeptidase tACE is responsible for release of GPI proteins from sperm membrane that is important for sperm-zona pellucida binding, necessary for fertilization. Acting like a GPI-anchored protein releasing factor, tACE shed various GPI-anchored proteins, mostly PH-20 and Tesp5 from the cell surface of germ cells [20]. Therefore, tACE may serve as marker for fertilizing ability of spermatozoa and tACE contributes to fertilization as a dipeptidase at least in the epididymis [10].

ACE activity in the testicular complex is possibly linked with androgens and is involved with spermatogenesis and sperm maturation. The testicular ACE is expressed at high level by developing germ cells and is present in mature sperm. Using of indirect immunofluorescence and immunoperoxidase method, tACE was found in elongating spermatids in the testicular seminiferous tubules as well as in spermatozoa within the epididymal tubular lumen in sexually mature, but not in immature rabbits, suggesting that the presence of tACE is dependent on sexual maturation on stage-specific manner [25]. The same results were observed in mice and human tACE in the testis. Species-specific expression of tACE was demonstrated in human testis where ACE was found only in adluminal membranes of post meiotic germ cells later than step 3 round spermatids corresponding to step 7 round spermatids in rat [13, 26]. The same cellular distribution was described in mice.

For better understanding of the role of tACE and sACE in the male reproduction, an insertional disruption of the somatic but not the testicular ACE gene was generated. Males homozygous for this mutation have normal amounts of testicular ACE mRNA and protein but completely lack of somatic ACE (equal to complete knockout of sACE) is responsible for severe kidney pathology. Nevertheless, homozygous for sACE mutation males have normal fertility, proving conclusively that somatic ACE in males is not essential for their fertility [16]. ACE null mice lacking both somatic and testicular ACE are infertile suggesting that only tACE has critical importance for male fertility by acting differently compared to sACE [25]. Infertility, independently

of normal testis weight, sperm count and morphology, is due to altered sperm migration in the oviduct and their ability to bind zona pellucida [31]. Mutants exhibit also low blood pressure and renal dysfunction. Experiments with transgenic expression of testicular ACE in ACE null mice restored fertility, whereas transgenesis of somatic ACE in ACE mutants does not and mice are infertile. Therefore sACE cannot substitute tACE in male reproduction.

Materials and Methods

The role of tACE as a marker for evaluation of mammalian and human spermatogenesis in normal and pathological condition was established by application of proper experimental approach involving treatments that lead to disturbance of spermatid development and inappropriate testosterone support. We use three experimentals as follow:

1) Spontaneously Hypertensive Rats (SHR) - model for genetic hypertension – testes were sampled at 4^{th} month [5];

2) Androgen withdrawal after selective ablation of Leydig cells by injection of ethane dimetanesulfonate (EDS) at dose of 75 mg/bw in adult rats. Testes were sampled at days 7^{th} , 14^{th} , 21^{st} , 35^{th} post EDS [8];

3) Streptozotocin (65 mg/kg) induced diabetes mellitus – neonatally on pnd 1, prepubertally on pnd 10 where testes were sampled on pnd 50. Diabetes mellitus in adulthood was induced on pnd 60 and testes were sampled at 1 and 2 months after Streptozotocin injection [21].

Testicular ACE was visualized by ABC-HRP immunohistochemistry using a polyclonal antibody in dilution of 1:500 (Santa Cruz) [5]

In all the three models measurement of Plasma T levels was performed by RIA.

Results and Discussion

Detailed immunohistochemical analysis in our previous studies [4, 6] revealed stage-specific pattern of tACE expression in post meiotic germ cells in rat testis. The cycle of the seminiferous epithelium in the rat comprises fourteen stages and spermiogenesis involved 19 steps. Schematic and semi-quantitative expression of tACE was shown in **Fig. 1** and **Table 1**, respectively.

Table 1. Semi-quantitative evaluation of tACE immunoexpression at the stages of the seminiferous epithelium and steps of spermiogenesis in adult rats

Stages of the seminiferous epithelium								
Steps of spermiogenesis								
VII		VIII		IX	X–XI	XII–XIV	I–III	IV–VI
7	19	8	19	9	10–11	12–14	15–16	17–18
–	++++	–/+	++++	+	++	++/+++	+++	++++

First faint immunoreactivity appeared in the cytoplasm of round spermatids step 8 (stage VIII of the cycle) in a round shape manner (**Fig. 2A**). Weak intensity was found in elongating spermatids step 9 at stage IX of the cycle of seminiferous epithelium. Later that stage, the immunostaining progressively increased and was located in cau-

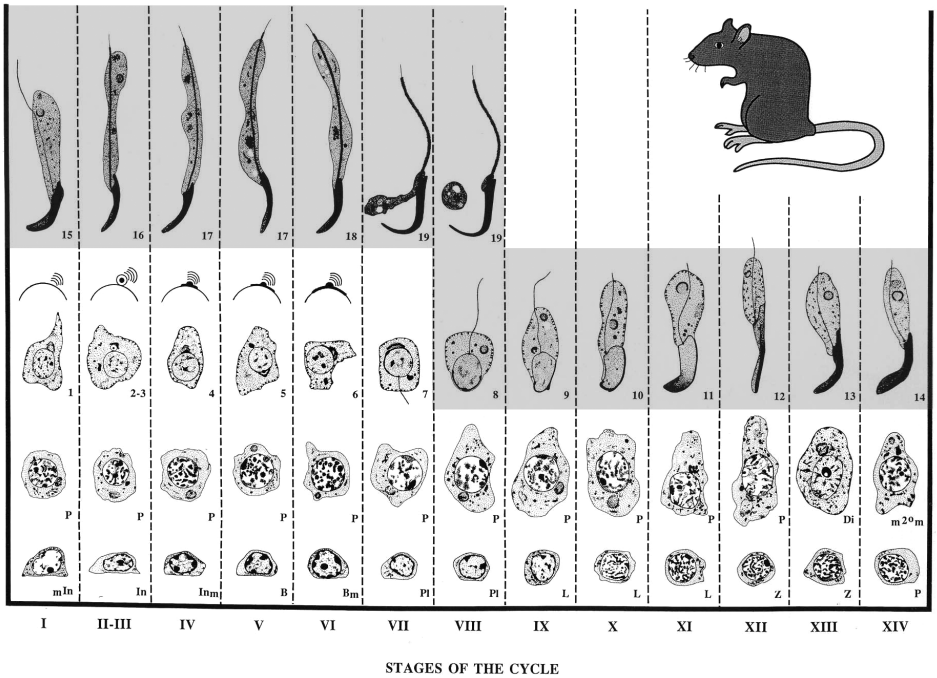

Fig. 1. Schematic presentation of expression of ACE during stages of seminiferous epithelium. On the scheme of the rat spermatogenesis all germ cell types and fourteen stages of the spermatogenesis are illustrated. Expression of tACE spanned from step 8 to step 19 of spermiogenesis (marked with grey)

dally organized cytoplasm of elongating spermatids. Immunoexpression became strong later than steps 12 of spermiogenesis (stage XII of the cycle) and reached maximum in steps 17–19 (stages IV–VIII of the cycle). No immunoexpression was observed in other germ cell types (spermatogonia, spermatocytes) as well as in somatic cells (peritubular cells, Leydig and Sertoli cells).

With one exception our results are consistent with the data by Sibony et al. [30] and Langford et al. [22]. The difference between these author groups could be explained by using different protocols and antibodies against the portion common to the testicular and somatic ACE.

Our data for stage specificity of tACE localization during spermatogenic cycle characterizes tACE [5] as a good marker for the stage of spermatid differentiation. In the rat testis expression of tACE starts and reaches maximum in androgen dependent stage VIII of spermatogenic cycle that implies androgen regulation of enzyme production in germ cells. Localization pattern of tACE revealed the importance of elongation phase of spermatids in male germ cell differentiation with respect to gene expression and not only to morphological modifications. Expression of tACE in post meiotic germ cells is an example for specific gene activation and translation during spermiogenesis.

In the course of the first spermatogenesis tACE appeared in stage-specific manner. Lack of tACE expression in the testis is due to absence of corresponding type of spermatids. Mid-pubertal testis (28-day-old) is negative for tACE as germ cell development proceeds to stage round spermatids 1-3 step. In late pubertal testis (42-day-old) spermatogenesis is not completed and proceeds to elongating spermatid 16 step in stage III. Immunoreactivity is observed in all the stages with an exception of stages IV–VI.

Lack of reaction in these stages is due to that elongating spermatids step 17-19 did not appear yet. Therefore, in the course of the first spermatogenic wave tACE is a marker for developmental stage of germ cell differentiation [4].

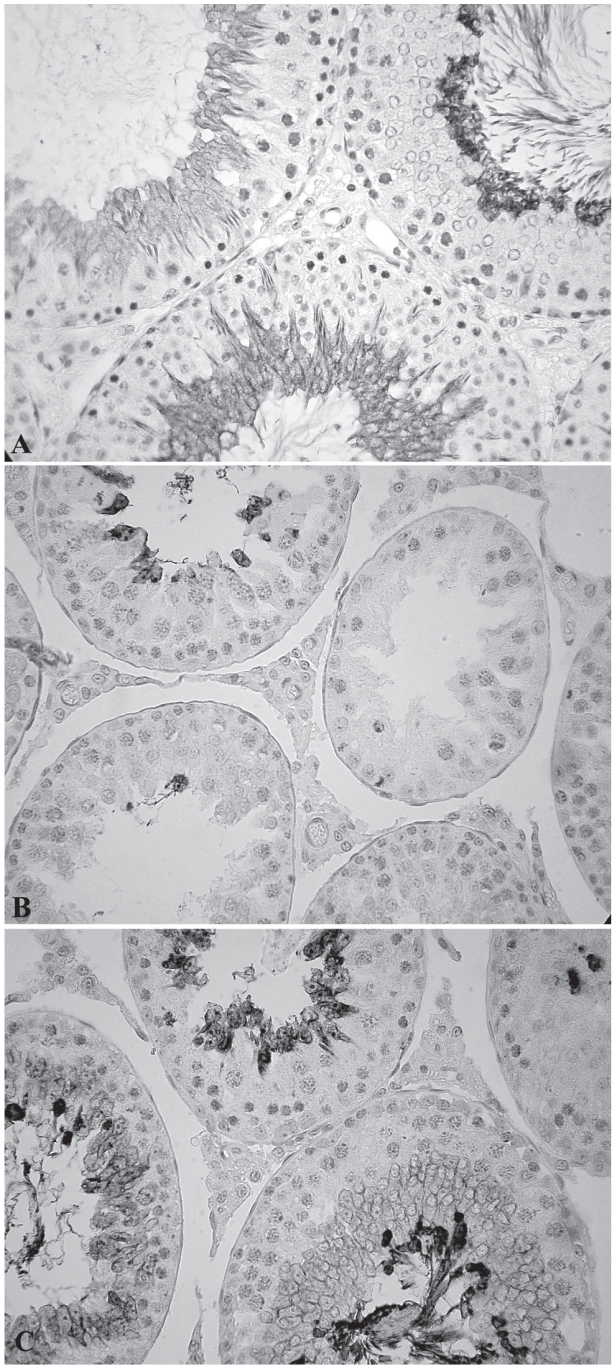

Fig. 2. Immunohistochemistry for tACE in adult rat testis. Localization of tACE in developing spermatids later step 8 (×400): **A**) Testis from control rat; **B**) Testis from SHR rat with depletion of elongating spermatids; **C**) Testis from SHR rat with stronger expression of tACE in elongating spermatids steps 9–14

Changes in the expression of tACE were reported in some pathological conditions such as hypertension and cancer. Advantages of genetic model for spontaneous hypertension rats (SHR) were well described by Azu [7]. Our previous data [5, 6] in SHR suggested relationship between hypertension, disturbance of spermatogenesis and elevated androgen production. In 20% of adult SHR (4-month-old) destructive changes in testicular histology were seen manifested by germ cell depletion, and reduced diameter of seminiferous tubules. Loss of elongated spermatids was proven by lack of immunopositive cells (**Fig. 2B**). In experimental group immunoexpression of tACE in spermatids steps 9-14 were more intensive than corresponding steps of the controls. As a result stage-specificity in SHR was not as prominent as in control (**Fig. 2C**). Plasma testosterone levels were obviously higher in SHR rats but significance was not reached due to highly variable values. High blood pressure development in SHR is suggested to be androgen-modulated [19].

Loss of tACE expression in germ cell depleted tubules in SHR is due to absence of corresponding stages of spermatid differentiation. Therefore, tACE can be used as a marker for germ cell depletion due to hypertension. Expression of tACE in post meiotic germ cell, specifically altered by SHR, suggested possible involvement of component of RAS in the process of spermiogenesis.

EDS experimental model is widely applied as a useful tool for investigation of androgen dependent events of spermatogenesis. Our previous data [3] revealed that expression of rat tACE started and reached maximal expression in androgen dependent stage VIII of spermatogenic cycle suggesting androgen regulation of the enzyme and EDS model was used for that case. By day 7th post EDS the Leydig cell completely absent from testicular interstitium as validated by negative reaction of marker enzyme, 3β-HSD and that is associated by drop in testosterone levels below 0.1 ng/ml [8]. Moreover, we previously found that androgen withdrawal induced profound germ cell apoptosis especially spermatocytes and round spermatids, demonstrated by maximal value of apoptotic index on day 7th [9]. In addition, lack of testosterone production coincides with loss of androgen receptor in Sertoli cells. Compromised cross-talk between Sertoli cells, Leydig cells and germ cells was suggested.

Morphological observations on testicular section from rats by 7th day after EDS injection showed total loss of elongating spermatids, steps 9-14 in corresponding stages IX–XIV of the cycle (**Fig. 3A**). Immunohistochemical study of tACE revealed that some seminiferous tubules do not contain positive cells whereas in some tubules single immune-reactive cells are seen (data not shown). Therefore, not all of the tubules in stages IX–XIV were completely depleted from elongating spermatids steps 9-14 (data not shown). Intensity of immune reaction in EDS testes is normal and stage-specific pattern of tACE expression was not different from that in controls. As far as, early (I–VI) and middle (VII–VIII) stages, they contained normal location of elongating spermatids steps 15-19. On day 7th post EDS we found stronger immunoexpression of tACE in round spermatids at stage VIII compared with the control (**Fig. 3B**). Our finding could be explained as a compensatory mechanism to androgen withdrawal due to absence of Leydig cells.

By day 14th post EDS single Leydig cells appeared in testicular interstitium proved by positive immunoreactivity for 3β-HSD and it is associated with considerable rise in plasma testosterone levels but significantly quite lower than controls [3]. Androgen receptor reappeared in Sertoli cells with no evidence for stage specific pattern. Histological observations revealed loss of elongating spermatids in all the stages of spermatogenic cycle. Immunohistochemistry for tACE details extent of loss of elongating spermatids. We found seminiferous tubules in all the stages of the spermatogenic cycle that were immunonegative for tACE, indicative completely depleted from elonga-

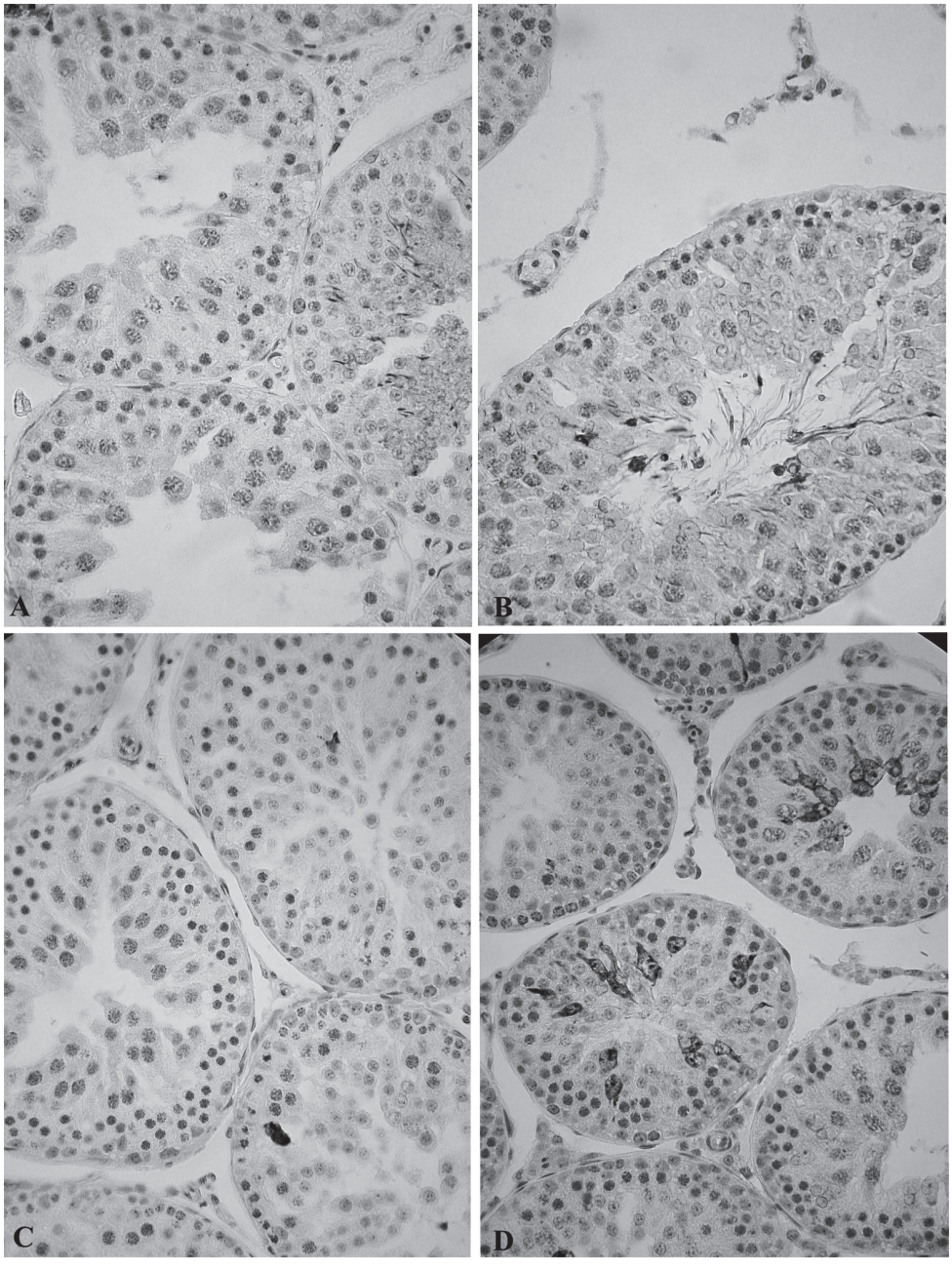

Fig. 3. Immunohistochemistry for tACE in adult rat testis after treatment with EDS (×400): **A**) Rat testis at 7th day after EDS treatment with loss of elongating spermatids steps 9-14; **B**) Rat testis at 7th day after EDS treatment with stronger expression of tACE in elongating spermatids step 8; **C)** Rat testis at 14th day after EDS treatment with complete loss of elongating spermatids; **D**) Rat testis at 14th day after EDS treatment with incomplete loss of elongating spermatids

ting spermatid (**Fig. 3C**). Moreover, tubules with single immunoreactive cells were also seen that suggested for incomplete loss of elongated spermatids (**Fig. 3D**). Depletion of elongating spermatids could be explained as a result of germ cell apoptosis that affected spermatocytes and round spermatids. Moreover germ cell apoptotic index still has significantly higher value compared to the controls [9]. The role of androgen signaling in Sertoli cells for post meiotic differentiation/spermatid development is demonstrated in knockout model for targeted disruption of androgen receptor in Sertoli cells (SCARKO) [33].

By day 21st post EDS more Leydig cells were found that is associated with higher testosterone levels compared to 14th post EDS even lower than normal value [8]. First signs for recovery of spermiogenesis we observed by histological and immunohistochemical studies. We found immunoreactive elongating spermatids step 9-14 in late stages of the cycle, IX–XIV. Occasionally, spermatids step 15-16 can be seen in early stages I–III (data not shown).

In conclusion, our data from immunohistochemical studies on tACE in EDS treated testes suggested that depletion and recovery of elongating spermatids occurred in stage-specific pattern. Therefore, application of tACE could be considered as a new tool for evaluation of post meiotic stages of spermatogenesis under conditions of hormonal/androgen deprivation. In particular, tACE can be recommended for precise visualization and evaluation of spermatid loss that is not optional by routine histological technique.

Reproductive dysfunction is a consequence of diabetes mellitus (DM), but the underlying mechanisms are poorly understood. Abnormal sperm production and failure of reproduction is a long time recognised consequence of DM, and it is accepted that infertility is a common complication in diabetic men [32]. In rats DM induces decreased testicular weight, sperm number and motility, testosterone levels that are an expression of abnormal spermatogenesis [28]. Nevertheless, the cellular alteration of testes has never been deeply studied, and the molecular mechanisms underlying this dysfunction are poorly understood.

We developed experimental approach for diabetes mellitus (DM) induced neonatally on pnd 1 (NDM) or prepubertally on pnd 10 (PDM) or in adulthood (ADM) [21]. In that study we aimed to evaluate which of three types of hyperglycaemia is the most severe risk factor for male fertility.

Our data reported recently [21] revealed that hyperglycaemia in adulthood revealed significant reduction of body weight by 20-30% whereas the 10% decrease in testis weight was not significant. The similar tendency for testis weight was found in animals with induced DM neonatally (NDM) or prepubertally (PDM) (data not shown). Blood glucose levels were strongly elevated up to 4 times in ADM and they were higher by 20-30% in NDM and PDM compared to the controls. Plasma testosterone levels were not significantly lower than controls in all the experimental groups.

Immunohistochemistry for tACE showed intact stage specific pattern of expression of tACE on day 50th in all the experimental group spermatogenesis starting in step 8 round spermatid at stage VIII of the spermatogenic cycle and reaching maximum in step 19 mature elongated spermatids at the same stage. Gross morphology of the testis in ADM rats is relatively normal. Histology of the testes from 50-day-old NDM rats is more altered than in ADM rats. Differential response to the hyperglycaemia was found as in some animals ST with enlarged lumen were seen and in other rats shrinkage of seminiferous tubules in stage VIII was found (**Fig. 4A**). Comparative analysis revealed that testicular morphology was most affected in 50-day-old PDM. Spermatogenesis is not completed and different degree of delay in spermatid development was observed (**Fig. 4B**). It was indicated by lack of elongating spermatids in stages IV–VII or in all the early stages (I–VII), or total loss of elongating spermatids in all the fourteen stages.

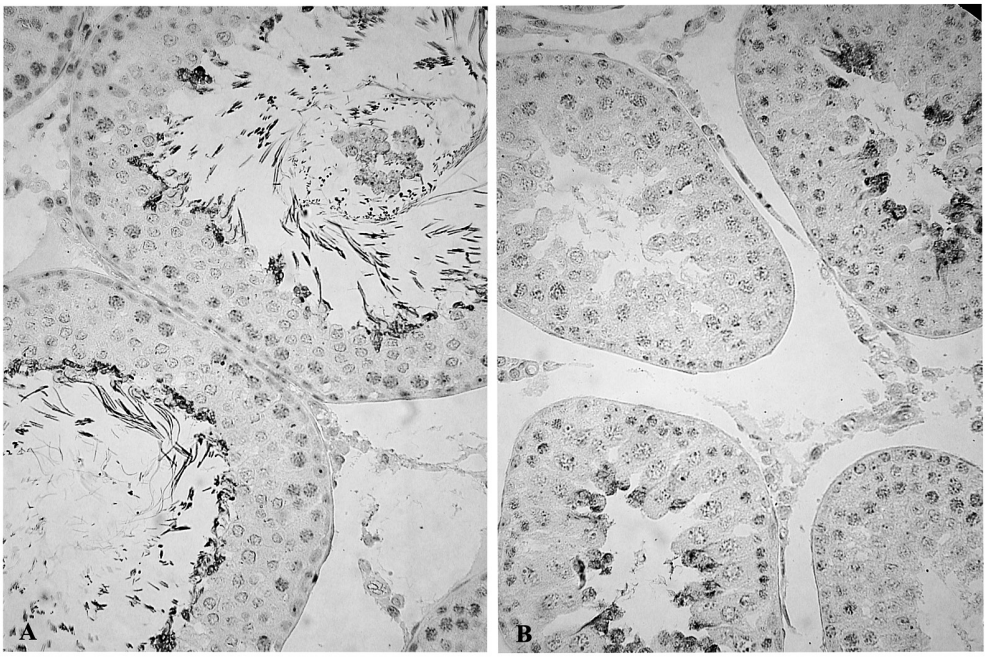

Fig. 4. Immunohistochemistry for tACE in 50-day-old rat testis after Streptozotocin induced diabetes mellitus (DM) in developing rats (×400): **A)** Adult testis from rat after NDM; **B)** Adult testis from rat after PDM with incomplete spermatogenesis

Alteration in spermatogenesis in diabetic state is mainly due to Leydig cell functional impairment caused by oxidative stress. As a consequence decreased testosterone production is responsible for the suppression of germ cell development [27].

The application of immunohistochemistry for tACE in diabetic condition demonstrated the dynamics of spermatid population, in particular the delay in development of post meiotic stages of spermatogenesis after PDM. Testicular ACE also could be considered as a marker for assessment of developmental stage of delayed spermatogenesis. Moreover, our comparative analysis provided the first evidence that prepubertal testis is more affected by hyperglycaemia than adult testis. Induction of DM on d10, when the first proliferative waves have started, affects germ cell development in a stronger extent compared to DM induced on day 1 when gonocytes are still quiescent [17, 24]. Our data indicate that the spermatogenesis is more vulnerable to DM at the time of proliferative phase of spermatogonia (4.5^{th} -12^{th} day) rather than the time of their mitotic arrest/quiescent period before 4.5^{th} day p.p. Long-term diabetes with sustained hyperglycemia leads to significant testicular dysfunction associated with decreased fertility potential.

Conclusion

The summary of our data obtained so far characterized tACE as a proper cellular marker for elongating spermatids and mature spermatozoa. Application of tACE in other experimental condition leading to subfertility or male infertility could provide better understanding for cellular and molecular mechanisms involved in regulation of sper-

matogenesis. For example, metabolite syndrome often associated with overweight, hypertension, DM type II, poor male reproduction and hence tACE could be used for detailed investigations of spermatogenesis applying proper experimental design as developmental studies under condition of hyperglycaemia and application of high fat diet on rats. Comparative investigations on the expression of other germ cell and Sertoli cell markers will develop broad view on the role of tACE in cell-cell interactions and such studies are in progress.

Our review provides new vision for tACE as a unique tool for evaluation for spermiogenesis, in particular stage in spermatid elongation. Assessment of germ cell depletion during experimental and pathological conditions could open future perspectives for development of new strategies for treatment of male infertility as well as for development of male contraception program.

Acknowledgements: This study was supported by grants from Medical University of Pleven No 1/2008, No 7/2009, No 2/2010, and Program for Carreer Development of Young Scientists – Grant DFNP – 72/2016.

References

1. **Akman, Q., Y. Ozkanlar, S. Ozkanlar, E. Oruc, N. Ulas, T. Ziypak, N. C. Lehimcioglu, M. Turkeli, O. Ucar.** Erythropoietin hormone and ACE inhibitor protect the sperm parameters of adult male rats against doxorubicin toxicity. – Kafkas. Univ. Vet. Fak. Derg., **21**(6), 2015, 805-812.
2. **Atanassova, N., L. Kancheva, B. Somlev.** Bradykinin stimulates prepubertal rat germ cell proliferation in vitro. – Immunopharmacology, **40**, 1998, 173-178.
3. **Atanassova, N., Y. Koeva, M. Bakalska, E. Pavlova, B. Nikolov, M. Davidoff.** Loss and recovery of androgen receptor protein expression in the adult rat testis following androgen withdrawal by ethane dimethanesulfonate. – Folia Histochem. Cytobiol., **44**(2), 2006, 81-86.
4. **Atanassova, N., E. Lakova, Y. Bratchova, G. Krasteva.** Stage specific expression of angiotensin-converting enzyme in adult and developing rat testis. – Acta morphol. anthropol., **15**, 2008, 52-56.
5. **Atanassova, N., E. Lakova, Y. Bratchkova, G. Krasteva.** Expression of testicular angiotensin-converting enzyme in adult spontaneously hypertensive rats. – Folia Histochem. Cytobiol., **47**, 2009, 117-122.
6. **Atanasova, N., E. Lakova, S. Popvska, M. Donchev, G. Krasteva, V. Nikolov.** Expression of testicular angiotensin I-converting enzyme in aging spontaneously hypertensive rats. – Acta morphol. anthropol., **17**, 2011, 79-83.
7. **Azu, O.** Testicular morphology in spontaneously hypertensive rat model: oxidant status and stereological implications. – Andrologia, **47**(2), 2014, 123-137.
8. **Bakalska, M., N. Atanassova, P. Angelova, Y. Koeva, B. Nikolov, M. Davidoff.** Degeneration and restoration of spermatogenesis in relation to the changes in Leydig cell population following ethane dimethanesulfonate (EDS) treatment in adult rats. – Endocrine Regulations, **35**, 2001, 211-217.
9. **Bakalska, M., N. Atanassova, Y. Koeva, B. Nikolov, M. Davidoff.** Induction of male germ cell apoptosis by testosterone withdrawal after ethane dimethanesulfonate treatment in adult rats. – Endocrine Regulations, **38**, 2004, 103-110.
10. **Deguchi, E., T. Tani, H. Watanabe, S. Yamada, G. Kondoh.** Dipeptidase-inactivated tACE action in vivo: selective inhibition of sperm-zona pellucida binding in the mouse. – Biol. Reprod., **77**(5), 2007, 794-802.
11. **Dingh, D. T., A. G. Frauman, C. I. Johnston, M. E. Fabiani.** Angiotensin receptors: distribution, signaling and function. – Clin. Sci., **100**, 2001, 481-492.
12. **Franke, F. E., K. Pauls, L. Kerkman, K. Steger, T. Klonisch, R. Metrger, et al.** Somatic isoform of angotensin I converting enzyme in the pathology of testicular germ cell tumors. – Hum.Pathol., **31**, 2000, 1466-1476.
13. **Franke, F. E., K. Pauls, R. Metzger, S. M. Danilov.** Angiotensin-converting enzyme and potential substrates in human testis and testicular tumors. – APMIS, **111**, 2003, 234-244.

14. **Fraser, L. R., M. D. Pondel, G. P. Vinson.** Calcitonin, angiotensin II and FPP significantly modulate mouse sperm function. – Mol. Hum. Reprod., **7**, 2001, 245-253.
15. **Gabrielle, C. Douglas, M. K. O'Bryan, M. P. Hedger, D. K. Lee, M. A. Yarski, A. I. Smith.** The novel angiotensin-converting enzyme homolog, ACE2, is selectively expressed by adult Leydig cells of the testis. – Endocrinology, **145**, 2004, 4703-4711.
16. **Hagaman, J. R., J. S. Moyer, E. S. Bachman, M. Sybony, P. L. Magyar, J .E. Welch, O. Smithies, J.H. Krege, D.A. O'Brien.** Angiotensin-converting enzyme in male fertility. – Proc. Natl. Acad. Sci., **95**(5), 1998, 2552-2557.
17. **Hilscher, W., B. Hilscher.** Kinetics of the male gametogenesis. – Andrologia, **8**(2), 1976, 105-16.
18. **Howard, T., S. Shai, K. Langford, B.Martin, K.E. Bernstein.** Transcription of testicular angiotensin-converting enzyme (ACE) is initiated within the 12th intron of the somatic ACE gene. – Mol. Cell Biol., **10**, 1990, 4294-4302.
19. **Kienitz, T., M. Quinkler.** Testosterone and blood pressure regulation. – Kidney Blood Press Res., **31**, 2008, 71-79.
20. **Kondoh, G., H. Tojo, Y. Nakatani, N. Komazawa, C. Murata, K. Yamagata, Y. Maeda, T. Kinoshita, M. Okabe, R. Taguchi, J. Takeda.** Angiotensin-converting enzyme is a GPI-anchored protein factor crucial for fertilization. – Nat. Medicine, **11**, 2005, 160-166.
21. **Lakova, E., S. Popovska, I. Gencheva, M. Donchev, G. Krasteva, E. Pavlova, D. Dimova, N. Atanassova.** Experimental Model for Streptozotocin-induced diabetes mellitus neonatally or in adulthood - comparative study on male reproduction in condition of hyperglycaemia. – Acta Morphol. Anthropol., **19**, 122-126.
22. **Langford, K. G., Y. Zhou, L. D. Russell, J. N. Wilcox, K. E. Bernstein.** Regulated expression of testis angiotensin-converting enzyme during spermatogenesis in mice. – Biol. Reprod., **48**, 1993, 1210-1218.
23. **Leung, P. S., S. Sernia.** The rennin-angiotensin system and the male reproduction: new functional for old hormones. – J. Mol. Endocrinology, **30**, 2003, 263-270.
24. **Orth, J. M., W. F. Jester, Jr., J. Qiu.** Gonocytes in testes of neonatal rats express the c-kit gene. – Mol. Reprod. Dev., **45**(2), 1996, 123-131.
25. **Paul, M., A. P. Mehr, R. Kreutz.** Physiology of local rennin-angiotensin system. – Physiol. Rev., **86**, 2006, 747-803.
26. **Pauls, K., R. Metzeger, K. Steger, T. Klonisch, S. Danilov, F. E. Franke.** Isoforms of angiotensin I-converting enzyme in the development and differentiation of human testis and epididymis. – Andrologia, **35**, 2003, 32-43.
27. **Ricci, G., A. Catizone, R. Esposito, F. A. Pisanti, M. T. Vietri, M. Galdieri.** Diabetic rats testis: morphological and functional alterations. – Andrologia, **41**, 2009, 361-368.
28. **Scarano, W. R., A. G. Messias, S. U. Oliva, G. R. Klinefelter, W. G. Kempinas.** Sexual behaviour, sperm quantity and quality after short-term streptozotocin-induced hyperglycaemia in rats. – Int. J. Androl., **29**, 2006, 482-488.
29. **Schill, W. B., W. Miska.** Possible effects of the kalikrein-kinin system of male reproductive functions. – Andrologia, **24**, 1992, 69-75.
30. **Sibony, M., D. Segretain, J. M. Gasc.** Angiotensin-converting enzyme in murine testis: step-specific expression of the germinal isoform during spermatogenesis. – Biol. Reprod., **50**, 1994, 1015-1026.
31. **Smith, T. T., W. B. Nothnick.** Role of direct contact between spermatozoa and oviductal epithelial cells in maintaining rabbit sperm viability. – Nothnick. Biol. Reprod., **56**, 1997, 83-89.
32. **Steger, R. W.** Testosterone replacement fails to reverse the adverse effects of streptozotocin-induced diabetes on sexual behavior in the male rat. – Pharmacol. Biochem. Behav., **35**, 1990, 577-582.
33. **Tan, K. A., K. De Gendt, N. Atanassova, M. Walker, R. M. Sharpe, P. T. K. Saunders, E. Denolet, G. Verhoeven.** The role of androgens in Sertoli cell proliferation and functional maturation: studies in mice with total or Sertoli cell-selective ablation of the androgen receptor. – Endocrinology, **146**, 2005, 2674–2683.
34. **Tipnis, S. R., N. M. Hooper, R. Hyde, E. Karran, G. Christie, A. J. Turner.** A human homolog of angiotensin-converting enzyme. Cloninig and functional expression as a captopril-intensive carboxypeptidase. – J. Biol. Chem., **275**, 2000, 33238-33243.

35. **Vickers, M., P. Hales, V. Kaushik, L. Dick, J. Gavin, J. Tang, K. Godbout, T. Parson, E. Baronas, F. Hsieh, S. Acton, M. Patane, A. Nichols, P. Tummino.** Hydrolysis of biological peptides by human angiotesin-converting enzyme-related carboxypeptidase. – J. Biol. Chem., **277**, 2002, 14838-14843.
36. **Wong, P. Y. D., C. N. Uchendu.** The role of angiotensin-converting enzyme in the rat epididymis. – J. Endocrinol., **125**, 1990, 287-293.

Institute of Experimental Morphology, Pathology and Anthropology with Museum
Bulgarian Anatomical Society

Acta morphologica et anthropologica, 23
Sofia ● 2016

CGRP- and VIP-Immunoreactivity in the Rat Carotid Body

D. Atanasova[1,2], N. Dimitrov[2], A. Dandov[3], N. Lazarov[1,3]

[1]*Institute of Neurobiology, Bulgarian Academy of Sciences, Sofia, Bulgaria*
[2]*Department of Anatomy, Faculty of Medicine, Trakia University, Stara Zagora, Bulgaria*
[3]*Department of Anatomy and Histology, Medical University of Sofia, Sofia, Bulgaria*

The carotid body (CB), the primary peripheral chemoreceptor in mammals, is a mass of vascular tissue located near the bifurcations of the carotid arteries. It registers changes in the oxygen concentration of arterial blood and helps to control respiratory activity. The most striking anatomical features of the CB are its rich vascularization and dense innervation. At a light microscopical level using immunohistochemistry we identified the localization and distribution of calcitonin gene-related peptide (CGRP) and vasoactive intestinal peptide (VIP)-containing nerve structures in the CB of rats. Both investigated vasoactive neuropeptides were expressed, although in a different manner, in periglomerular and intraglomerular nerve fibers which innervate blood vessels. Moreover, we observed strong VIP-like immunoreactivity not only in nerve fibers but also in the glomus cells. Our data provide immunohistochemical proof that the rat CB uses perivascular neuropeptides, which probably manage chemosensory activity through their actions on the vessels and neuron-like glomus cells.

Key words: carotid body, CGRP, VIP, immunohistochemistry, chemosensitivity.

Introduction

The carotid body (CB) is the main peripheral chemoreceptor responsible for monitoring changes in arterial blood levels of pO_2, pCO_2 and pH, and participates in the ventilatory responses to hypoxia, hypercapnia and acidosis [1, 4]. It is a neural crest-derived ovoid mass of tissue bilaterally located at the bifurcation of the common carotid artery, just before blood chemicals reach the brain, an organ that is quite sensitive to oxygen and glucose deficiency. The CB is composed of clusters of cells, surrounded by a dense meshwork of capillaries and penetrated by bundles of sensory nerve endings of the carotid sinus nerve, a branch of the glossopharyngeal nerve, and by sympathetic postganglionic nerve fibers from the superior cervical ganglion [4, 17, 23].

The cell clusters, also known as glomoids or glomeruli, are the essential morphofunctional units of the CB. The glomeruli consist of two juxtaposed cell types, neuron-like oxygen sensitive type I, or glomus cells, incompletely invested by glial-like type II or sustentacular cells [1, 4].

Besides classical neurotransmitters, possible involvement of various neuropeptides such as CGRP and VIP in the chemoreception has been proposed immunohisto-

chemically. Since the calcitonin gene-related peptide (CGRP), a 37-amino acid peptide, has been isolated the expression of CGRP was demonstrated to occur entirely in primary sensory neurons [8, 21]. Such a localization totally implies that CGRP is a specific marker for the identification of some sensory nerve endings in the peripheral nervous system [8].

Materials and Methods

The experiments were carried out on adult male Wistar rats, weighing 250-300 g. The study was conducted according to the European Communities Council Directive 2010/63/EU for the protection of animals used for scientific purposes. All experimental procedures have been approved by the Bioethical Commission of the Biomedical Research at the Institute of Neurobiology of the Bulgarian Academy of Sciences.

For the immunohistochemical experiments, the rats were deeply anesthetized and transcardially perfused first with 0.05 M phosphate-buffered saline (PBS), pH 7.4, followed by 4% paraformaldehyde (PFA) in 0.01 M phosphate buffer (PB), pH 7.4. The carotid bifurcations were dissected out and postfixed in the same fixative overnight at 4 °C. Afterwards, the tissues were embedded in paraffin and cut into 7 μm thick sections. The samples were then deparaffinized with xylene and ethanol, and subsequently processed for avidin-biotin-horseradish peroxidase complex (ABC) immunohistochemistry. Briefly, the sections were treated with hydrogen peroxide (1.2% in absolute methanol; 30 min) to inactivate endogenous peroxidase and the background staining was blocked with 5% normal goat serum (NGS) in PBS for 1 hour. Between the separate steps, the sections were rinsed with cold PBS/Triton X-100. After that they were incubated for 24 hours with the corresponding primary antibodies, rabbit anti-CGRP (diluted 1:1000, PEPA 27, Serotec) and rabbit anti-VIP (1:500; Amersham International, Buckinghamshire, UK) overnight at 4 °C in a humid chamber, followed by biotinylated goat anti-rabbit IgG (Sigma, 1:250) for 2 h at room temperature, and finally the ABC complex (Vector Labs, Burlingame, CA, USA) was applied for 2 hours at room temperature. Lastly, the peroxidase activity was visualized using diaminobenzidine as a chromogen. After the immunoreaction, the sections were dehydrated in ethanols, cleared in xylene and coverslipped with Entellan (Merck, Darmstadt, Germany). The specimens were observed and photographed with a Nikon research microscope equipped with a DXM 1200c digital camera.

The specificity of the immunostaining was controlled by the omission of the primary antiserum from the incubation medium or its replacement by PBS. No immunoreactivity was detected in either case.

Results

Numerous intraglomerular and periglomerular nerve fibers immunoreactive for CGRP were found throughout the parenchyma of the CB (**Fig. 1B, C**). At a higher magnification, the immunoreactive nerve fibers appeared as fine and beaded fibers, and they were seen as enclosing small blood vessels and cell clusters of glomus and sustentacular cells (**Fig. 1C**). When omitting the specific primary antibodies, or applying PBS or non-immune serum at the same dilution as the primary antibody, no specific immunostaining was found (**Fig. 1A**).

On the other hand, the immunohistochemical experiments demonstrated VIP-like immunoreactivity in some of neuron-like glomus cells (**Fig. 1D, E**). The periglomerular

and intraglomerular nerve fibers appeared as thin varicosities and most of them were associated with blood vessels.

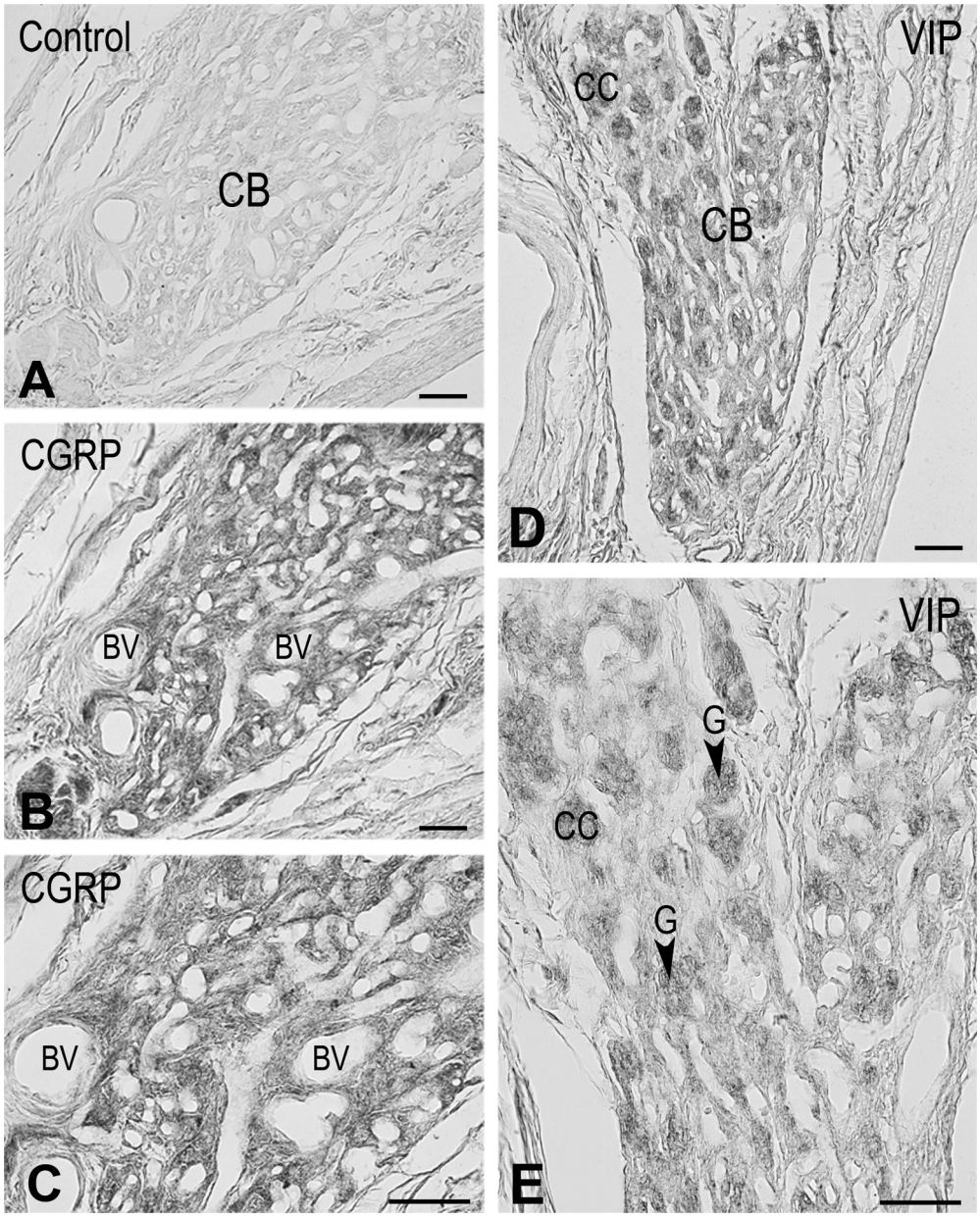

Fig. 1. Immunohistochemical demonstration of CGRP and VIP in the CB of adult rats. (**A**) No immunoreactivity is observed in the section incubated with PBS; (**B, C**) CGRP-immunoreactive intraglomerular and periglomerular nerve fibers in CB parenchyma; (**D, E**) Representative photomicrograph indicating the presence of VIP-immunoreactive perivascular nerve fibers and immunostained glomus cells (G) in cell clusters (CC). Blood vessels (BV). Scale bars = 50 μm

Discussion

The present results demonstrate that both examined dilatory neuropeptides are strongly expressed perivascularly in the rat CB, although in a different manner. In this study, we find that the vast majority of nerve fibers appear to contain certain sensory neuropeptides like CGRP. Furthermore, the most numerous CGRP-immunopositive sensory nerve fibers are associated with blood vessels and glomus cells, although some immunoreactive varicosities can be seen around the glomeruli too. We confirm results from previous immunohistochemical studies that also find CGRP-immunoreactivity in nerve endings close to blood vessels and glomic cell clusters in amphibians, birds and mammals [2, 5, 7, 8, 9, 11, 12, 13]. In addition, denervation experiments show that these nerve endings are sensory in nature, and most have their soma in the petrosal ganglion. In another study performed on the rat CB, it was observed that CGRP-immunopositive sensory fibers start to appear on the third day after birth, and increase continuously in number afterwards [8]. CGRP-immunoreactivity was not demonstrated in the glomus cells of chronically hypoxic or normoxic rat CBs [14, 20]. It was reported that in chronically hypoxic rat CB the density of CGRP-immunostained nerve fibers decreases significantly [14], and then increases several weeks after the termination of hypoxia [15, 16]. Various implications were described in different animal species, and it has been proposed that the action of CGRP is more likely to modulate the effects of neurotrophic factors than to impose a direct impact [3, 20]. Nevertheless, CGRP has been established in nerve fibers and not in glomic cells, it cannot be excluded that the release of CGRP by nervous terminations may exert some local trophic effect.

On the other hand, we have found VIP immunoreactivity in both the nerve fibers and glomus cells in the rat CB as opposed to studies performed by other authors who have been reported that VIP-immunoreactivity is confined to nerve terminations within the CB in different animal species [7, 10, 13, 19, 24]. Furthermore, immunohistochemical studies have also shown that weak VIP-immunoreactivity is located in type I cells of the human CB [22], although their data were not confirmed in the glomus cells of chronically hypoxic or normoxic rat CBs by another working group of researchers [14]. In the chronically hypoxic rat CB, the density of VIP-immunostained nerve fibers significantly increases [14, 19] and returns to a normoxic state in a few weeks after termination of hypoxia [16, 20]. Taken together with previous immunohistochemical and physiological [14] reports, our findings indicate that VIP most likely modulates the CB chemosensitivity and changes in spontaneous chemoreceptor discharges. VIP, a peptide abundant in autonomic nerve fibers, evokes vasodilation of blood vessels and it may be associated with chemosensory mechanisms by controlling local circulation [14, 20]. Furthermore, VIP may increase neuronal survival indirectly by the secretion of activity-dependent neurotrophic factors, cytokines, and chemokines [18, 20].

Conclusion

It can be inferred for this study that the two neuropeptides examined are strongly expressed in both sensory and autonomic nerve endings apposed to glomus cells, pericytes or vascular smooth muscle cells. The latter leads to the assumption that CGRP- and VIP-immunopositive nerve fibers may regulate the blood flow within the rat CB.

References

1. **Atanasova, D. Y., M. E. Iliev, N. E. Lazarov.** Morphology of the rat carotid body. – Biomed. Rev., **22**, 2011, 41-55.
2. **Atanasova, D. Y., N. E. Lazarov.** Expression of some neuropeptides in the rat CB. – Acta Morphol. Anthropol., **19**, 2012, 15-19.
3. **Connat, J. L., V. Schnüriger, R. Zanone, C. Schaeffer, M. Gaillard, B. Faivre, L. Rochette.** The neuropeptide calcitonin gene-related peptide differently modulates proliferation and differentiation of smooth muscle cells in culture depending on the cell type. – Regul. Pept., **101**, 2001, 169-178.
4. **Gonzaez, C., L. Almaraz, A. Obeso, R. Rigual.** Carotid body chemoreceptors: from natural stimuli to sensory discharges. – Physiol. Rev., **74**, 1994, 829-898.
5. **Heath, D., M. Quinzanini, A. Rodella, A. Albertini, R. Ferrari, P. Harris.** Immunoreactivity to various peptides in the human carotid body. – Res. Commun. Chem. Pathol. Pharmacol., **62**, 1988, 289-293.
6. **Heym, C., W. Kummer.** Immunohistochemical distribution and colocalization of regulatory peptides in the carotid body. – J. Electron. Microsc. Tech., **12**, 1989, 331-342.
7. **Kameda, Y.** Distribution of CGRP-, somatostatin-, galanin-, VIP-, and substance P-immunoreactive nerve fibers in the chicken carotid body. – Cell Tissue Res., **257**, 1989, 623-629.
8. **Kondo, H., M. Yamamoto.** Occurrence, ontogeny, ultrastructure and some plasticity of CGRP (calcitonin gene-related peptide)-immunoreactive nerves in the carotid body of rats. – Brain Res., **473**, 1988, 283-293.
9. **Kummer, W.** Retrograde neuronal labelling and double-staining immunohistochemistry of tachykinin- and calcitonin gene-related peptide-immunoreactive pathways in the carotid sinus nerve of the guinea pig. – J. Auton. Nerv. Syst., **23**, 1988, 131-141.
10. **Kummer, W.** Three types of neurochemically defined autonomic fibres innervate the carotid baroreceptor and chemoreceptor regions in the guinea-pig. – Anat. Embryol., **181**, 1990, 477-489.
11. **Kummer, W., A. Fischer, C. Heym.** Ultrastructure of calcitonin gene-related peptide- and substance P-like immunoreactive nerve fibers in the carotid body and carotid sinus of the guinea pig. – Histochemistry, **92**, 1989, 433-439.
12. **Kummer, W., J. O. Habeck.** Substance P- and calcitonin gene-related peptide-like immunoreactivity in the human carotid body studied at light and electron microscopical level. – Brain Res., **554**, 1991, 286-292.
13. **Kusakabe, T.** Ontogeny of substance P-, CGRP-, and VIP-containing nerve fibers in the amphibian carotid labyrinth of the bullfrog, Rana catesbeiana. An immunohistochemical study. – Cell Tissue Res., **269**, 1992, 79-85.
14. **Kusakabe, T., Y. Hayashida, H. Matsuda, Y. Gono, F. L. Powell, M. H. Ellisman, T. Kawakami, T. Takenaka.** Hypoxic adaptation of the peptidergic innervation in the rat carotid body. – Brain Res., 806, 1998, 165-174.
15. **Kusakabe, T., H. Hirakawa, H. Matsuda, T. Kawakami, T. Takenaka, Y. Hayashida.** Peptidergic innervation in the rat carotid body after 2, 4, and 8 weeks of hypocapnic hypoxic exposure. – Histol. Histopathol., **18**, 2003, 409-418.
16. **Kusakabe, T., H. Hirakawa, S. Oikawa, H. Matsuda, T. Kawakami, T. Takenaka, Y. Hayashida.** Morphological changes in the rat carotid body 1, 2, 4, and 8 weeks after the termination of chronically hypocapnic hypoxia. – Histol. Histopathol., **19**, 2004, 1133-1140.
17. **McDonald, D.M.** Peripheral chemoreceptors. Structure-function relationships of the carotid body. In: Regulation of Breathing (Ed. T. F. Hornbein), New York, Dekker, 1981, 105-319.
18. **Moody, T. W., J. M. Hill, R. T. Jensen.** VIP as a trophic factor in the CNS and cancer cells. – Peptides, **24**, 2003, 163-177.
19. **Poncet, L., L. Denoroy, Y. Dalmaz, J. M. Pequignot, M. Jouvet.** Chronic hypoxia affects peripheral and central vasoactive intestinal peptide-like immunoreactivity in the rat. – Neurosci. Lett., **176**, 1994, 1-4.
20. **Porzionato, A., V. Macchi, A.R. Parenti, R. De Caro.** Trophic factors in the carotid body. – International Review of Cell and Molecular Biology, **269**, 2008, 1-58.

21. **Rodrigo, J., J.M. Polak, L. Fernandez, M.A. Ghatei, P. Mulderry, S.R. Bloom.** Calcitonin gene-related peptide immunoreactive sensory and motor nerves of the rat, cat, and monkey esophagus. – Gastroenterology, **88**, 1985, 444-451.
22. **Smith, P., J. Gosney, D. Heath, H. Burnett.** The occurrence and distribution of certain polypeptides within the human carotid body. – Cell Tissue Res., **261**, 1990, 565-571.
23. **Verna, A.** The mammalian carotid body: morphological data. – In: The carotid body chemoreceptors (Ed. C. Gonzalez), Texas, U.S.A, Landes Bioscience Austin, 1997, 1-29.
24. **Wharton, J., J. M. Polak, A. G. Pearse, G. P. McGregor, M. G. Bryant, S. R. Bloom, P. C. Emson, G. E. Bisgard, J. A. Will.** Enkephalin-, VIP- and substance P-like immunoreactivity in the carotid body. – Nature, **284**, 1980, 269-271.

Institute of Experimental Morphology, Pathology and Anthropology with Museum
Bulgarian Anatomical Society

Acta morphologica et anthropologica, 23
Sofia ● 2016

An Unusual Case of Peripheral T-cell Lymphoma

V. Broshtilova[1], M. Gantcheva[2]

[1]Department of Dermatology and Venereology, Faculty of Medicine, Medical University, Sofia, Bulgaria
[2]Institute of Experimental Morphology, Pathology and Anthropology with Museum, Bulgarian Academy of Sciences, Sofia, Bulgaria

A 24-year-old woman presented with 2-year history of erythematous patches, papules and plaques on her trunk and extremities. Skin lesions were unpainful, slightly itchy, and showed tendency to resolve spontaneously. Medium to large atypical lymphoid cells with focal epidermotropism were seen on routine histology. Immunophenotyping revealed CD2+, CD3+, CD5+ and partly CD4+, PD-1+, Bcl-6+, CXCL-13+, βF1+. TCR-gamma, TIA-1, Granzyme B, CD8 were negative. Only few cells stained positive for CD56 and CD30. This constellation was more suggestive of peripheral T-cell lymphoma, not otherwise specified (PTCL/NOS). The lack of negative prognostic factors such as multifocal skin involvement with ulceration, concurrent extracutaneous disease, age older than 70 years and predominantly large cell morphology favor the diagnosis of atypical immunohistochemical variant of mycosis fungoides (MF). PTCL/NOS are extremely rare cases with bad prognosis and rapid fatal outcome, which must always be ruled out from all cases of MF by complete work-up and accurate clinical history.

Key words: mycosis fungoides, peripheral T-cell lymphoma, not otherwise specified.

Introduction

Peripheral T-cell lymphomas, not otherwise specified (PTCL, NOS), represent a heterogeneous group of T-cell neoplasms that do not fit to any defined T-cell entities [2, 3]. Most cases represent late stage of nodal disease, although extranodal involvement is common. Only 20% of PTCLs show skin involvement [5]. These are extremely rare cases with bad prognosis and rapid fatal outcome, which must always be ruled out from all cases of mycosis fungoides (MF) by complete work-up and accurate clinical history [4].

Case report

A 24-year-old Caucasian female presented with 2-year history of erythematous patches, papules and plaques on her trunk and extremities. Skin lesions were unpainful, slightly itchy, and showed tendency to resolve spontaneously. The first lesion reportedly appeared on the left arm, with the most recent ones developing on the face and eyebrows. The patient claimed episodes of pruritus and dry patches on her hands during childhood that usually disappeared under sun. She had 10-time elevated total IgE, which was first

detected two years ago and persisted to date. Her brother had severe atopic dermatitis presented by refracting erythematous patches and diffuse xerosis.

Examination revealed multiple uniform firm erythematous papules with a diameter of 1 cm on her upper and lower extremities (**Figs. 1, 2**). Multiple skin biopsies were subjected to histological examination showing parakeratosis, irregular acanthosis, mild to moderate medium and large atypical lymphoid cells (**Figs. 3, 4**). There were some

Fig. 1. An erythematous patch of uniform firm papules on the left elbow

Fig. 2. An erythematous plaque of the right cubital fold

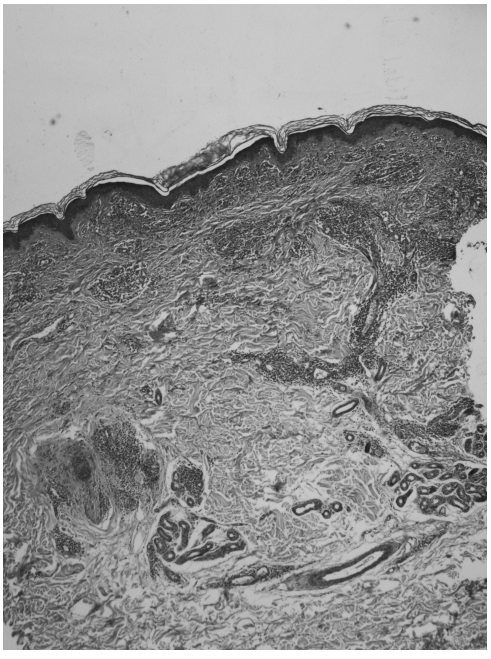

Fig. 3. Parakeratosis, acanthosis, mild to moderate perivascular and periadnexal infiltrate of atypical medium to large lymphoid cells in the dermis. HE × 100

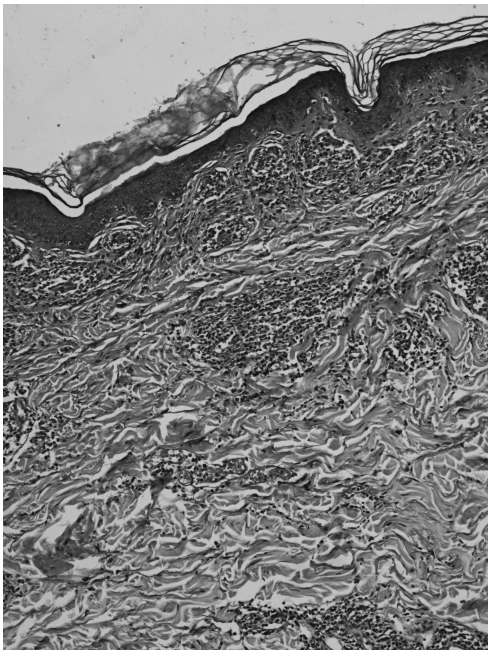

Fig. 4. Medium to large atypical lymphoid cells, focal perivascular necrosis. HE × 400

areas of peri-follicular necrosis. Immunophenotyping revealed CD2+, CD3+, CD5+ and partly CD4+, PD-1+, Bcl-6+, CXCL-13+, ßF1+. TCR-gamma, TIA-1, Granzyme B, CD8 were negative. Only few cells stained positive for CD56 and CD30. Flow cytometry did not find any peripheral aberrant lymphoid proliferation.

Abdominal CT scan and ultrasound ruled out systemic involvement. PET scan showed hypermetabolic activity in a solitary right inguinal lymph node, which upon histology turned out to be free of specific involvement. Narrow band UV B therapy was introduced with good clinical outcome, therefore, 5000 mJ/sq. cm was recommended on a weekly basis.

Discussion

Skin lymphomas usually show T-cell origin. Mycosis fungoides and Sezary syndrome comprise the majority of these cases. The primary skin lesions encompass co-existent patches, plaques or nodules, which may or may not ulcerate spontaneously. Erythroderma is typical for Sezary syndrome. Clinical picture corresponds to atypical lymphoid cells that show specific immunophenotypical characteristics, according to which the complicated classification of the various types of peripheral T-cell lymphomas is structured [6].

Interestingly, our case did not meet the histopathological or immunophenotypical criteria for any of the other well-defined subtypes of peripheral T-cell lymphoma. According to these criteria, it has to be classified as PTCL/NOS [1, 3].

Less than 100 patients were described with PTCL/NOS to date [2, 7]. In these limited reports, patients tend to present with generalized lymphadenopathy and gastrointestinal involvement. Cutaneous disease is usually represented with disseminated nodules. One fifth of the patients observed had concurrent nodal involvement at the time of presentation of the first skin lesions.

In contrast, our patient did not show any of the clinical features described. She had rather indolent course of the disease presented by erythematous papules and patches that resolved spontaneously and did not ulcerate. The lack of systemic involvement and peripheral aberrant lymphoid clone, together with favorable response to phototherapy, suggest more of an atypical immunohistochemical variant of MF.

Coclusions

We ruled out the negative prognostic indicators – multifocal skin involvement with ulceration, concurrent extracutaneous disease, lack of spontaneous improvement, age older than 70 years and large cell morphology, to favor our diagnosis. A close clinical, histological and laboratorial follow-up is, however, needed to confirm our suggestion.

References

1. **Bekkenk, M. W., M. H. Vermeer, P. M. Jansen, A. M. van Marion, M. R. Canninga-van Dijk, P. M. Kluin et al.** Peripheral T-cell lymphomas unspecified presenting in the skin: Analysis of prognostic factors in a group of 82 patients. – Blood, **102**(6), 2003, 2213-2219.
2. **Friedman, B. J., C. McHargue, M. Nauss.** Peripheral T-cell lymphoma, not otherwise specified with prominent cutaneous involvement. – Ind. J. Dermatol. Venereol., **81**(5), 2015, 535-537.

3. **Kempf, W., S. Rozati, K. Kerl, R. Dummer.** Cutaneous peripheral T cell lymphomas, unspecified /NOS and rare subtypes: A heterogeneous group of challenging cutaneous lymphomas. – G. Ital. Dermatol. Venereol., **147**(6) 2012; 553-562.
4. **Schmitz, N., L. Trümper, M. Ziepert, M. Nickelsen, A. D. Ho, B. Metzner et al.** Treatment and prognosis of mature T-cell and NK-cell lymphoma: An analysis of patients with T-cell lymphoma treated in studies of the German High-Grade Non-Hodgkin Lymphoma Study Group. – Blood, **116**(18), 2010, 3418-3425.
5. **Swerdlow, S. H., E. Campo, N. L. Harris, E. S. Jaffe, S. A. Pileri, H. Stein et al.** WHO Classification of Tumours of Haematopoietic and Lymphoid Tissues. Lyon, France: IARC Press; 2008.
6. **Wallett, A., J. S. Ibbetson, D. Kearney, K. Newland, S. Sidhu.** Cutaneous manifestations of peripheral T-cell lymphoma, not otherwise specified: a case series highlighting the diagnostic challenges for this heterogeneous group. – Australasian J. Dermatol., **56**(3), 2015, 197-201.
7. **Weisenburger, D. D., K. J. Savage, N. L. Harris, R. D. Gascoyne, E. S. Jaffe, K. A. MacLennan et al.** Peripheral T-cell lymphoma, not otherwise specified: A report of 340 cases from the International Peripheral T-cell Lymphoma Project. – Blood, **117**(12), 2011, 3402-3408.

Institute of Experimental Morphology, Pathology and Anthropology with Museum
Bulgarian Anatomical Society

Acta morphologica et anthropologica, 23
Sofia ● 2016

Distribution of Histamine-Positive Mast Cells in the Vicinity of the Needle Tract Following Acupuncture in "Zusanli" (ST_{36}) Acupoint in Rats

N. Dimitrov[1], D. Atanasova[1,2], N. Tomov[1], I Ivanova[1], Y. Staykova[3], K. Dinkova[4], I. Ganeva[4], D. Sivrev[1]

[1]*Department of Anatomy, Trakia University, Stara Zagora, Bulgaria*
[2]*Institute of Neurobiology, Bulgarian Academy of Sciences, Sofia, Bulgaria*
[3]*Department of General Medicine, Faculty of Medicine, Trakia University, Stara Zagora, Bulgaria*
[4]*Department of General and Clinical Pathology, Forensic Medicine and Deontology, Faculty of Medicine, Trakia University, Stara Zagora, Bulgaria*

"Zusanli"(ST_{36}) acupoint is commonly used in acupuncture. The mast cells are important object in experimental acupuncture. Histamine is stored in the granules of rat mast cells. The aim of the present study is to examine the distribution of histamine-positive mast cells in the vicinity of needle tract following acupuncture in ST_{36} acupoint in rats. Acupuncture in ST_{36} disrupted the integrity of the epithelium, derma, subcutis, fascia, epimysium and striated muscle tissue. In our research we observed thickening and displacement of the connective tissue in the direction of the needle tract and folding of the fascia. We noticed histamine-positive mast cells in the proximity of needle tract in the tissues of ST_{36} acupoint in rats. We could not establish considerable differences in the number and distribution of histamine-positive mast cells in the needle tract vicinity. Few histamine-positive mast cells in the proximity of the needle tract showed signs of degranulation.

Key words: mast cells, histamine, acupuncture, needle tract, Zusanli (ST_{36}).

Introduction

During the 20th century Traditional Chinese Medicine (TCM) which has been used for thousands of years in China and other countries of the Far East, is being extensively applied in modern medicine both as a modality for treatment or general conditioning in chronic disease as well as supplementary physical therapy, in support of the main therapeutic methods. The acupuncture is one of the main methods of TCM.

"Zusanli"(ST_{36}) acupoint is one of the most commonly used in acupuncture. Acupuncture points, described in the classical texts, are usually detected with the method of standard proportion of anatomical structures under the control of the apparatus measuring skin resistance [17, 4]. The acupuncture channels and acupuncture points of human and animals (including rats) share certain similarities [3], which allows researchers to

use animals as model for experimental acupuncture. Many studies have been devoted to research the local mechanism of acupuncture but there is relatively little research for changes in the vicinity of the acupuncture needle tract, although the regional anatomy has been previously described to include nerve fibres, small vessels and muscle spindles in the proximity of the acupuncture needle tract in the tissue of the acupoints [11].

Histamine is a neurotransmitter involved in local immune responses as well as in regulation of physiological functions [13]. Histamine is stored in the granules of rat mast cells [1, 8, 16]. The mast cells are heavily involved in local acupuncture reaction and are thus important object for experimental acupuncture in rats [18, 14, 20]. Histamine is also the subject of many experimental researches [7, 9, 10, 15].

The normal morphological structures in ST_{36} acupoint are: epidermis, dermis, subcutis, fascia, epimysium and muscle with blood vessels and nerves. There are many hair follicles with piloerector muscles and sebaceous glands in dermis. There are clusters of mast cells in certain areas close to the blood vessels [6]. Our previous results show that the impact of the acupuncture needle in the ST_{36} acupoint induces morphological changes in the tissues and mast cells. As a result of acupuncture of ST_{36} acupoint the integrity of the epithelium, dermis, subcutis, fascia, epimysium and striated muscles are disrupted in the direction of the needle tract [5]. However, the distribution of mast cells in the tissues of the acupoint and their reaction to acupuncture have not been elucidated.

Materials and Methods

The aim of this research is to study histamine-positive cells in the vicinity of the needle tract following acupuncture in ST_{36} acupoint in rats. The studies were carried out on six adult Wistar normotensive rats, weighing between 220 and 350 g. All experiment were carried out in accordance with the standards for ethical treatment of animals in research, set forth by the Ethics Committee of Trakia University. The area around the acupoint was epilated, defined and marked using the method of standard proportion of anatomical structures under the control of the apparatus KWD-808 measuring skin resistance. We used steel acupuncture needle with size 0.25 × 13 mm. The animals were deeply anaesthetized and transcardially perfused with 4% paraformaldehyde solution. Tissue sample with size 5 × 5 × 5 mm from ST_{36} acupoint was taken together with the acupuncture needle, postfixed, embedded in paraffin and cut into 5 μm thick sections. The samples were then deparaffinized with xylene and ethanol, and processed for avidin-biotin-horseradish peroxidase complex (ABC) immunohistochemistry. Briefly, the sections were treated with hydrogen peroxide to inactivate endogenous peroxidase and the background staining was blocked with 5% normal goat serum (NGS) in PBS for 1 hour. Between the steps, the sections were rinsed with PBS/Triton X-100. After that they were incubated with the primary antibody, rabbit anti-histamine (diluted 1:2000, Sigma, Saint Louis, Missouri, USA) overnight at 4 °C in a humid chamber, followed by biotinylated goat anti-rabbit IgG (Sigma, 1:250) for 2 h at room temperature, and finally the ABC complex (Vector Labs, Burlingame, CA, USA) was applied for 2 hours at room temperature. Finally, the peroxidase activity was visualized using diaminobenzidine as a chromogen. After the immunoreaction, the sections were dehydrated in ethanols, cleared in xylene and coverslipped with Entellan.

The specimens were photographed with a Nikon research microscope equipped with a DXM 1200c digital camera. Statistical analysis was performed using SigmaStat®11.0 software package (Systat Software Inc). Experimental data were evaluated by Student's t-test. Differences were considered statistically significant if p-values were < 0.05.

Transmission electron microscopy was also used for visualization of mast cells.

The material from skin in the vicinity of the needle tract, with size 1 × 1 × 1 mm, was fixed in 2.5% glutaraldehyde and 2% paraformaldehyde in 0.1 M PBS. The sample was then dehydrated through ethanol series, passed through a propylene oxide and then infiltrated and embedded in a liquid resin such as epoxy. After embedding the resin block was cut into ultrathin sections by a diamond knife in an ultramicrotome. Each section, only 50-70 nm thick, is collected on metal mesh 'grids' and stained with electron dense stains before observation in the TEM.

Results

After acupuncture in ST_{36} acupoint the main alterations happen in the cutis, subcutis and the underlying muscle fibers and fascia. As a result of acupuncture the integrity of the epithelium is disrupted and it folds in the direction of the needle tract. Acupuncture of ST_{36} disrupted the integrity of derma, subcutis, deep fascia, epimysium and striated muscles. We observed thickening and displacement of the connective tissue and formation of folds in the direction of the needle tract and also histamine-positive mast cells

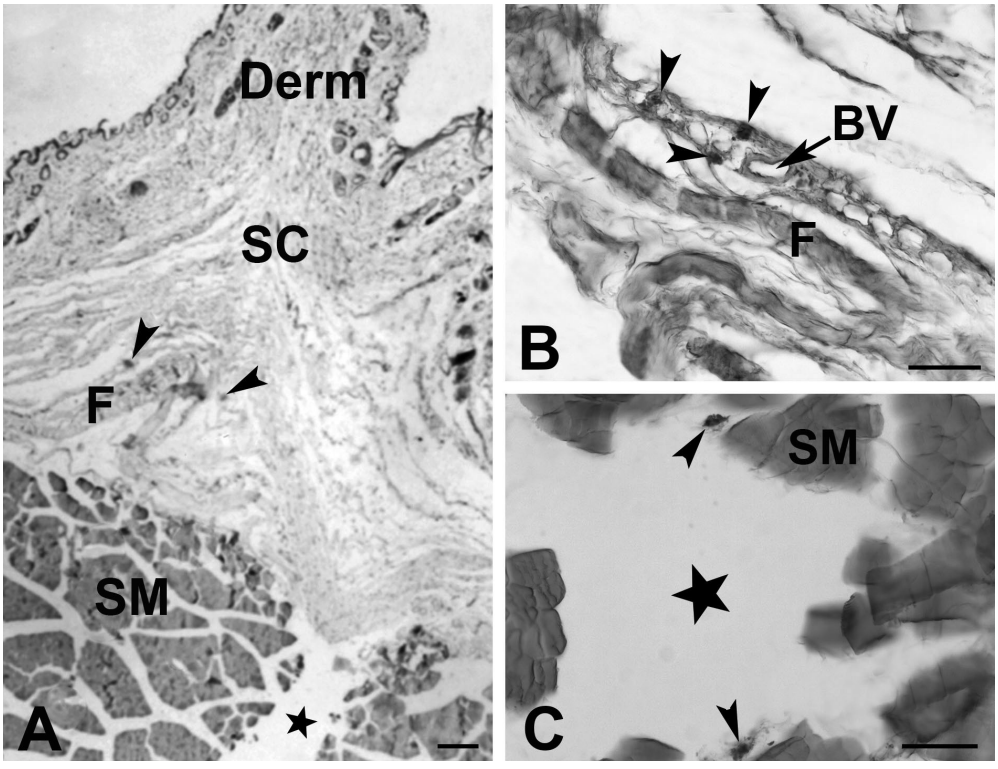

Fig. 1. (A, B, C) Histamine-positive mast cells in the needle tract vicinity of acupuncture point ST_{36} in rats: **A**) Distribution of histamine-positive mast cells (arrow) below the epidermis, dermis (Derm), fascia (F), subcutis (SC) and striated muscle (SM) in the needle tract (star) vicinity; **B**) Demonstrating the localization of histamine-positive mast cells (arrow) next to folded fascia (F) and blood vessel (BV); **C**). Histamine-positive mast cells (arrow) in the connective tissue of striated muscle (SM) in the needle tract (star) vicinity whith signs of partial degranulation. Scale bars = 50 μm

in the vicinity of needle tract in the tissues of ST_{36} acupoint in rats (**Fig. 1A, B, C**). Striated muscle fibers are partially destroyed and we noticed clear evident needle tract (**Fig. 1A, C**). Larger blood vessels are not affected, but rather displaced, by the needle.

The distribution of histamine-positive mast cells in tissue (dermis, subcutis and striated muscle) in the vicinity of the needle tract in ST_{36} acupoint in rats was uneven. The histamine-positive mast cells tended to form clusters in close proximity to the blood vessels (**Fig. 1B**). In our study we were not certain of the presence of histamine-positive mast cells in the epidermis. In the dermis histamine-positive mast cells were located mainly around the blood vessels and close to the hair follicle and sebaceous glands. The number of histamine-positive mast cells in the proximity of needle tract was larger in the border zones epidermis–dermis, dermis–subcutis, subcutis–fascia.

We observed thickening and displacement of the connective tissue in the vicinity of the needle tract (**Fig. 1A**). We also found histamine-positive mast cells adjacent to the folded fascia and blood vessels (**Fig. 1B**). More histamine-positive mast cells were visualized in subcutis and dermis than in striated muscles. Histamine-positive mast cells were also identified in the connective tissue of striated muscle in the vicinity of needle tract (**Fig. 1B**). We investigated the distribution of histamine-positive mast cells in the tissues in the vicinity of needle tract after acupuncture in Zone I (0-50 μm from the center of the needle tract) and Zone II (50-100 μm from it) (**Fig. 4**). In our results we could not establish considerable differences in the number and distribution of histamine-positive mast cells between Zone I and Zone II in ST_{36} acupoint. There were not statistically significant differences between the two areas ($p > 0.05$) (**Fig. 3**). We observed that mast cells show signs of partial degranulation in the proximity of the needle tract (**Fig. 1C, Fig. 2**).

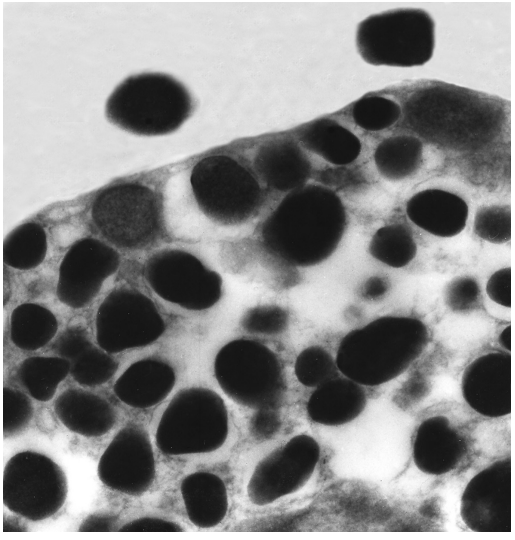

Fig. 2. Electron micrograph with signs of degranulation of mast cells in the needle tract vicinity (12700×)

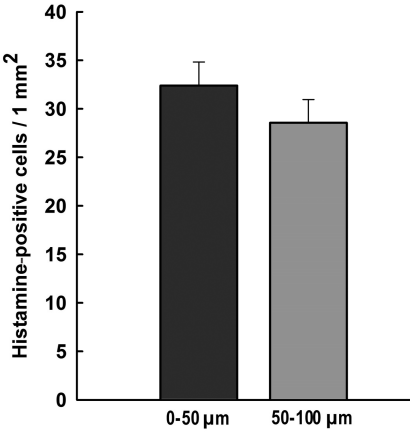

Fig. 3. Graphical representation of the distribution of histamine-positive mast cells in the tissues in the vicinity of the needle tract after acupuncture in acupoint ST_{36} in rats. Distribution of histamine-positive mast cells in Zone I (0-50 μm from the needle tract) and Zone II (50-100 μm from the needle tract). There are not statistically significant differences between the two areas ($p > 0.05$). Experimental data were evaluated by Student's t-test to parametric data. The data represent the average of the distribution of histamine-positive mast cells in an area of 1 mm^2 + SEM

Discussion

The results of the present study show thickening and displacement of the connective tissue in the proximity of needle tract. Our previous results also reported alterations in the connective tissue after acupuncture [7]. In the present study we observed single histamine-positive mast cells with signs of degranulation in the vicinity of the needle tract. The observed single histamine-positive mast cells with signs of degranulation were consistent with our research in rats, since we were able to show that degranulation of some mast cells takes place after acupuncture [5]. The influence of acupuncture on mast cell degranulation has been confirmed by other authors [2, 12]. Researchers have found that the acupuncture causes degranulation of closely located histamine-positive mast cells [19]. Other researchers reported that there were no significant differences in the distribution of mast cells between ST_{36} acupoint area and the nonacupoint areas, and most of the mast cells were mainly arranged along the small blood vessels. These researchers have also found that the influence of acupuncture on the cell number and degranulation of mast cells was unremarkable [21]. In our study we also could not establish considerable differences in the number and distribution of histamine-positive mast cells between center of acupoint with the needle tract and neighboring tissues in ST_{36} acupoint in rats. We suppose that the observed thickening and shifting of the connective tissue (together with the histamine-positive mast cells contained in it) by the needle could lead to small increase of the number of histamine-positive mast cells found in the connective tissue in the vicinity of the needle tract. We also confirm the presence of a large amount of histamine-positive mast cells in the proximity of blood vessels.

Conclusions

We could not establish considerable differences in the number and distribution of histamine-positive mast cells in the needle tract vicinity. Few histamine-positive mast cells in the proximity of needle tract are with signs of degranulation.

References

1. **Aldenborg, F., L. Enerbäck.** Histamine content and mast cell numbers in tissues of normal and athymic rats. – Agents and Actions, **17**, 1986, 454-459.
2. **Deng, Y., Z. Fu, H. Dong, Q. Wu, X. Guan.** Effects of electroacupuncture on the subcutaneous mast cells of zusanli acupoint in rat with unilateral sciatic nerve transection. – Acupunct. Res., **21**, 1996, 46-49.
3. **Dimitrov, N., D. Sivrev, Y. Staykova, Z. Goranova.** Comparative analisis of biological active channels in humans and animals. – Science in Globalization, **3**, 2008, 351-357.
4. **Dimitrov, N., D. Sivrev, N. Pirovski, A. Georgieva.** Methods for localization of BAP of the human body. – J.B.C.R., **2**, 2009, 19-21.
5. **Dimitrov, N.** Morphological changes in biologically active point /BAP/ ST_{36} after acupuncture in rat. – Acta Morphol. Anthropol., **19**, 2012, 30-33.
6. **Dimitrov, N.** Normal morphology of biologically active point BAP/ST_{36} rat. – Acta Morphol. Anthropol., **19**, 2012, 34-37.
7. **Enerbäck, L., U. Wingren.** Histamine content of peritoneal and tissue mast cells of growing rats. – Histochemistry, **66**, 1980, 113-124.
8. **Feng, Y., J. Wu.** Histochemical and immunohistochemical observations on heterogeneity in mast cells of rat. – Acta Anat. Sinica, **1**, 1989, 90-94.
9. **Hardwick, B.** Age changes in the histamine content of rat skin. – J. Physiol., **124**, 1954, 157-165.

10. **Huang, M., Y. Xie, G. Ding.** Acupoint-injection of histamine induced analgesic effect in acute adjuvant-induced-arthritis rats. – Acupunct. Res., **35**, 2010, 99-103.
11. **Kim, M., T. Nam, M. Kim, J. Kim, D. Kim, K. Lee, C. Song.** Histological observation of canine acupoints. – J. Vet. Clin., **23**, 2006, 102-104.
12. **Luo, M., J. He, Y. Guo, C. Li.** Effect of electroacupuncture and moxibustion of "Dazhui" (GV14) on the number and distribution of degranulated mast cells in GV14 region. – Acupunct. Res., **32**, 2007, 327-329.
13. **Marieb, E.** Human Anatomy & Physiology. San Francisco: Benjamin Cummings, 2001, 414.
14. **Ming, C., S. Cai, Y. Cai, T. Ma.** Observation of MC in the deep aponeurosis under the fluorescent microscope by electric needling in "Zusanli". – Acupunct. Res., **25**, 2000, 51-53.
15. **Riley, J., G.West.** Skin histamine; its location in tissue mast-cells. – AMA. Arch. Derm., **74**, 1956, 471-478.
16. **Schwartz, L., K. Austen.** Enzymes of the mast cell Granule. – J. Investig. Dermatol.,**74**, 1980, 349-353.
17. **White, A., M. Cummings, J. Fishie.** How to locate acupuncture points. – In: An introduction to western medical acupuncture. Ghurchil Livingstone Elsevier, 2008, 185-189.
18. **Wu, J., X. Chai, D. Cai, A. Zong.** Observation on mast cells in subcutaneous connective tissue at points in albino rats. – Acta Anat. Sinica, **1**, 1980, 308-312.
19. **Wu, M., D. Xu , W. Bai, J. Cui, H. Shu, W. He, X. Wang, H. Shi, Y. Su, L. Hu, B. Zhu, X. Jing.** Local cutaneous nerve terminal and mast cell responses to manual acupuncture in acupoint LI4 area of the rats. – J. Chem. Neuroanat., **68**, 2015, 14-21.
20. **Zhang, D., G. Ding, X. Shen, W. Yao, Z. Zhang, Y. Zhang, J. Lin, Q. Gu.** Role of mast cells in acupuncture effect: a pilot study. – Explore (NY), **4**, 2008, 170-177.
21. **Zong, A., X. Shi, F. Zhang.** Effects of electro-acupuncture on fascial mast cells in "Zusanli" acupoint area of rabbits. – J. Zhengzhou Univ. (Sci. Med.), **27**, 1992, 226-229.

Correspondence address:
**Department of Anatomy*
Faculty of Medicine
Trakia University
11, Armeyska Str.
6000 Stara Zagora, Bulgaria
e-mail: nikolaydd@abv.bg

Institute of Experimental Morphology, Pathology and Anthropology with Museum
Bulgarian Anatomical Society

Acta morphologica et anthropologica, 23
Sofia ● 2016

Histopathological Changes in the Testis of Hamsters with Experimentally Induced Myeloid Tumor of *Graffi*

I. Ilieva[1], R. Toshkova[1], I. Sainova[1], I. Vladov[1], E. Zvetkova[2]

[1]Institute of Experimental Morphology, Pathology and Anthropology with Museum, Bulgarian Academy of Sciences, Sofia, Bulgaria
[2] Bulgarian Biorheological Society

The secondary malignant tumors of the testes usually are a rare phenomenon. The presence of blood-testis barrier (BTB) is proposed as a reason about the seldom affection of the testes by metastatic developed tumor mass [1, 5, 17].

In this aspect, the current investigation is the first morphological study on testes, using experimental model of *Graffi* tumor in hamsters (GMT). The results indicate significant changes in the lumen diameter in capillaries, but also in the larger blood vessels in the testes of tumor-treated hamsters from day 25th and day 30th of the experiment, in comparison with the control. In parallel with these data, significant extension of the interstitial space between the seminiferous tubules is also established, as well as the presence of many atypical myeloid cells in the lumen of the whole blood vessels' length in the gonads of the tumor-treated animals. According to these results, the established changes in the blood vessels (in particular capillaries) and in the testicular tissue are probably caused by the developing GMT in the organism of the tumor-bearing hamsters (TBH).

Key words: Testicular metastases, blood-testis barrier, myeloid *Graffi* tumor, peritubular capillaries and intratubular blood vessels.

Introduction

The secondary malignant tumors of the testes usually are a rare phenomenon. Metastases in the testes can most often derive from hematological malignancies as leukemia and lymphoma, but also primary tumors with non-hematological origin [10, 17].

Testicular involvement is a rare and unusual case in patients with chronic myeloid leukemia (CML), but the testicular extramedullary myeloid cell tumors (TEM-MCTs) could be considered in the differential diagnosis of intra-testicular tumors [2, 7, 9, 14, 15, 20]. The literature review also revealed a report showing the simultaneous involvement of both testis and central nervous system in a three-year-old child with Philadelphia positive CML [3].

The functions of the blood-testis barrier and especially of testicular microcirculation (microvasculature) and Sertoli cells are of great importance – to protect testicular

interstitial tissue and developing male germ cells in the process of spermatogenesis against tumor/leukemia cell invasion (dissemination) [1, 5, 7, 20]. In this sense, further studies on histopathological changes in the testicular microcirculation (micro-vessel dilation and neo-angiogenesis) in the course of neoplastic diseases could characterize first steps of malignant cell metastasis through the blood-testis barrier and elucidate, at cellular and molecular levels, the etiology and pathogenesis of neoplastic blast cell dissemination. In this aspect, the current investigation is the first morphological study on testes, using experimental model of *Graffi* tumor in hamsters.

The transplantable myeloid tumor used in this study originated as a *Graffi* murine leukemia virus-induced tumor in newborn hamsters, adapted and maintained to mature Golden Syrian hamsters [6, 18, 19].

The *aim* of the present (pilot) study is to examine the early and late histopathological changes in the testis of hamsters with experimentally induced *myeloid tumor of Graffi* – defined in the literature as occurring at other extramedullary locations (skin, brain, lymph nodes, etc) [6, 16, 19].

Materials and Methods

Experimental hamster Graffi tumor model

Golden Syrian hamsters, 2 months old, were used in experiments. The experimental *Graffi* tumor was primary created by the Graffi-virus in new-born hamsters, and maintained monthly *in vivo* by subcutaneous transplantation of live tumor cells (2×10^6/ml PBS) in the interscapular area of hamsters, for keeping the tumor's survival [6, 18, 19]. The tumor is 100% cancerous, and the animals die usually up to the 30th day after transplantation. The animals were kept under standard conditions with free access to food and water.

Morphometric and histopathological examination

Samples of testes from control (healthy) and tumor bearing hamsters (TBH) were taken, fixed and embedded in paraffin using routine histological practice. Tissue sections (5-7 μm) were stained by hematoxylin-eosin and examined under light microscope Leica DM5000B. We obtained morphometric data from the light microscope at 400× magnification using an eyepiece micrometer. The luminal diameter was measured as perpendicular distance across the maximum chord axis of each vessels of control (n = 6) and TBH (n = 4 on the 10th, n = 6 on the 25th, and n = 3 on the 30th day after tumor implantation).

Statistical analysis: Results are reported as mean values ± SEM and statistically analyzed by Student's t-test.

All studies were performed in accordance with the Guide for Care and Use of Laboratory Animals, as proposed by the Committee on Care Laboratory Animal Resources, Commission on Life Sciences and National Research Council, and a work permit No 11130006.

Results

In the current study, the changes in the blood vessels diameter in testes from healthy (control group) and tumor-bearing hamsters are assessed on days 10th, 25th and 30th after the inoculation of the hamsters with tumor cells (post transplantation - p. t.). These findings are shown in **Table 1** and **Fig. 1**.

Table1. Morphometric data of blood vessels in the testes of tumor-bearing and healthy (control) hamsters (diameter of blood vessels lumen in μm)

Blood vessels (Luminal diameter)	6.0-15.0 μm	15.5-30.0 μm	30.5-50.0 μm	> 50 μm
Control	***9.19 ± 2.05***	***23.25 ± 2.36***	***34.62 ± 1.22***	***60.95 ± 6.11***
10th day	9.13 ± 3.38	23.97 ± 3.21	35.44 ± 2.41	62.36 ± 5.42
25th day	11.80 ± 1.89	24.82 ± 3.32	39.30 ± 6.06*	76.40 ± 9.10**
30th day	12.93 ± 1.66*	25.72 ± 3.26*	43.33 ± 4.95**	82.65 ± 7.77**

*p < 0.01, ** p < 0.001

Significant changes in the blood vessels diameter in the testes of hamster from day 10th p. t. are not established in comparison to the control group (**Table 1**). Considerable changes were observed in the lumen diameter of capillaries (vessels < 15.0 μm and vessels of 15.5-30.0 μm in diameter), but also of the larger blood vessels (vessels of 30.5-50.0 μm and >50.0 μm in diameter) in the testes of TBH from day 25th p. t. (mean luminal diameter of capillaries: 11.80 ± 1.89 μm; 24.82 ± 3.32 μm; and large vessels: 39.30 ± 6.06 μm; 76.40 ± 9.10 μm in diameter, respectively), and from day 30th p. t. (mean luminal diameter of capillaries: 11.80 ± 1.89 μm; 24.82 ± 3.32 μm, and large vessels: 39.30 ± 6.06 μm; 76.40 ± 9.10 μm in diameter, respectively), in comparison with the control. Lumens of capillaries with diameter > 30 μm were also assessed, and their rates were added to the blood vessels with a larger size (vessels of 30.5-50.0 μm and > 50.0 μm in diameter).

The percentage distribution of blood vessels with different size indicates an increase in the number of the large blood vessels – venules and arterioles (vessels of 30.5-50.0 μm and > 50.0 μm in diameter) in the testes of TBH on day 25th p. t. (8.09 % and 2.86%, respectively), and on day 30th p. t. (9.35 % and 5.14 %), in comparison with these from day 10th p. t. (3.88% and 1.46 %) and the controls (3.43 % and 1%) (**Fig. 1**).

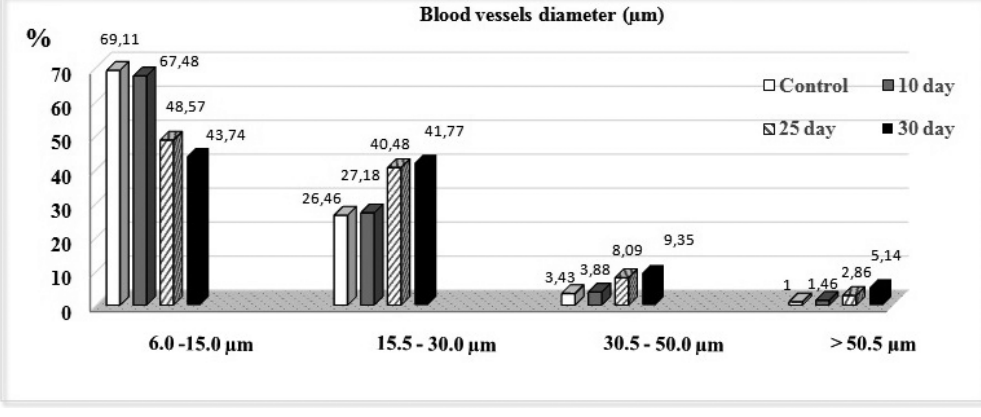

Fig. 1. Comparison of morphometric data of testis blood vessels of tumor treated and untreated (control) hamsters (relative part in %)

Besides, in the same experimental animals the number of blood vessels with lumen rate 15.5-30.0 μm in diameter (25th day – 40.48%, and 30th day – 41.77%) was significantly increased, and, hence the percent of these with the smallest size decreased (25th day - 48.57%, and 30th day – 43.74%), in comparison with the hamsters from the control group (69.11% and 26.46, respectively) (**Fig. 1**).

The results from the light microscopy observation of testes from hamsters on days 25th and 30th p. t. are shown in **Figs. 2** and **3**.

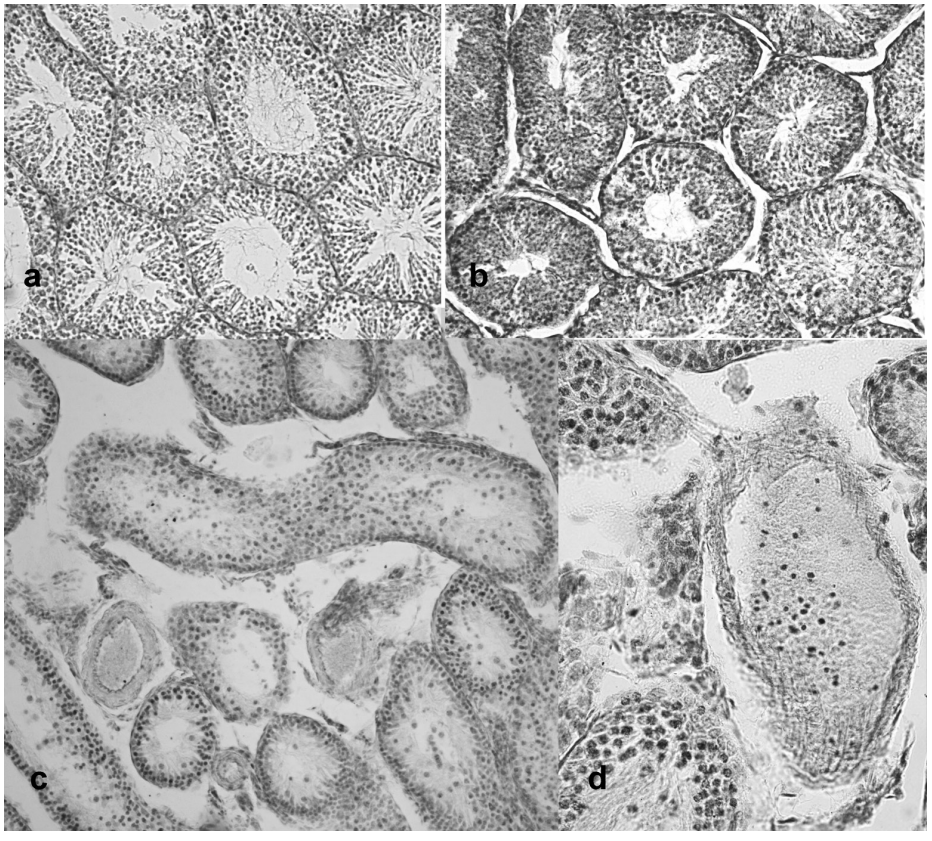

Fig. 2. Testicular cross-sections of control and tumor-treated hamsters (10th, 25th 30th):
(a) Healthy hamster (control); **(b)** Cross-section of tumor-treated hamster from day 10th. Region from the testicular tissue, slight enlargement of the interstitial space (in the normal values), as well as normal micro-vasculature; **(c)** Section of TBH from day 25th. Enlarged interstitial space with three large blood vessels (arterioles); **(d)** Section of TBH from day 30th. A large blood vessel (venula) with many atypical myeloid and erythroid cells in the lumen. Hematoxylin-eosine staining, × 200, × 400

Regions from the testicular tissue with blood vessels (mainly capillaries), located in peritubular and intratubular space, respectively with sinusoidally extensions of the lumen and branched, or thin excrescences derive from them, which are parallel directed to the main blood vessel are monitored (**Fig. 2** and **Fig. 3**). Short and thin capillary "bridges" (probably anastomoses) between nearly-located peritubular capillaries, as well as between peritubular and intratubular blood vessels (capillaries, arterioles and venules) could also be noted (**Fig. 3e**). In the blood vessel lumen, including in the whole

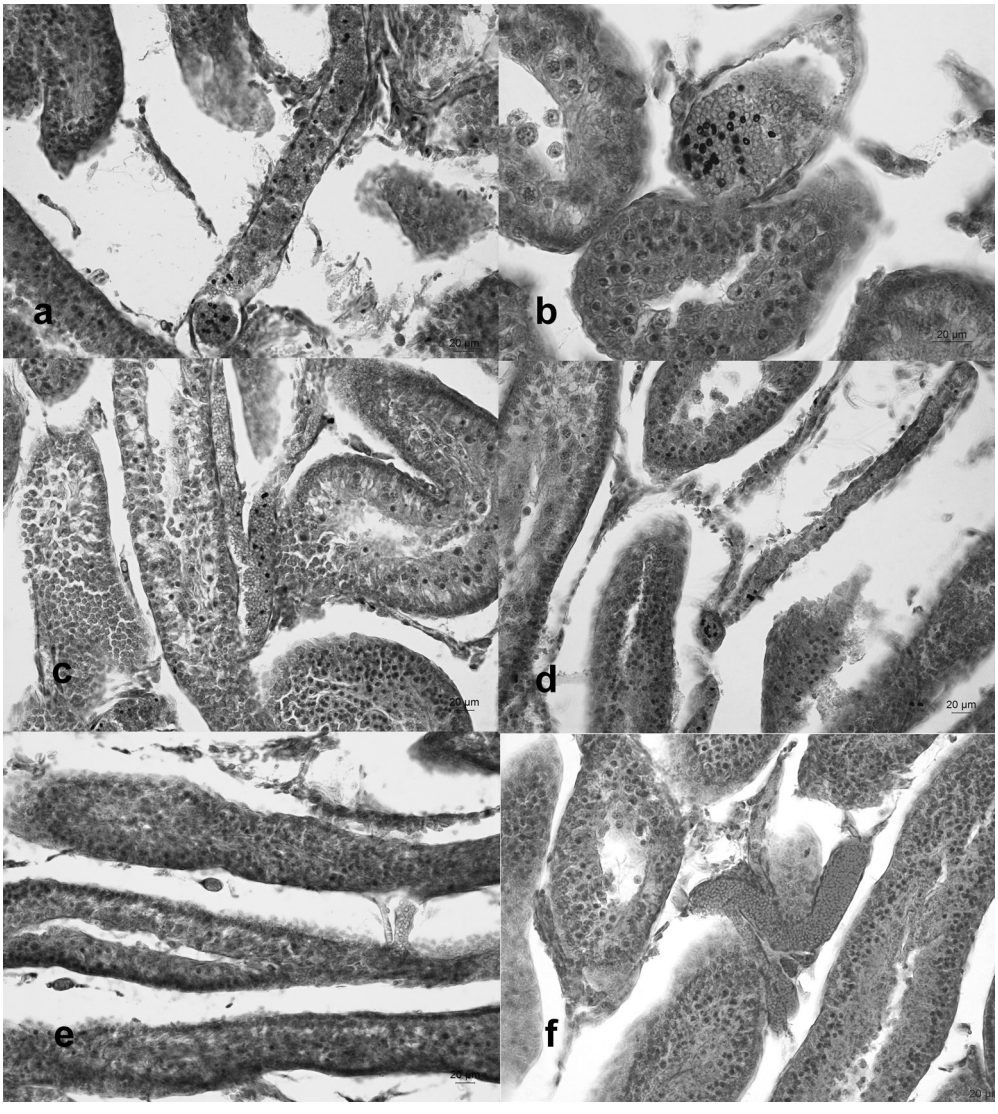

Fig. 3. Testicular cross-sections of tumor treated hamsters on 30th (a-d) and 25th (e-f) day: **(a)** Enlarged interstitial space with two branched blood vessels (sinusoidally extended capillaries), tightly put close to each other, in the upper part of the micrograph. A lot of erythroid cells, as well as nuclei of atypical myeloid cells, in the lumen of the whole blood vessel; **(b)** A large blood vessel (venula) with a presence of many nuclei of atypical myeloid cells, but also erythroid cells, in the blood vessel lumen; **(c)** Sinusoidally extended and branched capillary between two seminiferous tubules with injured vessel wall and atypical myeloid cells in the whole blood vessel; **(d)** Formation of venula with a presence of nuclei from atypical myeloid cells in the lumen; **(e)** Thin capillary "bridges" between two nearly located peritubular blood vessels (capillaries); **(f)** Sinusoidally extended capillary, with two thin branches and with injured vessel wall, deriving from it and located between three seminiferous tubules. Hematoxylin-eosine staining, × 200, × 400

vessel in some cases, many nuclei of atypical myeloid cells are often visualized (**Fig. 2d** and **Fig. 3a, b, c, d**). The capillaries are filled mainly with erythroid cells. In the cases from day 30th p. t., blood vessels with injured integrity of the vessel wall and with infiltrate of cells in the surrounding area could also be established in the testis.

The changes in the blood vessels are combined with extended interstitial spaces (especially in the peritubular tissue), as well as with injured structure in the most seminiferous tubules. These results from the morphometric measures of the peritubular tissue thickness in the TBH on day 25th p.t. (60.30 ± 26.78 μm) and on day 30th p.t., respectively (60.70 ± 28.79 μm) show considerable increase in comparison with the animals, treated on day 10th p.i. (16.39 ± 4.73 μm) and in the controls (14.16 ± 4.34 μm) ($p < 0.05$).

Discussion

In our study, the blood-testes barrier is accepted as a main factor about the secondary invasion and dissemination of the tumor cells in the male gonads. This suggestion is in support of some literature data [1, 5, 9, 20], according to which this barrier is very important about the early dissemination of neoplastic disease in the male reproductive system.

The blood stream regulation in the microcirculation of the testes takes place by active vasomotor function of the terminal afferent and efferent vessels – arterioles, venules as well as anastomoses between small vessels from both types. The blood reaches to the seminiferous tubules by adjacent peritubular and intertubular capillaries. The substance metabolism between the blood, Leidigh cells and seminiferous tubules occurs namely through these capillary vessel walls [8, 20]. This is the main reason for the investigation on the changes in the blood vessels (especially in the capillaries), because it plays a role as early sign for invasion and development of metastases in the testes.

The results in this study indicate statistically significant change in the mean luminal diameter and with dilatation of capillaries, but also of the larger blood vessels (arterioles and venules), in tumor progression process in the testes of TBH from day 25th and day 30th of the experiment, in comparison with the control. In the same treated animals, the percentage of blood vessels with large (vessels of 30.5-50.0 μm in diameter) and larger size (> 50.0 μm in diameter) is significantly increased, as at day 30th their number reached above 9% (9.35%) and above 5% (5.14%), respectively, in comparison with the control (3.43% and 1%).

In these cases, the percentage distribution of the capillaries can be noted. The number of the smallest capillaries (vessels < 15.0 μm in diameter) is significantly decreased (25th day – 48.57%, and 30th day – 43.74%), but that of the larger of them is enhanced (vessels of 15.5 – 30.0 μm in diameter) (25th day – 40.48%, and 30th day – 41.77%), in comparison with the hamsters, treated on day 10th and the control group, where the percent of the smallest size capillaries is the highest (67.48 and 61.11%, respectively).

Taking in consideration the indicated above performance of the blood vessel lumen in the tumor-bearing hamsters, as well as the microscopic observations, which reveal the presence of casual short, "blind" capillary excrescences and sinusoidal extensions, these results could be accepted as an indication for myeloid tumor cell-induced neoangiogenesis. Moreover, often the establishment of small "bridges" (anastomoses) between the capillaries, the presence of blood vessels with injured integrity of their wall, as well as the extended interstitial space between the seminiferous tubules, wholly change the normal look of the testicular tissue, and could be supplied as signs of initial tumor-induced neoangiogenesis. The establishment of many atypical myeloid cells in the blood vessels' lumen suggests the initiation of tumor cell invasion in the testes in tumor-bearing hamsters on days 25th and 30th post transplantation.

Analogical processes of interstitial region infiltration with blast cells have been described by Yuceturk et al. [20], in cases of chronic myeloid leukemia. Other authors have observed a presence of atypical myeloid cells with multiple mitochondria inside cytoplasm and nucleus in periphery blood of *Graffi* tumour-bearing hamster [21]. Similar morphological destructive changes have been observed by Ormandzhieva & Toshkova [16] in blood vessels from cheroid plexus of the brain in the same experimental model of *Graffi* tumor in hamster.

Supporting other experimental models and findings of authors on tumor blood vessel- and capillary-like structures formation *in vivo*, with the presence of erythrocytes in their lumens, we could point out recent data in this field concerning expression of several tumor vasculogenic- and angiogenic genes and cell growth factors (including VE-cadherin, FGFR1, VEGFA etc.), from the neoplastic cells, e.g. in cases of human melanoma and ovarian (Hey 1B) cancer [4, 12].

Human melanoma cells are known to produce various angiogenic factors which promote tumor angiogenesis through *in-growth* in the the tumor vasculature from pre-existing blood vessels [12]. To verify and confirm whether blood vessels in the course of malignant cell dissemination are a part of the prime organ vasculature or they grow as tumor cell "vasculogenic mimicry channels", probably as in our experimental model, firther studies and observations on VE-cadherin expression in Graffi myeloid tumor cells, accompanied by co-expression of tumor cell marker protein could be performed. The existence of new medicines suppressing tumor neo-angiogenesis and VE-cadherin expression in melanoma- and other malignant cells [4, 11, 13] could be also discussed by us in the course of our further experimental studies on *Graffi myeloid tumor models*.

The current study for the first time shows the histopathological changes in the testes in experimental model of induced transplantable myeloid *Graffi* tumor in hamsters. Furthermore, for the first time the lumen diameter rates of blood vessels with different size in testes of hamster are measured.

The observed by us changes in the integrity of the testicular tubules and of their membranes, but also the invasion of atypical myeloid cells in them together with the following changes in the spermatogenesis in hamsters on the influence of both tumor cells' dissemination and neoplastic process toxicity, would be an object of our future publication.

Conclusion

According to the results of the current study, the contrasted changes in the blood vessels (in particular in the capillaries), as well as in the testicular tissue, are probably the result of the developing myeloid *Graffi* tumor in the inoculated hamsters. We proposed the pathological changes in the diameter of capillary lumen and the extended interstitial regions between the seminal tubules as predominating obvious factors about the appearance of initial conditions (indication for angiogenesis) for distribution and development of metastases in the testes of the experimental animals. Additional investigations for clarification the histopathology of the testicular tissue in tumor-bearing hamsters are necessary.

Acknowledgements: This research was financially supported by the Bulgarian National Science Fund (Grant BO2/5-2014). The authors wish to thank M. Pavlova, medical laboratory assistant, for the excellent technical assistance of the histological preparation of tissue.

References

1. **Bart, J., H. J. Groen, W. T. van der Graaf, H. Hollema, N. H. Hendrikse, W. Vaalburg, et al.** An oncological view on the blood-testis barrier. – Lancet Oncol., **3**(6), 2002, 357-363.
2. **Beedassy, A., D. Topolsky, M. Styler, P. Crilley**. Extramedullary blast crisis in a patient with chronic myeloid leukemia in complete cyto-genetic and molecular remission on interferonalfa therapy. – Leukemia, **24**, 2000, 733-735.
3. **Carlson, N. L., G. Erichson, L. Lissel**. Simultaneous meningeal and testicular lymphoblastic transformation of Philadelphia positive CML in a three year old. – Anticancer Res., **10**, 1990, 1739-41.
4. **Cao, Z., D. Yu, S. Fu, G. Zhang, Y. Pan, M. Bao, J. Tu, B. Shang, P. Guo, P. Yang, Q. Zhou.** Lycorine hydrochloride selectively inhibits human ovarian cancer cell proliferation and tumor neovascularization with very low toxicity. – Toxicology Letters, **218**, 2013, 174-185.
5. **Dave, D. S., J. T. Leppert, J. Rajfer.** Is the testis a chemo-privileged site? Is there a blood-testis barrier? – Rev. Urol., **9**, 2007, 28-32.
6. **Jakimov, M., Z. Mladenov, A. Konstantinov, I. Yanchev.** Transplantable myeloid tumor in hamsters (MTH) induced by Graffi virus. – Gen. Compar. Pathol., **6**, 1979, 24-35.
7. **Holstein, A.F., W. Schulze, M. Davidoff.** Understanding spermatogenesis is a prerequisite for treatment. – Reproductive Biology Endocrinology, **1**(107), 2003, 1-16.
8. **Kawashima, H., W. Sakamoto, T. Nishijima, M. Hanada, K. Mori, M. Maekawa.** Granulocytic sarcoma of the testis preceding acute myeloid leukemia. – Urol. Int., **43**, 1988, 310-312.
9. **Kusumakumari, P., S. R. Kumar, G. R. Pillai**. Unusual course of chronic myeloid leukemia. A report. – Am. J. Clin. Oncol., **17**, 1994, 19-21.
10. **Lu, L. Yi.**, **J. Y. Kuo, T. L. A. Lin, Y. H. Chang, K. K. Chen, C. C. Pan, L. S. Chang**. Metastatic Tumors Involving the Testes. – J. Urol. Roc., **11**(1), 2000, 12-16.
11. **Liu, R., Z. Cao, J. Tu, Y. Pan, B. Shang, G. Zhang, M. Bao, S. Zhang, P. Yang, Q. Zhou.** Lycorine hydrochloride inhibits metastatic melanoma cell-dominant vasculogenic mimicry. – Pigment Cell & Melanoma Research, **25**, 2012, 630-638;
12. **Maniotis, A. J., R. Folberg, A. Hess, E. A. Seftor, L.M. Gardner, J. Pe'er, J. M. Trent, P. S. Meltzer, M. J. Hendrix**. Vascular channel formation by human melanoma cells in vivo and in vitro: vasculogenic mimicry. – American Journal of Pathology, **155**, 1999, 739-752.
13. **Nair, J. J., J. Bastidab, J. van Stadena.** In vivo effects of Amaryllidaceae alkaloids. – Natural Product Communications, **11**(1), 2016, 121-132.
14. **Neiman, R. S., M. Barcos, C. Berard, H. Bonner, R. Mann, R. E. Rydell, et al.** Granulocytic sarcoma: a clinico-pathologic study of 61 biopsied cases. – Cancer, **48**, 1981, 1426-1437.
15. **Ohyashiki, J. H., K. Ohyashiki, H. Shimizu, M. Miki, N. Kimura, S. Mori, et al.** Testicular tumour as the first manifestation of B-lymphoid blastic crisis in a case of Ph-positive chronic myelogenous leukemia. – Am. J. Hematol., **29**, 1988, 164-167.
16. **Ormandzhieva, V., R. Toshkova.** Morphometrical study of the choroid plexus blood vessels in experimental hamster *graffi* tumor model. Acta morphologica et anthropologica, **22,** 2015, 31-36.
17. **Shafer, D. W., H. A. Burris, T. J. O'Rourke.** Testicular Relapse in Adult Acute Myelogenous Leukemia. – Cancer, **70**(6), 2002, 1541-1544.
18. **Toshkova, R.** Attempts for immunomodulation in hamsters with transplanted myeloid tumor, previously induced by Graffi virus. PhD Thesis, 1995, Sofia, Bulgaria, p. 168.
19. **Toshkova, R., N. Manolova, E. Gardeva, M. Ignatova, L. Yossifova, I. Rashkov, M. Alexandrov.** Antitumor activity of quaternized chitosan-based electrospun implants against Graffi myeloid tumor. – J. Intern. Pharm., **400** (1-2), 2010, 221-233.
20. **Yuceturk, C. N., B. C. Ozgur, H. Sarici, P. Borcek, O. Telli.** Testicular Involvement of Chronic Myeloid Leukemia 10 Years after the Complete Response. – J. Clin. Diagn. Res., **8**(4), 2014.
21. **Zvetkova and Toshkova.** – In: BloodMed - Slide Atlas, 2006, (http://www.bloodmed.com/home/slide.asp?id=741).

Corresponding author:
e-mail: iilieva@abv.bg

Institute of Experimental Morphology, Pathology and Anthropology with Museum
Bulgarian Anatomical Society

Acta morphologica et anthropologica, 23
Sofia ● 2016

The Use of Neuronal Networks, Cultured on Microelectrode Arrays, to Explore the Pharmacological and Neurotoxicological Effects of Different Compounds

E. Kirazov[1], L. Kirazov[1], C. Naydenov[2], V. Mitev[2]

[1]Institute of Experimental Morphology, Pathology and Anthropology with Museum, Bulgarian Academy of Sciences, 1113 Sofia, Bulgaria
[2]Department of Chemistry and Biochemistry, Medical University, Sofia, 1431 Sofia, Bulgaria

Microelectrode arrays (MEAs) have been in use over the past decade and a half to study multiple aspects of electrically excitable cells. In particular, MEAs have been applied to explore the pharmacological and toxicological effects of numerous compounds on spontaneous activity of neuronal and cardiac cell networks. The MEA system enables simultaneous extracellular recordings from multiple sites in the network in real time, increasing spatial resolution and thereby providing a robust measure of network activity.

Key words: Microelectrode arrays, amyloid-beta peptides, neuronal networks, Alzheimer's disease.

Introduction

In the mid-70s the young neurobiologists Guenter Gross and Dieter Weiss, who worked under the guidance of the renowned neuropathologist Georg Kreuzberg at the Max Planck Institute for Psychiatry in Martinsried, Munich, shared the idea of "eavesdropping" on the "conversations" between cultured neuronal cells. For this purpose, however, they lacked the appropriate spyware.

In 1979, Gross published an article [4] describing a tissue culture chamber which bottom was covered by a dense grid of microelectrodes, created by photo-etching and electroplating. He considered that such a camera can be used for simultaneous long-term recordings of the extracellular electrical activity of more than 30 individual neurons in culture. However, a number of problems had to be solved - the substrate must not be toxic to the culture, the electrodes must be well insulated, with only their tips allowed to communicate with the neurons. And he had an additional goal – to find electrodes which are completely transparent to allow light-microscopic observation of the morphological characteristics of neurons during treatment.

In the late 70s Gross left Germany and returned to the USA where he continued his work on the creation of the so-called MEA (microelectrode array – array of microelectrodes on which neuronal cells are cultured).

Methods

In 1985 Gross published an article in which he described the newly created MEA [5], with transparent electrodes from indium tin oxide on a 5 × 5 cm glass plate (chip). The bottom of the chip was isolated with a layer of polysiloxane. The isolation of the contact tips of the electrodes was removed by a single laser pulse and the tip was coated with colloidal gold to reduce impedance. The recording end of the electrode is located on the periphery of the chip where it is connected to an amplifier. On the chip there are 64 electrodes. Before seeding the MEAs are processed so as to create conditions for maximum adhesion of cells. For this purpose the central part of the MEA is flamed through a mask of stainless steel, whereby the methyl groups of the polysiloxane are oxidized to hydroxyl groups, which creates a hydrophilic surface that provides good adhesion of the cells. Polylysine and laminine stick only to the flamed area of the MEA.

Monolayer tissue cultures are grown on MEA from dissociated tissues that are prepared from certain areas of the brain or spinal cord of 14-15-day-old mouse embryos (**Fig. 1**).

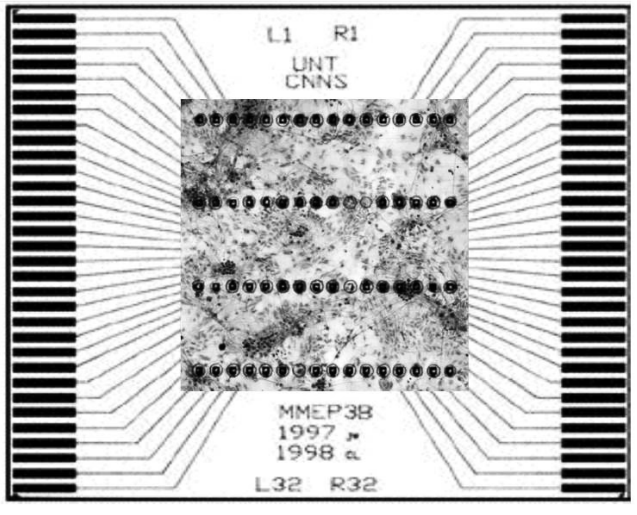

Fig. 1. Microelectrode array with neuronal network cultured on the microelectrodes

The spatiotemporal pattern of electrical activity (extracellular action potentials) provides important information regarding network structure and function that is difficult or impossible to obtain using other electrophysiological techniques. The electrical activity of the individual neurons is recorded on the tip of the electrode and is fed to its terminus at the periphery of the chip and then through an external amplifier into a computer with specialized software.

Around the end of the first week after seeding the cultures develop spontaneous electrical activity, which is stabilized about the third week in culture. Each tissue cul-

ture, which is a network of interconnected neurons, acquires characteristic electrical activity, which is considered native. This native activity is used as a basis for comparison in experimental treatments of the cultures with various agents.

Up to 4 different single neuron activities can be distinguished from the electrical activity derived from one electrode.

Action potentials (impulses), also called spikes, are integrated according to certain criteria, such as frequency, maximum and minimum interval between single spikes etc., resulting in defined groups of pulses termed bursts. These two parameters – spikes and bursts characterize the electrical activity of every culture.

Hereafter we shall call the network of neuronal cells cultured on MEA simply MEA. This experimental model proved to be very suitable for testing the toxicity of various substances as it provides information about the chemical effects leading to disruption of the function of nerve cells, which allows to reveal the mechanisms of action of a particular compound.

Results

The neurotoxin trimethyl-tin (TMT) is one of the first substances whose effect was investigated on neurons cultured on MEA, as it is known that TMT causes acute changes in the function of nerve cells, which directly affect the transmission of signals (signal transduction) between the neurons [1].

It can be seen that the cells begin to react at low concentrations (2-3 μM) and at 4 μM one signal disappears completely. Removing TMT from the culture by medium change results in recovery of the native activity (**Fig. 2**).

When the amplitude and the form of the action potential remain unchanged upon treatment with a particular agent, it can be concluded that the metabolism of the cell is not impaired, and the effect is directly on the synapse. No morphological changes in

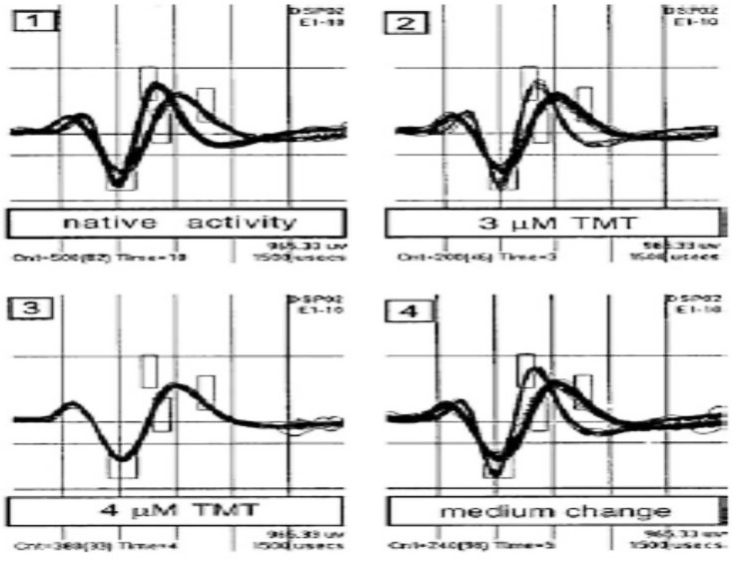

Fig. 2. Reversible inhibition of electrical activity by TMT

the cells have been observed at these concentrations. At higher concentrations (50-100 mM), there was total inhibition of electrical activity which cannot be restored with repeated medium changes. Such concentration of TMT are in the range of concentrations that are lethal to mice when administered *in vivo*. This and many other examples demonstrate the comparability of the results obtained *in vitro* with the MEA to those obtained *in vivo*.

Employing the MEA model system we investigated the effect of the amyloid β-peptides on the electrical activity of neuronal networks, cultured on MEA. The amyloid β-peptides are aberrant metabolic products of the amyloid precursor protein (APP) and are involved in the etiology of Alzheimer's disease. There are various assumptions about the mechanism of their toxicity. There are numerous publications that describe different effects of the amyloid β-peptides on neuronal cells. Some of the major ones are: inhibition of cell adhesion in cultures; inhibition of the outgrowth of neurites; disruption of calcium homeostasis; inducing oxidative stress; causing abnormal phosphorylation of the τ-protein; initiation of apoptotic mechanisms; participation in inflammatory mechanisms; effects on electrophysiological processes etc.

In our initial experiments with the peptide which is the carrier of the biological activity, consisting of the amino acid sequence of Aβ25-35 [6], we found a concentration-dependent inhibition of the electrical activity of cultured neuronal networks (**Fig. 3**).

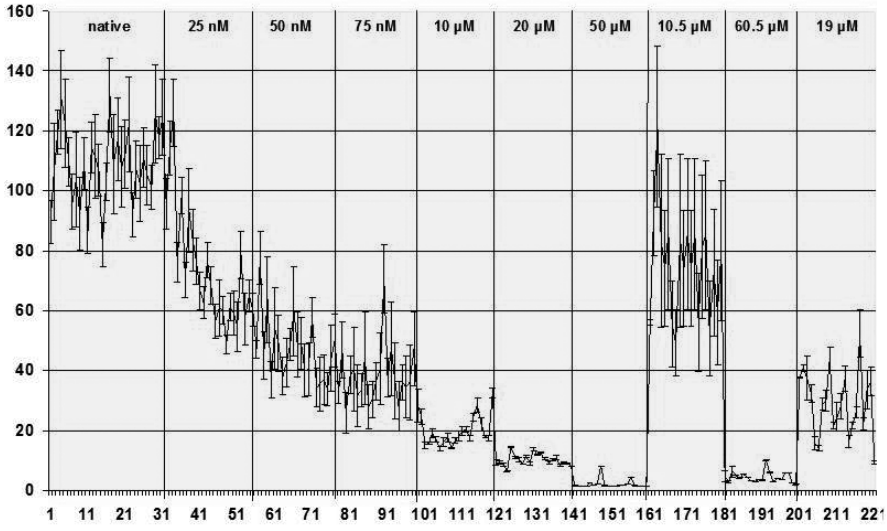

Fig. 3. Effect of Aβ25-35 on the spike rate of a spinal cord network

The effect is rapid, in the first three to five minutes after the addition of peptide, and reversible. Upon lowering of the concentration of the peptide by medium changes, the electrical activity of the neurons recovers.

Treatment with Aβ25-35 influences neither the amplitude nor the shape of action potentials, which indicates that the energy metabolism of neurons is not affected.

In summary, the effects of Aβ25-35 on the electrical activity of the neuronal networks are as follows: fast – 3-5 min after addition of the peptide; concentration-dependent; reversible; do not influence the amplitude or the shape of the action potentials; Central Nervous System region-specific.

Having established the inhibitory effect of Aβ25-35, we naturally had to think about the mechanism of action of this peptide. One of the most frequently reported effects of Aβ-peptides is the induction of oxidative stress. Therefore, we compared the effect of Aβ25-35 with that of the well-known agent causing peroxidation of membrane lipids – divalent iron ions (Fe^{2+}) [7].

We found that in comparison to the effect of the amyloid peptide, the effects of Fe^{2+} ions was slower (90 min after addition) and irreversible (**Fig. 4**). On the basis of these results we can suggest that unlike the non-specific general toxic effect of lipid peroxidation, the effect of Aβ has a specific site of action.

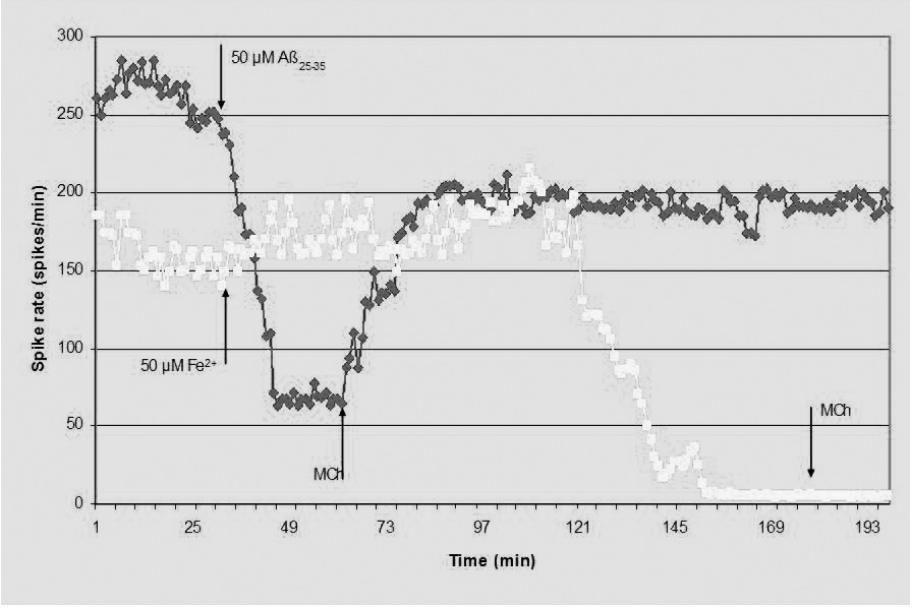

Fig. 4. Differential effects of Aβ25-35 and Fe^{2+} ions on the spike rate of cultured neuronal networks

This conclusion is supported further by additional experiments in which the effects of Aβ25-35 were compared with that of the well-known oxidants – divalent iron ions and hydrogen peroxide on the redox activity and viability of cultured neuronal cells. The effect of Aβ is always the fastest and most prominent one. It is not affected by the antioxidants vitamin E and propyl gallate, unlike the protective effect these antioxidants exhibit against the effects of the iron ions and hydrogen peroxide.

Almost identical results were obtained in studies of the effect of two Aβ-peptides with different amino acid chain length - Aβ1-40 and Aβ1-42 [8].

Starting in 2001, colleagues from the Universities in Rostock and Leipzig have taken upon themselves the laborious task of creating a database, encompassing the effects of numerous neuro-active substances, with a known mechanism of action, on neuronal networks, cultured on MEA. They record about 100 characteristics of the effects of these substances on the electrical activity of cultured neuronal networks. In this way they create a kind of pharmacological "fingerprint" of each substance. These features are introduced in the database, which is then used to compare the effects of unknown substances with those of well-known and characterized ones. This allows to get direc-

tion to search for the mechanism of action of the unknown substance and significantly shortens the period of experimental search [2, 3].

Using this approach in the database the characteristics of the effects of the investigated by us Aβ-peptides have been introduced and compared with those of neuroactive substances with known mechanisms of action [9]. The observed effects are illustrated with 5 characteristics of neuronal electrical activity:

– Burst shape: the average duration of plateaus in bursts (burst plateau);
– Synchronisation: the number of coordinated spikes within 1 ms (simplex);
– General activity in bursts: mean burst amplitude (burst amplitude);
– General spiking activity: mean spike rate (spike rate).

Employing the data analyzing tool for pattern recognition – Pattern Expert, we compared the influence of four "fingerprinted" compounds to the effects of Aβ peptides. The compounds are as follows: baclofen (a direct agonist of GABAB receptors), levetiracetam (opposes the activity of negative modulators of GABA and glycine-gated currents and partially inhibits N-type calcium currents in neuronal cells), fentanyl (a strong agonist at μ- and kappa-opiate receptors), and diazepam (a GABAA receptor agonist). The effects of the first three compounds on cultured neuronal networks are shown in **Fig. 5**.

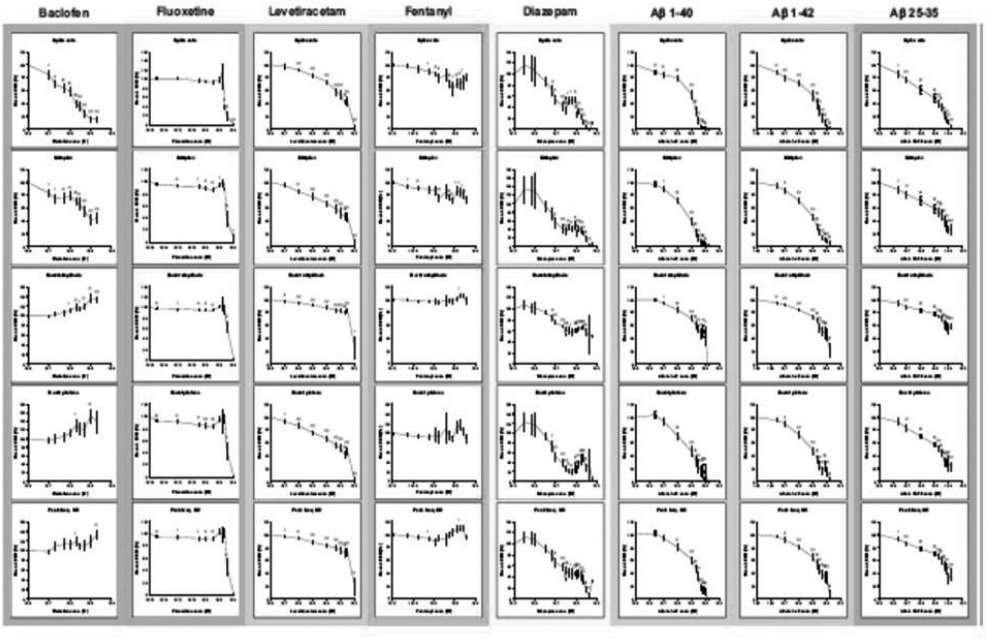

Fig. 5. Selected spike train parameters for 5 compounds and the 3 Aβ peptides

Pattern recognition and classification experiments indicate a similarity of the effects of Aβ peptides with GABAA receptor agonists such as diazepam, clonazepam and propofol (**Fig. 6**). We observe a course of cessation, which is known for example from GABAA agonists. This allows us to suggest the involvement of at least one ion-channel receptor mechanism, as it is controversially discussed in literature.

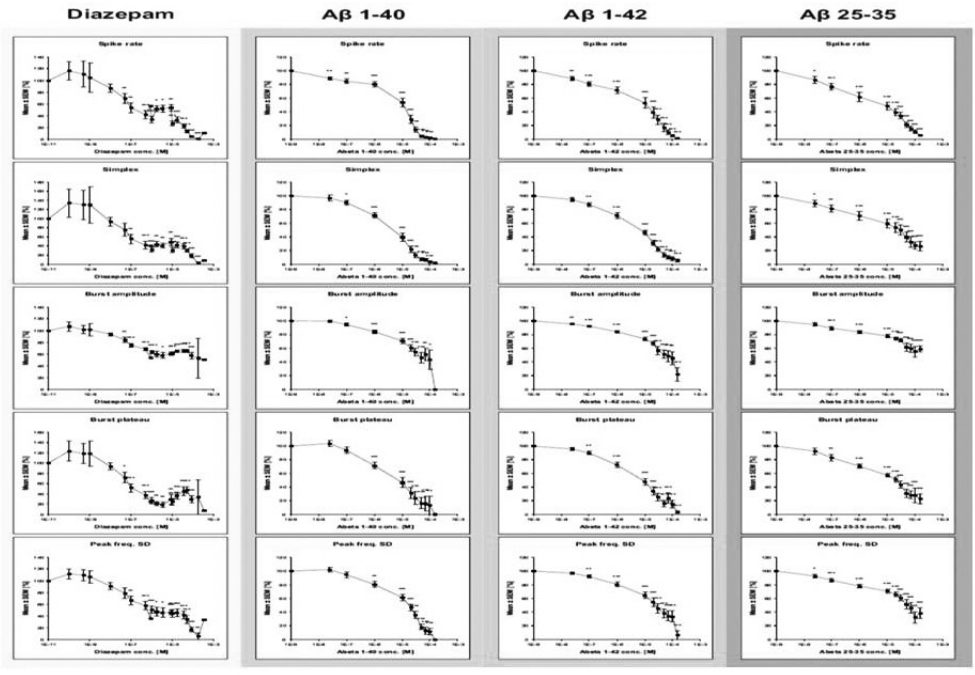

Fig. 6. Selected spike train parameters for diazepam and the 3 Aβ peptides

Discussion

These results lead us to the hypothesis that the rapid neurotoxic effect of increased amyloid beta peptide concentrations on the synaptic function could cause the early memory loss in Alzheimer's disease, preceding the synaptic loss and neuron degeneration. By hypothesis this mechanism seems to be a similar mechanism as it is described in literature for amnesia caused by benzodiazepine treatment.

At present modern MEA systems have different applications. There are numerous attempts MEA chips to be used for monitoring of toxic substances in the environment – air and water. For instance, water samples could be constantly fed to MEA chips. The presence of toxic substances in the water would change immediately the electrical activity of cells in the chip and will be reported instantly.

MEA systems offer greater flexibility in terms of biological tissue and experimental design. Electrodes of the MEA can be placed flat – for monolayer cultures, as the example discussed. A wide variety of electrically excitable biological tissues can be placed on the MEA. This includes tissue from the heart muscle, primary cultures of nervous system tissues from various regions of the central nervous system, whole tissue pieces – for example a slice of the hippocampus or the retina. MEA chips specialized for a particular tissue can be purchased from commercial suppliers.

MEAs may also have a three-dimensional structure, which allows the penetration of the electrodes through the outer layer of the damaged cells in tissue sections, thereby allowing the electrode to contact with the neighboring healthy cells. The spatial

arrangement of the electrodes can be changed, for example to place more electrodes in specific regions of the hippocampal slice or retina.

After use, the biological tissue can be removed from the MEA and can be used repeatedly. If treated carefully MEAs can be quite economical ($ 10-30 / per use).

The added value of this experimental model is significant. The approach to determining the toxicity is in the transition state from intensive *in vivo* testing the toxicity of various agents on animals, to approaches based on *in vitro* screening, which also allow the processing of large numbers of samples in a short time. The requirement for a better understanding of the potential hazards of tens of thousands of substances, currently used in everyday life, and the need to increase the number of substances whose potential toxicity is characterized, are the main driving force behind this change. In addition, the need to reduce the time, cost and number of animals used in modern test methods for toxicity also highlights the need for changes in the approach to hazard assessment.

References

1. **Gramowski A., D. Schiffmann, G. W. Gross.** Quantification of acute neurotoxic effects of trimethyltin using neuronal networks cultures on microelectrode arrays. – Neurotoxicology, **21**, 2000, 331-342.
2. **Gramowski, A., K. Juegelt, S. Stuewe, R. Schulze, G. P. McGregor, A. Wartenberg-Demand, et al.** Functional screening of traditional antidepressants with primary cortical networks grown on multielectrode neurochips. – Eur. J. Neurosci, **24**, 2006, 455-465.
3. **Gramowski, A., S. Stuewe, K. Juegelt, D. Schiffman, J. Loock, O. Schroeder, et al.** Detecting neurotoxicity through electrical activity changes of neuronal networks on multielectrode neurochips. – ALTEX, **23**, 2006, 410–415.
4. **Gross, G.W.** Simultaneous single unit recording in vitro with a photoetched laser deinsulated gold multi-microelectrode surface. – IEEEE Trans. Biomed. Eng. BME, **26**, 1979, 273-279.
5. **Gross, G.W., W. Wen, J. Lin.** Transparent indium-tin oxide patterns for extracellular, multisite recording in neuronal cultures. – J. Neurosci. Meth., **15**, 1985, 243-252.
6. **Kirazov, L., E. Kirazov, L. Venkov, E. Vassilewa, S. Stuewe, D. G. Weiss.** The amyloidogenic A-ß-peptide affects the electric activity of neuronal cells. – Compt. rend. Acad. bulg. Sci., **55**(4), 2002, 103-108.
7. **Kirazov, E., M. Inchovska, L. Kirazov, L. Venkov, E. Wasilewa, S. Stuewe, D. G. Weiss.** Differential effects of the soluble amyloidogenic $A\beta_{25-35}$ and an oxidative stress inducing agent (Fe^{2+}) on the electrical activity of cultured neuronal networks. – Compt. rend. Acad. bulg. Sci., **55**(12), 2002, 91-94.
8. **Kirazov, E., M. Inchovska, L. Kirazov, L. Venkov, E. Vassileva, S. Stuewe, D. G. Weiss.** Comparative studies on the cytotoxicity of the soluble amyloidogenic peptide fragment Aß25-35 and oxidative stress inducing agents (Fe^{2+} and H_2O_2). – Compt. rend. Acad. bulg. Sci., **57**(10), 2004, 75-80.
9. **Kirazov, E., L. Kirazov, O. Schroeder, A. Gramowski, E. Vassileva, C. Naydenov, D. G. Weiss.** Amyloid beta peptides exhibit functional neurotoxicity to cortical network cultures. – Compt. rend. Acad. bulg. Sci., **61**(7), 2008, 905-910.

Institute of Experimental Morphology, Pathology and Anthropology with Museum
Bulgarian Anatomical Society

Acta morphologica et anthropologica, 23
Sofia ● 2016

Phospholipid and Free Fatty Acid Content of Rat Brain Mitochondria Following Linseed Dietary Supplementation

E. Petrova, T. Gramatikova

Department of Experimental Morphology, Institute of Experimental Morphology, Pathology and Anthropology with Museum, Bulgarian Academy of Sciences, Bulgaria
1113 Sofia, Acad. G. Bonchev Str., Bl. 25

In this study, we report changes in the phospholipid and free fatty acid (FFA) content in rat brain mitochondria following linseed dietary supplementation. Male Wistar rats at the age of three months were fed a standard chow diet supplemented with linseed at a dose of 3 g/day for three weeks. Afterwards, the control and experimental animals were sacrificed by decapitation, the brain mitochondrial fraction was isolated and lipids were extracted. The phospholipid content was measured by thin-layer chromatography and spectrophotometrically. FFA content was measured by gas-liquid chromatography.

In the brain mitochondria of rats fed linseed, we found 9% increase of the total phospholipids. Phosphatidylserine, phosphatidylethanolamine and phosphatidylcholine were the predominant phospholipid classes and they together accounted for 88.8% of the total phospholipids. The content of the total FFA increased by 42.3% and stearic acid and arachidonic acid were the most pronounced components of the FFA pool.

Key words: phospholipids, free fatty acids, mitochondria, rat brain, dietary linseed.

Introduction

Brain maintains a unique lipid environment that is essential for normal brain function. It is well known that the membrane fluidity, transport of proteins and ions, and membrane enzyme activities are affected by the lipid membrane composition.

The relationship between the membrane lipid environment and its intrinsic enzymes is well documented in mitochondrial membranes [4]. The maintenance of the mitochondrial phospholipid composition is essential for the function and structure of mitochondria. It depends on the metabolism of phospholipids, their transport into and out of the mitochondrial membrane and the supply of lipids from the diet. Studies have demonstrated that dietary changes modify the fatty acid composition of the major mitochondrial phospholipids, thus influencing the membrane physical properties, respiration and other processes. Dietary interventions that contribute to the remodeling of phospholipids and mitochondrial membrane homeostasis are emerging as novel therapeutic

strategies against cancer, metabolic disorders, cardiovascular and neurodegenerative diseases and other pathologies [9].

Our experiment was conducted to examine the effect of feeding dietary linseed on the FFA and phospholipid content of rat brain mitochondria.

Materials and Methods

Experimental animals and dietary linseed intake

Twenty-five male Wistar rats at the age of three months were used in the experiment. Animals were divided into: one control group (n=5) and experimental one (n=20). The control group was fed a standard chow diet. The experimental group diet was supplemented with ground linseed at a dose of 3 g/day for three weeks. Afterwards, control and experimental rats were deprived of food for 24 hours, lightly anesthetized with diethyl ether and sacrificed by decapitation.

The animal experiments were performed in accordance with the animal protection guidelines approved by the Ethics Committee for Experimental Animal Use at IEMPAM, BAS.

Brain phospholipid and FFA analysis

A 10% brain homogenate was prepared in ice-cold 0.32M sucrose and the mitochondrial fraction was isolated as described by Venkov [20] using discontinuous two-step sucrose gradient. Lipids were extracted according to the method of Kates [21] using the following eluates: chloroform:methanol 1:2 (v/v) and chloroform:methanol:water 1:2:0.8 (v/v/v).

Total phospholipids were measured spectrophotometrically at 820 nm [2]. All major phospholipid classes were separated by thin-layer chromatography using eluate from chloroform:methanol:water 65:25:4 (v/v/v). Perkin-Elmer scanning spectrophotometer was used to estimate the concentration of migrated spots.

The FFA content was determined by gas-liquid chromatography. The fatty acids were converted to fatty acyl methylesters (FAME) by addition of methanol and 25% hydrochloric acid. The FAME were extracted by petroleum ether, then concentrated in a rotary vacuum evaporator and subjected to a gas-liquid chromatographic analysis. A gas chromatograph with a flame ionization detector and connected with Trio Vector computing integrator was used. The analysis was performed by injecting 5 μl of the sample into a SE-35 column. The temperature was programmed from 85 ºC to 205 ºC (2.5 ºC/min). Nitrogen was used as a carrier gas at a flow-rate of 40 ml/min.

Statistical analysis

Results are reported as mean values ± SD and statistically analyzed by Student's *t*-test.

Results and Discussion

It is known that biochemical functions of mitochondria strongly depend on membrane lipids. The membrane phospholipids are essential for the mitochondrial respiration and the inner mitochondrial membrane integrity. Besides, free fatty acids and especially polyunsaturated fatty acids (PUFA) are an important component of the brain cellular membranes, including mitochondrial membrane. PUFA are crucial in multiple aspects of the neuronal development and function [3]. They are involved in modification of

membrane fluidity, membrane-bound enzymes activity, the number and affinity of receptors, the function of membrane ion channels [16].

The majority of membrane PUFA are synthesized from linoleic acid (LA, C18:2 n-6) and α-linolenic acid (ALA, C18:3 n-3), which act as precursors for the synthesis of longer-chain PUFA through a series of elongation and desaturation reactions [18]. α-Linolenic and linoleic acids have been identified as essential fatty acids, because they cannot be synthesized de novo and they must be provided in the diet. Dietary sources of LA and ALA are vegetable oils, seeds, and some vegetables. Linseed is a rich source of PUFA, including mainly LA and ALA. The percentage contribution of both these acids is around 73%. In addition, linseed oil contains 53.3% of ALA and 12.7% of LA, yielding the highest n-3/n-6 FFA ratio amongst plant sources [10]. Linseed has a high nutritional value and it is easily accessible, which makes it a beneficial rat diet supplement.

Several studies have indicated that mitochondrial lipid composition is susceptible to dietary manipulation [9, 13]. It is reported that the changes generally reflect the fatty acid pattern present in the diet [6].

In the present study, we examined the effect of linseed dietary supplementation on the FFA and phospholipid content of rat brain mitochondria. The control FFA pool was enriched in stearic acid ($C_{18:0}$) and arachidonic acid (AA, $C_{20:4}$ n-6) (**Fig. 1**). They represented 63% and 32% of the total FFA in the mitochondria, respectively. Smaller amounts of myristic ($C_{14:0}$), myristoleic ($C_{14:1}$), palmitic ($C_{16:0}$) and arachidic ($C_{20:0}$) acids were also estimated. Among the phospholipid classes, phosphatidylserine (PS), phosphatidylethanolamine (PE) and phosphatidylcholine (PC) were the most prominent and they together accounted for 88.6% of total phospholipids in the brain mitochondria (**Fig. 2**). In fact, the mitochondrial membrane is enriched in PE, in comparison to other

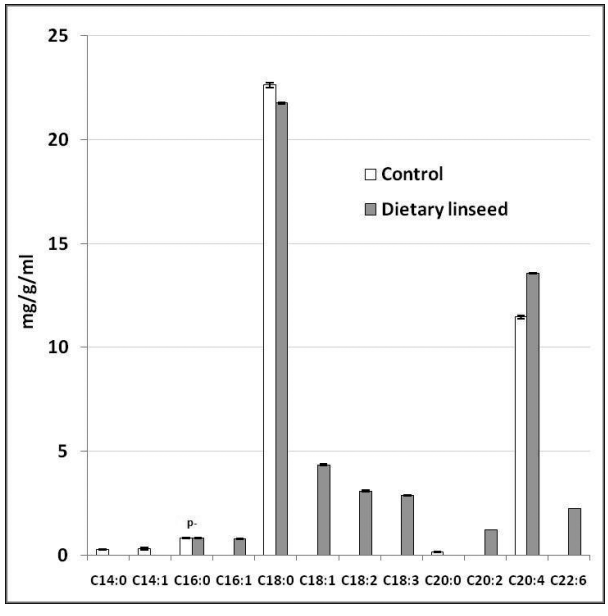

Fig. 1. Free fatty acid pool composition of the rat brain mitochondria following linseed dietary supplementation. Values are expressed in mg/g dry lipid residue/ml. $P < 0.001$

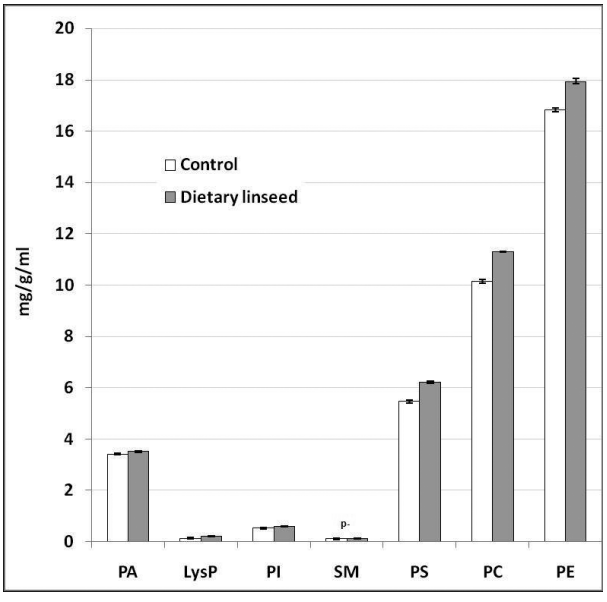

Fig. 2. Phospholipid composition of the rat brain mitochondria following linseed dietary supplementation. Values are expressed in mg/g dry lipid residue/ml. $P < 0.001$

cellular membranes. The PE is the only phospholipid that is primarily synthesized in mitochondria by the decarboxylation of PS. In contrast, the majority of phospholipids are synthesized in the endoplasmic reticulum, transported to, and imported in the mitochondria [15].

Phosphatidic acid (PA; 9.3%), lysophospholipids (LysP; 0.3%), phosphatidylinositol (PI; 1.4%) and sphingomyelin (SM; 0.3%) were also estimated in the phospholipid composition of the control animals.

Feeding linseed resulted in a significant increase in the total FFA content of brain mitochondria by 42.3% (from 35.666 ± 0.2 to 50.765 ± 0.15 mg/g dry lipid residue/ml, $p < 0.001$). The most notable effect was observed for AA, whose concentration increased by 18.5% (from 11.46 ± 0.08 to 13.578 ± 0.03 mg/g/ml, $p < 0.001$) and it comprised of 26.7% of the total FFA (**Fig. 1**). In contrast, other studies have shown that increasing dietary intake of the n-3 PUFA decreases the desaturation of LA, and thus, the production of arachidonic acid [7]. Furthermore, we found decreased content of stearic acid by 3.8% (from 22.629 ± 0.1 to 21.759 ± 0.03 mg/g/ml, $p < 0.001$), though it had the highest percentage in the FFA pool of the experimental rats. No statistically significant changes were observed in the level of palmitic acid. Besides the FFA pool size, the composition of the FFA pool was also modified by linseed supplementation. The latter was comprised of mono- and polyunsaturated FFA, some of which were absent in controls: palmitoleic acid ($C_{16:1}$ n-7) – 1.6%, oleic acid ($C_{18:1}$ n-9) – 8.6%, LA – 6.1%, ALA – 5.7%, eicosadienoic acid ($C_{20:2}$ n-6) – 2.4%, DHA – 4.5%. Other studies have also reported an increased content of ALA and long-chain PUFA following dietary linseed supplementation [1]. Our findings indicate that the FFA pattern resembles those of linseed regarding the presence of LA and ALA.

The increased PUFA content of the diet is shown to increase the metabolic rate [14]. For example, treatment of rats with n-3 PUFA is reported to decrease proton leakage from the respiratory chain and this is related to the incorporation of PUFA into mitochondrial PC, PE and cardiolipin [11]. Similarly, the presence of ALA in the diet is shown to contribute to a greater resistance to certain neurotoxic agents.

The nutritional importance of the n-3 to n-6 fatty acid ratio in the diet has aroused a great interest. It is reported that the ratio is important to avoid imbalance of membrane fluidity. Studies in animal models also demonstrate that the ratio influences various aspects of serotoninergic and catecholaminergic neurotransmission, as well as prostaglandin formation [8]. Our findings in controls indicated that the n-6 series predominated among the polyenoic acids in the mitochondrial FFA pool. Feeding linseed resulted in enhanced n-3 fatty acids synthesis, though the n-6 FFA had a prevalence (n-3/n-6=0.29). In contrast, we have previously shown a higher content of the n-3 FFA in comparison to the n-6 FFA in a whole brain homogenate [12]. Moreover, the ratio of PUFA to saturated fatty acids in the mitochondrial FFA pool increased from 0.48 to 1.02 with linseed dietary supplement.

Furthermore, we also examined the changes in the phospholipid composition of brain mitochondria. Adding linseed to rat diet led to 9% higher content of the total phospholipids (from 36.598 ± 0.05 to 39.889 ± 0.16 mg/g/ml, $p < 0.001$). All the individual phospholipid classes increased as follows: PA by 3%, LysP by 65.6%, PI by 15.8%, PS by 13.6%, PC by 11.4%, PE by 6.6% (**Fig. 2**). Their concentrations rose to 3.514 ± 0.02, 0.212 ± 0.02, 0.602 ± 0.01, 6.206 ± 0.05, 11.294 ± 0.02 and 17.938 ± 0.1 mg/g/ml, respectively. As we have established in controls, PS, PC and PE were still the predominant classes in the phospholipid composition and they together accounted for 88.8% of the total phospholipids. However, no statistically significant changes were observed in the level of sphingomyelin.

As seen from the results, the most notable increase was found for LysP, though they remained poorly presented in the phospholipid composition of the brain mitochondria following linseed intake. Lysophospholipids are intermediates in phospholipid metabolism and turnover and they are now recognized as important membrane-derived bioactive lipid mediators. Although LysP are usually found in small amounts in biological cell membranes, they have been shown to play a role in a wide range of cellular processes that involve membrane-protein or membrane-membrane interactions. The “shape” of the molecules in the membrane is among the factors that affect the mechanical properties of a bilayer. Phospholipids have an approximately cylindrical molecular shape, whereas LysP are cone shaped and promote the formation of curved (or nonbilayer) structures. It has been shown that if lysophospholipids accumulate in a membrane, they will tend to lower the membrane electrical resistance, increase the permeability, inhibit the fusion and alter the channel-gating kinetics. In the bilayer phase LysP would introduce membrane tensions that may influence the conformation and activity of membrane proteins [5].

It is known that the fatty acid composition of membrane phospholipids is affected by the exogenous fatty acids from the diet [19]. The degree of fatty acid unsaturation in membrane phospholipids determines the biophysical properties of the membrane, which in turn influences many critical membrane-associated functions. For example, a phospholipid made from a saturated fat has a different structure and is less fluid than one that incorporates an essential fatty acid [17]. Moreover, studies have reported that the changes in the phospholipid fatty acid composition depend not only on the dietary fatty acid profile, but also on the classes of phospholipids affected. It has been shown that the response to dietary fatty acids varies according to the phospholipid class. PC is found to be more susceptible to variation in dietary monounsaturated fatty acid (MUFA) content than the other phospholipid classes, whereas PE is more responsive than PC to both dietary n-6 PUFA and the n-3 PUFA [8].

Although the present study does not explore the changes in the fatty acid composition of phospholipids, the results suggest that the increased PE content may cause an increase in the unsaturation index, and thus increased fluidity.

In conclusion, alterations in the phospholipid and FFA content of the rat brain mitochondria were observed in response to linseed dietary supplementation. The results indicate the tendency to synthesize high amounts of long-chain PUFA which is associated with changes in the n-3/n-6 PUFA ratio and the ratio of unsaturated to saturated FFA. These changes suggest possible dietary modifications of the membrane biophysical characteristics.

References

1. **Barceló-Coblijn, G., L. W. Collison, C. A. Jolly, E. J. Murphy.** Dietary alpha-linolenic acid increases brain but not heart and liver docosahexaenoic acid levels. – Lipids, **40**(8), 2005, 787-798.
2. **Bartlett, G. R.** Phosphorus assay in column chromatography. – J. Biol. Chem., **234**(3), 1959, 466-468.
3. **Benatti, P., G. Peluso, R. Nicolai, M. Calvani.** Polyunsaturated fatty acids: biochemical, nutritional and epigenetic properties. – J. Am. Coll. Nutr., **23**(4), 2004, 281-302.
4. **Daum, G.** Lipids of mitochondria. – Biochim. Biophys. Acta, **822**, 1985, 1-42.
5. **Fuller, N., R. P. Rand.** The influence of lysolipids on the spontaneous curvature and bending elasticity of phospholipid membranes. – Biophys. J., **81**(1), 2001, 243-254.
6. **Haag, M.** Essential fatty acids and the brain. – Can. J. Psychiat., **48**(3), 2003, 195-203.
7. **Hochgraf, E., S. Mokady, U. Cogan.** Dietary oxidized linoleic acid modifies lipid composition of rat liver microsomes and increases their fluidity. – J. Nutr., **127**(5), 1997, 681-686.
8. **Hulbert, A. J., N. Turner, L. H. Storlien, P. L. Else.** Dietary fats and membrane function: implications for metabolism and disease. – Biol. Rev., **80**(1), 2005, 155-169.
9. **Monteiro, J. P., C. V. Pereira, A. M. Silva, E. Maciel, I. Baldeiras, F. Peixoto, M. R. Domingues, A. S. Jurado, P. J. Oliveira.** Rapeseed oil-rich diet alters hepatic mitochondrial membrane lipid composition and disrupts bioenergetics. – Arch. Toxicol., **87**(12), 2013, 2151-2163.
10. National Research Council. Composition of Feed Ingredients. Washington, DC: National Academy Press, 1993, 64-71.
11. **Pehowich, D. J.** Thyroid hormone status and membrane n-3 fatty acid content influence mitochondrial proton leak. – Biochim. Biophys. Acta – Bioenergetics, **1411**(1), 1999, 192-200.
12. **Petrova, E., A. Dishkelov, E. Vasileva, T. Gramatikova.** Effect of linseed dietary supplementation on free fatty acid and phospholipid content in rat brain. – Med. Data, **2**(3), 2010, 181-184.
13. **Stillwell, W., L. J. Jenski, F. T. Crump, W. Ehringer.** Effect of docosahexaenoic acid on mouse mitochondrial membrane properties. – Lipids, **32**(5), 1997, 497-506.
14. **Takeuchi, H., T. Matsuo, K. Tokuyama, Y. Shimomura, M. Suzuki.** Diet-Induced Thermogenesis Is Lower in Rats Fed a Lard Diet Than in Those Fed a High Oleic Acid. – J. Nutr., **125**(4), 1995, 920-925.
15. **Vance, J. E.** Compartmentalization and differential labeling of phospholipids of rat liver subcellular membranes. – Biochim. Biophys. Acta - Lipids and Lipid Metabolism, **963**(1), 1988, 10-20.
16. **Yehuda, S.** Omega-6/omega-3 ratio and brain-related functions. – In: Omega-6/omega-3 essential fatty acid ratio: the scientific evidence (Eds. A. P. Simopoulos, L. G. Cleland), World Rev. Nutr. Diet., Basel, Karger, 2003, **92**, 37-56.
17. **Yehuda, S., S. Rabinovitz, D. I. Mostofsky.** Essential fatty acids and the brain: from infancy to aging. – Neurobiol. Aging, **26**(1), 2005, 98-102.
18. **Youdim, K. A., A. Martin, J. A. Joseph.** Essential fatty acids and the brain: possible health implications. – Int. J. Dev. Neurosci., **18**(4-5), 2000, 383-399.
19. **Zhao, J., M. E. Gillam, C. G. Taylor, H. A. Weiler.** Deposition of docosahexaenoic acid (DHA) is limited in forebrain of young obese fa/fa Zucker rats fed a diet high in α-linolenic acid but devoid of DHA. – J. Nutr. Biochem., **22**(9), 2011, 835-842.
20. **Венков, Л.** Получаване на обогатени фракции на елементи, изграждащи нервната тъкан. – Съвр. пробл. невроморфол., **11**, 1983, 1-60.
21. **Кейтс, М.** Техника липидологии. Москва, Мир, 1975. 322 p.

Corresponding author:
e-mail: emiliapetrova@abv.bg

Institute of Experimental Morphology, Pathology and Anthropology with Museum
Bulgarian Anatomical Society

Acta morphologica et anthropologica, 23
Sofia ● 2016

Pathology of Experimental Poisoning Induced by Lead Shot Pellets in Mallards

P. Stamberov[1], M. Alexandrov[2], T. Todorov[1], T. Yankovska[3] and E. Taneva[1]

[1]*University of Forestry – Sofia, Faculty of Veterinary Medicine, 1797 Sofia, Bulgaria, 10 Kliment Ohridsky Blvd.*
[2]*Institute of Experimental Morphology, Pathology and Anthropology with Museum, Bulgarian Academy of Sciences, 1113 Sofia, Bulgaria, Acad. G. Bonchev Str., bl. 25*
[3]*Central Laboratory for Veterinary Sanitary Expertise and Ecology, 1528 Sofia, Bulgaria, 5 Iskarsko shose Str.*

Clinical, radiological, elemental and histopathological analyses were carried out on mallards (*Anas platyrhynchos*) dosed orally with lead shot pellets #3. The clinical signs and pathological changes of mortally poisoned ducks were proportional to the dosage of lead and the length of time the birds were exposed. It was concluded that like the field cases the lead shot poisoned mallards developed severe and fatal ailment, which could be induced even with a single lead pellet in a range of two to five weeks. An important and pathognomonic microscopic finding was the detection of acid-fast intranuclear inclusions within the epithelial cells of the proximal renal tubules of all cases and in the hepatocytes of birds with longer course of intoxication.

Key words: mallard, lead shot, lead poisoning, acid-fast intranuclear inclusions.

Introduction

Lead hunting ammunition sources have been implicated in the deaths of many avian species, best known and documented in waterfowl. All birds are susceptible to the effects of lead but their response shows distinct intraspecific and interspecific differences (2, 4, 5, 9, 11, 14). Lead poisoning is especially problematic for the mallards because their populations are frequently exposed to ingestion of lead pellets in the areas of intensive hunting. Therefore, the abundant epidemiological data in this field was used to develop regulations regarding the use of lead ammunitions in many countries around the world (1, 3, 7, 11). However, studies about the severity of the ailment induced by lead pellets in susceptible birds are insufficient; therefore, the objectives of our study were to assess the severity of the pathology in mallards orally dosed with lead pellets #3.

Materials and Methods

This study was approved by the Animal Care Commission at the Faculty of Veterinary Medicine, University of Forestry – Sofia (permition number: No 80 valid until 2018 to train students and conduct research of Veterinary Medicine) and performed according to the EU and national regulations.

Animals and study design. Sixteen clinically healthy mallards (*Anas platyrhynchos*) 9 to 12 months old were randomly divided into four groups (n = 4/ group) and housed in separate isolators. After a 7-day period of adaptation the birds in group 1 were orally dosed with 3 lead shot pellets #3 (average weight of 0.26746 g), group 2- with 2 lead pellets and group 3- with 1 lead pellet. The last four mallard (group 4) were kept untreated and used as a negative control group. All ducks were monitored daily for the occurrence of clinical signs including growth stunt and diarrhea. Body weight measurings were performed on the 0th, 7th, 14th, 21st, 28th, 35th and 42nd day after administering the pellets.

Radiology. At the beginning and at the end of the experiments each mallard, orally dosed with lead pellets, was examined by native radiography in a ventro-dorsal projection using an Innovet X-ray machine (V 125 Eickemeyer®).

Elemental analysis. Lead concentrations in the livers of all ducks were estimated by atomic absorption spectroscopy (Atomic absorption spectroscopy system "SpectrAA 800").

Histopathology. Tissue samples from the liver, spleen, kidney, heart, cerebrum and cerebellum were fixed in 10% neutral buffered formalin, embedded in paraffin, prepared in 5 to 8 μm sections and stained with hematoxylin and eosin (H&E). Double sections of kidney and liver were stained for acid-fast nuclear inclusions according to the Ziehl-Neelsen.

Results

The surviving period, severity of the clinical signs and pathologic lesions correlated to the lead concentrations in the liver and were proportional to the dosage of the lead pellets and the length of time the birds were exposed (**Table 1**).

One of the earliest symptoms to appear was the lowered food intake. Either the appetite of the affected bird decreased completely or the food consumption decreased to a level below the minimum nutritional requirements, which lead to a progressive weight loss. Passage of characteristic bright green droppings was established as early as the seventh day after the ducks were dosed with commercial #3 shot pellets. Later greenish diarrhoea and greenish staining of the vent were observed in some cases following by signs of weakness and fatigue. Ataxia, convulsions, paralysis of legs or wings, inability to fly, swim or dive and prostration were also a common clinical observations in the diseased birds.

By means of radiology, it was observed that the shot pellets were stopped in the gizzard and remained there to the end of the experiments. The final radiographs and post mortem findings showed that destruction of the shot in the gizzard was progressive and regular (**Fig. 1**)

In fatal cases, the main macroscopic findings included emaciation, decreasing of body fat, bright green staining of the vent area, mottled bile-stained liver, enlarged and distended with bile gallbladder and presence of lead pellets in the gizzard, as well.

Table 1. Initial and endpoint body weight (BW), the day of death and contents of lead in the liver of experimental mallards

Group	Sex	No of shot per treatment	Initial BW(g)	End point BW(g)	Loss of weight (%)	Day of death	Lead in the liver mg/kg
Group 1	female	3	1120	830	25.8	14	26.2
	male	3	1250	850	32	28	37.6
	male	3	1220	860	29.5	28	37.1
	male	3	1153	740	35.8	21	42.5
Group 2	male	2	1230	900	26.8	35	26.2
	female	2	1180	600	49.2	32	17.5
	male	2	1300	870	33	37	25.3
	male	2	1150	580	49.56	42	73,9
Group 3	female	1	1150	1200	2.61	*	2.5
	male	1	1140	1152		*	1.9
	male	1	1130	1075	4.86	*	8.7
	male	1	1070	525	50.93	35	28.4
Group 4	female		1130	1234		**	0.19
	male		1142	1274		Excluded alive	Not performed
	male		1115	1260		Excluded alive	Not performed
	male		1035	1232		**	0.69

* Euthanized on the 62th day of experiment
** Euthanized on the 75th day of experiment

The pronounced histopathological features were diffuse congestion of the liver, kidney, spleen, heart, cerebrum and cerebellum (**Fig. 2a, b**). Canalicular and intracellular holestasis, hepatic necrosis and hypertrophic nucleoli of the hepatocytes were commonly seen. In the cases with longer course of disease well-developed intranuclear inclusion bodies were detected in many hepatocytes. Focal tubulonephrosis and constantly occurring acid-fast intranuclear inclusion bodies within the epithelium of the proximal tubules were the most specific findings at all. Morphologically, the inclusions could

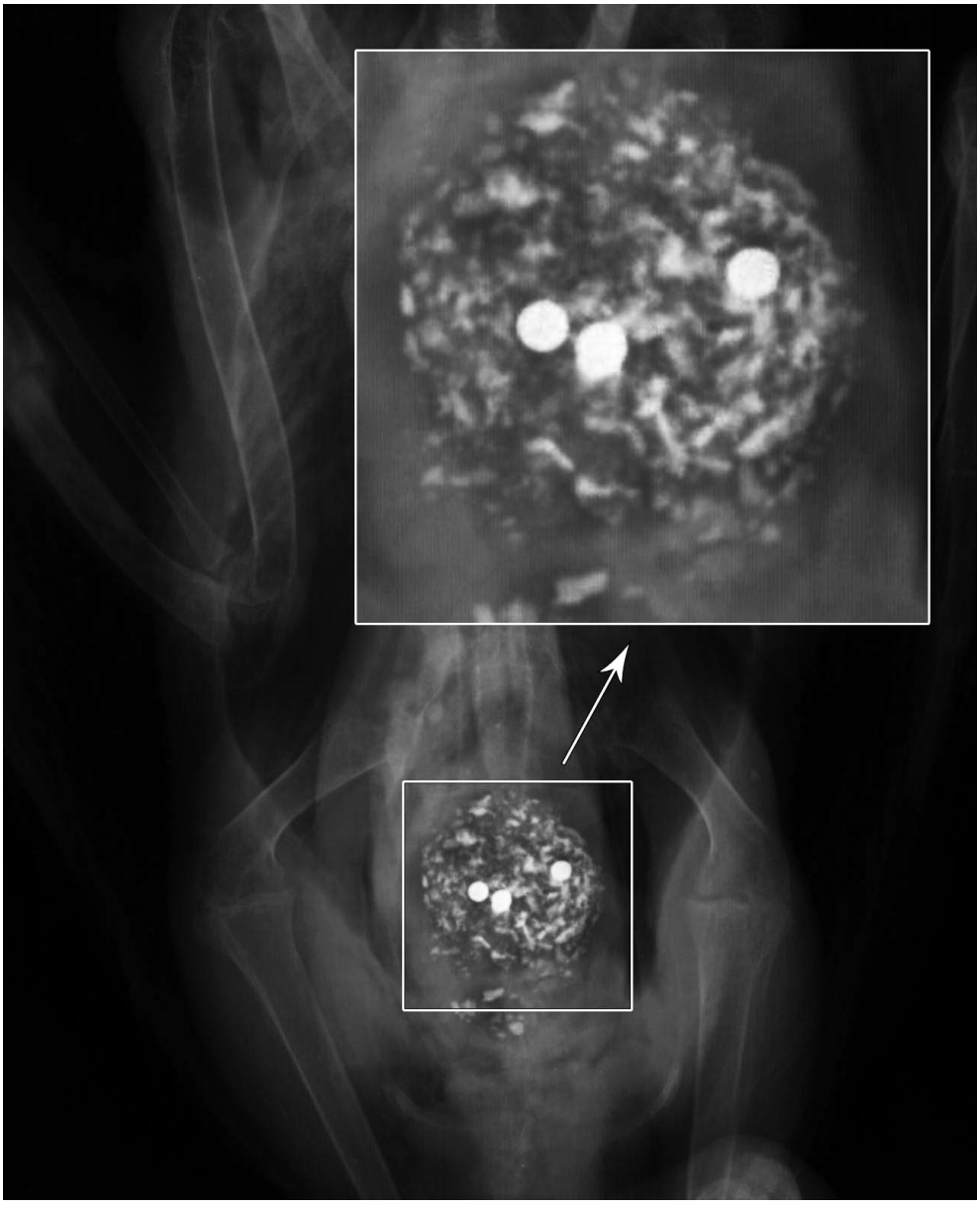

Fig. 1. X-Ray of a dead mallard on the 21st day after it had been orally dosed with three lead pellets #3. The pellets permanently remained in the gizzard decreasing in diameter and eroding asymmetrically

be divided into two types. Inclusions from the first type were observed in birds with acute course of poisoning in a range of a two or three weeks and were found within the epithelial cells of some proximal renal tubule. They were clearly acid-fast appearing as single or granulated small bodies (**Fig. 3a**). Inclusions from the second type were observed in ducks with the chronic cases. They were larger round inclusions in both

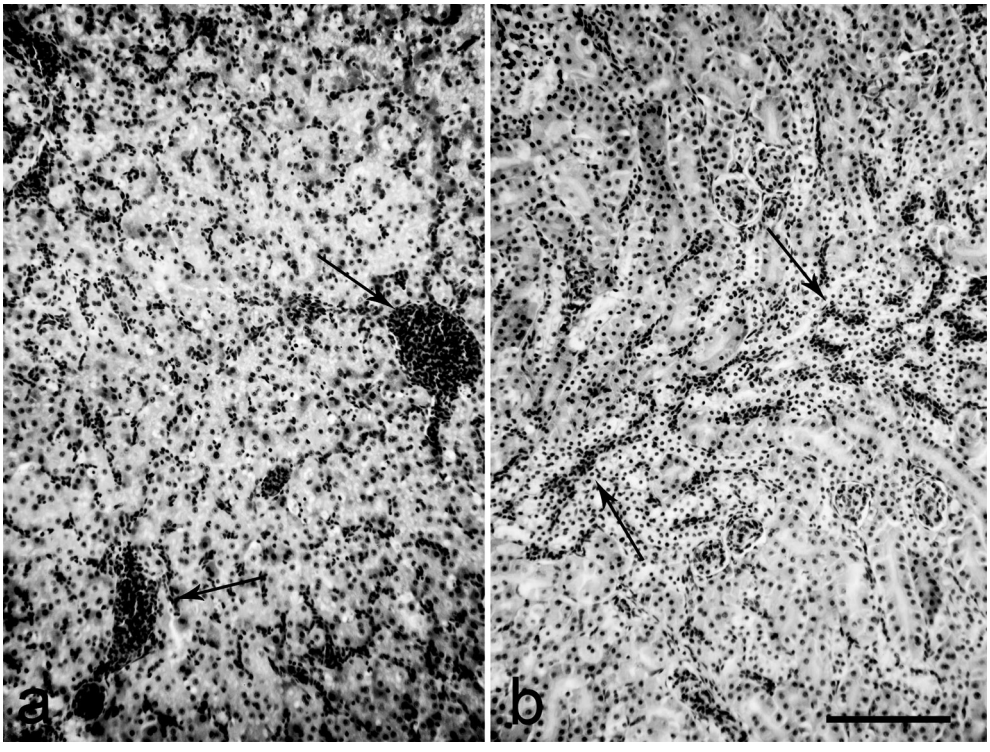

Fig. 2. Histological features of a mallard's liver (a), and kidney (b) – dead on the 28th day after it had been orally dosed with three lead pellets #3. Both organs are severely congested (arrows). Paraffin sections stained with hematoxylin-eosin (H&E). Bar = 100 μm

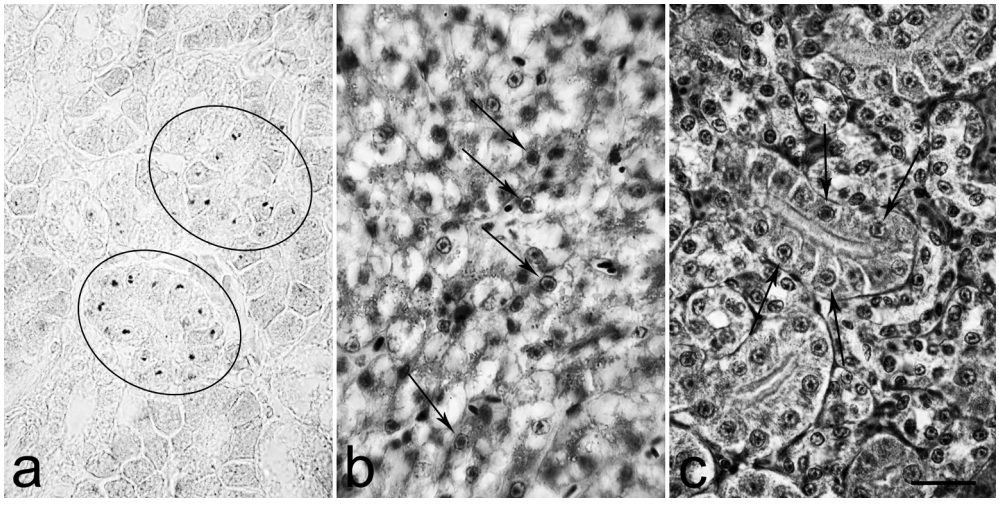

Fig. 3. Acid-fast intranuclear inclusion bodies in the mallard's renal (a and c) and liver (b) cells. Clearly distinguishable acid-fast inclusions (encircled) as single or granulated small bodies within the epithelial cells of two proximal renal tubules of a mallard, dosed with three lead pellets and died on the 28th day (a). Larger nuclear inclusion bodies (arrows) in hepatocytes (b) and renal tubular cells (c) of a mallard that had been dosed with two lead pellets and died on the 37th day. Ziehl-Neelsen stain (a), and H&E (b, c). Bar = 20 μm

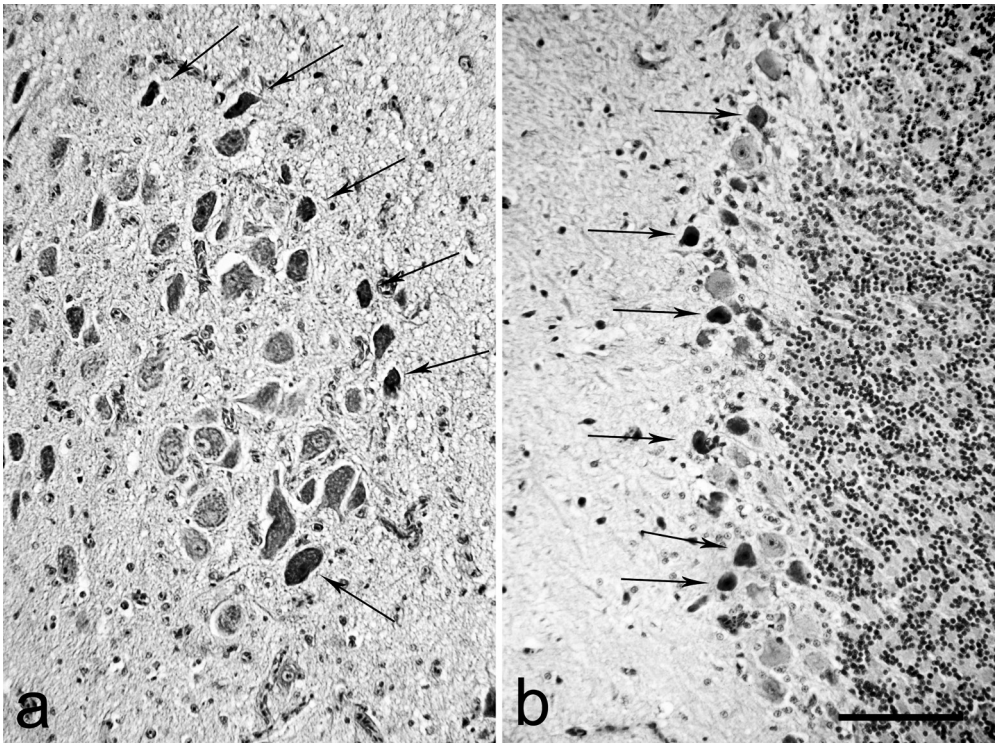

Fig. 4. Medulla oblongata at the obex level (a), and cerebellum (b) from a mallard died on the 37th day after had been dosed orally with two lead shot pellets #3. Necrotic neurons (arrows) within the dorsal vagal nucleus (a), and Purkinje cell layer (b). H&E. Bar = 100 μm

hepatocytes and renal tubular cells. These type inclusions were not strongly acid fast but were well visible in haematoxylin-eosin stained preparations (**Fig. 3b, c**). Marked distention of many blood vessels with swollen and hyperplastic endothelial cells as well as neuronal necrosis were a common findings throughout the brain (**Fig. 4a, b**). Additionally necrotic foci infiltrated with heterophil granulocytes were frequently established within the heart.

Discussion

The data of the present study clearly indicate that the ingestion of one to three lead pellets #3 in a mallard induces acute to subacute fatal ailment with clinical, radiological, toxicological and pathological features, which are in agreement with the data published by other researchers in this field (1, 6, 8, 10, 12, 13, 15). The macroscopic and microscopic findings in liver, spleen, kidneys, heart, cerebrum and cerebellum were not sufficiently different from many other metabolic or toxic changes to make a definitive diagnosis of lead poisoning and were not with significant diagnostic properties. However, the acid-fast inclusion bodies in liver and kidney cells were a constant finding and could be considered as useful diagnostic criteria as it was stated by other researchers as well (1, 6, 7, 13, 16). Therefore, the lead poisoning in this study was confirmed on the basis

of microscopic detection of nuclear acid-fast inclusions in kidney and liver cells and high lead levels estimated by atomic absorption spectroscopy in the liver. Finally, based on the present study and the data of other investigators (6, 9, 17, 18 and 19) we could conclude that the lead shot toxicosis in mallards should be treated as a fatal systemic disease where the hematopoietic system, nervous system, immune system, reproductive system, kidney, liver, bones and heart are general targets of toxic injuries.

Acknowledgements: These investigations were supported by University of Forestry, Sofia, Bulgaria.

References

1. **Bates, F. Y., D. M. Barnes, J. M. Higbee.** Lead toxicosis in mallard ducks. – Wildl. Dis., **4**(4), 1968, 116-125.
2. **Beyer, W. N., J. W. Spann, L. Sileo, J. C. Franson.** Lead poisoning in six captive avian species. – Archives of Environmental Contamination and Toxicology, **17**, 1988, 121-130.
3. **Binkowski, Ł. J., K. Sawicka-Kapusta.** Lead poisoning and its *in vivo* biomarkers in Mallard and Coot from two hunting activity areas in Poland. – Chemosphere, **127**, 2015, 101-108. (doi: 10.1016/j.chemosphere.2015.01.003).
4. **Carpenter, J. W., Oliver H. Pattee, Steven H. Fritts, Barnett A. Rattner, Stanley N. Wiemeyer, J. Andrew Royle, and Milton R. Smith.** Experimental lead poisoning in turkey vultures (*Cathartes aura*). – Journal of Wildlife Diseases, **39**(1), 2003, pp. 96-104.
5. **Chiai, K. K. Lin, M. G Oryo, T. Tsuzuki, C. Itakura.** Pathomorphologic Findings of Lead Poisoning in White-fronted Geese (*Anser albifrons*). – Vet. Path., **30**, 1993, 522-528.
6. **Clemens, E. T., L. Krook, A. L. Aronson, C. E. Stevens.** Pathogenesis of lead shot poisoning in the mallard duck. – Cornell Vet., **65**(2), 1975, 248-285.
7. **Del Bono, G., G. Braca.** Lead poisoning in domestic and wild ducks. – Avian Pathology, **2**(3), 197, 195-209.
8. **Douglas-Stroebel, E., D. J Hoffman, G. L. Brewer, L. Sileo.** Effects of lead-contaminated sediment and nutrition on mallard duckling brain growth and biochemistry. – Environ. Pollut., **131**(2), 2004, 215-222.
9. **Ferreyra, H., Pablo M. Beldomenico, Krysten Marchese, Marcelo Romano, Andrea Caselli, Ana I. Correa, Marcela Uhart.** Lead exposure affects health indices in free-ranging ducks in Argentina. – Ecotoxicology, **24**, 2015, 735–745 (doi 10.1007/s10646-015-1419-7).
10. **Finley, M. T., M. P. Dieter, L. N. Locke.** Sublethal effects of chronic lead ingestion in mallard ducks. – J. Toxicol. Environ. Health., **1**(6), 1976, 929-937.
11. **Haig, S., J. D'Elia, C. Eagles-Smith, J. Fair, J. Gervais, G. Herring, J. Rivers, J. Schulz.** The persistent problem of lead poisoning in birds from ammunition and fishing tackle. – The Condor: Ornithological Applications, **116**, 2014, 408-428. (doi: 10.1650/CONDOR-14-36.1).
12. **Hoffman, D. J., G. H. Heinz, L. Sileo, D. J. Audet, J. K. Campbell, L. J. LeCaptain.** Developmental toxicity of lead-contaminated sediment to mallard ducklings. – Arch. Environ. Contam. Toxicol., **39**, 2000, 221-232. (doi: 10.1007/s002440010099).
13. **Locke, L., G. Bagley, H. Irby.** Acid-fast intranuclear inclusion bodies in the kidneys of mallards fed lead shot. – Bull. Wildlife Disease Assoc., **2**, 1966, 127-131.
14. **Pattee, O. H., S. N. Wiemeyer, B. M. Mulhern, L. Sileo, J. W. Carpenter.** Experimental leadshot poisoning in bald eagles. – Journal of Wildlife Management, **45**, 1981, 806-810.
15. **Plouzeau, E., O. Guillard, A. Pineau, P. Billiald, P. Berny.** Will leaded young mallards take wing? Effects of a single lead shot ingestion on growth of juvenile game-farm Mallard ducks Anas platyrhynchos. – Sci. Total Environ., **409**(12), 2011, 2379-2383. (doi: 10.1016/j.scitotenv.2011.03.012).
16. **Richter, G., Y. Kress, C. Cornwall.** Another look at lead inclusion bodies. – Am. J. Pathol., **53**(2), 1968, 189-217.
17. **Rocke, T. E., M. D. Samuel.** Effects of lead shot ingestion on selected cells of the mallard immune system. – J. Wildl. Dis., **27**(1), 1991, 1-9.

18. **Romero, D., A. Hernández-García, C.A. Tagliati, E. Martínez-López, A.J. García-Fernández.** Cadmium- and lead-induced apoptosis in mallard erythrocytes (Anas platyrhynchos). – Ecotoxicol. Environ. Saf., **72**(1), 2009, 37-44. (doi: 10.1016/j.ecoenv.2008.05.004).
19. **Vallverdú-Coll, N., A. López-Antia, M. Martinez-Haro, M. E. Ortiz-Santaliestra, R. Mateo.** Altered immune response in mallard ducklings exposed to lead through maternal transfer in the wild. – Environ Pollut., **205**, 2015, 350-356. (doi: 10.1016/j.envpol.2015.06.014).

Institute of Experimental Morphology, Pathology and Anthropology with Museum
Bulgarian Anatomical Society

Acta morphologica et anthropologica, 23
Sofia ● 2016

Petri Nets Representation and Analysis of the Synthesis of Dolichol-Linked Precursor of N-Glycans

J. Stoyloff

Institute of Experimental Morphology, Pathology and Anthropology with Museum,
Acad. G. Bonchev Str., bl.25, 1113 Sofia, Bulgaria

Synthesis of dolichol-linked precursor of N-glycans is a complex biological system with numerous interdependent processes. Modeling this process is indispensable if we want to analyze this system for potential problems. We used Petri nets mathematical formalism to construct the synthesis of dolichol-linked precursor of N-glycans. Our analysis show that Dol-P is a critical point, but reduced levels of this substrate can be compensated by the oxidative pathway involving dolichol [9], from Dol pool by phosphorylation (EC 2.7.1.108) or PP-Dol pool by dephosphorylation (EC 3.6.1.4). Reactions of dolichol pathway can be controlled at least at three places by availability of substrates Man-GDP [6], Man (β) – P – Dol [5] and Glc(β) – P – Dol. Reduced levels of proteins with consensus Asn-X-Ser or Asn-X-Thr sites, through lack of essential amino acids, can also be a bottleneck in the synthesis.

Key words: petri net, glycosylation.

Introduction

The process of N-linked glycosylation starts with the formation of dolichol-linked sugar precursor [3]. Sugar molecules are attached to the dolichol through a pyrophosphate linkage and extended through the addition of various sugar molecules to form a precursor oligosaccharide. The assembly of this precursor oligosaccharide occurs in two stages: first stage, which takes place on the cytoplasmic side of the ER, and second stage, which takes place on the luminal side of the ER [2]. Steps involved in stage 1 include addition of two UDP-GlcNAc residues to the dolichol molecule followed by addition of five GDP-Man residues. After stage 1 the lipid-linked glycan is translocated across the membrane into the ER lumen. On the luminal side of the ER membrane 4 mannose and 3 glucose monosaccharides are added. The final product is dolichol - GlcNAc2 - Man9-Glc3. Once the precursor oligosaccharide is formed, the completed glycan is transferred to the newly formed polypeptides in the lumen of the ER membrane [10]. For protein glycosylation completed glycan is attached to asparagine located in a specific consensus sequence in the primary structure (Asn-X-Ser or Asn-X-Thr) [1]. Oligosaccharyltransferase is responsible for the recognition of the consensus sequence and the transfer of the precursor glycan to a polypeptide acceptor.

Materials and Methods

The main source of pathway information was N-Glycan biosynthesis pathway represented in KEGG/ENZYME database. Bipartite Petri graphs $G = (V_1, V_2; E)$ were constructed from two disjoint sets of nodes, called places ($V = P$) and transitions ($V = T$), $V_1 \cup V_2 = V$, which are connected by edges $e \in E \subseteq V$. The input range $I(x)$ of an element $x \in P \cup T$ of a Petri net is given by $I(x) = \{y|(y, x) \in E\}$, the output range as $O(x) = \{y|(x, y) \in E\}$ – [7] and [8].

Results

Dolichol is converted to dolichyl phosphate (Dol-P) by CTP:dolichol *O*-phosphotransferase (EC 2.7.1.108) as shown in **Fig. 1**. The next step is synthesis of *N,N*'-diacetylchitobiosyl-diphosphodolichol catalysed by *N*-acetylglucosaminyldiphosphodolichol *N*-acetylglucosaminyltransferase (EC 2.4.1.141). chitobiosyldiphosphodolichol β-mannosyltransferase (EC 2.4.1.142) catalyse synthesis of β-(1->4)-D - mannosylchitobiosyldiphosphodolichol. D-Man-α-(1->3)-D-Man-β-(1->4)-D-GlcNAc-β-(1->4)-D-GlcNAc-diphosphodolichol is obtained from GDP-D-mannose and D-Man-β-(1->4)-D-GlcNAc-β-(1->4)-D-GlcNAc-diphosphodolichol by EC 2.4.1.132. Next in the chain of synthesis is D-Man-α-(1->3)-[D-Man-α-(1->6)]-D-Man-β-(1->4)-D-GlcNAc-β-(1->4)-D-GlcNAc-diphosphodolichol, which is product of GDP-Man:Man2GlcNAc2-*PP*-dolichol α-1,6-mannosyltransferase (EC 2.4.1.257). Finally D-Man-α-(1->2)-D-Man-α-(1->2)-D-Man-α-(1->3)-[D-Man-α-(1->6)]-D-Man-β-(1->4)-D-GlcNAc-β-(1->4)-D-GlcNAc-diphosphodolichol is synthesised from 2 GDP-D-mannose and D-Man--α-(1->3)-[D-Man-α-(1->6)]-D-Man-β-(1->4)-D-GlcNAc-β-(1->4)-D-GlcNAc-diphosphodolichol by sucrose synthase (EC 2.4.1.13).

The next eight reactions of synthesys of dolichol-linked precursor are catalyzed by following enzymes: dolichyl-*P*-Man:Man5GlcNAc2-*PP*-dolichol α-1,3-mannosyltransferase (E.C. 2.4.1.258), dolichyl-*P*-Man:Man6GlcNAc2-*PP*-dolichol α-1,2-mannosyltransferase (E.C. 2.1.4.259), dolichyl-*P*-Man:Man7GlcNAc2-*PP*-dolichol α-1,6-mannosyltransferase (E.C. 2.4.1.260) and dolichyl-*P*-Man:Man8GlcNAc2-*PP*-dolichol α-1,2-mannosyltransferase (E.C. 2.4.1.261), which add dolichyl β-D-mannosyl phosphate to various intermediate products.

In the next three reactions dolichyl-*P*-Glc:Man9GlcNAc2-*PP*-dolichol α-1,3-glucosyltransferase (E.C. 2.4.1.267), dolichyl-*P*-Glc:Glc1Man9GlcNAc2-*PP*-dolichol α-1,3-glucosyltransferase (E.C. 2.4.1.265) and dolichyl-*P*-Glc:Glc2Man9GlcNAc2-*PP*-dolichol α-1,2-glucosyltransferase (E.C. 2.4.1.256) add dolichyl β-D-glucosyl phosphate to obtain the dolichol-linked precursor of glycosylation. This precursor is transferred to protein L-asparagine with the help of dolichyl-diphosphooligosaccharide:protein-L-asparagine oligopolysaccharidotransferase (E.C. 2.4.1.119) to obtain glycoprotein with an oligosaccharide chain attached by *N*-glycosyl linkage to protein L-asparagine.

Discussion

Analysis of **Fig. 1** shows that Dol-P is a critical point of synthesis of dolichol-linked precursor of N-glycans. Reduced levels of dolichol and its derivative Dol-P affect N-glycosylation of proteins and results in a congenital disorders of glycosylation type I (CDG I)[4]. SRD5A3 is required for converting polyprenol to dolichol and is mutated

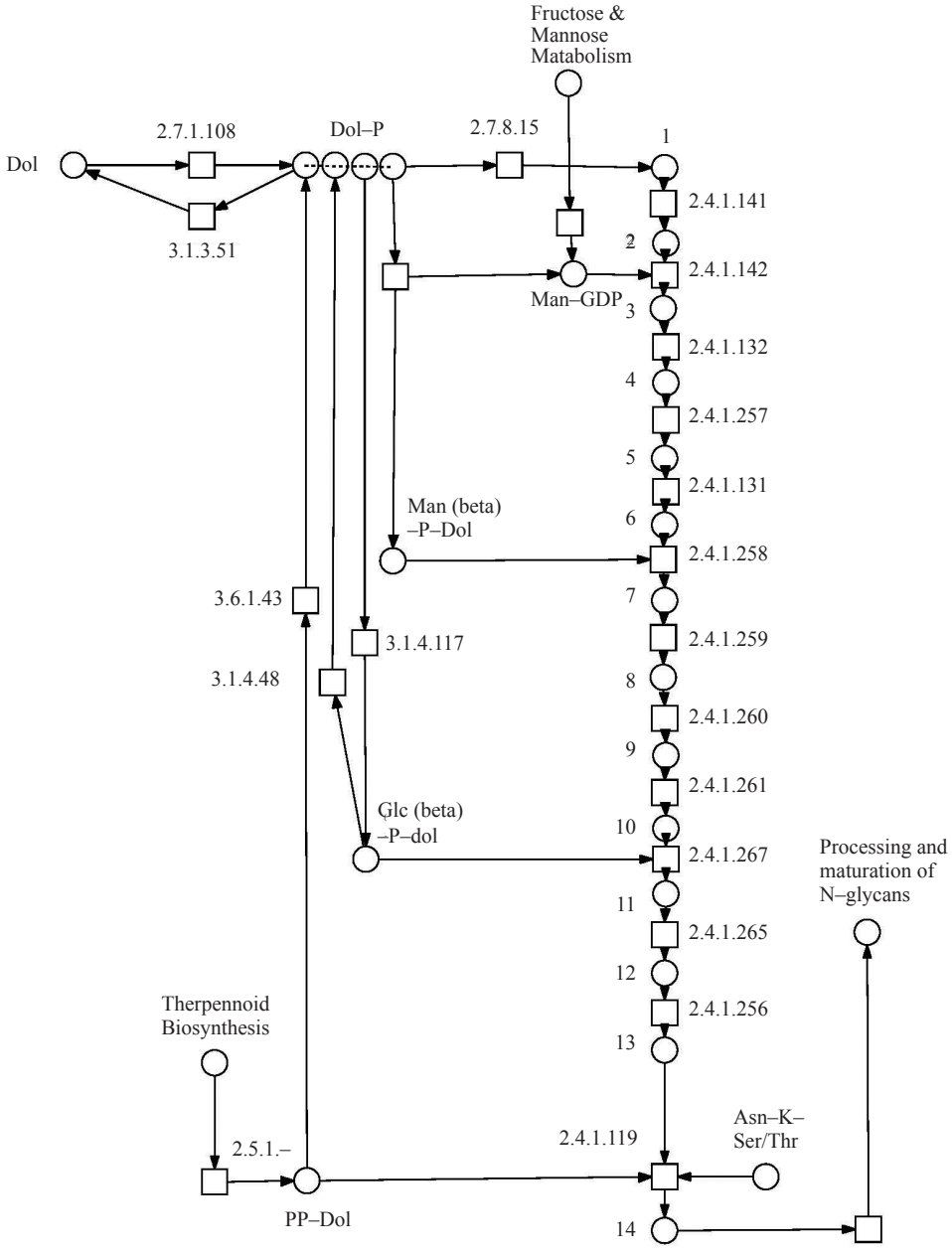

Fig. 1. Petri Net presentation of synthesis of dolichol-linked precursor of N-glycans

Legend: *circles represent metabolites and squares represent transitions according to accepted convention. Enzymes are represented according to their number in IUBMB Enzyme Nomenclature.*

in a congenital glycosylation disorder [7]. An alternative pathway for dolichol synthesis must be present, to avoid such disorders. For example, the oxidative pathway involving dolichol could play such a role [9]. Dol-P is precursor for *N*-acetyl-D-glucosaminyl-di-

phosphodolichol, Man (beta)-P-Dol and Glc(beta)-P-Dol. Dol-P can also be consumed by dolichyl-phosphate phosphohydrolase.

Dol-P is replenished from Dol pool by phosphorylation (EC 2.7.1.108) or PP-Dol pool by dephosphorylation (EC 3.6.1.4). PP-Dol comes either from therpenoid biosynthesis or as byproduct after transfer of dolichyldiphosphooligosaccharide to protein L-asparagine. Another source of Dol-P may be Gcl(beta)-P-Dol through the action of dolichyl-β-D-glucosyl-phosphate dolichylphosphohydrolase (EC 3.1.4.48).

These series of reactions can be controlled at least at three places by availability of substrates Man-GDP [6], Man (β) – P – Dol [5] and Glc(β) – P – Dol. Man-GDP is substrate for 2.4.1.142 and lack or low quantities of this substrate can block or impede all subsequent 10 enzymatic reactions and lead to different disorders.

References

1. **Apweiler, R., H. Hermjakob, N. Sharon.** On the frequency of protein glycosylation, as deduced from analysis of the SWISS-PROT database. – BBA – General Subjects, **1473**(1),1999, 4-8.
2. **Berg, J. M., J. L. Tymoczko, L. Stryer.** Carbohydrates Can Be Attached to Proteins to Form Glycoproteins. – In: Biochemistry (5th Edition), New York, W. H. Freeman, 2002, Section 11.3.
3. **Bieberich, E.** Synthesis, processing, and function of N-glycans in N-glycoproteins. – Adv. Neurobiol., **9**, 2014, 47-70.
4. **Cantagrel, V., D. J. Lefeber, Z. Guan, J. L. Silhavy, S. L. Bielas, L. Lehle.** SRD5A3 is required for converting polyprenol to dolichol and is mutated in a congenital glycosylation disorder. – Cell, **142**(2), 2010, 203-217.
5. **Dirk, J., L. Lefeber, J. Schönberger, E. Morava, M. Guillard, K. M. Huyben.** Deficiency of Dol-P-Man synthase subunit DPM3 bridges the congenital disorders of glycosylation with the dystroglycanopathies. – Am. J. Hum. Genet., **85**(1), 2009, 76-86.
6. **Janik, A., M. Sosnowska, J. Kruszewska, H. Krotkiewski, L. Lehle, G. Palamarczyk.** Overexpression of GDP-mannose pyrophosphorylase in Saccharomyces cerevisiae corrects defects in dolichol-linked saccharide formation and protein glycosylation. – BBA – General Subjects, **1621**(1), 2003, 22-30.
7. **Lefeber, D. J., A. P. de Brouwer, E. Morava, M. Riemersma, J. H. M. Schuurs-Hoeijmakers, B. Absmanner, K. Verrijp, W. M. R. van den Akker, K. Huijben, G. Steenbergen, J. van Reeuwijk, A. Jozwiak, N. Zucker, A. Lorber, M. Lammens, C. Knopf, H. van Bokhoven, S. Grünewald, L. Lehle, L. Kapusta, H. Mandel, R. A. Wevers.** Autosomal recessive dilated cardiomyopathy due to DOLK mutations results from abnormal dystroglycan O-mannosylation. – PLoS Genet., **7**(12), 2011, e1002427.
8. **Murata, T.** Petri Nets: properties, analysis and applications. – Proc. IEEE, **77**, 1989, 541-80.
9. **Nagasaki, M., A. Doi, H. Matsuno.** A versatile Petri net based architecture for modeling and simulation of complex biological processes. – Genome Inform., **15**, 2004, 180-197.
10. **Sagami, H, Y. Igarashi, S. Tateyama, K. Ogura, J. Roos, W. J. Lennarz.** Enzymatic formation of dehydrodolichal and dolichal, new products related to yeast dolichol biosynthesis. – J. Biol. Chem., **271**(16), 1996, 9560-9566.
11. **Shwarz, F., M. Aebi.** Mechanisms and principles of N-linked protein glycosylation. – Curr. Opinion in Struct. Biol., **21**, 2011, 576-582.

Institute of Experimental Morphology, Pathology and Anthropology with Museum
Bulgarian Anatomical Society

Acta morphologica et anthropologica, 23
Sofia ● 2016

Comparative Study of Several Cases of Human Breast Cancer and Mammary Cancer in Domestic Dogs and Cats

K. Todorova[1], P. Dimitrov[1], R. Milcheva[1], S. Roga[2] and R. Russev[1]

[1]*Institute of Experimental Morphology, Pathology and Anthropology with Museum, Bulgarian Academy of Sciences, 1113 Sofia, Bulgaria*
[2]*Riga Hospital No 1, Department of Pathology, Riga, Riga Stradins University, Department of Study, LV-1007, Latvia*

A useful model for studying tumor systems, which is close to the human analogue, is very necessary for development of modern approaches and methods in cancer researches. As breast cancer is the second leading cause of cancer deaths in women, spontaneous mammary tumors in domestic animals are feasible solution for valid tumor systems model. In this study we present histological diagnosis and grading of human, canine and feline mammary tumors and evaluate their histological and biological behavior. Histological diagnosis of animal tissue samples found five cases of ductal carcinoma (n=5, 62.5%), one lobular carcinoma, one squamous cell carcinoma and one case of metaplastic carcinoma with osteosarcomatous differentiation, graded from I to III: I (n=1, 12.5%), II (n=4, 50%) and III (n=3, 37.5%). Four of the human cases were diagnosed as invasive ductal (n=2, 40%) and lobular (n=2, 40%) carcinoma, one case - metaplastic carcinoma, all scored as grade III.

Key words: mammary cancer in dogs and cats, breast cancer, histological grading.

Introduction

The most common breast malignant tumors in women are epithelial ductal and lobular cancer. They invade the nearby tissues or spread on distant organs of the body. Staging of the cancer is crucial for successful treatment and most often the TNM classification is used. It is based on the primary tumor size (T) and whether it has invaded nearby tissue, if the tumor has reached regional lymph nodes (N), and its distant metastases (M) [21].

The breast cancer is the second leading cause of cancer deaths in women in Europe and the United States [8], and a useful model for studying tumor systems which is close to the human analogue is very necessary.

Like in humans, spontaneous canine and feline malignant mammary tumors represent a heterogeneous group. The prevalence of mammary tumors in dogs is about three times more often than in human females [9]. They are the second most common tumors in dogs and the third most common malignant disease in cats [3, 22].

Histological diagnosis and grading of tumors are crucial for treatment and prognosis of neoplastic diseases and are accepted in the standard clinical practice. In women, the noninvasive proliferative breast lesions such as ductal and atypical ductal hyperpla-

sia, and ductal carcinoma *in situ*, found during regular medical checks, are recognized as risk preconditions preceding the invasive cancer development and they predetermine the subsequent management decisions [1, 18, 20]. In domestic dogs and cats, however, the tumor progress is seen only when growth of the formation is obvious. In middle-aged dogs and cats malignant mammary tumors with histological and biological behavior similar to human carcinomas occur spontaneously. Because the lifespan of animals is shorter, they can be used for a histological model of malignant mammary tumors for studies on the morphology, development and metastatic pattern, mainly at regional lymph nodes, lungs and liver, as it is done in humans.

In order to predict individual prognosis and respond to therapy in early stages of breast cancer and its hormonal dependence, immunohistochemical studies of markers of proliferation, hormone receptors and specific tumor markers are used, which revealed similarities in tumor development in humans, and in dogs and cats [2, 4, 5, 6, 7, 13, 14].

In this study, we evaluated a series of operable canine, feline and human mammary carcinomas, and compared their suitability for a routine assessment of histological diagnosis and grading with prognostic value of further development of this particular subset of carcinomas.

Materials and Methods

Patients. Tissue samples from altered mammary glands of seven dogs and one cat, at the age between 7 and 16 years and incomplete data about their reproductive status, were compared with breast tissue excisions from five middle-aged women, diagnosed with breast cancer. The animals were not castrated before the surgical operation and some of them were sporadically treated with steroidal progestins. The animal tumor formations ranged between 0.5 and 15.6 cm in diameter and were collected mainly from the caudal mammary glands. The human tissue formations ranged between 6 and 9 cm in diameter and were accompanied by metastases in the adjacent lymph nodes.

Light microscopy. Tissue samples from surgically removed tumors of mammary glands were routinely fixed in 10% buffered formalin, dehydrated in graded ethanol, and embedded in paraffin. Tissue sections, 3-5 μm thick, were stained in H&E and examined by light microscope (Leica DM 5000B, Wetzlar, Germany). Nottingham Histologic Score system (the Elston-Ellis grading system) [7] was used to evaluate the results.

Results

Histopathological diagnosis of animal tissue samples estimated seven cases of simple or complex carcinoma (n=7, 87.5%) and one carcinosarcoma subtype (n=1, 12.5%). Histological evaluation found five cases of ductal carcinoma (n=5, 62.5%) (**Fig. 1a**), one lobular carcinoma (**Fig. 2a**), one squamous cell carcinoma and one case of metaplastic carcinoma with osteosarcomatous differentiation. All duct carcinomas originated in the epithelial cells of ducts, while lobular carcinomas arose in alveoli and developed into progressively larger lobules. Invasion was observed in four cases (n=4, 50%), necrosis in one (n=1, 12.5%). According to the Nottingham Histologic Score system tumors were classified as stage of anaplasia: grade I (n=1, 12.5%), grade II (n=4, 50%) and grade III (n=3, 37.5%). One of the excisions was taken *post mortem*, with anamnesis of prolonged suffering of mammary tumors. Pathomorphological studies revealed ductal carcinoma grade III and changes that had taken place in the internal organs of an old animal, accompanied with disseminated metastases in the associated lymph nodes,

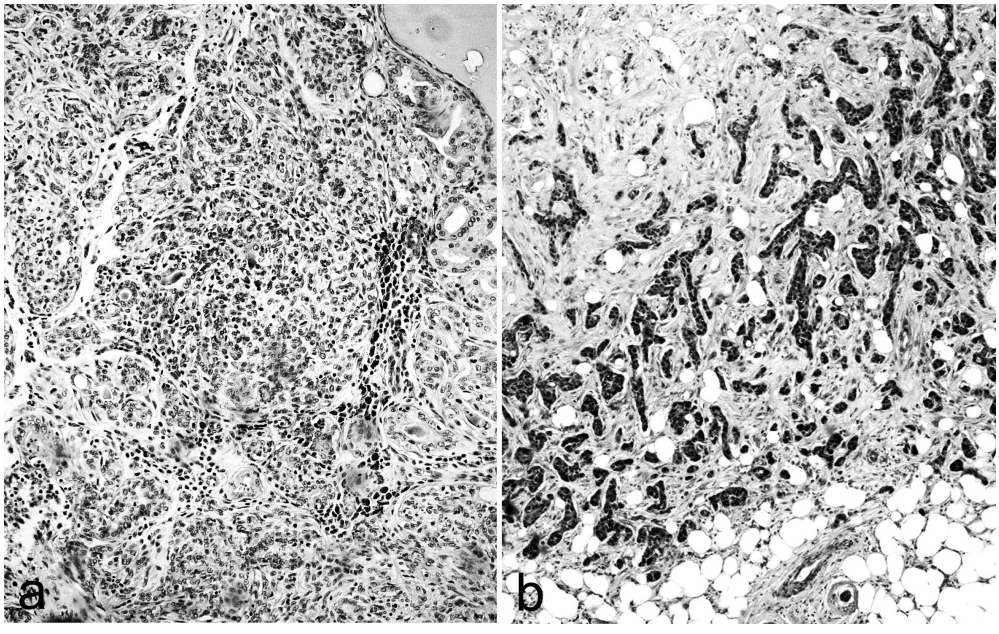

Fig. 1. Invasive ductal carcinoma, stage of anaplasia grade III - poorly differentiated pleomorphic epithelial cells, high mitotic counts and prominent nucleoli: in female dog (a) H&E, 10×; and in human female (b), H&E, 10×

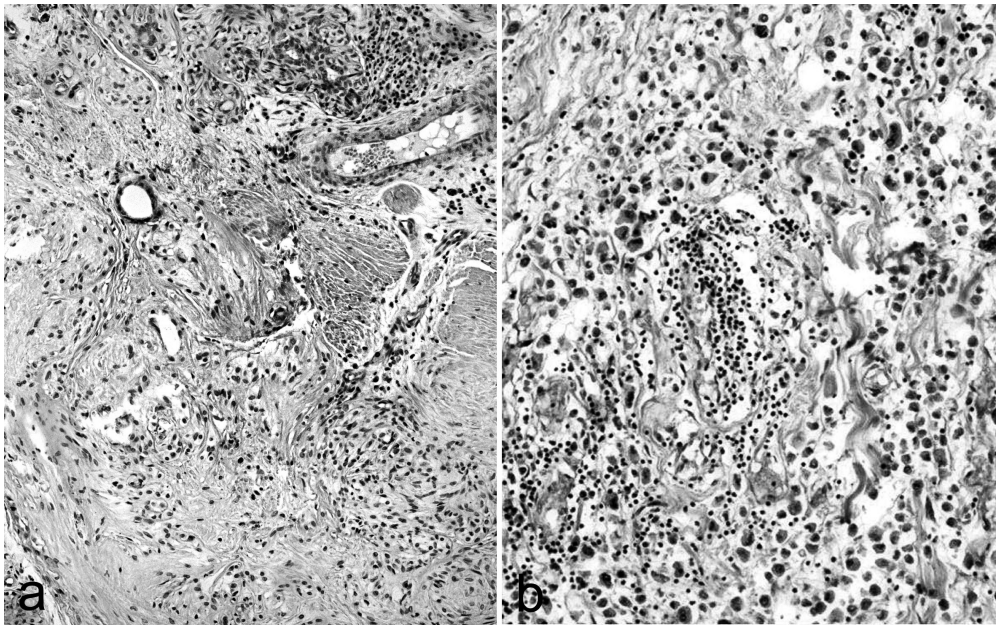

Fig. 2. Invasive lobular carcinoma: in female dog, stage of anaplasia grade II - arranged in cords epithelial cells (a) H&E, 10×; in human female, stage of anaplasia grade III poorly differentiated epithelial cells with considerable nuclear and cellular pleomorphism and prominent nucleoli (b), H&E, 20×

lungs and liver, mainly causing the lethal end. During the one year follow-up period of observation of all cases, one more animal had died, diagnosed with invasive ductal carcinoma grade III, where disseminated metastases in nearby lymph nodes, lungs and liver resulted in a lethal end. Four of the human cases were pathomorphologically diagnosed as invasive ductal (n=2, 40%) (**Fig. 1b**), and lobular (n=2, 40%) (**Fig. 2b**), carcinoma. One case of metaplastic carcinoma was recognized. All five cases were scored as grade III. All women were undergoing chemotherapy.

Discussion

Variety of etiological factors can result in severe abnormalities in the processes of cell proliferation and differentiation, consequently leading to non-cancerous (benign), precancerous or cancerous (malignant) conditions. Domestic dogs and cats share almost the same living conditions as their owners, and usually use industrially made food and cosmetics containing the same carcinogenic chemicals as for the humans. In animals compared to humans, the role of stress factors in tumor development is less possible. In both humans and animals, among the most often causes for cancer development is the probable involvement of imbalances due to mutations in tumor suppressor genes such as: BRCA1, BRCA2, p53 and endocrine dysfunctions. The canine BRCA1 gene that has 84% homology with its human analog is very likely to play a role in malignancy as it is in humans, even though its role in mammary cancer in dogs has not been determined clearly yet [16]. The BRCA1-related protein TopBP1 is expressed at a higher percentage also in feline mammary malignant neoplasms [12]. Like in humans, in dogs and cats oophorectomy in early age significantly reduces tumor development frequency [15] showing connection with hormonal status in these species.

In this study we used the grading of canine mammary gland tumors which follows as much as possible on the classification of human breast tumors and dysplasias, approved by the World Health Organization [17]. As it was shown from our histological examinations, the neoplastic mammary parenchyma in mastectomy specimens from the operated pets was histologically similar to that of human breast tissue. Most often simple epithelial carcinomas and rarely complex carcinomas were identified. Carcinosarcomas were relatively rare and no sarcomas were found in our survey, as reported by other authors [10, 11]. The malignant neoplasia in the examined animals was expressed by abnormal growth of the mammary tissues and impairment of gland functions. Metastases were found on the lymph nodes, lungs and liver, which is common for the malignancy events also in the examined women. As our results showed, dogs, cats and humans develop tumors with similar frequency of histological subtype and their behavior can vary from indolent to very aggressive, according to the histological grade. The histological subtype of tumors is highly important for prognostic determination of the survival time and the treatment options [19].

We consider that the non-castrated domestic dogs and cats are suitable animal model for studies on mammary cancer in humans because of their short lifespan, comparable hormonal background and similarities in the shared with humans environmental risk factors. This model can be used for investigations in cancer biology, prognosis and therapies with possible potential in clinical researches of anticancer drugs.

Acknowledgements: The article was supported by the framework of the project BALTINFECT. This project has received funding from the European Union's 7th Framework Programme for research, technological development and demonstration under grant agreement No 316275.

References

1. **Antuofermo, E., M. A. Miller, S. Pirino, J. Xie, S. Badve, S. I. Mohammed.** Spontaneous Mammary Intraepithelial Lesions in Dogs – A Model of Breast Cancer. – Cancer Epidemiol. Biomarkers Prev., **16**(11), 2007, 2247-2256.
2. **Basset, P., C. Wolf, P. Chambon.** Expression of the stromelysin-3 gene in fibroblastic cells of invasive carcinomas of the breast and other human tissues: a review. – Breast Cancer Research and Treatment, **24**(3), 1993, 185-193.
3. **Benjamin, S., A. Lee, W. Saunders.** Classification and behavior of canine mammary epithelial neoplasms based on life-span observations in beagles. – Vet. Pathol., **36**(5), 1999, 423-436.
4. **Brearley, M. J.** Mammary gland tumours in the dog. – Practice, Nov., 1989, 248-253.
5. **Cribier, B., G. Noacco , B. Peltre, E. Grosshans.** Stromelysin 3 expression: a useful marker for the differential diagnosis dermatofibroma versus dermatofibrosarcoma protuberans. – J. Am. Acad. Dermatol., **46**(3), 2002, 408-413.
6. **Esteva, F. J., G. N. Hortobagyi.** Prognostic molecular markers in early breast cancer. –Breast Cancer Res., **6**, 2004, 109-118.
7. **Gama, A., A. Alves, F. Schmitt.** Identification of molecular phenotypes in canine mammary carcinomas with clinical implications: application of the human classification. – Virchows Arch., **453**(2), 2008, 123-132.
8. **Jemal, A., R. Siegel, E. Ward, T. Murray, J. Xu, M. J. Thun.** Cancer statistics. – CA Cancer J. Clin., **57**, 2007, 43-66.
9. Mammary Tumors: Introduction. The Merck Veterinary Manual, 2006. Retrieved 2007. Available at: (http://www.merckvetmanual.com/mvm/reproductive_system/mammary_tumors/overview_of_mammary_tumors.html).
10. **Misdorp, W.** Tumors of the mammary gland. Meuten D. J., editor. Tumors in domestic animals. Ames (IA), Iowa State Press, 2002, 575-606.
11. **Misdorp, W., R. W. Else, E. Hellmen, T. P. Lipscomb.** Histological classification of mammary tumors of the dog and the cat. 2nd series. Vol. VII. Washington (DC), Armed Forces Institute of Pathology and World Health Organization, 1999, 11-25.
12. **Morris, J. S., C. Nixon, A. Bruck, L. Nasir, I. M. Morgan, A. W. Philbey.** Immunohistochemical expression of TopBP1 in feline mammary neoplasia in relation to histological grade, Ki67, ERα and p53. – Vet. J., **175**(2), 2008, 218-226.
13. **Moulton, J. E.** Tumors of the Mammary Gland. Tumors in Domestic Animals. Berkeley, University of California Press, 1978, 346-371.
14. **Mouser, P., M. A. Miller, E. Antuofermo, S. S. Badve, S. I. Mohammed.** Prevalence and Classification of Spontaneous Mammary Intraepithelial Lesions in Dogs Without Clinical Mammary Disease. – Vet. Pathol., **47**(2), 2010, 275-284.
15. **Mulligan, R. M.** Mammary cancer in the dog: a study of 120 cases. – Am. J. Vet. Res., **36**(9), 1975, 1391-1396.
16. **Nieto, A., M. D. Pérez-Alenza, N. D. Castillo, E. Tabanera, M. Castaño, L. Peña.** BRCA1 Expression in Canine Mammary Dysplasias and Tumours: Relationship with Prognostic Variables. – J. Comp. Pathol., **128**(4), 2003, 260-268.
17. **Owen, L. N.** A comparative study of canine and human breast cancer. – Invest. Cell Pathol., **2**(4), 1979, 257-275.
18. **Page, D. L., W. D. Dupont.** Anatomic markers of human premalignancy and risk of breast cancer. – Cancer, **66**, 1990, 1326-35.
19. **Rakha, E. A., M. E. El-Sayed, A. H. S. Lee, C. W. Elston, M. J. Grainge, Z. Hodi, R. W. Blamey, I. O. Ellis.** Prognostic Significance of Nottingham Histologic Grade in Invasive Breast Carcinoma. – J. Clin. Oncol., **26**(19), 2008, 3153-3158.
20. **Skinner, K. A., M. J. Silverstein.** The management of ductal carcinoma in situ of the breast. – Endocr. Relat. Cancer, **8**, 2001, 33-45.
21. **Sobin, L. H., M. K. Gospodarowicz, C. Wittekind.** TNM Classification of Malignant Tumours, UICC International Union Against Cancer, Paul Hermanek, L.H. Sobin, edition 4, Springer Science & Business Media, 2012.
22. **Viste, J., S. Myers, B. Singh, E. Simko.** Feline mammary adenocarcinoma: tumor size as a prognostic indicator. – Can. Vet. J., **43**(1), 2002, 33-37.

Institute of Experimental Morphology, Pathology and Anthropology with Museum
Bulgarian Anatomical Society

Acta morphologica et anthropologica, 23
Sofia ● 2016

Професор Олег Сотников и тайните на живата аксоплазма

„Смисълът на фундаменталната наука, по мое мнение, се състои не само в това да се открива новото в природата, живота или да се изяснят възможни механизми на описани процеси. Особено увлекателна е научната работа, при която изследователят успява да открие, да докаже невероятното, това, което за болшинството съвсем не може да бъде, т.е. е небивалица.“

Тези думи на автора на монографията „Тайны живой аксоплазмы“ са първите за читателя, който ще разкрива непрекъснато нови изключителни данни за аксоплазмата. Авторът е проф. О. С. Сотников, директор на Лабораторията по функционална морфология и физиология на неврона в Института по физиология „Ив. П. Павлов“ на Руската академия на науките.

В монографията са отразени изследвания на нови свойства на аксоплазмата, получени при експерименти на жив (нефиксиран) аксон от ганглий на молюската Lymnaea stagnalis (вид сладководно коремоного мекотело). Описана е удивителната еластичност на аксоплазмата, способна да се удължава на големи разстояния, наличието в нея на ретрактилен тонус и на интензивна агрегация при неблагоприятни условия.

Анализът на белтъчните полимери на аксоплазмата и проведените експерименти чрез прерязване на аксона показват, че аксоплазмата не е течност, а интензивно се ретрахира и се впива в тялото на неврона. При опити с изменение на зоните на адхезия на аксона е установена възможност за регулиране на транспорта на аксоплазмата. Тя се ретрахира с цялата си маса, включително и цитоскелета, като едно цяло, едновременно в противоположни направления.

Това са първи експерименти, които потвърждават оригиналната хипотеза за двупосочно съкращаване. Открита е и нова форма на това съкращаване – изомерна ретракция. При тази ретракция се осъществява съкращаване не в резултат на намаляване на дължината, а чрез съкращаване на нейния диаметър. Демонстрирана е възможност за рязко изтъняване и удължаване на аксоните, при което се получават влакна – „невидимки“, и с тяхното участие се наблюдават различни физиологични процеси. Използвайки свойството на изомерната ретракция, учените успяват да намерят обяснение за изчезването и бързото възстановяване на апикалните дендрити в хипокампа при стрес и хибернация. В тъканни култури се потвърдила повтарящата се ретракция на аксоплазмата, като едновременно се съкращава в противоположни страни.

С цел да се спре ретракцията на аксоплазмата са проведени експерименти с различни блокатори. Получено е инхибиране както на безмиелиновите, така и на миелиновите влакна. Тъй като методите за лечение на диастазата не са много

ефективни, предложен е нов подход – фармакологично блокиране на ретракцията на двата края на прерязания нерв.

Проведените експерименти върху живи аксони, детайлно описани в настоящата монография, потвърждават концепцията на автора за ретрактилните свойства на аксоплазмата и за способността ѝ да решава необичайни морфо-физиологични задачи. Възможно е ретрактилният тонус и ретракцията да се явяват основни неелектрични функции на аксоплазмата.

Монографията съдържа изключителна колекция от микрофотографии, с надписи на руски и английски език. Със своите оригинални научни приноси, както и с изящното си оформление и отпечатване тя представлява безспорен интерес за широк кръг специалисти.

Проф. д.м.н. Емилия Запрянова

Institute of Experimental Morphology, Pathology and Anthropology with Museum
Bulgarian Anatomical Society

Acta morphologica et anthropologica, 23
Sofia ● 2016

Anthropology and Anatomy

Roma People – Genetics and Anthropology

L. Macuga

Torun University, Poland

Roma people are from long ago suspected of Indian ancestry. At first this supposition was proved by somatological observations. Generally different Roma appearance from neighbouring European populations was obvious but only since start of genetic surveys it was evident that Indian hypothesis is valid, and fully concordant with older anthropometric data.

Keywords: Roma, genetics, anthropometry, origins.

I. Historical background

Gypsies, who call themselves Roma, originated from people who left northern India between 5th and 11th century, probably around 8th century [5, 6, 9], and then reached through variety of ways almost all European countries (about 900 years ago appeared in the Balkans) [6], in turn, related to them Dom people [9] are present at the Middle East and north Africa. The two most likely are derived from the tribe Domba from north–western India [8].

II. Y–DNA

The main proof of the origin of the Gypsies from the Indian subcontinent is a very high percentage of "Indian" haplogroup H (exactly H1a1a–M82)[8]. Apart from India, does not meet such high frequency of this haplogroup. Moreover, among the Gypsies this haplogroup is more numerous than among the Hindus, which indicates so-called "founder effect" and the origin of Gypsies from a small group of Indian immigrants.

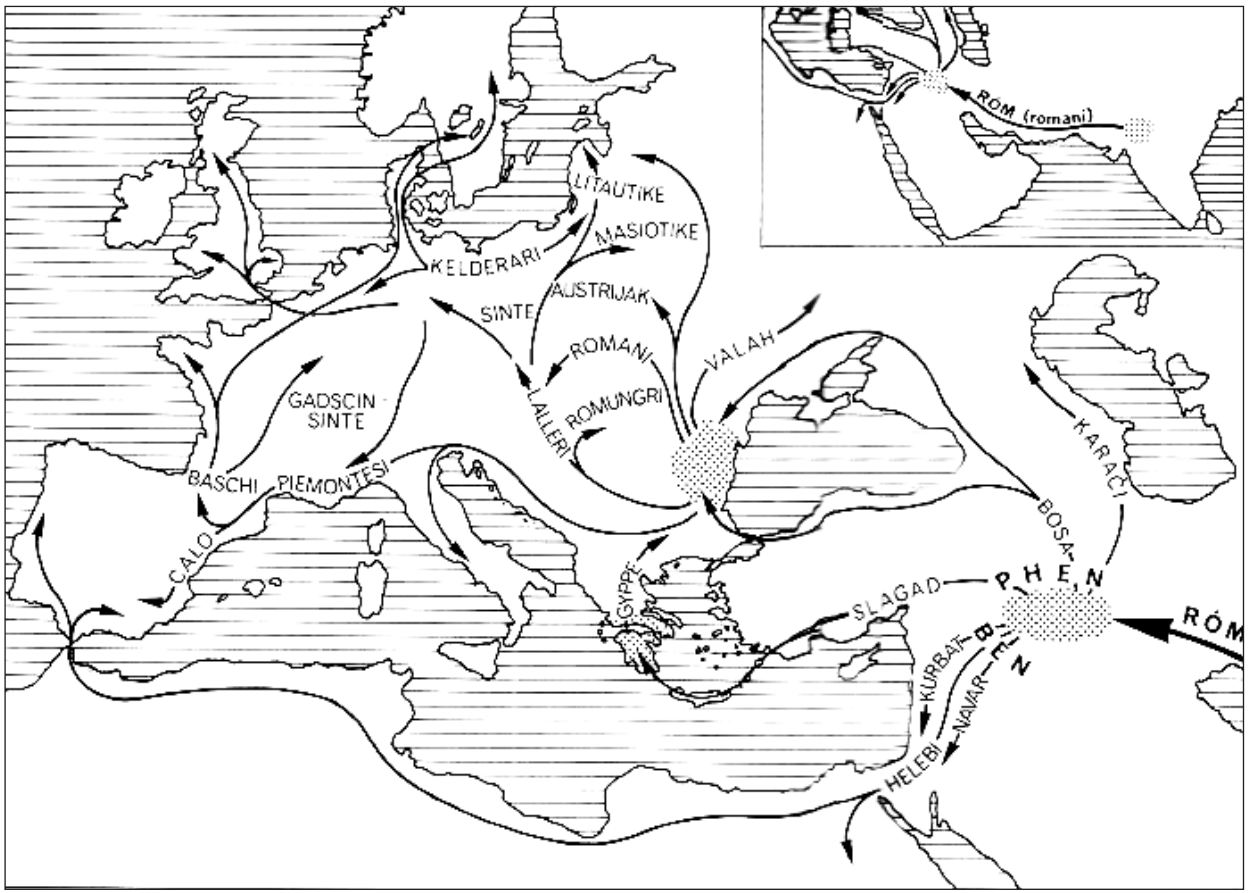

Fig 1. Migration routes of early Roma [2]

In Europe, only among the Serbs and Ukrainians H percentage oscillates around 1%, elsewhere is practically non-existent.

Table 1. European Roma samples and two non-Roma European samples with biggest percentage of H haplogroup [11]

Population sample	n	H–haplogroup, %	Author
Slovakian Romani	62	30.65%	Pamjev et al. 2011
Portuguese Romani	126	16.67%	Gusmao et al. 2008
Kosovo, Belgrade, Vojvodina Romani	88	43.18%	Regueiro et al. 2011
Bulgarian Romani	248	39.52%	Gresham et al. 2001
Spanish Romani	27	18.52%	Gresham et al. 2001
Croatian Romani	377	20.16%	Battaglia et al. 2009
Macedonian Romani (Skopje)	257	13.23%	Peričić et al. 2005
Hungarian Romani	424	16.98%	Pamjav et al. 2011
Lithuanian Romani	20	50%	Gresham et al. 2001
Ukrainians (Slav)	92	1.1%	Battaglia et al. 2009
Serbians, Belgrade (Slav)	113	0.9%	Peričić et al. 2005

Table 2. Indian samples of H haplogroup [11]

Population sample	n	H–haplogroup, %	Author
Terai–Nepal	197	10.66%	Fornarino et al. 2009
Hindu New Delhi	49	10.2%	Fornarino et al. 2009
Andhra Pradesh Tribals	29	27.6%	Fornarino et al. 2009
Northwest India	842	14.49%	Rai et al.2012
South India	1845	20.05%	Rai et al.2012
Central India	863	14.83%	Rai et al.2012
North India	622	13.99%	Rai et al.2012
East India	1706	8.44%	Rai et al.2012
West India	501	17.17%	Rai et al.2012

III. mtDNA

Also, mtDNA haplogroups [5, 10] indicate the Indian origin of Roma, especially frequency of the South-Asian haplogroup M (exactly M5A1, M18 and M35b), which is present in Europe only in trace amounts in non-Gypsy populations.

IV. Blood groups

Also, since first studies of blood groups [9] it was showed a greater frequency of gene B (or group B) from blood group system AB0, than average frequency in Europe and comparable with India.

Table 3. Frequency of blood group B in some Roma populations and populations related to them [9]

Population	Blood group B – min–max, %	Blood group B in Roma from the same territory, min–max, %
Romania	8–24	18–37
Former Yugoslavia and Hungary	15–26	20–41
Former USSR – Asiatic part	15–31	29
Other European populations	2–27	18–41
Turkey	11–28	
Syria		30–46
Iran	19–35	
Pakistan	21–44	
India	10–50	

V. Anthropometry

A very extensive list of masurements, cephalofacial indices and descriptive features presented Djaczenko [1] for Ukrainian Gypsies (area Starokozacze in southern Bessarabia belonging to Ukraine, n = 108). They gradually came to Ukraine from Romania in the fifteenth and eighteenth centuries.

Table 4. Anthropometric characteristics of Roma in Ukraine [12]

Anthropological feature	**Mean**	**SD**
height	165.1	6.3
Cephalic index	**79.1**	–
head length [g-op]	186.4	5.2
head width [eu-eu]	147.4	5.7
less frontal width [ft-ft]	103.1	5
fronto–parietal index	69.99	–
Morphological facial index (calculated from dimensions: zy-zy i n-gn)	**88.82**	–
facial index (calculated from facial height from lower border of the eyebrows and zy-zy)	91	–
Morphological facial height [n–gn], calculated: (facial height from the lower border of the eyebrows) – (nasal height from the lower border of the eyebrows – nasal height n-ns)	121.6	–
facial height (from lower border of the eyebrwos)	124.6	6.7
facial width [zy-zy]	36.9	5.1

Table 4 – continued

physionomical facial height [tr-gn]	186	8.6
physionomical facial index	135.8	–
nasal index (calculated from dimensions al-al i n-ns)	**71.01**	–
nasal idnex (calculated from nasal height from the lower border of the eyebrows and al-al	65.9	–
nasal width [al-al]	36.5	2.8
Nasal height [n-sn]	51.4	3.5
nasal height from the lower border of the eyebrows	55.4	3.9
mandibular width [go-go]	107.5	5.2
mandibulo-zygomatic index	79.16	–
zygo-parietal index	92.13	–
nasal height index	42.26	–
height of upper lip (skin part)	12.3	2.6
height of both lips	16.4	3.1
width of the mouth	56.3	4.1
mouth index	29.12	–

Technical notes: *Soviet authors use non-Martin nasal and morphological height (from lower border of eyebrows), so I provide also proper morphological facial height (nasal height from nasion was given by Djacenko in addition) and proper nasal index and morhplogical facial index.*
Also nasal profile was given for bony part of the nose and cartilagous part separately. And later the mean profile was calculated from the two. More or less only profile for cartilagous part of the nose can be comapred with nasal profile figures given by non-Soviet authors, so I provide only this. I calculated also from the following dimensions, some indices like: zygomatico-parietal, fronto-parietal, zygomatico-mandibular, the height of the nose index and mouth index.

Table 5. Anthroscopic characteristics of Roma in Ukraine [12]

Trait	Grades					
Eye color on Bunak scale (1-12)	(2 grade) dark (1-4) 54%	(1 grade) mixed (5-8) 42%, and green–brown (5) 15%	(0 grade) light (9-12) 4%	mean value: 1.5 (0-2)		
Hair color in Fischer scale	(4 grade) black (27) 18%	(3 grade) brownish black (4) 59%	(2 grade) dark brown (5) 19%	(1 grade) medium brown (7) 3%	(0 grade) darkblond (25) 1%	mean value: 2.9 (0-4)
Height of nasal bridge	(2) medium: 44%	(3) high: 56%	mean value: 2.56 (1-3)			

Table 5 – continued

Flattening of the nose ridge	(2) medium flattened: 15%	(3) arched: 85%	mean value: 2.85 (1–3)			
Nasal profile (cartilagous part)	(1) concave: 14%	(2) straight: 81%	(3) convex: 5%	mean value: 1.91 (1–3)		
Nasal tip	(1) up–turned: 47%	(2) horizontal: 34%	(3) depressed: 19%	mean value : 1.72 (1–3)		
Beard density	(1) very weak: 2%	(2) weak: 2%	(3) medium: 30%	(4) strong: 30%	(5) very strong: 36%	mean value: 3.96 (1–5)
Hairness of the torso	(1) very weak or absent: 37%	(2) weak: 21%	(3) medium: 24%	(4) strong: 15%	(5) very strong: 3%	mean value: 2.26 (1–5)
Eyebrows density	(1) weak: 17%	(2) medium: 44%	(3) strong: 39%	mean value e: 2.22 (1–3)		
Palpebral opening width	(1) narrow: 4%	(2) medium: 67%	(3) wide: 29%	mean value: 2.61 (1–3)		
Eyefold	(0) absent: 40%	(1) weak: 40%	(2) medium: 18%	(3) strong: 2%	mean value : 0.82 (0–3)	
Facial profile	(1) flat: 1%	(2) medium: 63%	(3) sharp: 36%	mean value : 2.35 (1–3)		
Malars prominency	(1) weak: 55%	(2) medium: 44%	(3) strong: 1%	mean value : 1.46 (1–3)		
Chin	(1) receding: 8%	(2) vertical: 39%	(3) pointed: 53%	mean value : 2.63 (1–3)		
Occiput	(1) prominent: 29%	(2) rounded: 57%	(3) flattened: 14%	mean value: 1.85 (1–3)		

In comparison with other studied groups from Ukraine (mainly Ukrainians but also other minorities) Djaczenko found that Gypsies have the lowest cephalic index, the widest nose, darkest pigmentation, and the most dense beard. Generally those features are rather alien to Eastern European populations.

Those set of traits indicate Southern Caucasoid phenotypical influences with some affinities to Indian subcontinent (wider nose, or straight or less so concave profile which can be summarized as Robust Mediterranean or South-Asian morphotype) than for example Western Asia (which is known from narrow noses, with large convex minority – Balkan-Anatolian or Armenoid and South-Western Asiatic or Oriental morhotypes).

The trend is clear. The height is mostly low, rarely medium. Cephalic index is in mesocephalic range, except in Bosnia. The nose in Turkey, Bulgaria, Romania is medi-

Table 6. Roma's anthropological data from Balkans and Central Europe [9]

Author		A. Weisbach	L. Gluck	E. Pittard	E. Pittard	E. Pittard	V. Lebzelter	F. Stampach	Schade, Pilaric	G. Pilaric	J. Benes	J. Benes
Country and year of investigation		Hungary 1889	Bosnia 1897	Turkey 1902	Romania 1902	Bulgaria 1904	Serbia 1922	Czecho-slovakia 1929	Croatia 1961	Macedonia 1961	Slovakia 1962	Hungary 1962
Height (cm)		165.5	167.8	163.6	161	165.6	162.7	163.7		163.6	164.3	167.1
Weight (kg)		62.6	–	–	–	–	–	–	–	–	60.4	60.7
g - op (mm)		188	190	189.1	188.5	189.9	185.5	190	188.2	186.1	185.7	187.5
eu - eu (mm)		150	145	148.2	150	146.8	147	149	152	146.1	151.3	151.1
Cephalic index, %		79.7	76.4	78.4	79.5	77.3	78.3	78.5	80.8	78.6	79.4	80.9
zy - zy (mm)		139	135	137	139.9	137.2	135.6	–	138.5	135.7	134.4	136.9
n - gn (mm)		–	–	–	–	–	120	–	127	120.5	121.6	122.8
Morph. facial index, %.		–	–	–	–	–	88.4	–	91.8	88.9	90.3	89.6
n - sn (mm)			54	52.1	50.8	50.5	52	–	–	51.5	55.6	55
al - al (mm)		35	34	36.3	36.3	36.5	33	–	–	35.7	33.4	33.9
Nasal index, %.			63.9	69.4	71.9	72.9	63.3	–	–	69.8	61.7	61.7
Skin color	light	0	0	–	–	–	0	–	–	–	11.9	2.8
	light swarthy	27	28.6	–	–	–	100	–	–	–	88.1	97.2
	swarthy	73	71.4	–	–	–						
Hair color	light	0	0	0.6			0	0	–	–		
	brown	5.9	3.6	14.5			7	15.3	–	–	0	0
	dark/ black	94.1	96.4	84.9			93	84.7	–	–	6.3	7.6
Eye color	light	3.8	17.8	13.3			2.2	9.3	7.2	22	93.7	92.4
	mixed	13.6	35.7	0.6			9	3.7			2.8	3.8
	dark	82.6	46.5	86			87.8	87	92.8	78	36.9	40

um wide, and in Western Balkans and Central Europe is narrow. When it comes to face the data is very scarce, but everywhere is on average in the narrow range. Pigmentation of hair is very dark. Eyes are dark but there is a large mixed minority. Skin color is dark as for Europan standards.

In addiditon Coon[1] wrote that in France Roma's cephalic index is 79 and height is 166 cm (pre-war data). He also stated that straight hair are dominant among Roma people.

We can summarize those data in similar way as above Djaczenko evidence on Ukrainian Roma. There is a clear deviation from average south-eastern and central European phenotype toward South Asian morphological complex.

As an example we can use Serbian Roma sample [4, 9] from **Table 1**. Polish anthropologist Michalski [7] analyzed them individually by use of morphological-comparative method. He estimated frequencies of phenotypical combinations (morphotypes) among Serbian Roma and concluded that Southern Caucasoid complex of traits dominated and Northern and Eastern European were in small minority in comparison to ethnic Serbian sample. Balkan-Anatolian (Armenoid) complex have similar frequency in both groups. Also among Roma's Southern phenotypical complex (composed mainly from European Mediterranean morhotype) there was quite numerous minority of South-Asian (Robust Mediterranean) and South-Western Asiatic (Oriental) sets of traits.

Conclusion

As it has been shown above, despite their longtime coexistance with European peoples Roma people reserves high specifity in their genetics and consequently in their phenotype. This specifity is due to their origin from the Indian subcontinent.

As a graphical illustration of those suggestions it could be fair to show some random Roma phenotypes from Hungary and Balkans.

Fig 2. Serbian Roma – early 20th century [4]

Fig. 3. Hungarian Roma – women – late 20th century [2, 3]

Fig. 4. Hungarian Roma – women – late 20th century [2, 3]

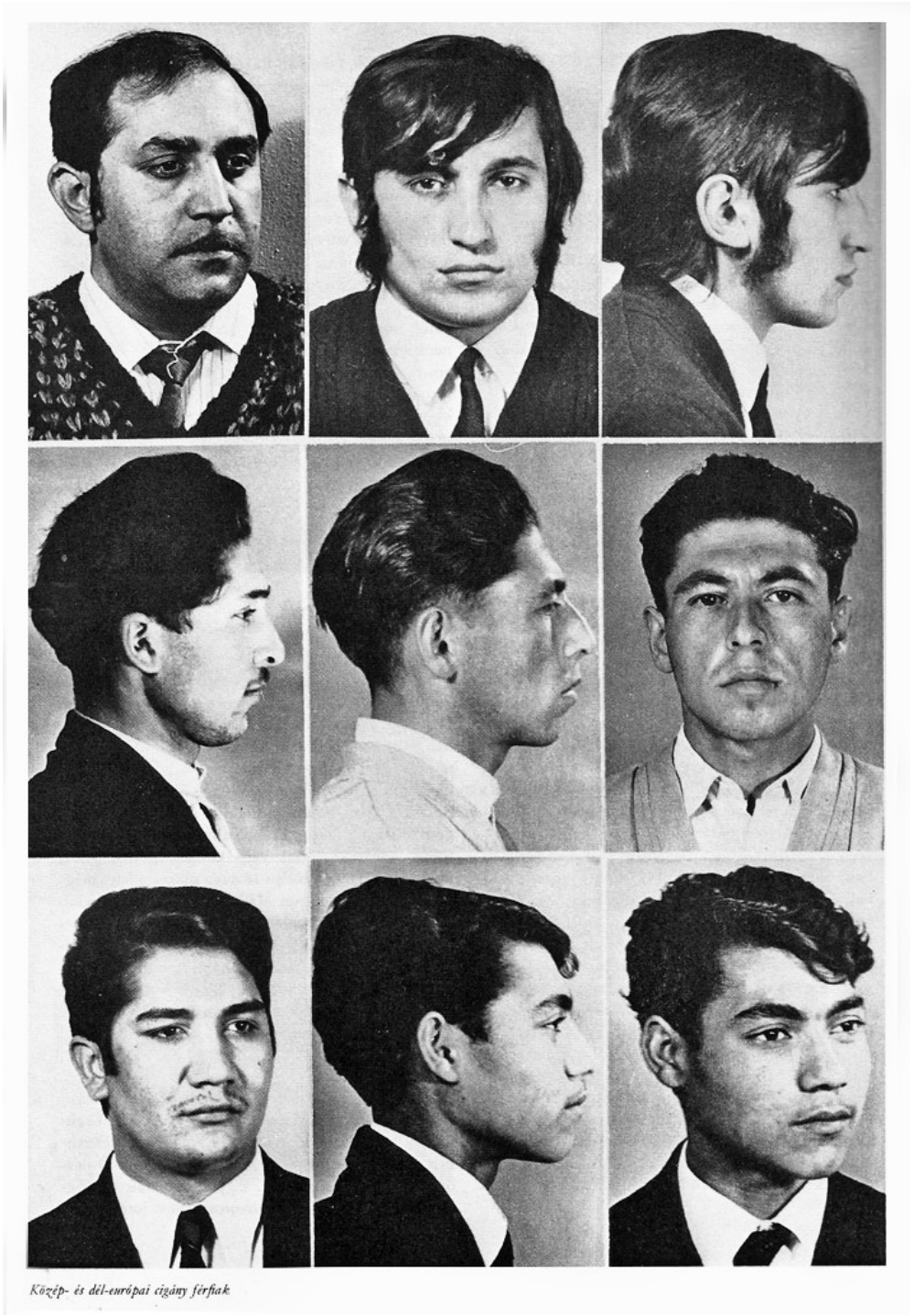

Fig. 5. Hungarian Roma – men – late 20th century [2, 3]

References

1. **Coon, C. S.** The Races of Europe, 1939.
2. **Kiszely, I.** A föld népei. Európa,1979.
3. **Kiszely, I.** A magyar ember. – A Kárpát Medencei Magyarság Embertörténete, 1-2, 2004.
4. **Lebzelter, V.** Anthropologische untersuchungen an Serbischen Zigeunern. – Mitteilungen der Anthropologischen Gesellschaft in Wien, **52**, 1922, 23-42.
5. **Mendizabal, I., C. Valente, A. Gusmão, C. Alves, V. Gomes, A. Goios, W. Parson, F. Calafell, L. Alvarez, A. Amorim, L. Gusmão, D. Comas, M. J. Prata.** Reconstructing the Indian origin and dispersal of the European roma: A Maternal genetic perspective. – PlosOne, **6**(1), 2011, e15988.
6. **Mendizabal, I., O. Lao, U. M. Marigorta, A. Wollstein, L. Gusmão, V. Ferak, M. Ioana, A. Jordanova, R. Kaneva, A. Kouvatsi, V. Kučinskas, H. Makukh, A. Metspalu, M. G. Netea, de R. Pablo, H. Pamjav, D. Radojkovic, S. J. Rolleston, J. Sertic, M. Jr. Macek, D. Comas, M. Kayser.** Reconstructing the population history of European Romani from genome-wide data. – Current Biology, **22**(24), 2012, 2342-2349.
7. **Michalski, I.** Struktura antropologiczna Polski. – Acta anthropologica Universitatis Lodziensis, **1**, 1949, 1-236.
8. **Rai, N., G. Chaubey, R. Tamang, A. K. Pathak, V. K. Singh, M. Karmin, M. Singh, D. S. Rani, S. Anugula, B. K. Yadav, A. Singh, R. Srinivasagan, A. Yadav, M. Kashyap, S. Narvariya, A. G. Reddy, G. van Driem, P. A. Underhill, R. Villems, T. Kivisild, L. Singh, K. Thangaraj.** The phylogeography of Y-chromosome haplogroup H1a1a-M82 reveals the likely Indian origin of the European romani populations. – PlosOne, **7**(11), 2012, e48477.
9. **Sûchy, J.** Die Zigeneur. red. Saller K., Rassengeschichte der Menschheit. Lfg 1. Australien. Indochina. Indopkaistan. Die Zigeneur, 1968.
10. **Vilar, M.** *Genographic Scientists Trace the Origins of Europe's Roma.* National Geogrpahic, 2015, (http://voices.nationalgeographic.com/2015/10/23/genographic-scientists-trace-the-origins-of-europes-gypsies/) https://en.wikipedia.org/wiki/Haplogroup_H_(Y-DNA).
11. **Дяченко, В. Д.** Антропологичний склад українського народу. – Наукова думка, Київ, 1965, 1–130.

Institute of Experimental Morphology, Pathology and Anthropology with Museum
Bulgarian Anatomical Society

Acta morphologica et anthropologica, 23
Sofia ● 2016

A persistent Metopic Suture – Incidence and Influence on the Frontal Sinus Development (Preliminary Data)

S. Nikolova[1], D. Toneva[1], I. Georgiev[2,3]*

[1] *Department of Anthropology and Anatomy, Institute of Experimental Morphology, Pathology and Anthropology with Museum, Bulgarian Academy of Sciences, 1113 Sofia, Bulgaria*
[2] *Department of Scientific Computations, Institute of Information and Communication Technologies, Bulgarian Academy of Sciences, 1113 Sofia, Bulgaria*
[3] *Department of Mathematical Modeling and Numerical Analysis, Institute of Mathematics and Informatics, Bulgarian Academy of Sciences, 1113 Sofia, Bulgaria*

The relation between *metopism* and underdevelopment of the frontal sinus is controversial. This study aimed to evaluate the incidence of the metopic suture as well as to assess its influence on the frontal sinus development. The frequency of the metopic suture was investigated in a series of 1373 dry skulls from contemporary adult males. The frontal sinus development was examined into two series: a control one (n=42), and a series with preserved metopic suture (n=40). The visualization was performed via digital radiography. The statistical significance of the differences between both series was assessed using chi-square test.

The metopic suture was found in 6.85% (94 out of 1373 skulls). The incidences of uni- and bilateral aplasia of the frontal sinus were more frequent in the metopic suture series compared to the control one. The cases of uni- and bilateral hypoplasia were commensurable in both series. A frontal sinus hyperplasia was observed only in the control. The differences between both series were significant at $p < 0.01$. The frontal sinus underdevelopment in the metopic suture series was exclusively expressed on the right side. Generally, the metopic suture seems to exert a repressive influence on the frontal sinus development. Thus, the metopic suture is not a certain indicator, but is a prerequisite for an underdeveloped frontal sinus.

Key words: metopic suture; frontal sinus; dry skulls.

Introduction

The metopic suture (MS) is located between the halves of the fetal frontal bone. It is a dentate suture [2] considered to be an anterior extension of the sagittal suture [31]. The MS is the first one to close physiologically, since the fusion usually takes place during the first or second year, but the completion can last until the fourth year of age [27], as the MS can be patent to the seventh year [31]. Sometimes the MS persists in adults as the frontal bone is composed of two symmetrical halves joined in the sagittal midline and this condition is known as *metopism* [27].

There are different hypotheses focused on the reasons for non-fusion of the frontal bone. The persistent MS has not been established to be related either to the skull shape

or the cranial capacity but has been positively correlated with an increase in the frontal curvature [27]. A familial study implies that metopism is under genetic control [34]. The presumptive factors for *metopism* include an abnormal growth of the cranial bones, hydrocephalus, growth retardation, heredity and heredospecific factors, sexual influence, atavism, stenocrotaphia, plagiocephaly, scaphocephaly, mechanical causes, and hormonal dysfunction [11]. The preserved MS was found to range from 0.8% up to 15% in different population groups [1, 2, 4, 6, 8, 9, 11, 13, 17, 22, 23, 25, 33, 37]. The MS can be easily misdiagnosed as vertical traumatic skull fractures extending in the mid-line in head injury patients or even for the sagittal suture on posteroanterior roentgenograms in the clinical practice [5].

It is supposed that the persistent MS could be a prerequisite for an underdevelopment of the frontal sinus [3, 26, 33], despite the fact that the frontal bones and MS appear during early fetal life, while the pneumatization of the frontal sinus occurs after the fifth or sixth postnatal year and reaches the full size after puberty [7]. This assumption is based on the fact that the development of the frontal sinus occurs together with the growth of the frontal bone, most probably with a feedback regulating mechanism. Thus, if the frontal bones do not fuse, the MS persists and the pneumatization of the frontal sinuses may be retarded or suppressed, or they may fail to develop altogether [3, 33]. However, other studies do not show a significant association between *metopism* and aplasia of the frontal sinus [7]. In such cases, the frontal sinuses develop separately on either side of the suture and this entity can be used to differentiate a persistent MS from a fracture of the frontal bone [10]. The frontal sinus is of great importance in the forensic medicine for identification of unknown human remains [7]. In this study, we aimed to evaluate the frequency of the MS among contemporary adult males from Bulgaria as well as to assess its influence on the frontal sinus development.

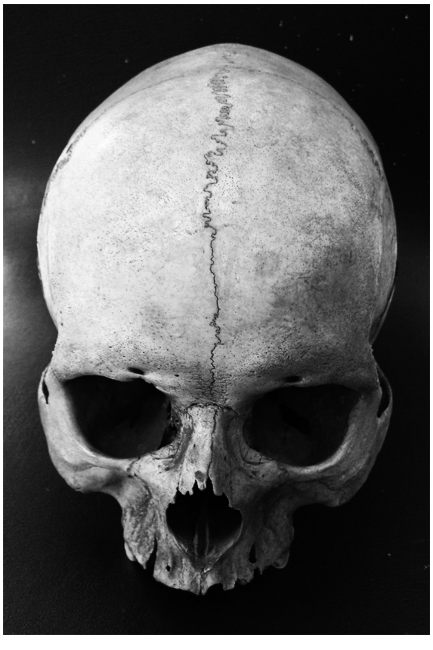

Fig. 1. Skull with entirely preserved metopic suture

Materials and Methods

The frequency of the persistent MS was investigated in a total of 1373 dry skulls of contemporary adult males. The skulls belonged to soldiers who served and died in the wars at the beginning of the 20th century: the First Balkan War, the Second Balkan War and the First World War. Their bone remains were preserved in the Military Mausoleum with Ossuary at the National Museum of Military History (Bulgaria).

The persistence of the MS was established by macroscopic inspection of the frontal bone. Only skulls with a completely preserved MS (**Fig. 1**) were accounted, i.e. the skulls with continuous suture extending from *nasion* to *bregma*.

The frontal sinus development was investigated in sample of 82 skulls grouped into two series: a control one – consisted of 42 skulls without traces from a MS, and a second series – of 40 skulls with an entirely preserved MS.

The frontal sinus was visualized through the digital radiography performed on a Nikon

XT H 225 system. The settings varied dependent on the specimens: voltage 95-126 kV, 80-100 μA tube current, exposure time of 1000 ms and 32 frames averaged. The skulls were oriented and radiographed in the occipitofrontal projection (Caldwell's view).

The development of the frontal sinus was observed bilaterally and was assessed as hyperplasia, medium, hypoplasia and aplasia according to the classification of Guerram et al. (2014) (**Fig. 2**). The facial reference lines were used after Schmittbuhl and Le Minor [28] and Schmittbuhl et al. [29]:

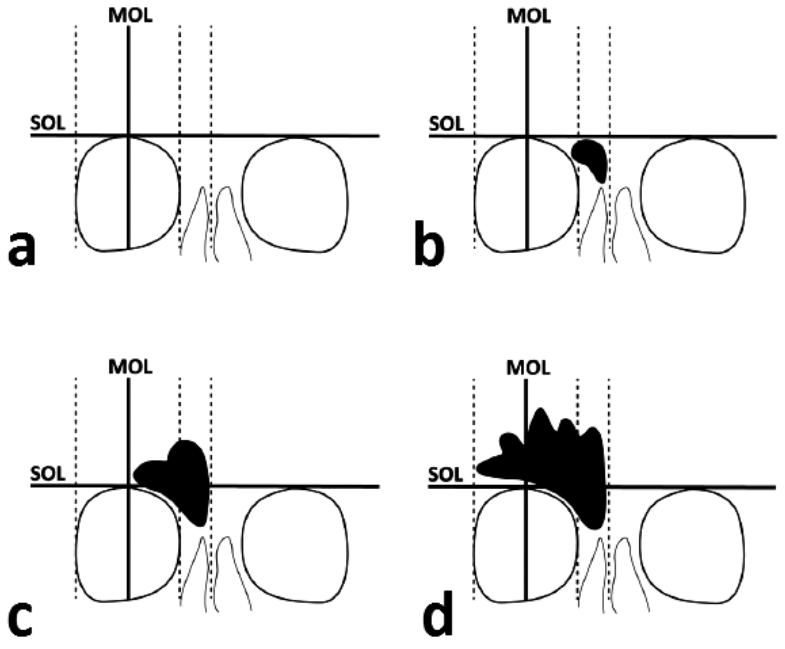

Fig. 2. Morphological quantification of the frontal sinus size after Guerram et al. (2014): a) aplasia; b) hypoplasia; c) medium; d) hyperplasia. Abbreviations: SOL – supraorbital line; MOL – midorbital line; Dotlines – midsagittal line; medial orbital line (vertical line passing through the most medial orbital point); lateral orbital line (vertical line passing through the most lateral orbital point)

1. Supraorbital line (SOL): horizontal line tangent to the superior margin of both orbits;
2. Midorbital line (MOL): vertical line, drawn for each orbit, parallel to the midsagittal line, and passing through the middle of the orbital breadth defined between the lateral orbital line (vertical line passing through the most lateral orbital point) and the medial orbital line (vertical line passing through the most medial orbital point).

The statistical significance of the differences between both series was assessed using chi-square test (χ^2).

Results

The overall incidence of the entirely preserved MS was 6.85% (94 out of 1373 skulls). The incidences of the uni- and bilateral aplasia of the frontal sinus were more frequent in the series with a persistent metopic suture (27.5%) compared to the control one

(4.8%) (**Table 1**). The cases of uni- and bilateral hypoplasia were commensurable in both series (22.5% MS; 28.6% control). Hyperplasia of the frontal sinus was observed only in the control series (11.9%). The differences between both series were statistically significant at $p < 0.01$. The frontal sinus underdevelopment in the MS series was exclusively expressed on the right side. Moreover, the aplasia was in a combination with a hypoplastic left sinus in 5 cases and with a developed left sinus in 3 cases (**Table 2**). In the control series, only 2 cases of aplasia were found as both were bilateral (**Table 3**). Bilateral hypoplasia of the frontal sinus was observed in 4 cases from the MS series and in 7 cases from the control one. Right-sided hypoplasia was found in 4 cases from the MS series and in 3 cases from the control one. Left-sided hypoplasia was observed in only 1 metopic and in 2 non-metopic skulls.

Table 1. Relation between metopic suture and development of the frontal sinus

Study	Series	Σn	Aplasia			
			bilateral		unilateral	
			n	%	n	%
Welcker [36]	MS (German)	20	4	20	5	25
Rochlih and Rubaschewa, [24]	MS Control Control (Russian)	110 80 100	31 6 7	28.2 7.5 7	18 9 4	16.4 11.2 4
Monteiro et al. [21]	MS (Portuguese)	80	6	7.5	2	2.5
Torgersen, [33]	MS–roentgenograms Non–metopic	62 400	15 20	24.2 5	– –	– –
Marciniak and Nizankowski, [19]	MS– roentgenograms MS–museum material	252 26	20 3	8 14	18 2	7.1 10.5
Baaten et al. [4]	MS (Lebanese)	8	7	87.5	0	0
Bilgin et al., [7]	MS Control	61 570	6 60	40 46.9	9 68	60 53.1
Guerram et al. [14]	MS Control (Upper Rhine)	63 80	3 1	4.8 1.25	3 2	4.8 2.5
Present study	MS (Bulgarians) Control (Bulgarians)	40 42	3 2	7.5 4.8	8 0	20 0

Table 2. Comparison of the development of the frontal sinus in our MS series with the data reported by Guerram et al. (2014)

Frontal sinus size – MS	Aplasia L		Hypoplasia L		Medium L		Hyperplasia L		Total	
Aplasia R	3	3*	5	2*	3	0*	0	0*	11	2*
Hypoplasia R	0	1*	4	29*	4	2*	0	0*	8	8*
Medium R	0	0*	1	1*	20	23*	0	1*	21	60*
Hyperplasia R	0	0*	0	0*	0	1*	0	0*	0	10*
Total	3	4*	10	32*	27	26*	0	1*	40	63*

* data after Guerram et al. (2014)

Table 3. Comparison of the development of the frontal sinus in our control series with the data reported by Guerram et al. (2014)

Frontal sinus size – Control	Aplasia L		Hypoplasia L		Medium L		Hyperplasia L		Total	
Aplasia R	2	1*	0	1*	0	0*	0	0*	2	2*
Hypoplasia R	0	1*	7	5*	3	2*	0	0*	10	8*
Medium R	0	0*	2	1*	23	56*	0	3*	25	60*
Hyperplasia R	0	0*	0	0*	0	4*	5	6*	5	10*
Total	2	2*	9	7*	26	62*	5	9*	42	80*

* data after Guerram et al. (2014)

Discussion

The observed MS incidence is in agreement with those reported for the Europeans [8, 9, 25]. In a previous study of the MS among medieval series from Bulgaria was found that the suture was more frequently observed in the female series (10.6%, 16 out of 159 skulls) compared to the male one (8.18%, 13 out of 159 skulls), but the differences were not statistically significant [23]. A comparison between the contemporary (6.85%) and the medieval (8.18%) male series showed a slightly lower frequency of the MS in the contemporary one.

Aplasia of the frontal sinus is a relatively rare but not uncommon finding. Complete agenesis of the frontal sinus occurs in 5-15% of adults and the percentage may vary in different geographic groups [16]. According to Martin [20], a congenital absence of the frontal sinuses was found in about 7% of Europeans and 30% of Australians. In our control series, aplasia of the frontal sinus was observed in 4.8%.

The relationship between the MS and a congenital absence of the frontal sinuses is contraversial. Rochlin and Rubaschewa [24] have observed a higher incidence of uni- and bilateral congenital aplasia of the frontal sinus in a MS series compared to two control ones. Torgersen [33] has also found aplasia of the frontal sinus to be more frequent in the metopic skulls. Furthermore, when the sinuses are present in metopic skulls, they tend to be reduced [32]. However, Marciniak and Nazankowski [19] and Bilgin et al. [7] have not found any strong association between both MS and frontal sinus agenesis. Baaten et al. [4] have reported an absence of the frontal sinus in 7 from 8 skulls with a MS. Slight prevalence of the frontal sinus aplasia in a MS series was also observed by Guerram et al. [14].

The frequency of the unilateral aplasia is varying as the failure of the development of one of the frontal sinuses occurs in 1-15% of adults [12]. The unilateral aplasia has been found to be more common than the considerably rarer bilateral one [26]. However, in the studies of Rochlin and Rubaschewa [24], Marciniak and Nazankowski [19] and Bilgin et al. [7] on MS series, such a tendency could not be established. Our results showed a considerable prevalence of the frontal sinus aplasia in the MS series as the unilateral cases were more frequent (**Tables 2, 3**) and exclusively expressed on the right side (**Fig. 3**).

Guerran et al. [14] have found that both aplasia and hypoplasia of the frontal sinus were considerably more frequent in the MS skulls as the differences generally came from the higher frequency of the cases with hypoplasia. As it could be seen from our results, the overall cases of absence and underdeveloped frontal sinus were also more

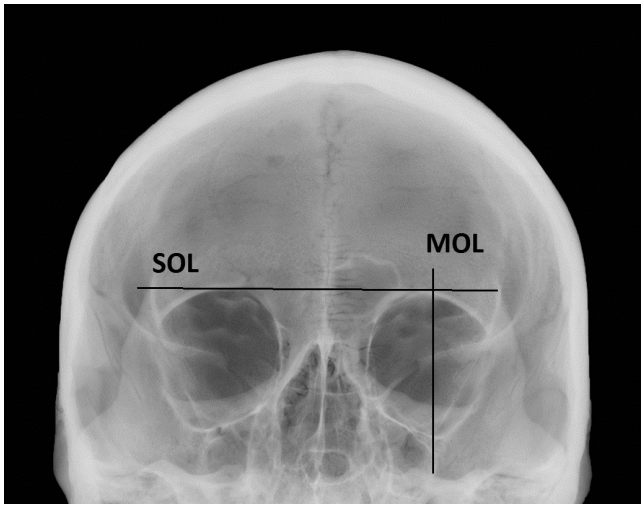

Fig. 3. Roentgenogram of the skull with a metopic suture showing right side aplasia and left side sinus of medium size. Abbreviations: SOL – supraorbital line; MOL – midorbital line

frequent in the MS compared to the control series as the prevalence was at the expense of the cases of aplasia which was entirely right-sided (**Tables 2, 3**).

The right and left lobes of the frontal sinus develop independently and often display asymmetry, which is generally attributed to a more rapid development on one side at the expense of the other [35]. Some authors have reported that the right lobe of the sinus tends to be larger than the left counterpart [15, 18, 27]. Other researchers have found a predominance of the left lobe [16, 19]. According to other studies, there have not been established any significant differences between the dimensions of both frontal lobes [32]. Our results showed clearly a tendency to left lobe dominance as in the MS series this tendency was expressed even more strongly (**Table 2**).

Conclusion

The MS frequency in the contemporary adult males from Bulgaria was comparable to those reported for the Europeans. The persistence of the MS was often related to a frontal sinus aplasia and/or hypoplasia, so it could be considered that it exerts a repressive influence. Thus, the MS is not a certain indicator but is a prerequisite for an underdeveloped frontal sinus.

Acknowledgements: This study was supported by the "Program for career development of young scientists, Bulgarian Academy of Sciences", research grant DFNP – 73/27.04.2016. The authors would like to acknowledge the kind assistance given by the staff of the National Museum of Military History (Bulgaria).

References

1. **Agarwal, S. K., V. K. Malhotra, S. P. Tewari.** Incidence of the metopic suture in adult Indian crania. – Acta Anat., **105**, 1979, 469-474.

2. **Ajmani, M. L., R. K. Mittal, S. P. Jain.** Incidence of the metopic suture in adult Nigerian skulls. – J. Anat., **137**, 1983, 177-183.
3. **Alyea, O. E.** Nasal sinuses: an anatomic and clinical consideration. Baltimore, The Williams & Walkins Company, 1951.
4. **Baaten, P. J., M. Haddad, K. Abi-Nader, A. Abi-Ghosn, A. Al-Kutoubi, A. R. Jurjus.** Incidence of metopism in the Lebanese population. – Clin. Anat., **16**, 2003, 148-151.
5. **Bademci, G., T. Kendi, and F. Agalar.** Persistent metopic suture can mimic de skull fractures in the emergency setting? – Neurocirugía, **18**, 2007, 238-240.
6. **Berry, A. C., R. J. Berry.** Epigenetic variation in the human cranium. – J. Anat., **101**, 1967, 361-379.
7. **Bilgin, S., U. H. Kantarci, M. Duymus, C. H. Yildirim, B. Ercakmak, G. Orman, Beser C. Gunenc, M. Kaya, M. Gok, A. Akbasak.** Association between frontal sinus development and persistent metopic suture. – Folia Morphol., **72**, 2013, 306-310.
8. **Breathnach, A. S.** Frazer's Anatomy of the Human Skeleton. London, Churchill, 5th ed., 1958.
9. **Bryce, T. H.** Osteology and Arthrology. – In: Quain's Elements of Anatomy, London, Longmans Green, 11th ed., vol. **4**, pt. I, 1915, 177.
10. **Christensen, A. M.** An Empirical Examination of Frontal Sinus Outline Variability Using Elliptic Fourier Analysis: Implications for Identification, Standardization, and Legal Admissibility. PhD Thesis, Knoxville, University of Tennessee, 2003.
11. **del Sol, M., O. Binvignat, P. D. A. Bolini, J. C. Prates.** Metopismo no individuo brasileiro. – Rev. Paul Med., **107**, 1989, 105-107.
12. **Donald, P. J., J. L. Gluckman, D. H. Rice.** The Sinuses. New York, Raven Press, 1994.
13. **Eroğlu, S.** The frequency of metopism in Anatolian populations dated from the Neolithic to the first quarter of the 20th century. – Clin. Anat., **21**, 2008, 471-478.
14. **Guerram, A., J.-M. le Minor, S. Renger, G. Bierry.** The size of the human frontal sinuses in adults presenting complete persistence of the metopic suture. – Am. J. Phys. Anthropol., **154**, 2014, 621-627.
15. **Hajek, M.** Normal Anatomy of the Frontal Sinuses. In: Pathology and Treatment of the Inflammatory Diseases of the Nasal Accessory Sinuses. (editors M. Hajek, and J.D. Heitger), 5th edition, St. Louis, The C.V. Mosby Company, 1926, 35-43.
16. **Harris, A. M., R. E. Wood, C. J. Nortje, C. J. Thomas.** Gender and Ethnic Differences of the Radiographic Image of the Frontal Region. – J. Forensic. Odontostomatol., **5**, 1987, 51-57.
17. **Keith, A.** Human Embryology and Morphology. London, Edward Arnold, 6th ed, 1948.
18. **Lang, J.** Clinical anatomy of the nose, nasal cavity and paranasal sinuses. New York, Thieme, 1989.
19. **Marciniak, R., C. Nizankowski.** Metopism and its correlation with the development of the frontal sinuses. – Acta Radiol., **51**, 1959, 343-352.
20. **Martin, R.** Lehrbuch der Anthropologie. Jena, G. Fischer, Bd. II, 1928.
21. **Monteiro, H, S. Pinto, A. Ramos, A. S. Tavares.** Aspects morphologiques des sinus para-nasaux. – Acta. Anat., **30**, 1957, 508-522.
22. **Murlimanju, B. V., V. Prabhu Latha, M. Mangala et al.** Median Frontal Sutures – Incidence, Morphology and Their Surgical, Radiological Importance. – Turk. Neurosurg., **21**, 2011, 489-493.
23. **Nikolova, S., D. Toneva.** Frequency of metopic suture in male and female medieval cranial series. – Acta Morphologica et Anthropologica, **19**, 2012, 250-252.
24. **Rochlin, D. G., A. Rubaschewa.** Zum Problem des Metopismus. – Z. Konstitutiouslehre, **18**, 1934, 339.
25. **Romanes, G. J.** Cunningham's Textbook of Anatomy. London, Oxford University Press, 11th ed., 1972, 133.
26. **Samuel, E., G. A. S. Lloyd.** Clinical Radiology of the Ear, Nose and Throat. Philadelphia: W. B. Saunders Company, 1978.
27. **Scheuer, L., S. Black.** Developmental Juvenile Osteology. London, Academic Press, 2000.
28. **Schmittbuhl, M, J. M. Le Minor.** New approaches to human facial morphology using automatic quantification of the relative positions of the orbital and nasal apertures. – Surg. Radiol. Anat., **20**, 1998, 321-327.
29. **Schmittbuhl, M, J. M. Le Minor, A. Schaaf.** Relative orbitonasal overlap in African great apes and humans quantified by the automatic determination of horizontal and vertical lines of reference. – Primates, **40**, 1999, 301-310.

30. **Schuller, A.** A note on the identification of skulls by X-ray pictures of the frontal sinuses. – Med. J. Aust., **1**, 1943, 554-557.
31. **Skrzat, J., J. Walocha, J. Zawilinski.** A note on the morphology of the metopic suture in the human skull. – Folia Morphol., **63**, 2004, 481-84.
32**. Strek, P., K. Kaczanowski, A. Skawina, K. Pitynski, Z. Kitlinski, D. Mrowka, B. Naklicka.** The morphological evaluation of frontal sinuses in Human Skulls. – Folia Morphol. (Warsz.), **51**, 1992, 319-328.
33. **Torgersen, J.** A roentgenological study of the metopic suture. – Acta Radiol., **33**, 1950, 1-11.
34. **Torgersen, J.** The developmental genetics and evolutionary meaning of the metopic suture. – Am. J. Phys. Anthropol., **9**, 1951, 193-207.
35. **Turner, A. L.** The Accessory Sinuses of the Nose. New York, Longmans, Green & Co., 1902.
36. **Welcker, H.** Untersuchungen über Wachstum und Bau des menschlichen Schädels. 1. Allgemeine Verhältnisse des Schädelwachsthums und Schädelbaues. Normaler Schädel deutschen Stammes. Leipzig, Engelmann, 1862, 92–93.
37. **Woo, Ju-Kang.** Racial and sexual differences in the frontal curvature and its relation to metopism. – Am. J. Phys. Anthropol., **7**, 1949, 215-226.

*Corresponding author:
Silviya Nikolova, PhD
Department of Anthropology and Anatomy,
Institute of Experimental Morphology,
Pathology and Anthropology with Museum,
Bulgarian Academy of Sciences
E-mail: sil_nikolova@abv.bg

Institute of Experimental Morphology, Pathology and Anthropology with Museum
Bulgarian Anatomical Society

Acta morphologica et anthropologica, 23
Sofia ● 2016

Anthropological Types in Bulgarian Population around 1940 – Regional and Local Level

R. Stoev

Institute of Experimental Morphology, Pathology and Anthropology with Museum, BAS, Sofia, Bulgaria

The largest anthropological survey in Bulgaria has been organized by M. Popov in 1938-1943. Its materials include individual data of 5725 men. Only this study gives a possibility to analyze complex individual anthropological characteristics on regional and local level. The data of the distribution of six anthropological types collected in this survey are analyzed by regions and by counties and an anthropological map of Bulgaria has been made. The analysis shows that recent Bulgarian population is highly heterogeneous. Brachycephalic Dinaric and Alpine types dominate in North and especially in Northwest Bulgaria. Mesocephalic Pontian and Mediterranean types dominate in South and especially in Southeast Bulgaria. However, there are bands of mesocephalic population in North Bulgaria (along the Black Sea coast and along the Danube river) and islands of brachycephalic population in South Bulgaria (in the Rhodopes and in Eastern Thrace). The anthropological composition of Northwest Bulgaria is similar to the Central European one.

Key words: anthropological types, ethnic anthropology, modern Bulgarians, regional anthropological characteristics, local anthropological characteristics.

There were four major ethnoanthropological surveys in Bulgaria, which cover all the territory of the country – carried out by: acad. Stefan Vatev around 1899, acad Methody Popov at 1938-1943, Aris Poulianos at 1963, and the National Anthropological Program at 1989-1993 [14, 17, 8, 16]. Their results show that the anthropological structure of the present Bulgarian population is very heterogeneous. Unfortunately, their results are presented only at national and regional levels. Only few data are published on lower level [14, 17]. The survey of Krum Dronchilov [2], perhaps the best exact and best known outside Bulgaria, also presents anthropological data on local level, but it do not cover the whole territory of Bulgaria. The materials of the extensive anthropological studies of Peter Boev, Luchia Kavgazova and their collaborators, collected at 1970s and 1980s are only partly published and also do not cover the whole country [3, 4, 5].

The largest anthropological survey in Bulgaria of these four studies, mentioned above, is the study organized by M. Popov in 1938-43. Part of the collected by him and his collaborators materials was destroyed at the time of bombing of Sofia at 1943-1944. The survived materials include individual data of 5759 men. This material has been elaborated and the results were published only after his death (1954) by his student

Georgi Markov in 1959 [17]. However, because of political reasons he had to make a conscious error in the text (not in the numeral data), probably for to insure that the results could be published. This mistake has been repeated in some later Bulgarian works about the anthropology of Bulgarians for inner use [12, 13]. But the anthropologists outside the borders of Bulgaria were not influenced by it [15, 10, 11]. The published material of this study gives a possibility to analyze anthropological characteristics and the distribution of anthropological types on regional and local level (by counties – "okolias") as it has been made, for example in Poland or Switzerland long ago [9, 6].

Materials and Methods

The published materials of the anthropological survey of M. Popov are used at regional level, namely for each regional population the share of the anthropological type is calculated. The classification of anthropological types is taken as in the original publication, which is close to the classification of Cheboksarov [19] and coincides with the classification of Henzel-Michalski in the main points [6, 7]. The share of individuals of intermediate type are divided between the main anthropological types after Michalski [6]. Then euclidean distances are calculated between the local samples and cluster analysis is made by UPGMA [1]. The classification of the distances as very small, small, medium, large and very large is made after Heet [18].

On local (county) level only the percent distribution of five anthropological traits has been given on maps (height, cephalic index, morphological face index, percentage of individuals of dark complexion (dark eyes, dark hair), percentage of individuals of light complexion). Based on this, it is possible to combine these traits and to calculate the approximate theoretic share of the major anthropological types. For example:

County of Vidin – height over 170 cm – ca 62.5% (60-64.9%); cephalic index over 81 – ca 52.5% (45-59.9%); morphological face index over 88 – ca 77.5% (75–79.9%); dark complexion – ca 62.5% (60-64.9%); light complexion – ca 6% (under 7.9%).

Mediterranean type – height under 170, cephalic index under 81, face index over 88, dark complexion : $0.375 \times 0.\ 475 \times 0.775 \times 0.625 \approx 0.086 = 8.6\%$;

Pontian (Atlanto-mediterranean) type – height over 170, cephalic index under 81, face index over 88, dark and mixed complexion + height under 170, cephalic index under 81, face index over 88, mixed complexion: $0.625 \times 0.475 \times 0.775 \times 0.94 + 0.375 \times 0.475 \times 0.775 \times 0.315 \approx 0.260 = 26.0\%$;

Dinaric type – height over 170, cephalic index over 81, face index over 88, dark and mixed complexion: $0.625 \times 0.525 \times 0.775 \times 0.94 \approx 0.239 = 23.9\%$

Alpine type – height under 170, cephalic index over 81, face index under 88, dark and mixed complexion: $0.375 \times 0.525 \times 0.225 \times 0.94 \approx 0.942 = 4.2\%$

Atlanto-baltic (Nordic) type - height over 170, cephalic index under 81, face index over 88, light complexion: $0.625 \times 0.475 \times 0.775 \times 0.06 \approx 0.014 = 1.4\%$

Eastern Baltic (White see-Baltic) type: cephalic index over 81; face index under 88; light complexion: $0.525 \times 0.225 \times 0.06 \approx 0.007 = 0.7\%$

The names of the anthropological types and their description and borderlines between them are that of the original publication.

Results and Discussion

The share of the basic anthropologic types in the regional population samples are presented in **Table 1**.

Table 1. Regional distribution of major anthropologic types

Region	Vratsa	Pleven	Ruse	Varna	Sofia	Plovdiv	St. Zagora	Burgas	Blagoevgrad	Total	Macedonians	Bulgarians-Muslims
n	593	861	234	316	1615	1274	377	299	156	**5725**	413	356
Type. %												
Mediterranean	1.85	2.15	2.78	2.78	4.61	**11.93**	7.96	11.04	9.94	**6.19**	6.05	10.25
Pontian	27.32	30.31	34.62	34.62	32.07	33.28	38.06	**40.13**	31.09	**33.82**	30.15	26.26
Dinaric	19.48	18.18	**20.94**	**20.94**	13.03	9.30	12.33	9.20	6.73	**13.88**	14.77	5.48
Alpine	**4.89**	4.24	3.63	3.63	3.10	1.57	0.80	0.84	1.60	**2.75**	1.94	1.69
Atlanto-Baltic	4.89	4.12	3.63	3.63	6.90	10.05	6.37	7.19	7.05	**6.75**	3.39	**10.39**
Eastern Baltic	2.45	2.44	1.92	1.92	2.01	0.59	0.80	0.84	**2.56**	**1.63**	0.85	1.26
Undefined	39.12	38.56	32.48	32.48	38.27	33.28	33.69	30.77	41.03	**35.00**	42.86	44.66

Note: The maximum share of every anthropological type is bolded.

As it can easily be seen, the major concentration of Pontian type is in Southeast, not in Northeastern Bulgaria, as in the text written by G. Markov for to stress the role of Slavic elements in the formation of Bulgarian people (17). The most extreme position in the table have the samples from Southeast Bulgaria (St. Zagora and Burgas)from one side with very high concentration of Pontian type and of North Bulgaria (especially Northwest Bulgaria) from other side with high concentration of Dinaric type. The samples of Sofia, the Macedonians, of Blagoevgrad and Plovdiv have something intermediate position. This can easy be seen in the diagram of Czekanowski **(Fig. 1).**

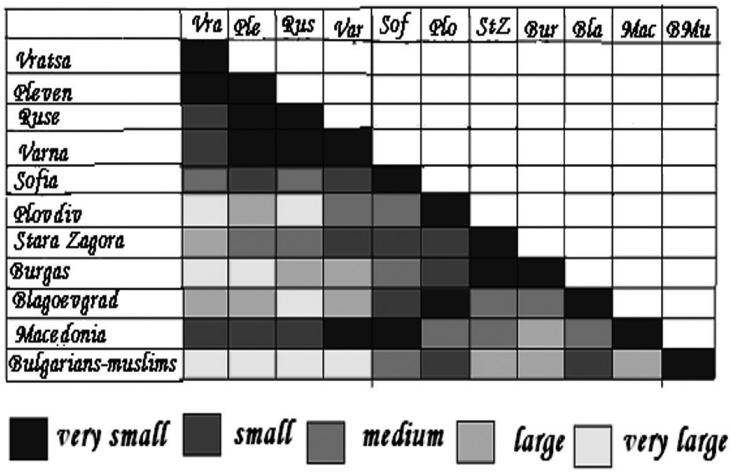

Fig. 1. Euclidean distances between regional Bulgarian populations based on the share of the major anthroplogical types

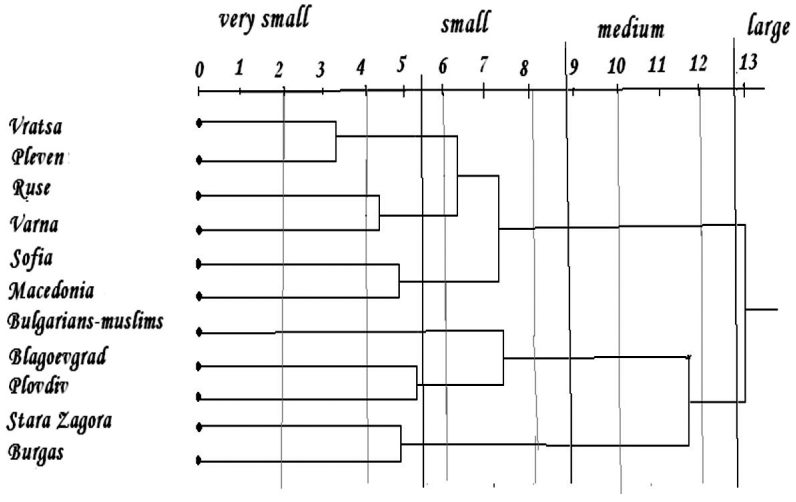

Fig. 2. Cluster analysis of the Euclidean distances between the regional anthropological samples

The cluster analysis of the euclidian distances between these samples (**Fig. 2)** shows that they present two well defined clusters. The first of them includes all samples from Danube Basin + Macedonians, the second – all Southern Bulgaria from Struma to the Black Sea.

Table. 2. Theoretic share of major anthropological type in the population – county level

	Mediterranean	Pontian	Dinaric	Alpine	Atlanto-Baltic	Eastern Baltic	Predominance
County	%	%	%	%	%	%	
Vidin	8.6	26.0	23.9	4.2	1.4	0.7	PD
Kula	3.6	5.8	21.1	14.0	0.7	4.3	Da
Belogradchik	2.2	6.8	24.5	13.4	0.6	3.5	Da
Lom	1.9	8.4	35.1	8.0	0.5	1.9	D
Montana	1.9	7.6	32.3	9.1	0.4	2.1	D
Berkovitsa	3.2	6.9	25.1	11.0	0.9	3.8	Da
Oryahovo	4.1	12.6	19.9	8.8	2.1	4.6	Dp
Byala Slatina	1.7	8.1	29.0	10.4	0.7	3.1	Da
Vratsa	2.2	7.7	29.0	10.4	0.7	3.1	Da
Nikopol	6.1	18.5	12.9	10.5	1.3	2.2	pda
Pleven	7.7	23.3	19.7	5.5	2.0	1.4	Pd
Lukovit	2.2	8.1	27.9	12.4	0.4	1.9	Da
Teteven	1.7	6.5	26.3	9.3	1.2	**6.3**	D
Troyan	1.6	8.3	33.6	7.7	0.8	3.1	D
Lovech	4.5	14.4	26.4	6.1	2.1	3.1	Dp
Sevlievo	3.6	17.6	29.7	5.4	1.6	1.9	Dp
Gabrovo	3.3	16.1	27.1	4.9	2.9	3.3	Dp
Dryanovo	2.2	9.3	36.3	6.6	0.9	2.3	D
Svishtov	2.2	10.0	36.0	6.3	0.8	1.9	Dp
Pavlikeni	2.5	8.1	31.3	9.0	0.7	2.7	D
Tarnovo	2.5	8.1	31.3	9.0	0.7	2.7	D
Gorna Oryahovitsa	2.9	7.7	28.8	10.3	0.7	2.7	Da
Elena	3.8	6.8	26.3	11.5	0.6	2.7	Da
Ruse	6.3	14.9	25.3	7.1	1.4	1.9	Dp
Byala	3.0	6.5	23.4	**15.7**	0.3	2.1	Da
Razgrad	2.5	7.1	28.5	8.2	1.3	4.8	D
Popovo	4.3	13.7	23.4	6.7	2.5	3.9	Dp
Silistra	9.8	24.8	22.0	4.7	1.3	0.7	PD
Targovishte	2.9	10.1	41.3	4.2	1.0	1.4	Dp
Omurtag	2.3	9.9	41.7	4.6	1.0	1.9	D

Table 2 – continued

Preslav	2.5	11.1	46.4	3.7	0.6	0.9	Dp
Shumen	7.2	24.4	21.9	3.8	3.2	1.7	PD
Novi Pazar	10.6	22.6	21.1	4.5	2.1	1.2	PDm
Provadiya	9.1	23.2	20.6	5.8	1.2	0.9	PD
Varna	7.0	24.0	23.1	4.2	2.3	1.4	PD
Balchik	5.5	18.2	33.2	4.6	1.0	0.9	Dp
Dobrich	5.5	14.3	19.5	10.4	1.0	2.2	dpa
Godech	8.2	30.8	13.4	3.8	3.6	1.4	PD
Sofia	8.0	19.6	16.0	7.0	2.4	2.4	pd
Elin Pelin	2.6	7.1	26.3	9.3	1.2	4.8	D
Samokov	6.4	13.8	22.1	7.6	1.7	2.6	Dp
Ihtiman	4.9	14.8	23.6	8.4	1.3	2.2	Dp
Pirdop	8.2	29.0	12.8	3.6	4.7	1.9	Pd
Botevgrad	2.2	7.7	29.0	10.4	0.7	3.1	Da
Tran	7.2	29.9	13.9	3.2	5.1	1.9	Pd
Breznik	7.6	32.5	7.9	2.8	3.0	1.0	P
Pernik	8.8	25.0	11.7	6.4	1.2	1.0	Pd
Radomir	12.5	25.4	12.0	5.2	2.2	1.2	Pmd
Kyustendil	6.1	24.8	12.5	4.5	3.4	2.2	Pd
Dupnitsa	7.7	25.9	12.6	4.5	3.4	2.0	Pd
Blagoevgrad	8.7	24.9	11.6	5.1	3.1	2.0	Pd
Sandanski	8.7	24.9	11.6	5.1	3.1	2.0	Pd
Petrich	8.7	24.9	11.6	5.1	3.1	2.0	Pd
Razlog	12.8	32.2	7.5	2.7	4.2	1.0	Pm
Gotse Delchev	8.7	24.9	11.6	5.1	3.1	2.0	Pd
Panagyurishte	11.5	29.3	15.3	3.5	2.8	1.0	Pdm
Pazardzhik	7.8	20.5	16.4	5.6	3.3	2.6	Pd
Velingrad	12.5	33.5	6.4	2.7	4.8	1.1	Pm
Peshtera	7.7	33.0	16.5	3.0	3.1	1.0	Pd
Karlovo	10.2	34.2	16.6	2.1	4.5	0.9	Pd
Plovdiv	12.9	28.8	14.4	3.1	3.9	1.2	Pdm
Asenovgrad	17.6	34.8	7.2	1.7	5.5	0.7	Pm
Chepelare	10.1	27.0	12.8	3.6	4.7	1.9	Pdm
Devin	7.3	28.0	28.3	2.3	2.8	0.9	DP
Smolyan	8.1	22.9	21.4	4.9	2.2	1.4	PD
Ardino	8.1	22.9	21.4	4.9	2.2	1.4	PD
Kazanlak	7.3	26.4	25.1	2.6	3.7	1.3	PD

Table 2 – continued

Chirpan	6.1	30.2	15.8	2.9	4.3	1.7	Pd
Parvomay	10.6	31.0	16.9	2.4	4.6	1.2	Pdm
Stara Zagora	10.8	32.8	15.0	3.2	2.8	0.8	Pdm
Nova Zagora	5.9	33.0	17.0	2.4	4.6	1.4	Pd
Haskovo	6.7	27.1	14.7	4.1	1.6	1.0	Pd
Harmanli	5.1	25.1	24.2	4.4	1.4	1.0	PD
Svilengrad	1.8	9.1	37.3	5.4	1.3	3.2	D
Ivaylovgrad	**22.7**	32.3	7.6	1.8	4.3	0.6	PM
Sliven	9.2	**45.8**	11.6	0.9	**6.5**	0.6	Pd
Kotel	9.4	26.9	12.5	4.5	3.4	1.7	Pd
Yambol	15.9	27.7	12.4	4.0	2.3	0.8	Pmd
Elhovo	9.0	25.6	22.0	4.7	1.3	0.7	PD
Karnobat	12.1	40.7	9.6	2.2	2.1	0.4	Pm
Aytos	15.3	31.1	14.6	2.8	2.7	0.7	Pmd
Pomorie	13.2	43.3	11.1	1.5	2.4	0.3	Pmd
Burgas	10.6	22.6	21.1	4.5	2.1	1.2	PDm
Tsarevo	15.0	42.6	10.4	1.3	4.0	0.4	Pmd
Malko Tarnovo	15.0	42.6	10.4	1.3	4.0	0.4	Pmd
Mean arithmetic	**7.2**	**21.2**	**20.9**	**5.7**	**2.3**	**1.9**	PD
SD	**4.3**	**10.6**	**9.0**	**3.2**	**1.4**	**1.2**	

Note: In the column "predominance" is shown the major anthropological types according to their share – P = Pontian, D = Dinaric, M = Mediterranean, A = Alpine. By capital letters types with share more than 20% are presented, by small letters – types with 10 to 19.9%. The maximal share of every anthropological type is bolded.

The analysis on anthropological type distribution on local level, presented in **Table 2** and **Fig. 3** clearly present how heterogeneous modern Bulgarians are. However, one can see that there is some order in the picture – Northern Bulgaria is an area of predominance of Dinaric type, Southern – of Pontians. Dinars are predominating also in a belt in the eastern part of Sofia district, which is connected with the predominantly dinaric Northern Bulgaria – this brachycephalic belt can be well observed also in the materials of St.Vatev's and Kr. Donchilov's surveys [14, 2]. Dinaric islands can also be found in Central Rhodopes and Eastern Thrace. Pontians and other meso-dolichocephals can be found also in Notheast Bulgaria and along Danube up to Vidin – this can also be traced and even more clear in the materials of St. Vatev's survey, but the colonization of Danube plain by brachycephalic Balkandzhi –Bulgarians from the Balkan Mountains valleys in the end of 19th and in the beginning of the 20th century has obscured the picture. However, Pontian type on a local level is concentrated in Northeast Bulgaria, but the major concentration being in Southeast Bulgarian counties – Sliven, Pomorie, Tsarevo, Malko Tarnovo, Karnobat. Thus this type has been renamed as Poulianos Thracian type [8].

If we have to look for Slavic heritage in modern Bulgarians, we surely have not to look in the regions of predominance of Pontian type, which is only sporadically

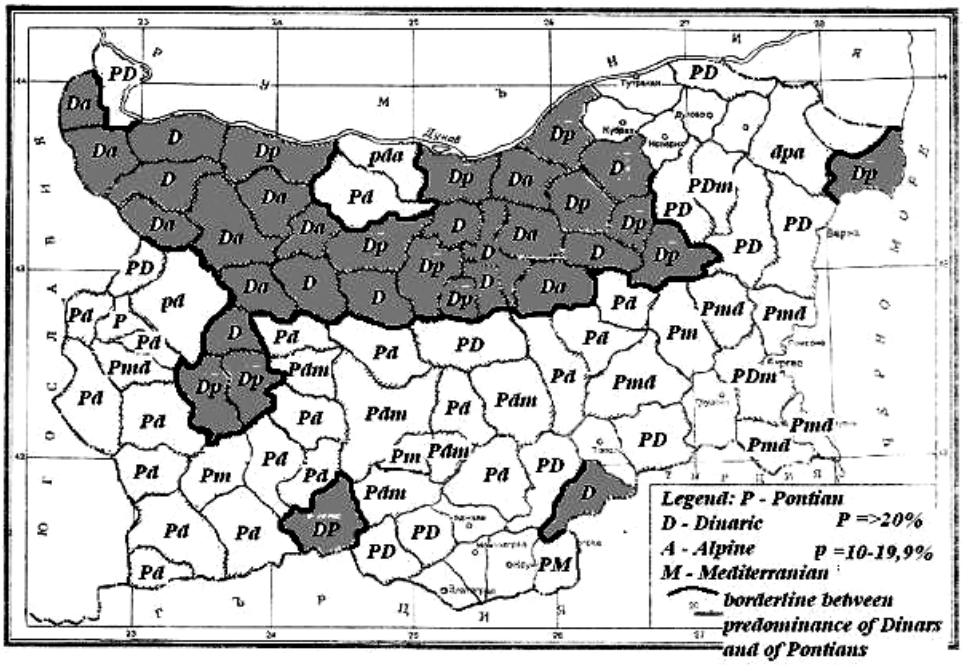

Fig 3. Predominating anthropological types in Bulgarians around 1940

Note: There were insufficient numbers of investigated from some counties and thus they are left empty on the map.

presented in significant degree in Eastern Slavic populations [15, 10, 11]. The Northern Bulgarians with their brachycephaly and mixed pigmentation are more similar to the populations of Central Europe north of Danube and thus are better candidates to be Slavic descendents. Especially interesting are the counties with higher concentration of Eastern Baltic type, which is synonym with the Subnordic type. The latter is considered by the Polish anthropologists as typical for Slavic populations [6].

Conclusion

The analysis of the anthropological data collected by acad. M. Popov presents that modern Bulgarians anthropologically are very heterogeneous in territorial aspect. Southern Bulgaria is a region of predominance of Pontian Anthropologic type with higher concentration in Southeast Bulgaria. Northern Bulgaria is a region of predominance of Dinaric type. However, there are islands and belts of Dinaric predominance in Southern and of Pontian predominance in Northern Bulgaria.

References

1. **Chistov, Yu. K.** The use of Data Bases for the Analysis of Large Quantities of Anthropological Data. – In: Mathematics in Biological Sciences. Application in Anthropology. Commotini, Greece, **1996.**
2. **Drontschiloff, Kr.** Beiträge zur Anthropologie der Bulgaren. Friedr. Vieeg & Sohn, 1914, 1-80.

3. **Kavgazova, L. P. Boev, A. I. Hadjioloff**. Morphological characteristics of highland population in Central Rhodopes. – C. r. Acad. bulg. Sci., v. **37**, 1984, 5, 657-659.
4. **Kavgazova, L**., **P. Boev**. Anthrogical characteristics of Rhodope variant of Dinaric race. C. r. Acad. bulg. Sci., v. **37**, 1984, 5, 665-667
5. **Kavgazova, L., Zl. Filcheva, R. Stoev**. Anthropological characteristics of the population in the western part of Smolyan region. – Acta morphologica, **6**, 1987, 58-64.
6. **Michalski, I.** Struktura antropologiczna Polski. Lodz. Acta anthropologica universitatis Lodziensis, **1**, 1949, 1-236.
7. **Henzel, T, I. Michalski.** Podstawy klasyfikacji czlowieka w ujeciu Tadeusza Henzla i Ireneusza Michalskiego. – Przeglad Antropologiczny, tom XXI, zeszyt 2, 1955, 537-662.
8. **Poulianos, A. N.** Anthropologikes erevnes sta Valkania (Voulgaria – Ellada – Giougoslavia). Athina, 1967, 1-157.
9. **Schlaginhaufen, O.** Anthropologia Helvetica. Art. Institut Orell Füssli A.-G., Zürich**,** 1946, 1-700.
10. **Алексеев, В. П.** В поисках предков. Советская Россия, М., 1972, 1-304.
11. **Алексеева, Т. И.** Антропология. Онлайн учебник, 2004.
12. **Боев, П.** Антропологична характеристика на населението на НР България. – В: Етнография на България, т. 1. София, Изд. БАН, 1978, 261–269.
13. **Боев, П.** Антропологични типове. – В: Енциклопедия България, т. 1. София, Изд. на БАН, 1980, 97–98.
14. **Ватев, Ст.** Антропология на българите. С., 1939, 1–80.
15. **Дяченко, В. Д.** Антропологичний склад українського народу. Наукова думка, Київ, 1965, 1–130.
16. **Йорданов, Й.** Антропология на населението на България в края на XX век. С., Акад. изд. „Проф. Марин Дринов“, 2006, 1–432.
17. **Попов, М., Г. Марков.** Антропология на българския народ. С., Изд. БАН, 1959, 1–296.
18. **Хить, Г. Л.** Дерматоглифика народов СССР. М., Наука, 1983, 1–280.
19. **Чебоксаров, Н. Н., И. Ал Чебоксарова.** Народы, расы, культуры. М., Наука, 1985, 1–272.

Institute of Experimental Morphology, Pathology and Anthropology with Museum
Bulgarian Anatomical Society

Acta morphologica et anthropologica, 23
Sofia ● 2016

Intra- and Interobserver Measurement Error of Linear Measurements on Three-dimensional Computed Tomography Models of Dry Mandibles

D. Toneva[1], S. Nikolova[1], I. Georgiev[2,3], A. Tchorbadjieff[3]

[1] Institute of Experimental Morphology, Pathology and Anthropology with Museum, Bulgarian Academy of Sciences, 1113 Sofia, Bulgaria
[2] Institute of Information and Communication Technologies, Bulgarian Academy of Sciences, 1113 Sofia, Bulgaria
[3]Institute of Mathematics and Informatics, Bulgarian Academy of Sciences, 1113 Sofia, Bulgaria

The study aimed to establish the precision of linear measurements taken on 3D models of human mandibles created by computed tomography and to compare the measurement error with the one obtained for the corresponding measurements taken directly on the dry mandibles. Ten mandibles were scanned through computed tomography. The polygonal models in STL format were generated using VG Studio Max 2.2 software. Ten linear measurements were taken on both dry mandibles and 3D models. The conventional measurements of the mandibles were taken with a digital caliper and the digital measurements were accomplished on the 3D models using the software Geomagic Verify Viewer. All parameters were measured twice by two observers. The intra- and interobserver measurement error was estimated using the technical error of measurement and the reliability of the mandibular measurements was assessed with the coefficient of reliability. All digital measurements showed acceptable measurement error. According to the coefficients of reliability, most of the digital measurements had values above 0.95, indicating high reliability.

Key words: 3D models, mandible, computed tomography, technical error of measurement, coefficient of reliability.

Introduction

The integration of three-dimensional (3D) technologies in different anthropological fields has led to an increasing utilization of the 3D models in anthropometric studies. The steadily increasing usage of digital measurements inevitably puts the question for their precision and reliability. Precision is a measure of the closeness of repeated measurements of the same quantity [5], and reliability is the degree to which within-subject variability is due to factors other than measurement error [14]. Since measurements are not free of error due to instrument imprecision and human inconsistencies [5], the determination of the measurement error appears to be an important component of the anthropometric studies [15].

The most commonly used measures of precision are the technical error of measurement (TEM) and the coefficient of reliability (R). The use of these two errors estimates contributes sufficiently to the determination of the precision of a series of anthropometric measurements [15]. The TEM is the variability encountered between dimensions when the same specimens are measured multiple times by the same observer (intraobserver TEM) or by two or more observers (interobserver TEM) [5, 14]. The lower variability between repeated measurements indicates greater precision [3]. Furthermore, the coefficient of reliability (R) reveals the proportion of between-subject variance, which is free from measurement error [15].

This study aimed to establish the precision of linear measurements taken on 3D models of human mandibles created by computed tomography (CT) and to compare the measurement error with the one obtained for the corresponding measurements taken directly on the dry mandibles.

Materials and Methods

The study was conducted on a sample of ten mandibles from the Military Mausoleum with Ossuary, National Museum of Military History, Bulgaria. The bones belonged to adult male individuals, who served and died during the wars from the beginning of the 20th century.

To obtain 3D models, the mandibles were scanned through computed tomography. The CT scanning was performed on a Nikon Metrology XT H 225 system with reflection head and a voltage of 85 kV with a power of 8.1 W and 95 μA tube current. To generate a 3D CT volume, a series of sequential 2D X-ray images (projections) were captured as the object was rotated through 360°. For each scan 3000 projections were registered, where each projection was taken with an exposure time of 500 ms. The images were then reconstructed to generate a 3D volumetric representation of the object with voxel size of 86 μm. The polygonal models in STL format were generated from voxel data by surface determination and surface extraction using VG Studio Max 2.2 software.

Ten linear measurements between definite landmarks (**Fig. 1**), described according to Martin and Saller [8], were taken on both dry mandibles and 3D models (**Table 1**). The

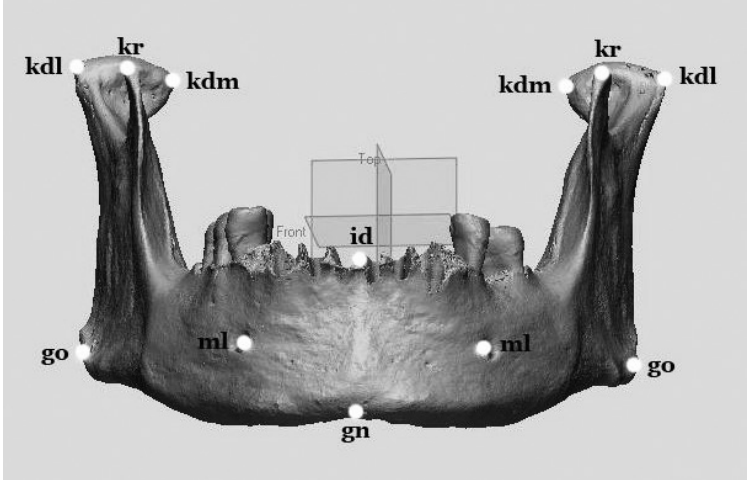

Fig. 1. Location of the landmarks used in the study

Table 1. Mandibular measurements

Measurements		Definition
M1	kdl-kdl	The direct distance between the left and right kondilion laterale (kdl)*.
M2	kdm-kdm	The direct distance between the left and right kondilion mediale (kdm).
M3	kr-kr	The direct distance between the left and right koronion (kr).
M4	go-go	The direct distance between the left and right gonion (go).
M5	ml-ml	The direct distance between both landmarks mentale (ml).
M6	id-gn	The direct distance from infradentale (id) to gnation (gn).
M7	kdl-kdm (L)	The direct distance between left kondilion laterale and left kondilion mediale.
M8	id-kr (L)	The direct distance from infradentale to the left koronion.
M9	id-kdl (L)	The direct distance from infradentale to the left kondilion laterale.
M10	id-kdm (L)	The direct distance from infradentale to the left kondilion mediale.

*Landmarks' abbreviations are written according to Martin and Saller [8].
(L) – left

conventional measurements of the mandibles were taken with a digital caliper (Würth, Germany) with a measuring unit of 0.01 mm and accuracy to 0.03 mm. The digital measurements were accomplished on the 3D models using the free software Geomagic Verify Viewer (3D Systems, Inc).

All parameters were measured twice by two observers. The 1st and 2nd measurements of all samples were taken on separate days.

Statistics

The intra- and interobserver measurement error was estimated using TEM and the reliability of the mandibular measurements was assessed with R. The intraobserver measurement error was computed for each parameter using the duplicate measurements taken by each observer. The interobserver measurement error was calculated based on the values of repeated measurements of both observers.

The absolute TEM was calculated by the following equitation [15]:

$$TEM = \sqrt{\left(\sum D^2\right)/2N} \ ,$$

where $\sum D^2$ is the sum of the deviations raised to the second degree and N is the number of the measured specimens.

However, the absolute TEM depends on the magnitude of the measurements and thus, the different parameters are not comparable. Therefore, the absolute TEM was transformed into relative TEM (%TEM or rTEM) [14]:

$$\%TEM = (TEM/mean) \times 100 \ .$$

For comparison of different studies with more than one observer involved, the total TEM was computed in the following way:

$$total\ TEM = \sqrt{(((TEM_{(intra_1)}{}^2 + TEM_{(intra_2)}{}^2)/2) + TEM_{(inter)}{}^2)},$$

where TEM(intra$_1$) is the intraobserver TEM for the first observer, TEM(intra$_2$) is the intraobserver TEM for the second observer, and TEM(inter) is the interobserver TEM between the two of them [14]. The relative total TEM (% total TEM) was obtained using the equation: % total TEM = ((total TEM)/mean) × 100.

According to the calculations of the total TEM, the measurement error of the digital and direct mandibular measurements was classified as acceptable and non-acceptable. A threshold of 5% was chosen as an admissible cut-off in accordance with the osteometric studies of Richard et al. [11], Franklin et al. [2], Lottering et al. [7].

The coefficient of reliability (R) was calculated from the total TEM [14]:

$$R = 1 - \left(\frac{(total\ TEM)^2}{SD^2}\right),$$

where SD^2 is the total between subject variance, including measurement error. The R values can range from 0 (all between-subject variation was due to measurement error) to 1 (no measurement error). Values of R greater than 0.95 indicate high reliability of the measurements with more than 95% of the variance due to factors other than measurement error [14].

Comparisons between the TEMs of both observers for digital and direct measurements as well as between the TEMs of the digital and conventional measurements of each observer were performed using a paired t-test.

Results

The basic descriptive statistics of the measurements of both observers are presented in **Table 2**. The values obtained for the intra- and interobserver absolute TEM, %TEM, total TEM and R are given in **Tables 3** and **4**.

Intraobserver TEM and %TEM

The intraobserver absolute TEMs for the **digital measurements** ranged within 0.26–0.60 mm for the first observer and 0.26-0.59 for the second one. The values of the %TEM ranged up to 2.18% and 1.34%, respectively. As can be seen from **Table 3**, the most affected by measurement error was the measurement with smallest magnitude (M7). The mean %TEMs for the digital measurements were 0.80% for the first and 0.70% for the second observer.

The TEMs observed for the **direct measurements** were lower than these for the digital ones (**Table 4**). The intraobserver absolute TEMs for both observers ranged within 0.17-0.53 mm. The largest values of the %TEM reached up to 1.04% for the first and 0.95% for the second observer. The most precise measurement was M1 and the least one – M7. The mean %TEMs for the direct measurements of both observers were very close – 0.48% and 0.47%, respectively.

Table 2. *Means* and *SD* of the two measurement sets of both observers. Deviations (*D*) between the measurements of each observer or both observers

Measurements	Observer I			Observer II			Interobserver *D*
	Trial 1	Trial 2	$D^2 \pm SD$	Trial 1	Trial 2	$D^2 \pm SD$	$D^2 \pm SD$
	Mean ± SD	*Mean ± SD*		*Mean ± SD*	*Mean ± SD*		
Digital measurements							
M1	115.84±7.57	116.06±7.46	0.13±0.18	116.52±7.23	116.21±7.36	0.35±0.52	0.31±0.35
M2	80.54±6.08	80.43±6.11	0.39±0.60	80.11±6.08	80.24±5.88	0.26±0.36	0.17±0.23
M3	92.90±3.95	92.72±4.12	0.32±0.27	93.44±3.93	93.29±3.71	0.61±0.79	0.84±0.88
M4	99.42±5.06	99.72±5.00	0.41±0.37	99.28±4.62	99.08±4.32	0.70±1.01	1.02±1.42
M5	44.29±2.93	44.65±2.64	0.60±0.85	44.98±2.53	44.98±2.92	0.45±0.48	0.38±0.50
M6	31.06±2.27	31.01±2.20	0.24±0.32	30.85±2.14	30.87±2.29	0.27±0.38	0.36±0.31
M7	18.52±2.26	18.49±2.37	0.33±0.29	19.06±2.16	19.09±2.36	0.13±0.22	0.44±0.43
M8	82.13±3.31	81.99±4.00	0.68±0.69	82.97±3.77	82.96±3.62	0.50±0.52	1.16±1.21
M9	107.06±2.66	107.29±2.34	0.71±0.72	107.93±2.84	107.96±2.59	0.52±1.21	1.38±1.66
M10	103.15±2.42	103.08±2.31	0.69±0.98	103.24±1.98	103.22±2.07	0.20±0.28	0.72±0.87
Direct measurements							
M1	116.82±7.33	116.84±7.42	0.06±0.05	117.06±7.36	117.14±7.40	0.06±0.08	0.11±0.14
M2	79.41±6.22	79.54±6.20	0.39±0.43	79.85±6.09	80.02±5.89	0.37±0.38	0.39±0.48
M3	92.51±4.54	92.54±4.43	0.15±0.13	92.37±4.66	92.38±4.47	0.55±0.68	0.29±0.33
M4	100.56±4.72	100.40±4.86	0.18±0.27	100.50±4.86	100.46±4.86	0.07±0.10	0.10±0.18
M5	44.98±2.66	44.85±2.59	0.12±0.14	44.82±2,59	44.89±2.71	0.07±0.10	0.11±0.10
M6	32.71±2.01	32.74±1,90	0.11±0.13	32.62±1,77	32.53±1.88	0.10±0.11	0.17±0.41
M7	19.41±2.57	19.50±2.43	0.08±0.17	19.58±2.48	19.63±2.24	0.07±0.10	0.11±0.18
M8	82.66±4.29	82.94±3.91	0.33±0.53	82.52±4.00	82.56±4.34	0.42±0.41	0.49±0.76
M9	107.59±2.97	107.57±2.87	0.29±0.27	107.38±3.16	107.42±3.00	0.11±0.19	0.25±0.28
M10	103.52±2.52	103.59±2.35	0.29±0.33	103.47±2.33	103.47±2.39	0.34±0.51	0.32±0.42

Table 3. TEMs and R of the digital mandibular measurements

Measurements	Intraobserver TEM				Interobserver TEM		Total TEM		R
	Observer I		Observer II						
	Absolute	%	Absolute	%	Absolute	%	Absolute	%	
M1	0.26	0.22	0.42	0.36	0.39	0.34	0.37	0.32	0.997
M2	0.44	0.55	0.36	0.45	0.29	0.36	0.35	0.44	0.996
M3	0.40	0.43	0.55	0.59	0.65	0.69	0.57	0.61	0.978
M4	0.45	0.45	0.59	0.60	0.71	0.72	0.63	0.63	0.982
M5	0.55	1.24	0.47	1.05	0.44	0.98	0.48	1.06	0.968
M6	0.34	1.11	0.37	1.20	0.42	1.36	0.39	1.26	0.967
M7	0.40	2.18	0.26	1.34	0.47	2.51	0.41	2.18	0.966
M8	0.59	0.71	0.50	0.60	0.76	0.92	0.66	0.80	0.966
M9	0.60	0.56	0.51	0.47	0.83	0.77	0.71	0.66	0.923
M10	0.59	0.57	0.32	0.31	0.60	0.58	0.54	0.52	0.935

Table 4. TEMs and R of the direct mandibular measurements

Measurements	Intraobserver TEM				Interobserver TEM		Total TEM		R
	Observer I		Observer II						
	Absolute	%	Absolute	%	Absolute	%	Absolute	%	
M1	0.17	0.15	0.18	0.15	0.24	0.20	0.32	0.27	0.998
M2	0.44	0.56	0.43	0.54	0.44	0.56	0.69	0.87	0.986
M3	0.28	0.30	0.53	0.57	0.38	0.41	0.60	0.65	0.981
M4	0.30	0.30	0.18	0.18	0.23	0.23	0.40	0.40	0.993
M5	0.24	0.54	0.19	0.41	0.24	0.53	0.36	0.81	0.980
M6	0.23	0.70	0.22	0.68	0.29	0.90	0.40	1.24	0.951
M7	0.20	1.04	0.19	0.95	0.23	1.18	0.33	1.70	0.980
M8	0.41	0.49	0.46	0.55	0.49	0.60	0.72	0.87	0.968
M9	0.38	0.35	0.24	0.22	0.36	0.33	0.55	0.51	0.965
M10	0.38	0.37	0.41	0.40	0.40	0.39	0.62	0.60	0.927

Interobserver TEM and %TEM

The interobserver TEMs for the **digital measurements** were similar or slightly greater than the intraobserver TEMs, varying from 0.29 mm to 0.83 mm (**Table 3**). The %TEMs ranged from 0.34% to 2.51%. The largest interobserver %TEM was also observed for the M7. The mean interobserver %TEM obtained by all 10 digital measurements was 0.92%.

The interobserver TEM for the **direct measurements** varied from 0.23 mm to 0.49 mm (**Table 4**). The %TEM values were up to 1.18%. The mean %TEM for the direct measurements was 0.53%, which is approximately twice less than the mean %TEM established for the digital ones.

The mean interobserver TEMs did not exceed substantially the intraobserver TEMs. The intra-method differences between intra- and interobserver TEM and %TEM values were 0.11 mm and 0.17% for the digital measurements and 0.03 mm and 0.05% for the direct ones (calculations based on the averaged mean intraobserver TEM and %TEM of both observers).

Total TEM

All digital and direct measurements showed total TEMs below the 5% threshold, so the measurement errors were classified as acceptable. The largest total %TEM concerned the M7 and amounted to 2.18% for the digital and 1.70% for the direct measuring method.

R of digital and direct measurements

The coefficients of reliability showed that almost all **digital measurements** had values above 0.95, except for two measurements (M9 and M10), whose R values were below this threshold (**Table 3**). This result was indicative for low imprecision and demonstrated good repeatability of the mandibular measurements, especially the most used ones (M1-M7). On the other hand, only one of the **direct measurements** (M10) showed excessive variability ($R < 0.95$).

The most reliable measurements ($R > 0.99$) obtained on 3D models were M1 and M2. Concerning the direct measuring method, the most precise ones were M1 and M4.

Interobserver and inter-method comparisons of TEMs

The paired t-test did not establish statistically significant differences between the TEMs obtained by both observers ($p > 0.05$), which means that measurements produced by both observers were consistent. However, statistically significant differences were observed between the measurement errors of both measuring methods ($p < 0.05$). This was most likely due to the more consistent direct measurements performed by the observers compared to the digital ones.

Discussion

The precision of the digital measurements acquired from 3D CT bone models and the comparison of the obtained measurement error with the corresponding one of the direct bone measurements are very important topics for all anthropological subfields dealing with 3D models, especially forensic anthropology and paleoanthropology. Anthropometric measurement error is unavoidable, but could be minimized considering all aspects of the data collection process [14]. According to Harris and Smith [5], the landmark location is the major source of variability, since it depends mostly on the human judgement.

In previous studies using intraclass correlation coefficient for assessment of the reliability [12, 13], the mandibular measurements obtained by cone beam CT (CBCT) imaging were revealed to be highly reliable and reproducible. In our study, the digital measurements were assessed as highly precise based on the TEM widely used in an-

thropometry. According to the assumed 5% threshold of the total TEM, the measurement errors of all mandibular measurements from both measuring techniques were classified as acceptable. However, in some anthropometric studies, the acceptable levels for intra- and interobserver %TEM of the linear measurements were set at 1.5% and 2% for beginning anthropometrists and at 1% and 1.5% for skillful anthropometrists [9]. Thus, taking into account the acceptable level for intraobserver measurement error, the three digital measurements with smallest magnitude (M5, M6, and M7) were above the limit of 1% for both observers. According to the direct measurements, the M7 from the measurements of the first observer was the only one with %TEM over 1%, which illustrated again the least precision observed for this measurement. The interobserver %TEM, respectively, was above 1.5% for M6 and M7 from the digital measurements. Considering the conventional measuring method, there was no one measurement to pass the limit of 1.5% for interobserver measurement error. The interobserver absolute TEMs and %TEMs ranged within or slightly exceeded the intraobserver values. However, it has been noticed that the interobserver TEM was more susceptible to error [3].

The results of R showed that most of the digital and direct measurements had $R > 0.95$. Such values above 0.95 have been reported as indicative of good quality control [4]. However, in some studies, it has also been used a cut-off of 0.90 [2] or 0.75 [6, 10]. In case of accepting these thresholds, all digital and direct measurements in our study passed them.

Comparing the %TEM of both measuring techniques, we established lower %TEM values for direct bone measurements compared to the digital ones. Similar results were obtained by Franklin et al. [2]. However, Berco et al. [1] established that the CBCT-derived measurements tended to be more precise than the direct anthropometric standard. Although the direct measurements in our study were more precise, as a whole, the mean differences between both methods were very small (Observer I: TEM – 0.16 mm, %TEM – 0.32%; Observer II: TEM – 0.14 mm, %TEM – 0.23%).

Conclusion

The digital linear measurements taken on 3D models of human mandibles appeared to be highly precise (total TEM < 5%) with minimal measurement error and could be used for anthropometric research purposes. Taking into account the coefficients of reliability, almost all of the measurements indicated high reliability ($R > 0.95$).

Acknowledgement: This study was supported by the "Program for Career Development of Young Scientists, BAS", research grant DFNP – 75/27.04.2016.

The authors would like to acknowledge the kind assistance given by the staff of the National Museum of Military History, Bulgaria.

References

1. **Berco, M., P. H. Rigali, Jr, M. R. Miner, S. DeLuca, N. K. Anderson, L. A. Will.** Accuracy and reliability of linear cephalometric measurements from cone-beam computed tomography scans of a dry human skull. – Am. J. Orthod. Dentofac. Orthop., **136**, 2009, 17.e1-9.
2. **Franklin, D., A. Cardini, A. Flavel, A. Kuliukas, M. K. Marks, R. Hart, C. Oxnard, P. O'Higgins.** Concordance of traditional osteometric and volume-rendered MSCT interlandmark cranial measurements. – Int. J. Legal. Med., **127**, 2013, 505-520.

3. **Gómez-Cabello, A., G. Vicente-Rodríguez, U. Albers, E. Mata, J. A. Rodriguez-Marroyo, P. R. Olivares, N. Gusi, G. Villa, S. Aznar, M. Gonzalez-Gross, J. A. Casajús, I. Ara.** Harmonization process and reliability assessment of anthropometric measurements in the elderly EXERNET multi-centre study. – PLoS ONE, **7**(7), 2012, e41752.
4. **Goto, R., C. G. N. Mascie-Taylor.** Precision of measurement as a component of human variation. – J. Physiol. Anthropol., **26**, 2007, 253-256.
5. **Harris, E. F., R. N. Smith.** Accounting for measurement error: a critical but often overlooked process. – Arch. Oral. Biol., **54**(Suppl 1), 2009, S107-S117.
6. **Hemy, N.** Stature and sex estimation using anthropometry of feet and footprints in a Western Australian population. – Thesis, Perth, University of Western Australia, 2012.
7. **Lottering, N., D. M. MacGregor, M. D. Barry, M. S. Reynolds, L. S. Gregory.** Introducing standardized protocols for anthropological measurement of virtual subadult crania using computed tomography. – Journal of Forensic Radiology and Imaging, **2**, 2014, 34-38.
8. **Martin, R., K. Saller.** Kraniometrische Technik. – In: Lehrbuch der Anthropologie (Eds R. Martin, K. Saller), Band I, Stuttgart, Gustav Fischer, 1957.
9. **Perini, T. A., G. L. de Oliveira, J. S. Ornelia, F. P. de Oliveira.** Technical error of measurement in anthropometry. – Rev. Bras. Med. Esporte, **11**, 2005, 86-90.
10. **Reynolds, M. E., D. Franklin, M. A. Raymond, I. Dadour.** Bloodstain measurement using computer-fitted theoretical ellipses. – Journal of Forensic Identification, **58**(4), 2008, 469-484.
11. **Richard, A. H., C. L. Parks, K. L. Monson.** Accuracy of Standard Craniometric Measurements Using Multiple Data Formats. – Forensic Sci. Int., **242**, 2014, 177-185.
12. **Tarazona-Álvarez, P., J. Romero-Millán, D. Peñarrocha-Oltra, M. Á. Fuster-Torres, B. Tarazona, M. Peñarrocha-Diago.** Comparative study of mandibular linear measurements obtained by cone beam computed tomography and digital calipers. – J. Clin. Exp. Dent., **6**(3), 2014, e271-e274.
13. **Tomasi, C., E. Bressan, B. Corazza, S. Mazzoleni, E. Stellini, A. Lith.** Reliability and reproducibility of linear mandible measurements with the use of a cone-beam computed tomography and two object inclinations. – Dentomaxillofacial Radiology, **40**, 2011, 244-250.
14. **Ulijaszek, S. J., D. A. Kerr.** Anthropometric measurement error and the assessment of nutritional status. – Br. J. Nutr., **82**, 1999, 165-77.
15. **Ulijaszek, S. J., J. A. Lourie.** Intra- and inter-observer error in anthropometric measurement. – In: Anthropometry: The individual and the population. (Eds S. J. Ulijaszek, C. G. N. Mascie-Taylor), Cambridge, Cambridge University Press, 1994.

Institute of Experimental Morphology, Pathology and Anthropology with Museum
Bulgarian Anatomical Society

Acta morphologica et anthropologica, 23
Sofia ● 2016

Stress Levels and Risks among Casino Employees in Bulgaria

Vl. Vodenicharov[1], E. Vodenicharov[1], K. Mitov[2], Z. Stoyneva[3], I. Ivanova[4]

[1]Department of Hygiene, Medical Ecology and Nutrition, Medical University, 1612 Sofia, Bulgaria
[2]Department of Organization and Economics of Pharmacy, Medical University - Sofia, Bulgaria
[3]Department of Occupational Diseases, St. Ivan Rilski University Hospital, Medical University – Sofia, Bulgaria
[4]Department of Clinical Laboratory, St. Ivan Rilski University Hospital, Sofia, Bulgaria

The aim of this study was to measure the stress level and the risk of developing high levels of stress among female and male casino workers in Bulgaria. This quantitative study was conducted on 388 casino employees (221 women and 167 men) from 18 casinos, who completed Perceived Stress Scale questionnaire. The results show higher stress levels and risks of developing stress among the group of female casino workers.

Key words: work stress, casino workers, gender, Perceived Stress Scale.

Introduction

Stress has become a part of modern working life, but it can lead to increased rates of occupational stress and stress-related disorders [1, 2, 10]. Gender is one of the most important determinants of human health [6] and male and female possessed different capabilities of dealing with stress and understandings of what is stressful [1, 2, 5, 6, 11].

Casino employees experienced high levels of work stress [3, 8, 11] compared to other occupations and the general workforce [4, 9, 11] and have to be well prepared for meeting the requirements of their occupation [4, 11]. Furthermore, in the light of the above data, the purpose of the present study was to examine general levels of stress and their gender distribution in 18 casinos in the territory of Bulgaria.

Materials and Methods

In order to determine the general levels of stress among casino employees in this study, we used the Bulgarian adaptation of Perceived stress scale (PSS) [7]. There are three versions of the questionnaire. We used the 10 item version for the purposes of this study. There were 388 participants (221 women and 167 men) from 18 casinos who completed the questionnaire. The results were statistically processed with MED CALC.

The general stress levels for each of the participants were measured as the sum of the points of the answers to each of the 10 questions from the test. Data for general stress levels of those persons is written as variable general levels of stress (Total_T2). Classification of general stress levels for each of the participants was done in accordance with the code table of the questionnaire in one of these three categories: code "0" – no stress, code "1" – moderate level of stress, and code "2" – high level of stress.

Results and Discussion

Descriptive statistics, frequency and graphical analysis have been performed to evaluate the data for Total_T2 among men and women working in casinos. The data for these two groups (221 women and 167 men from 18 casinos) have equal variances and among them there are no highly diverted from their mean value. Data for the group of women are normally distributed, but not those from the group of men (**Table 1**).

Comparative analysis of the mean of data for general levels of stress is used in the groups of working women and men in casinos. The comparison is done with Kruskal-Wallis test, which in the case of two variables gives identical results to those of the test of Mann-Whitney for independent samples (**Table 2**).

Table 1. Data for the group of women are normally distributed, but not those from the group of men

	Gender							
	female				male			
	N	Mean	**SD**	Normal Distr.	N	Mean	SD	Normal Distr.
Total_T2	221	17.597	5.5453	0.2961	167	15.048	5.7955	0.0288

Table 2. General levels of stress in the group of working women and men in casinos

Descriptive statistics						
Factors	N	Minimum	25th percentile	Median	75th percentile	Maximum
Female	221	3.000	14.000	17.000	21.000	34.000
Male	167	4.000	11.000	15.000	19.000	33.000
Kruskal-Wallis test						
Test statistic						19.3743
Corrected for ties Hit						19.4313
Degrees of Freedom (DF)						1
Significance level						P = 0.000010
Factor				N		Average Rank
(1) female				221		216.29
(2) male				167		165.67

It was found that there was a highly statistically significant difference ($P < 0.0001$) at the average rank of these two groups (216.29 for the group of women, and 165.67 for the group of men). This means that there are statistically significant higher levels of stress in the group of working women than in the group of men.

Comparing risks of developing high stress levels among men and women displays 3.74 greater risk for stress among working women than men (**Table 3**).

Table 3. Risks of developing high stress levels among men and women. This risk is statistically significant ($P < 0.0001$) and with 95% confidence interval will vary from 2.42 to 5.79

Outcome	Code_for_T2_results			Relative risk & Odds ratio	
Group	Gender			Exposed group: female	
Outcome	Group			Relative risk	3.740
	female	male		95% CI	2.4176 to 5.7874
0	122	147	269 (69.3%)	z statistic	5.924
1	99	20	119 (30.7%)	Significance level	$P < 0.0001$
	221	167	388		

The principal findings were as follows: First, the group of women is normally distributed, but not those from the group of men. These results are generally similar to those observed in previous studies [1, 2]. Second, our data provide the evidence that there are statistically higher levels of stress and risk of developing stress in the group of working women than in the group of men.

Conclusion

The results show higher general stress levels among working women in casinos than men. The risk of developing stress is also higher in the group of women. The study of the levels of stress and risk of developing stress has never been done before among Bulgarian casino employees. These new data may open the way to new studies in working stress and perhaps, one of the future challenges for Bulgarian casinos will be integrating stress prevention and awareness programs to sensitize gaming employees to problems related to stress.

Acknowledgement: This work was supported by the Council for Science, Medical University, Sofia (project No 311 / 15.01.2015).

References

1. **Ahlberg, J., M. Könönen, M. Rantala, S. Sarna, H. Lindholm, M. Nissinen, K. Kaarent, A. Savolainen.** Self-reported stress among multiprofessional media personnel. – Occup. Med. (Lond), **53**(6), 2003, 403-405.
2. **Gabriel, P., M-R Liimatainen.** In: Mental Health in the Workplace, Introduction, International Labour. Office, Geneva, 2000, pp. 1-27.
3. **Hing, N., S. Gainsbury.** Risky business: gambling problems amongst gaming venue employees in Queensland, Australia. – J. Gambl. Issues, **25**(1), 2011, 4-23.

4. **Hu, S. X., A. Luk, C.U.C. Leong, F. Van.** The correlations of work conditions with unhealthy lifestyles and occupational health problems of casino croupiers in Macau. – J. Gambl. Stud., **29**(2), 2013, 255-268.
5. **Juster, R-P., M. L. Hatzenbuehler, A. Mendrek, J. G. Pfaus, N. G. Smith, P. J. Johnson, J. P Lefebvre-Louis, C. Raymond, M. F. Marin, S. Sindi, S. J. Lupien, J. C. Pruessner.** Sexual Orientation Modulates Endocrine Stress Reactivity. – Biol. Psychiatry, **77**(7), 2015, 668-676.
6. **Kajantie, E., D. I. Phillips.** The effects of sex and hormonal status on the physiological response to acute psychosocial stress. – Psychoneuroendocrinology, **31**(2), 2006, 151-178.
7. **Karastoyanov, G., A. Russinova-Hristova.** Bulgarian version of the Perceived Stress Scale, Psychological Res., **1-2**, 2000, 67-77.
8. **Lee, T. K., R. A. Labrie, H. S. Rhee, H. J. Shaffer.** A study of South Korean casino employees and gambling problems. – Occup. Med. (Lond), **58**(3), (2008) 191-197.
9. **Shaffer, H. J., M. N. Hall.** The natural history of gambling and drinking problems among casino employees. – J. Soc. Psychol., **142**(4), 2002, 405-424.
10. **Smith, A., C. Brice, A. Collins, V. Matthews, R. McNamara.** The scale of occupational stress: A further analysis of the impact of demographic factors and type of job. HSE Books. – Contact Res. Report, **311**, 2000, 1-61.
11. **Wong, I. L. K., P. S. Lam.** Work stress and problem gambling among Chinese casino employees in Macau. – Asian J. Gambling Issues and Public Health, **3**(7), 2013, 1-16.
12. **Wu, A, E. Wong.** Disordered gambling among Chinese casino employees. – J. Gambling Studies, **24(**2), (2008), 207-218.

Corresponding author:
e- mail: vlayko_vodenicharov@abv.bg

Institute of Experimental Morphology, Pathology and Anthropology with Museum
Bulgarian Anatomical Society

Acta morphologica et anthropologica, 23
Sofia ● 2016

Anthropometric Nutritional Status and Arterial Blood Pressure in 7-10 Years Old Children

I. Yankova, Y. Zhecheva, A. Nacheva

Institute of Experimental Morphology, Pathology and Anthropology with Museum, Bulgarian Academy of Sciences

The aim is to evaluate the associations of anthropometric nutritional status and abdominal obesity with arterial blood pressure (ABP) among 7-10 years old Bulgarian children. A total of 820 children (410 boys and 410 girls) aged 7-10 years were studied during the period 1993-2002. Body mass index (BMI) was calculated. Waist circumference (WC) and ABP were measured. Boys were heavier and had a higher mean BMI, WC and ABP than girls. The frequency of overweight boys and girls was 12.4% and 13.7%, respectively. Overall, 13.7% of the boys and 13.2% of the girls were abdominally obese (WC ≥ 90th percentile). The prevalence rates of prehypertension and hypertension were 4.5% and 0.45%, respectively in both genders. The correlations between BMI, WC and ABP in both sexes were positive and statistically significant. They were higher and highly significant in boys than in girls. BMI and WC values influenced the ABP values in schoolchildren.

Key words: body mass index, waist circumference, overweight, blood pressure, schoolchildren.

Introduction

Overweight and obesity are serious public health problem. The prevalence of obesity is rising rapidly during the last years and affects ever more children and adolescents. Childhood obesity is an important predictor of adult obesity [11, 21, 24]. More than 60% of children who are overweight before puberty will be overweight in early adulthood, which will probably reduce the age at which will occur variety of non-communicable diseases [9]. Furthermore, it is observed increased frequency of hypertension in childhood, especially of the essential, which manifests mainly in adolescence and more than 75% associated with overweight and obesity [27]. High blood pressure during childhood is a significant predictor of cardiovascular, metabolic and other diseases in adults [2, 7]. These findings are evidence of the importance of the discovery of high blood pressure during childhood, before the complications of this disease can lead to health problems later in life.

The aim of this report is to evaluate the associations of anthropometric nutritional status, and abdominal obesity with arterial blood pressure among 7-10 years old Bulgarian children.

Materials and Methods

During the period 1993-2002, totally 820 children from Sofia aged 7-10 years, of which 410 boys and 410 girls, distributed in four age groups were studied. The data of three directly measured anthropometric features - stature (St, cm), weight (W, kg) and waist circumference (WC, cm), and also arterial blood pressure (ABP, mmHg) were analyzed. The anthropometric measurements were carried out according to the Martin-Saller's classical method [14]. Blood pressure (BP) was measured with mechanical sphygmomanometer and stethoscope on the right arm, in sitting position.

On the basis of the data about stature and body weight, for each one of the studied individual the body mass index (BMI, kg/m^2) was calculated by the formula: Weight (kg)/Stature (m^2). The individuals were distributed into the categories underweight, normal weight, overweight and obese, according to the BMI cut-off points for 2-18 years old children, recommended by International Obesity Task Force (IOTF) and recently updated by Cole and Lobstein [4].

The distribution of children, according to the waist circumference values, into the categories under norm, norm and abdominal obesity was made in accordance with percentile cutoffs for European children (IDEFICS study 2007-2010) [19]:

WC $\leq P_{10}$ is taken as under norm;

WC between P_{10} and P_{90} is taken as norm;

WC $\geq P_{90}$ is taken as central obesity.

The evaluation of ABP as normal, high-normal BP (prehypertension) and hypertension was defined in accordance with the recommendations in the Fourth Report on the Diagnosis, Evaluation, and Treatment of High Blood Pressure in Children and Adolescents [20]. But for categorization of investigated children into four categories of ABP including hypotension was used percentile cutoffs for European children (IDEFICS study 2007-2010) [1]:

ABP $\leq P_3$ is taken as hypotension;

ABP between P_3 and P_{90} is taken as normal tension;

ABP between P_{90} and P_{97} is taken as high but normal ABP (prehypertension) and were considered to be an indication of heightened risk for developing hypertension;

ABP $\geq P_{97}$ is taken as hypertension.

The collected data were analysed by statistical software package SPSS 16.0. Mean and standard deviation for each of the anthropometric measurements and indexes were calculated. The frequency distribution of children from each gender and age into BMI, WC and ABP categories was made. Statistically signifficant differences between genders and age were evaluated by T-test of Student at P-level ≤ 0.05. Categorical variables were expressed as numbers (n) and percentages (%), and were compared by gender and age using the Chi-square test at P-level ≤ 0.05. The correlation analysis was used for the assessment of relationship between investigated morphological and functional features.

Results

The mean values of anthropometric (weight, height, BMI, and WC), and ABP (SBP and DBP) data for each gender and age are presented in **Table 1**. The values of anthropometric features and ABP increased with age in both genders. Boys were heavier and had a higher mean BMI, WC and ABP than girls. They had a significantly larger waist on 7 and 8 years of age and significantly higher SBP values on 8 years, compared to girls. Significant differences between separate age groups there were in the mean values of stature, body weight and waist circumference, systolic and diastolic blood pressure du-

ring the whole age period in both genders. There were no significance between values of waist circumference and systolic blood pressure in girls aged 7-8 and 9-10 years. The significant differences in the means of BMI were observed only between 8-9 years of age in both boys and girls.

Table 1. Data of the investigated features in 7-10 years old children

Age	Sex	N	Features											
			Stature		Body weight		Waist circumference		Body mass index		Systolic BP		Diastolic BP	
			mean	SD	mean	SD	mean	SD	mean	SD	mean	SD	mean	SD
7	♂	110	125.78	5.83	25.84	4.53	54.77*	4.60	16.24	1.95	91.56	10.25	53.20	8.97
	♀	110	125.85	5.23	25.55	4.48	53.33	4.86	16.06	2.04	91.36	8.80	53.04	8.69
8	♂	100	131.01#	5.93	28.22#	5.01	56.91*#	4.60	16.35	1.97	96.24*#	8.51	59.43#	7.86
	♀	101	130.52#	5.13	27.37#	4.51	55.05#	4.51	15.99	1.96	93.42	9.27	57.41#	7.72
9	♂	100	136.48#	5.94	32.39#	6.50	58.47#	5.59	17.27#	2.54	99.50#	7.50	65.74#	6.76
	♀	101	137.56#	6.47	32.88#	7.48	57.45#	6.00	17.23#	2.84	97.98#	7.51	64.93#	6.71
10	♂	100	142.05#	7.14	36.28#	8.68	60.97#	6.89	17.79	2.92	103.58#	9.17	68.79#	7.91
	♀	98	142.30#	6.44	35.81#	7.44	59.16	6.40	17.57	2.86	103.52#	9.03	68.56#	7.08

* Statistically significant gender differences at $P \leq 0.05$

Statistically significant interage differences at $P \leq 0.05$

Table 2 presents the percentage distribution of the investigated children from the various age groups, according to the categories of BMI and WC. Among the studied 7-10 years old children 75.9% of boys and 70.7% of girls have normal weight. Underweight was observed in 8.5% of boys and 13.4% of girls. The frequency of overweight boys and girls (without obesity) was 12.4% and 13.7% respectively. The frequency of children with obesity was 3.2% for boys and 2.2% for girls, as it reached 3.6% in girls of 7 years of age, and 5.0% in boys aged 10 years. Differences between genders and age groups were insignificant.

The prevalence of WC in the 10th – 90th percentile was, respectively, 70.5% and 63.9% of the entire group of the studied individuals. Overall, 13.7% of the boys and 13.2% of the girls were abdominally obese (WC ≥ 90th percentile). A higher percentage of abdominal obesity was found in children of 10 years of age from both genders. There were no significant sexual and interage differences in the percentage distribution of children into categories.

Table 2. Percentage distribution of children, according to the body mass index and waist circumference categories

Age/Sex/n	BMI				WC		
	1	2	3	4	1	2	3
	n (%)	n (%)	n (%)	n (%)	n (%)	n (%)	n (%)
7 y ♂ (110)	7 (6.4)	86 (78.2)	14 (12.7)	3 (2.7)	24 (21.8)	76 (69.1)	10 (9.1)
♀ (110)	10 (9.1)	83 (75.5)	13 (11.8)	4 (3.6)	23 (20.1)	73 (66.4)	14 (12.7)
8 y ♂ (100)	8 (8.0)	80 (80.0)	10 (10.0)	2 (2.0)	12 (12.0)	77 (77.0)	11 (11.0)
♀ (101)	14 (13.9)	75 (74.3)	12 (11.9)	0	20 (19.8)	71 (70.3)	10 (9.9)
9 y ♂ (100)	8 (8.0)	75 (75.0)	14 (14.0)	3 (3.0)	15 (15.0)	71 (71.0)	14 (14.0)
♀ (101)	16 (15.8)	66 (65.3)	16 (15.8)	3 (3.0)	26 (25.7)	62 (61.4)	13 (12.9)
10 y ♂(100)	12 (12.0)	70 (70.0)	13 (13.0)	5 (5.0)	14 (14.0)	65 (65.0)	21 (21.0)
♀ (98)	15 (15.3)	66 (67.3)	15 (15.3)	2 (2.0)	25 (25.5)	56 (57.1)	17 (17.3)
Total ♂(410)	35 (8.5)	311 (75.9)	51 (12.4)	13 (3.2)	65 (15.9)	289 (70.5)	56 (13.7)
♀ (410)	55 (13.4)	290 (70.7)	56 (13.7)	9 (2.2)	94 (22.9)	262 (63.9)	54 (13.2)

BMI – body mass index; 1 – Thinness; 2 – Norm; 3 – Overweight; 4 – Obesity;
WC – waist circumference; 1 – WC ≤ P_{10}; 2 – WC between P_{10} – P_{90}; 3 – WC ≥ P_{90}

Table 3. Percentage distribution of children, according to the arterial blood pressure categories

Age/Sex/n	Systolic blood pressure				Diastolic blood pressure			
	1	2	3	4	1	2	3	4
	n (%)	n (%)	n (%)	n (%)	n (%)	n (%)	n (%)	n (%)
7 y ♂ (110)	29(26.4)	77 (70.0)	3 (2.7)	1 (0.9)	58 (52.7)	48 (43.6)	4(3.6)	0
♀ (110)	31 (28.2)	77 (70.0)	2(1.8)	0	57 (51.8)	49 (44.5)	4 (3.6)	0
8 y ♂ (100)	9 (9.0)*#	85 (85.0)	5 (5.0)	1(1.0)	16 (16.0)#	76 (76.0)#	7 (7.0)	1 (1.0)
♀ (101)	28 (27.7)	69 (68.3)	4 (4.0)	0	26 (25.7)#	71 (70.3)	4 (4.0)	0
9 y ♂ (100)	3 (3.0)	94 (94.0)	3 (3.0)	0	0 #	81 (81.0)	19 (19.0)	0
♀ (101)	4 (4.0) #	96 (95.0)	1 (1.0)	0	4 (4.0) #	86 (85.1)	11 (10.9)	0
10 y ♂(100)	2 (2.0)	88 (88.0)	9 (9.0)	1 (1.0)	0	65 (65.0)	33 (33.0)	2 (2.0)
♀ (98)	0	87 (88.8)	10 (10.2)	1 (1.0)	0	73 (74.5)	22 (22.4)	3 (3.1)
Total ♂(410)	43 (10.5)	344 (83.9)	20 (4.9)	3 (0.7)	74 (18.0)	270 (65.9)	63 (15.4)	3 (0.7)
♀ (410)	63 (15.4)	329 (80.2)	17 (4.1)	1 (0.2)	87 (21.2)	279 (68.0)	41 (10.0)	3 (0.7)

1 – Hypotension; 2 – Normal ABP; 3 – High but normal ABP (prehypertension); 4 – Hypertension
* Statistically significant gender differences at P ≤ 0.05
# Statistically significant interage differences at P ≤ 0.05

Table 3 shows the percentage distribution of children according to the categories of systolic and diastolic blood pressure. Overall, the prevalence rates of prehypertension and hypertension, according to SBP were low - 4.5% (4.9% for boys and 4.1% for

girls), and 0.45% (0.7% for boys and 0.2% for girls), respectively. Boys were more often normotensive than girls (83.9% and 80.2%, respectively). The younger participants (aged 7-8 years) were more likely to have hypotension than the older children (aged 9-10 years). The children aged 10 years were more likely to have prehypertension and hypertension than these aged 7-9 years (9.0% till 10.0% versus 1.0% till 5.0%). There were statistically significant differences in the percentage distribution of the studied boys and girls only in 8-year-old hypotonic children. Significant interage differences in the percentage distribution of children according to SBP categories were established between 7 and 8 years in boys and between 8 and 9 years in girls of the hypotensive group. Significant differences in percentage distribution of children according to DBP categories were found between 7 and 8, 8 and 9 years for both genders in the hypotension category and between 7- 8-year-old normotensive boys.

The correlation coefficients between systolic and diastolic blood pressure and investigated anthropometric features and BMI were presented in **Table 4**. The correlations in both genders were positive and statistically significant ($p < 0.05$; $p < 0.001$), except for the relationship between diastolic blood pressure and stature in girls of 7 and 8 years of age ($p > 0.05$). The correlation coefficients between ABP and anthropometric measures were higher and highly significant in boys ($r = 0.194 \div 0.812$) than in girls ($r = 0.139 \div 0.800$).

Table 4. Correlation coefficients between arterial blood pressure, body mass index and anthropometrical features

Sex	Age (n)	Correlation coefficients								
		SBP/ DBP	**SBP/ Stature**	**SBP/ Weight**	**SBP/ BMI**	**SBP/ WC**	**DBP/ Stature**	**DBP/ Weight**	**DBP/ BMI**	**DBP/ WC**
Boys	7 y (110)	0.752**	0.302**	0.489**	0.468**	0.453**	0.194*	0.356**	0.367**	0.352**
	8 y (100)	0.812**	0.339**	0.579**	0.572**	0.578**	0.258**	0.549**	0.588**	0.540**
	9 y (100)	0.747**	0.433**	0.557**	0.497**	0.496**	0.312**	0.391**	0.344**	0.370**
	10 y (100)	0.801**	0.504**	0.617**	0.560**	0.586**	0.417**	0.566**	0.550**	0.529**
Girls	7 y (110)	0.752**	0.263**	0.302**	0.226*	0.235*	0.139	0.238*	0.219*	0.257**
	8 y (101)	0.800**	0.306**	0.431**	0.386**	0.391**	0.179	0.276**	0.265**	0.307**
	9 y (101)	0.607**	0.459**	0.458**	0.356**	0.453**	0.343**	0.451**	0.393**	0.383**
	10 y (98)	0.751**	0.473**	0.471**	0.350**	0.374**	0.409**	0.534**	0.465**	0.494**

SBP – Systolic blood pressure; DBP – Diastolic blood pressure; BMI – body mass index; WC – waist circumference;
** Correlation is significant at the 0.01 level (2-tailed); * Correlation is significant at the 0.05 level (2-tailed).

Table 5 presents average values of WC and ABP, according to the BMI categories.

Table 5. Data of BMI, waist circumference and arterial blood pressure, according to BMI categories

Age	BMI categories	N	Boys								N	Girls							
			BMI		WC		SBP		DBP			BMI		WC		SBP		DBP	
			mean	SD	mean	SD	mean	SD	mean	SD		mean	SD	mean	SD	mean	SD	mean	SD
7	1	7	13.63	0.42	50.47	2.12	83.14	8.07	48.57	5.13	10	13.30	0.53	49.83	3.24	87.70	8.27	48.10	5.63
	2	86	15.78	0.98	53.87	3.04	90.92	9.17	52.92	9.17	83	15.66	1.11	52.39	3.60	91.47	9.19	53.28	8.75
	3	14	18.93	0.92	59.24	3.69	96.21	11.64	54.64	7.84	13	18.83	0.62	57.82	3.51	92.54	4.61	54.23	10.06
	4	3	23.04	2.54	69.83	8.74	108.00	16.00	65.33	5.03	4	22.27	0.46	67.10	4.35	94.50	12.15	56.50	7.00
8	1	8	13.82	0.41	52.88	2.45	95.00	5.35	56.88	3.72	14	13.45	0.56	50.27	2.58	89.29	11.58	53.79	8.22
	2	80	16.02	1.18	56.23	3.46	94.33	6.71	57.98	6.75	75	15.84	1.14	54.79	3.38	93.20	8.25	57.60	7.23
	3	10	19.61	0.80	62.81	4.91	109.30	9.21	70.00	7.82	12	19.93	0.78	62.20	3.79	99.58	10.10	60.42	9.16
	4	2	23.43	1.12	70.60	2.26	112.50	10.61	75.00	7.07	0								
9	1	8	13.66	0.62	53.39	2.25	93.75	6.41	62.63	6.93	16	13.75	0.72	51.69	1.54	93.44	3.01	60.63	5.12
	2	75	16.67	1.34	57.09	3.52	99.00	7.07	65.17	6.42	66	16.77	1.29	56.52	4.10	98.53	7.88	65.65	6.65
	3	14	20.94	1.09	65.78	4.73	103.21	6.68	70.00	7.07	16	20.98	1.11	63.49	3.56	98.63	7.63	63.75	4.65
	4	3	24.65	1.28	72.43	9.06	110.00	10.0	68.33	7.64	3	26.01	1.82	76.33	4.51	106.67	2.89	78.33	2.89
10	1	12	14.45	0.31	54.46	2.64	100.08	7.99	67.42	7.43	15	14.13	0.67	52.15	2.18	100.67	7.99	63.67	4.42
	2	70	17.15	1.54	59.25	3.66	101.74	7.92	66.89	6.93	66	17.07	1.43	58.10	4.06	103.18	9.23	68.27	6.83
	3	13	21.14	0.86	68.70	2.89	109.62	7.49	75.23	6.51	15	22.23	1.37	69.46	3.79	106.33	8.12	73.87	6.76
	4	5	26.19	1.34	80.54	7.01	122.00	4.47	82.00	4.47	2	24.97	0.21	69.50	4.95	115.00	7.07	75.00	7.07

BMI – body mass index; WC – waist circumference; SBP – Systolic blood pressure; DBP – Diastolic blood pressure;
1 – Underweight; 2 – Normal weight; 3 – Overweight; 4 – Obesity

The results show that the boys and girls who were overweight and obese have higher mean values of the BMI, WC, systolic and diastolic blood pressure compared to their peers with normal weight and underweight during the whole age period. The differences for the average SBP and DBP between children with underweight and obesity were about 15.0-20.0 mmHg.

The results about mean values of the features in accordance with age and nutritional status assessed on the basis of the WC (**Table 6**) show that the children with abdominal obesity (WC ≥ 90th percentile) from four age groups have higher values of BMI, WC and ABP compared to their peers without abdominal obesity. The differences for the ABP values were established between 5.0 and 15.0 mmHg.

Discussion

This study presents the percentage distribution of children according to the categories of BMI, WC and ABP and relationship between anthropometric nutritional status (assessed on the basis of the BMI and WC) and ABP among 7-10 years old schoolchildren.

The body mass index is a measure commonly used to assess the nutritional status. Among the investigated 7-10 years old children frequency of boys with overweight was 12.4% and 13.7% in girls. The prevalence of obesity was 3.2% for boys and 2.2% for girls. A higher percentage of children with overweight and obesity was found in the group of the 9-10-year-olds. The similar frequency of overweight and obesity was established in 9-15 year-old Bulgarian children and adolescents [15]. Lower percent of Turkish children with overweight (7.7%) and similar percent of obese children (3.1%) was revealed by Gundoglu [10]. Other researchers reported for higher percentage of schoolchildren distributed in these categories of nutritional status [16, 26]. The study conducted in Lithuania showed lower prevalence of overweight and obesity among 12- to 15-year-old adolescents, except of overweight boys (14.3% for boys and 10.2% for girls and 2.7% for boys and 2.2% for girls, respectively) [5].

Another specific measurement for assessment of the nutritional status, especially of abdominal obesity, is the waist circumference. In boys of 7 years of age it was 54.8 cm, and in girls – 53.3 cm. The values of the trait increased with age in both genders and reached respectively 61.0 cm and 59.0 cm in 10-year-olds. In other studies carried out in Bulgaria and Greece higher values of WC in children and adolescents above 6 years were established [8, 23, 26]. The overall relative share of schoolchildren with abdominal obesity from our survey was 13.45% (13.7% for boys and 13.2% for girls). The frequency of abdominally obese Greek children was lower in boys (12.5%) and higher in girls (14.2%) compared to Bulgarians [23]. Over 50% of boys and girls with waist circumference > P90 were with overweight and obesity. A high percentage of overweight and obesity in children with waist circumference above the norm was found by Konstantinova [26].

The overweight, general and central obesity are risk factors of metabolic and cardiovascular diseases, including hyprtension, both in adults and children. The average ABP values among the studied 7 years old children was 91.5/53.1 mm Hg, and among the 10-year-olds was 103.5/68.7 mm Hg. Over 70.0% from boys and girls of 7-10 years old had normotensive ABP, and with prehypertension and hypertension were about 5.0% of children. The frequency of boys and girls with hypotension decreased with age, and prevalence of these with prehypertension and hypertension increased. Other studies of children and adolescents show similar results [10, 15, 17].

Table 6. Data of waist circumference, BMI and arterial blood pressure, according to waist circumference categories

Age	WC categories	N	Boys								N	Girls							
			WC		BMI		SBP		DBP			WC		BMI		SBP		DBP	
			mean	SD	mean	SD	mean	SD	mean	SD		mean	SD	mean	SD	mean	SD	mean	SD
7	1	24	49.72	1.26	14.87	0.72	87.37	8.71	50.25	7.52	23	47.80	1.66	14.46	0.75	89.78	10.33	50.52	7.87
	2	76	55.09	2.23	16.14	1.34	91.55	9.45	53.28	9.05	73	53.24	2.18	15.96	1.59	90.85	8.02	52.68	8.50
	3	10	64.52	5.99	20.33	2.43	102.70	13.23	59.70	8.84	14	62.87	3.90	19.20	2.18	96.64	8.76	59.00	8.88
8	1	12	50.80	1.24	14.67	0.75	90.58	3.99	56.25	3.77	20	49.65	1.52	14.25	0.83	90.50	11.91	56.30	9.07
	2	77	56.51	2.71	16.11	1.43	95.66	7.68	58.69	7.66	71	55.27	2.74	16.01	1.63	92.96	7.77	56.86	6.95
	3	11	66.35	2.91	19.88	2.15	106.45	9.76	68.09	7.22	10	64.25	1.77	19.32	1.24	102.50	8.58	63.50	8.18
9	1	15	52.03	0.95	14.60	1.02	94.33	4.57	61.0	4.71	26	51.66	1.08	14.62	1.18	93.65	5.40	61.08	5.91
	2	71	57.70	2.67	16.95	1.57	99.51	7.18	66.18	6.69	62	57.45	3.32	17.35	1.88	98.56	7.31	65.48	6.25
	3	14	69.24	4.71	21.75	2.05	105.00	8.09	68.57	6.91	13	68.98	5.00	21.89	2.79	103.85	7.68	70.00	6.45
10	1	14	53.14	1.14	15.12	1.00	98.43	9.15	64.57	8.08	25	52.04	1.84	14.88	1.21	97.80	5.96	63.20	4.97
	2	65	59.28	2.83	17.01	1.66	101.88	7.59	67.34	6.63	56	59.07	3.03	17.32	1.51	104.64	9.33	69.12	6.48
	3	21	71.40	6.52	22.02	2.63	112.29	8.38	76.10	7.19	17	69.93	3.10	22.35	1.95	108.23	7.89	74.59	6.15

WC – waist circumference; BMI – body mass index; SBP – Systolic blood pressure; DBP – Diastolic blood pressure;
1 – WC < P10; 2 – WC P10 – P90; 3 – WC ≥ P90 (abdominal obesity)

With increasing of BMI and WC the ABP and anthropometric features reached higher mean values. The values of systolic and diastolic blood pressure in children with overweight and obesity were higher compared to these of children with normal weight and underweight. Similar results were observed when comparing the ABP values of schoolchildren with different average waist circumference. In children with waist circumference over P90 (abdominal obesity) was observed higher mean values of SBP and DBP. Increased frequency of ABP in children with overweight and obesity showed a number of studies. According to Bogalusa Heart Study the children with overweight had 2.4-4.5 times higher risk of developing of arterial hypertension [6]. Sorof and Daniels examined the relationship between hypertension and BMI and found that in 94.0% of children with obesity was observed elevated systolic blood pressure [22]. The results obtained from Kolarova-Janeva also suggest that the presence of abdominal obesity and metabolic syndrome is associated with a higher risk of cardiovascular diseases in children [25].

In our report, as well as in the other studies, the variables weight, BMI and WC were positively and significantly associated with ABP values. The correlations between ABP and anthropometric measures were stronger and highly significant in boys than in girls [3, 12, 13, 17, 18].

This fact reinforces the importance of measuring these indicators to detect hypertension and future cardiovascular risks.

Conclusions

The children with overweight and obesity in both genders have higher values of systolic and diastolic blood pressure.

In boys a systolic blood pressure correlated positively with BMI and waist circumference, as in 8- and 10-year old children strength of the correlation is the highest.

In girls, the relationship between BMI, waist circumference and systolic and diastolic blood pressure was positive, but slighter.

The values of BMI and waist circumference affect blood pressure values in children of school age.

References

1. **Barba, G., C. Buck, K. Bammann, C. Hadjigeorgiou, A. Hebestreit, S. Marild, D. Molnár, P. Russo, T. Veidebaum, K. Vyncke, W. Ahrens, L. A. Moreno.** Blood pressure reference values for European non-overweight school children: The IDEFICS study. – International Journal of Obesity, **38**, 2014, 48-56.
2. **Chen, X., Y. Wang.** Tracking of blood pressure from childhood to adulthood: a systematic review and meta-regression analysis. – Circulation, **117**, 2008, 3171-3180.
3. **Choy, C., Y. Huang, Y. Liu, C. Yang, C. Liao, J. Li, W. Chiu, H. Chiou.** Waist circumference as a predictor of pediatric hypertension among normal-weight taiwanese children. – J. Exp. Clin. Med., **3**(1), 2011, 34-39.
4. **Cole, T. J., T. Lobstein.** Extended international (IOTF) body mass index cut-offs for thinness, overweight and obesity. – Pediatr. Obes., **7**, 2012, 284-294.
5. **Dulskiene, V., R. Kuciene, J. Medzioniene, R. Benetis.** Association between obesity and high blood pressure among Lithuanian adolescents: a cross-sectional study. – Italian Journal of Pediatrics, **40**, 2014, 102-111.

6. **Freedman, D. S., W. H. Dietz, S. R. Srinivasan, G. S. Berenson.** The relation of overweight to cardiovascular risk factors among children and adolescents. The Bogalusa heart study. – Pediatrics, **103**, 1999, 1175-1182.
7. **Fuentes, R. M., I. L. Notkola, S. Shemeikka, J. Tuomilehto, A. Nissinen.** Tracking of systolic blood pressure during childhood: a 15-year follow-up populationbased family study in Eastern Finland. – J. Hypertens, **20**, 2002, 195–202.
8. **Galcheva, S., V. Iotova, Y. Yotov, K. Grozdeva, V. Stratev, V. Tzaneva.** Waist circumference percentile curves for Bulgarian children and adolescents aged 6-18 years. – Int. J. Ped. Obes., **4**, 2009, 381-388.
9. Green Paper. Promoting healthy diets and physical activity: a European dimension for the prevention of overweight, obesity and chronic diseases. – Brussels, European Commission, 2005 (COM (2005) 637 final) (http://ec.europa.eu/health/ph_determinants/life_style/nutrition/documents/nutrition_gp_en.pdf).
10. **Gundogdu, Z.** Relationship between BMI and blood pressure in girls and boys. – Public Health Nutrition, **11**(10), 2008, 1085-1088.
11. **Lobstein, T., L. Baur, R. Uauy.** For the IASO International obesity task force. Obesity in children and young people: a crisis in public health. – Obesity Reviews, **5**(1), 2004, 4-85.
12. **Maffeis, C., A. Pietrobelli, A. Grezzani, S. Provera, L. Tatò.** Waist circumference and cardiovascular risk factors in prepubertal children. – Obes. Res., **9**, 2001, 179-187.
13. **Marrodán Serrano, M. D., M. D. Cabañas Armesilla, M .M. Carmenate Moreno, M. González-Montero de Espinosa, N. López-Ejeda, J. R. Martínez Álvarez, C. Prado Martínez, J. F. Romero-Collazos.** Association between adiposity and blood pressure levels between the ages of 6 and 16 years: Analysis in a student population from Madrid, Spain. – Rev. Esp. Cardiol. (Engl. Ed), **66**(2), 2013, 110-115.
14. **Martin, R., K. Saller.** Lehrbuch der Anthropologie in sistematischer Darstellung. – Bd. I. Stuttgart, Gustav Fischer Verlag, 1957, 322-324.
15. **Mitova, Z.** Relation between the nutritional status type and the arterial blood pressure in 9-15-year-old schoolchildren from Sofia. – Acta Morphol. Anthropol., **16**, 2010, 76-87.
16. **Mladenova, S., E. Andreenko.** Prevalence of underweight, overweight, general and central obesity among 8-15-year-old Bulgarian children and adolescents (Smolyan Region, 2012-2014). – Nutr. Hosp., **31**(6), 2015, 2419-2427.
17. **Mladenova, S., E. Andreenko.** The prevalence of high-normal blood pressure and hypertension among 8 to 15-year-old Bulgarian children and adolescents with various nutritional status (Smolyan region, 2012-2014). – Anthropologist, **21**(1, 2), 2015, 51-60.
18. **Moselakgomo, V., A. Toriola, B. Shaw, D. Goon, O. Akinyemi.** Body mass index, overweight, and blood pressure among adolescent schoolchildren in Limpopo province, South Africa. – Rev. Paul. Pediatr., **30**(4), 2012, 562-569.
19. **Nagy, P., E. Kovacs, L. A. Moreno, T. Veidebaum, M. Tornaritis, Y. Kourides, A. Siani, F. Lauria, I. Sioen, M. Claessens, S. Marild, L. Lissner, K. Bammann, T. Intemann, C. Buck, I. Pigeot, W. Ahrens, D. Molnár.** Percentile reference values for anthropometric body composition indices in European children from the IDEFICS study. – International Journal of Obesity, **38**, 2014, 15-25.
20. National High Blood Pressure Education Program Working Group on High Blood Pressure in Children and Adolescents. The fourth report on the diagnosis, evaluation, and treatment of high blood pressure in children and adolescents. – Pediatrics, **114** (2: 4), 2004, 555-576.
21. **Serdula, M. K., D. Ivery, R. J. Coates, D. F. Williamson, T. Byers.** Do obese children become obese adults? A review of the literature. – Preventive Medicine, **22**, 1993, 167-177.
22. **Sorof, J, S. Daniels.** Obesity hypertension in children. A problem of epidemic proportion. – Hypertension, **40**, 2002, 441-447.
23. **Tzotzas, T., E. Kapantais, K. Tziomalos, I. Ioannidis, A. Mortoglou, S. Bakatselos, M. Kaklamanou, L. Lanaras, D. Kaklamanou.** Prevalence of overweight and abdominal obesity in Greek children 6-12 years old: Results from the National Epidemiological Survey. – Hippokratia, **15**(1), 2011, 48-53.

24. **Wang, Y., K. Ge, B. M. Popkin.** Why do some overweight children remain overweight, whereas others do not? – Public Health Nutrition, **6**(6), 2003, 549-558.
25. **Коларова-Янева, Н.** Първична артериална хипертония в детска възраст – епидемиология, основни кардиоваскуларни рискови фактори и възможности за профилактика. Автореф. на дис. труд, Плевен, 2014.
26. **Константинова, М.** Тенденции в разпространението на поднормено, наднормено тегло и затлъстяване сред детското население в България през последните 40 години. Антропометрични, метаболитни и хормонални характеристики на клиничните типове затлъстяване в детска възраст. Автореф. на дис. труд, София, 2015.
27. **Попова, Г.** Наднормено тегло и затлъстяване – основен рисков фактор за артериална хипертония в детска възраст. – Мединфо, **8**, 2011, 48–51.

Institute of Experimental Morphology, Pathology and Anthropology with Museum
Bulgarian Anatomical Society

Acta morphologica et anthropologica, 23
Sofia ● 2016

Review Articles

Proteolytic Enzymes as Biological Markers for Tumor Diseases: Review

M. Dimitrova

Institute of Experimental Morphology, Pathology and Anthropology with Museum, Bulgarian Academy of Sciences, Acad. G. Bonchev Str., bl. 25, 1113 Sofia

Nowadays, about one thousand proteolytic enzymes are isolated and purified from different organisms. According to the catalytic mechanism, the structure of the active center and their tertiary structure, proteases are divided into four main groups – aspartic peptidases, metallopeptidases, cysteine and serine peptidases. Most of them not only perform various physiological functions but are also involved in pathogenic mechanisms of different diseases. The aim of the present mini-review is to outline the main groups of proteases and individual enzymes typically used as biomarkers for tumor diseases as well as to designate certain enzymes that are promising for future application in oncology.

Key words: proteolytic enzymes, biological markers, tumor diseases.

General

In principle, an enzyme can be nominated as biomarker for a disease in case its expression and/or activity levels are different (higher or lower) in pathologically altered tissues in comparison to those in healthy tissues. In such cases, the enzyme levels might be used for diagnostic and/or prognostic purposes. On the other hand, an enzyme can be defined as a target for therapy, if it has been proven beyond any doubt (in experimental model systems) that restoration of its normal levels can slow down or even reverse the pathological process, i.e. it can improve the patient's condition. Therapeutic agents can be:

– At higher enzyme levels – specific enzyme inhibitors or antibodies, small interfering RNA, or other suppressive agents;

– At lower enzyme levels – specific activators, the enzyme itself or its encoding DNA.

The use of proteases as biological markers has long been controversial. The main objection has been related to the low specificity of those enzymes. For example, if a peptidase hydrolyzes a single amino acid (AA) from N- or C-terminal of peptides, usu-

ally it is active to several AAs, e.g. Ala, Met and Cys. If a peptidase hydrolyzes two AAs, one can compile a whole library of potential enzyme substrates in connection with the numerous combinations of 2 AAs. These facts inevitably lead to the assumption that proteases can be interchangeable - if one of them is inactive for some reasons, others can assume its functions. However, over the years a lot of data accumulate that the above assumption is not quite true. Thus, a genetic deficiency of certain proteases leads to the development of serious genetic diseases. Additionally, suppression or overexpression of a number of these enzymes invariably accompanies certain pathological processes and is actually an integral part of them.

Studies on the marker role of enzymes in tumor diseases usually start *in vitro* via comparing their expression/activity levels in tumor cell lines and normal cell lines/primary cell cultures of the same origin. Finding a difference in the enzyme levels suggests a potential marker role, particularly if the altered expression/activity level can be directly correlated with the pathological phenotype of the cells. To verify this, re-expression or inhibition of the enzyme and tracking the effect on the cells are performed. Studies *in vivo* require the use of experimental animals. Intravenous injection leads to a transport of tumor cells with blood and formation of secondary tumors initially in the lung and then in other organs. Subcutaneous injections of tumor cells or subcutaneous xenografts directly transfer the tumor mass in the animals. Determination of the enzyme as a marker requires a number of confirmatory experiments to refine its diagnostic/prognostic significance. Identification of the enzyme as a target for therapy is associated with further complex tests, including clinical trials.

Matrix metallopeptidases (MMPs)

Matrix metallopeptidases are zinc-dependent enzymes. Taken together, they can degrade almost all the components of the extracellular matrix (ECM) – structural proteins, soluble protein components and proteins of the cell surface. Controlled expression of MMPs is connected with a number of physiological processes requiring changes in ECM like fetal development, mammary glands involution after weaning, ovulation, etc. However, abnormal regulation of MMPs leads to different kinds of pathological processes including cancer. Together with two more families of metal-dependent proteases – ADAMs (a disintegrin and metalloproteinase) and ADAMTs (a disintegrin and metalloproteinase with thrombospondin motifs), they participate in the complete formation of the microenvironment in which tumor cells develop [10].

So far, 28 MMPs have been described. Depending on their substrate specificity, they are divided into 4 types: 1. Interstitial collagenases (e.g. MMPs-1, -8 and -13); 2. Gelatinases (e.g. MMPs-2 and -9); 3. Stromelysins (e.g. MMPs-3, -7 and -10); 4. Membrane-type MMPs (e.g. MT-MMP-4). The role of individual MMPs is different in different types of tumors [reviewed in 15]. Additionally, some of them are tumor-promoters at certain stages of the oncological disease but tumor-suppressors at other stages [22]. MMPs participate in practically all processes related to the tumorigenesis and tumor progression.

Effects on the cell growth. Obviously, uncontrolled growth and division is a common feature of tumor cells. MMPs modify both the availability and functioning of growth factors in the cell microenvironment thus changing the balance between signaling molecules which control the cell growth. This may result in an appearance and distribution of tumor cells. For example, the transforming growth factor β (TGF-β) is important for maintaining tissue homeostasis and normally is considered a tumor-suppressor. However, during the tumor growth frequently mutations lead to changes in TGF-β receptor and tumor cells become insensitive to TGF-β. Accumulation of TGF-β

molecules in ECM whereas the tumor cells are insensitive to the factor is associated with an induction of tumor growth and metastasis [23]. MMP-9 is the main enzyme involved in the activation of TGF-β by hydrolyzing its inactive form. On the other hand, MMPs-2 and -14 hydrolyze TGF-β binding protein thus releasing additional active TGF-β in the ECM [6]. In this connection, the high levels of MMP-9 are accepted as a marker of poor prognosis.

Inhibition of apoptosis. Escaping apoptosis is another strategy for accumulation of cancer cells and tumor growth. MMPs accelerate the tumor spreading by blocking the receptor-dependent apoptosis. For example, MMP-7 participates in the formation of neoplastic lesions in the pancreas. This role of the enzyme has been supposed first by using immunohistochemistry [5]. The experiments have shown that the enzyme is not expressed in healthy pancreas. However, during the process of metaplasia from acinar to ductal cells, the metaplastic cells already express it and metaplastic ducts are highly positive for MMP-7. Later studies [9] have revealed the mechanism of MPP-7 involvement in pancreatic adenocarcinoma. The ligand of the Fas-receptor (FasL) which transfers pro-apoptotic signal, is a substrate of MMP-7. Through the hydrolysis of FasL by MMP-7, a soluble form of FasL is obtained, which is a powerful pro-apoptotic agent. On the other hand, by a yet unknown mechanism, MMP-7 induces the expression of anti-apoptotic proteins of Bcl2 family. Thus, the cells receive mixed signals leading to a selection of cells resistant to apoptosis. Those cells are involved in the formation of pancreatic intraepithelial neoplasia. This mechanism is activated in chronic pancreatitis which increases the probability of ductal adenocarcinoma. That is why overexpression of MMP-7 is regarded as a marker for pancreatic adenocarcinoma and resistance to chemotherapy [9].

Tumor vascularization. MMPs participate in angiogenesis by overcoming the physical barrier (degrading of ECM) and by generating pro-angiogenic factors. For example, the vascular endothelial growth factor (VEGF) is bound to ECM molecules and the free VEGF is generated through MMP-9 mediated degradation of collagen [3]. Active MMP-9 is secreted from neutrophils infiltrated in the tumor mass [24]. That is why the high number of infiltrated neutrophils is considered an indicator of intensive angiogenesis. Thus, a prolong treatment of experimental animals with an antibody selectively removing neutrophils from the blood leads to triple reduction of angiogenic lesions [24]. MMP-9 is identified as a target for therapy and it has been supposed to use its selective inhibitors along with radiotherapy in order to increase the positive effects of this treatment.

Regulation of adipocytes. Adipocytes are a part of the tumor stroma and contribute to the tumor progression by secreting products called adipokines. Certain adipokines control the expression and activity of MMPs. In turn, several MMPs regulate the growth and differentiation of adipocytes [30]. One of the most important MMPs influencing adipocytes is the so called stromelysine 3 (ST3). Mice that are deficient in the enzyme (knock-out mice) show a very quick differentiation of embryonal fibroblasts into adipocytes and greater weight and vice versa – treatment of those mice with recombinant ST3 results in a quick degradation of fats and regulation of body weight [1]. So, ST3 decreases pre-adipocytes differentiation and even reverses mature adipocytes into fibroblast-like cells. Accumulation of such cells modifies the tumor stroma so that it can meet the needs of the tumor cells. Therefore, the overexpression of ST3 in the tumor stroma is considered a marker of poor prognosis. The high ST3 gene expression is used to distinguish invasive ductal carcinoma of mammary gland from non-invasive ones.

Initiation of neoplastic progression (epithelial–mesenchymal transition - EMT). The initial process of tumor invasion is accompanied with a loss of cell-cell adhesion and cell polarity of epithelial cells and acquiring of mesenchymal phenotype, i.e. EMT.

All the MMPs able to degrade E-cadherin and β-catenin and/or activate TGF-β, participate in EMT. Especially important for this process is stromelysin 1 (ST1). Induced expression of ST1 in a primary culture of normal cells from mammary gland leads to a degradation of E-cadherin and β-catenin, detachment of the cells, loss of differentiation and increase of the cell migration, i.e. the cells acquire a tumor phenotype [20]. MMP-7 is also involved in EMT especially in the pancreas, uterus, mammary gland and prostate. Its enhanced expression in glandular epithelial cells results in an initiation of tumor progression. This enzyme is a subject of a great scientific interest due to the increased number of cases of adenocarcinomas. The serum levels of MMP-7 have a diagnostic value in pancreatic ductal carcinoma [9].

Tumor invasion and metastasis. Secondary tumors or metastases are the main cause for fatal outcomes in cancer. Invasion and metastases require that the cells overcome many physical barriers with the help of MMPs. Interstitial collagenases are the MMPs mostly involved in these processes. That is why they are the main marker enzymes for tumor invasion and the central targets for therapy. For example, MMP-1 is usually expressed in the invasive front of many types of advanced tumors [31]. It is expresses both by tumor and stromal cells. The appearance of this enzyme in the border parts of the tumor is connected with the most aggressive and metastatic phenotype.

Another interstitial collagenase that plays important role in the tumor invasion is MMP-13 [reviewed in 28], which is expressed in the invasive front of squamous cell carcinomas of the mammary gland, head and neck. Actually, the enzyme is present only in malignant lesions but not in non-malignant. In that respect, it is useful as a prognostic marker for the above types of tumors.

One more MMP directly involved in the tumor growth and metastasis is the membrane-type 1 MMP (MT1-MMP). It is usually expressed in the invadopodia and provides the cells with a great potential for migration by cleaving the ECM components and activating other MMPs [reviewed in 36]. The increased expression of MT1-MMP at the border membranes between the tumor and stroma is considered a poor prognostic marker for squamous cell carcinomas, some glyomas and neuroblastomas.

Kallikrein-related peptidases (KLKs)

Kallikrein-related peptidases or kalikreins are serine-type soluble proteases which, like MMPs. are directly involved in tumorigenesis and tumor progression. Till now, 15 members of KLK-family are identified, most of which are already used as diagnostic/prognostic markers of tumor diseases. Normally, KLKs participate in a number of physiological processes like regulation of the blood pressure, contractions of the smooth muscles, neutrophis' chemotaxis, etc. KLK2, 3, 5 and 11 are expressed in the prostate and seminal plasma, where they take part in the liquefaction of the sperm. Certain KLKs support the normal skin physiology, activate peptide hormones and growth factors and participate in myelination and demyelination in the central nervous system [25].

Altered expression of KLKs has been detected in many types of adenocarcinomas [8]. For example, the expression of KLK3 in the prostate is applied for differentiation between malignant and non-malignant lesions [4]. Also, KLK3 takes part in the attachment of metastatic cells to the bones thus favoring the development of bone metastases [29]. Actually, in most cases KLKs act as proteolytic cascades (PCs) both in healthy and pathologically altered tissues. PCs are highly organized sequences of proteolytic enzymes, which activate each other and operate coordinately to transfer a specific signal. PCs are activated when a well-directed and secure (from physiological point of view) signal transfer to the target cells is needed. The best studied PCs are those of the blood

coagulation, caspases at apoptosis and PCs of the innate and acquired immunity. Kallikreins` PC of the liquefaction of the sperm before ejaculation as well as the one of the physiological skin peeling, are also well known. Amongst the pathological kallikreins` PCs the best known is the one in prostate cancer. It results in increased angiogenesis, suppression of the immune reactions and acceleration of the tumor growth. Pathological PCs are used for the development of more accurate multifactorial methods for diagnosis and prognosis of cancer. Such a method has been introduced for diagnosis of prostate cancer, based on kallikreins' PC [8].

Aminopeptidase N (APN; EC 3.4.11.2)

In the group of aminopeptidases – enzymes which hydrolyze single AA from the N-terminal of peptides, most studies are directed to the marker role of aminopeptidase N, also known as CD13. APN is a membrane-bound, Zn-dependent peptidase hydrolyzing neutral AAs. The enzyme is normally expressed in many tissues and organs but in the development of tumor diseases its expression increases, which allows to be used as a biological marker for diagnostic purposes.

About 20 years ago, it has been found that phages expressing the motif Asp-Gly-Arg (NGR) selectively bind to the endothelium of growing capillaries and the receptor of this motif is APN [26, 27]. The high expression of APN in tumor capillaries can be applied for *in vivo* monitoring of the tumor growth and angiogenesis by using non-invasive techniques like e.g. fluorescence-mediated tomography. APN is used as a diagnostic marker for carcinomas of the mammary gland, colon, pancreas, thyroid gland and non-small cell carcinoma of the lung [reviewed in 35]. More than that, several anti-cancer strategies are developed, based on the overexpression of APN in tumors [reviewed in 35], the most promising of which is the delivery of medications directly into the tumor by means of NGR-peptide and more particularly by its cyclic analogue with two cysteine residues at both ends – CNGRC. This peptide can be used for precise delivery of TNFα, which potentiates the effect of chemotherapeutic agents. Attempts have been made for a directed delivery of chemotherapeutics, toxic medicines and small interfering RNAs. Those methods are still at experimental stage but they are promising for the development of more effective therapies.

Fibroblast activation protein alfa (FAP-α; EC 3.4.21.B28)

FAP-α is a membrane-associated serine-type protease belonging to the family of post-proline cleaving proteases. It is also called F19-antigene after the name of the monoclonal antibody by which the enzyme has been discovered. Another trivial name of FAP-α is Seprase (from ***s***urface ***e***xpressed ***pr***ote***ase***). Its soluble form entering the blood after shedding from cell surface is known as **A**nti**P**lasmin **C**leaving **E**nzyme (APCE). FAP-α is usually absent from normal adult tissues. In healthy adults it can be find only in single reactive fibroblasts, glucagon producing A-cells in the pancreas and individual endometrial cells [reviewed in 37]. On the other hand, lots of data show elevated expression in the fibroblasts of the tumor stroma as well as in tumor cells in several types of cancer. In fact, more than 90% of carcinomas and many types of sarcomas are FAP-α-positive [reviewed in 12 and 14]. Thus, the enzyme should be very convenient for diagnostic purposes. However, in some types of tumors it could be a tumor-promoter [19] and in others - a tumor suppressor [33, 34]. For example, in ductal mammary gland carcinomas and in some melanomas its expression is considered a good prognostic marker. Oppositely, in

ovarian carcinomas the high enzyme levels are regarded as a marker for poor prognosis. Similarly, in colorectal carcinoma the enzyme occurrence is a sign for the existence of metastases in the lymph nodes. The truth is that although many scientific groups work on the application of FAP-α as a biological marker in oncology, very little is still known about the mechanisms of the enzyme participation in tumor progression. All the same, FAP-α is very important for the development of novel therapies. For example, an experimental anti-tumor vaccine, based on FAP-α has been already proposed [21].

Dipeptidyl peptidase IV (DPPIV;EC 3.4.14.5)

DPPIV is a membrane-associated serine peptidase, cleaving off dipeptides from the N-terminal of peptides and small proteins. Together with FAP-**α** it is a member of the family of post-proline cleaving enzymes. DPPIV is considered a potential marker for thyroid carcinoma [16]. It is believed that DPPIV possesses a tumor-suppressor function in non-small cell lung carcinoma, prostate cancers, some melanomas, etc. That is why in those types of cancers the enzyme has a very low to lacking expression [2, 33]. For example, studies on DPPIV activity levels in tumor lung cells in comparison with normal lung-derived cells reveal that in normal cells it is about ten times more active than in tumor cell lines [34]. Additionally, our own results show a lack of activity in tumor cells in cryo-sections of lung squamous carcinoma and high activity in the surrounding stroma [7]. The re-expression of DPPIV in tumor cells by the use of a plasmid vector leads to a number of changes, showing a conversion of the cells to a normal phenotype – decrease of the cell growth, increase of the adhesion and loss of migration ability, re-expression of CD44 and FAP-α, which are known to inhibit the tumor growth and dissemination in lung carcinoma [34]. Obviously, the decreased DPPIV expression in lung carcinoma is a part of the tumor phenotype of the cells and vice versa - restoration of the enzyme activity can lead to a suppression of the tumor growth. The above results are promising for the development of novel anti-cancer therapies.

Tripeptidyl peptidase I (TPPI; EC 3.4.14.9)

TPPI is a lysosomal serine protease hydrolyzing a large number of tripeptides from the N-terminal of polypeptides and unfolded proteins. The enzyme is essential for the neuronal function - its genetically determined deficiency leads to the hereditary neurodegenerative disorder classical late-infantile neuronal ceroid lipofuscinose (LINCL), connected with severe symptoms and early death of affected individuals [32]. On the other hand, TPPI is widely distributed in many peripheral organs and tissues such as the spleen, kidney, liver, pancreas, lungs, male and female reproductive organs [18]. Therein, it is supposed to play a role not only in physiological but also in pathological processes like tumorigenesis and tumor growth. The mechanisms of the enzyme involvement in tumors are not elucidated yet. Nevertheless, TPPI has been proposed as a marker for breast carcinomas, since its activity during the tumor development is about 20 times higher than that in the normal tissue [13]. Increased TPPI levels has also been found in other types of cancer like carcinomas of the lower esophagus, colorectal carcinomas, thyroid adenocarcinoma, liver cancer, meningioma, mesothelioma, etc. [17]. Using enzyme histochemical method in a rare malignant epithelial neoplasm, i.e. pancreatic acinar cell carcinoma, we found an increased TPPI activity in tumor acinar cells with varying grades of differentiation (**Fig. 1B**), whereas in healthy pancreas the enzyme is absent in the pancreatic acini (**Fig. 1A**).

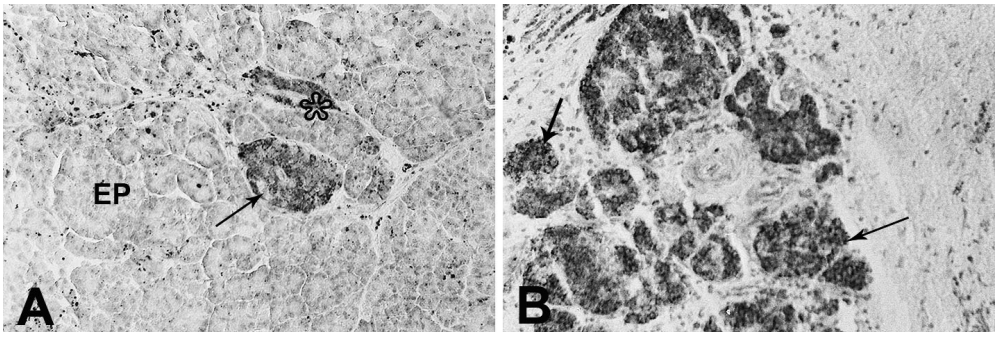

Fig. 1. TPPI activity in normal human pancreas (A) and in human pancreatic acinar cell carcinoma (B). A – TPPI in Langerhans islands (arrow) and in pancreatic ducts and stromal elements (asterisk); lack of the enzyme expression in the exocrine pancreas (EP). B – High TPPI activity in the tumor acinar cells at various grades of differentiation (arrows). A, B – 200×

In fact, all the studies on solid tumors show substantially elevated TPPI expression in the areas of tumor invasion into the adjacent tissues and/or in metastases, which is typical for the enzymes degrading ECM. However, the enzyme is lysosomal and is active only at pH about 4.5. On the other hand, secretion of TPPI pro-enzyme from cells over-expressing it has been already documented. In the ECM it binds to polyanionic glycosaminoglycans such as dextran sulfate, heparan sulfate and chondroitin sulfate B, which exert a protective effect on the enzyme molecule [11]. They not only protect TPPI from heat- or alkaline pH-induced degradation but also facilitate the enzyme activation at pH up to 6.0. These findings may explain the possible TPPI role as an extracellular (matrix) protease in tumor diseases.

In conclusion, many proteolytic enzymes are involved in tumorigenesis, tumor progression and metastasis. Some of them are already used as valuable markers for the diagnosis/prognosis of tumor diseases. Additionally, certain proteases are identified as promising targets for therapy. Those enzymes potential for application in oncology is huge and opens infinite possibilities for future research in the field of tumor diseases.

References

1. **Andarawewa, K. L., E. R. Motrescu, M.-P. Chenard, A. Gansmuller, et al.** Stromelysin-3 is a potent negative regulator of adipogenesis participating to cancer cell-adipocyte interaction/crosstalk at the tumor invasive front. – Cancer Res., **65**, 2005, 10862-10871.
2. **Baginski, L., G. Tachon, F. Falson, J. S. Patton, U. Bakowsky, C. Ehrhardt.** Reverse transcription polymerase chain reaction (RT-PCR) analysis of proteolytic enzymes in cultures of human respiratory epithelial cells. – J. Aerosol. Med. Pulm. Drug Deliv., **24**, 2011, 89-101.
3. **Bergers, G., R. Brekken, G. McMahon, T. H. Vu, T. Itoh et al.** Matrix metalloproteinase-9 triggers the angiogenic switch during carcinogenesis. – Nat. Cell Biol., **2**, 2000, 737-744.
4. **Catalona, W. J., A. W. Partin, K. M. Slawin, M. K. Brawer.** Use of the percentage of free prostate-specific antigen to enhance differentiation of prostate cancer from benign prostatic disease: a prospective multicenter clinical trial. – JAMA, **279**, 1998, 2542-2547.
5. **Crawford, H. C., C. R. Scoggins, M. K. Washington, L. M. Matrisian, S. D. Leach.** Matrix metalloproteinase-7 is expressed by pancreatic cancer precursors and regulates acinar-to-ductal metaplasia in exocrine pancreas. – J. Clin. Invest., **109**, 2002, 1437-1444.

6. **Dallas, S. L, J. L. Rosser, G. R. Mundy, L. F. Bonewald.** Proteolysis of latent transforming growth factor-beta(TGF-beta)-binding protein-1 by osteoclasts. A cellular mechanism for release of TGF-beta from bone matrix. – J. Biol. Chem., **277**, 2002, 21352-21360.
7. **Dimitrova, M., I. Ivanov, R. Todorova, N. Stefanova, V. Moskova-Doumanova, T. Topouzova-Hristova, V. Saynova, E. Stephanova.** Comparison of the activity levels and localization of dipeptidyl peptidase IV in normal and tumor human lung cells. – Tissue and Cell, **44**, 2012, 74-79.
8. **Emami, N., E. P. Diamandis.** Utility of kallikrein-related peptidases (KLKs) as cancer biomarkers. – Clinical Chemistry, **54**, 2008, 1600-1607.
9. **Fukuda, A., S. C. Wang, J. P. Morris, A. E. Folias, A. Liou et al.** Stat3 and MMP7 contribute to pancreatic ductal adenocarcinoma initiation and progression. – Cancer Cell, **19**, 2011, 441-455.
10. **Gialeli, C., A. D. Theocharis, N. K. Karamano.** Roles of matrix metalloproteinases in cancer progression and their pharmacological targeting. – FEBS Journal, **278**, 2011, 16-27.
11. **Golabek, A. A., M. Walus, K. E. Wisniewski, E. Kida.** Glycosaminoglycans modulate activation, activity, and stability of tripeptidyl-peptidase I in vitro and in vivo. – J. Biol. Chem., **280**, 2005, 7550-7560.
12. **Gorrell, M. D., J. E. Park.** Fibroblast activation protein α. – In: Handbook of proteolytic enzymes (Eds. N. D. Rawlings, G. S. Salvesen), Elsevier Ltd, 2013, 3395-3400.
13. **Junaid, M. A., G. M. Clark, R. K. Pullarkat.** A lysosomal pepstatin-insensitive proteinase as a novel biomarker for breast carcinoma. – Int. J. Biol. Markers, **15**, 2000, 129-134.
14. **Kelly, T., Y. Huang, A. E. Simms, A. Mazur.** Fibroblast Activation Protein-a: a key modulator of the microenvironment in multiple pathologies. – In: International review of cell and molecular biology, Academic Press – Elsevier, USA, UK, The Netherlands, 2012, 83-116.
15. **Kessenbrock, K., V. Plaks, Z. Werb.** Matrix metalloproteinases: regulators of the tumor microenvironment. – Cell, **141**, 2010, 52-67.
16. **Kholova, I., M. Ludvikova, A. Ryska, O. Topolcan, R. Pikner, L. Pecen, J. Cap, L. Holubec.** Diagnostic role of markers dipeptidyl peptidase IV and thyroid peroxidase in thyroid tumors. – Anticancer Res., **23**, 2003, 871-875.
17. **Kida, E., A. Golabek, M. Walus, P. Wujek, W. Kaczmarski, E. K. Wisniewski.** Distribution of tripeptidyl peptidase I in human tissues under normal and pathological conditions. – J. Neuropathol. Exper. Neurol., **60**, 2001, 280-292.
18. **Koike, M., M. Shibata, Y. Ohsawa, S. Kametaka, S. Waguri, E. Kominami, Y. Uchiyama.** The expression of trypeptidyl peptidase I in various tissues of rats and mice. – Arch. Histol. Cytol., **65**, 2002, 219-232.
19. **Lee, H.O., S. R. Mullins., J. Franco-Barraza, M. Valianou, E. Cukierman, J. D. Cheng.** FAP-overexpressing fibroblasts produce an extracellular matrix that enhances invasive velocity and directionality of pancreatic cancer cells. – BMC Cancer, **11**, 2011, 245.
20. **Lochter, A., S. Galosy, J. Muschler, N. Freedman, Z. Werb, M. J. Bissell.** Matrix metalloproteinase stromelysin-1 triggers a cascade of molecular alterations that leads to stable epithelial-tomesenchymal conversion and a premalignant phenotype in mammary epithelial cells. – J. Cell Biol., **139**, 1997, 1861-1872.
21. **Loeffler, M., J. A. Kruger, A. G. Niethammer, R. A. Reisfeld.** Targeting tumor associated fibroblasts improves cancer chemotherapy by increasing intratumoral drug uptake. – J. Clin. Invest., **116**, 2006, 1955-1962.
22. **Martin, M. D., L. M. Matrisian.** The other side of MMPs: Protective roles in tumor progression. – Cancer Metastasis Rev., **26**, 2007, 717-724.
23. **Massague, J.** TGFbeta in cancer. – Cell, **134**, 2008, 215-230.
24. **Nozawa, H., C. Chiu, D. Hanahan.** Infiltrating neutrophils mediate the initial angiogenic switch in a mouse model of multistage carcinogenesis. – PNAS, **103**, 2006, 12493-12498.
25. **Pampalakis G., G. Sotiropoulou.** Tissue kallikrein proteolytic cascade pathways in normal physiology and cancer. – Biochim. Biophys. Acta, **1776**, 2007, 22-31.
26. **Pasqualini, R., E. Koivunen, E. Ruoslahti.** A peptide isolated from phage display libraries is a structural and functional mimic of an RGD-binding site on integrins. – J. Cell Biol., **130**, 1995, 1189-1196.
27. **Pasqualini, R., E. Koivunen, R. Kain et al.** Aminopeptidase N is a receptor for tumor-homing peptides and a target for inhibiting angiogenesis. – Cancer Res., **60,** 2000; 722-727.

28. **Patrick, H., E. Yves.** Matrix metallopeptidase-13/collagenase 3. – In: Handbook of proteolytic enzymes (Eds. N. D. Rawlings, G. S. Salvesen), Academic Press – Elsevier, 2013, 735-744.
29. **Romanov, V. I., T. Whyard, H. L. Adler, W. C. Waltzer, S. Zucker.** Prostate cancer cell adhesion to bone marrow endothelium: the role of prostate-specific antigen. – Cancer Res., **64**, 2004, 2083-2089.
30. **Rutkowski, J. M., K. E. Davis, P. E. Scherer.** Mechanisms of obesity and related pathologies: the macro- and microcirculation of adipose tissue. – FEBS J., **276**, 2009, 5738-5746.
31. **Shiozawa, J., M. Ito, T. Nakayama, M. Nakashima, S. Kohno, I. Sekine.** Expression of matrix metalloproteinase-1 in human colorectal carcinoma. – Mod. Pathol., **13**, 2000, 925-930.
32. **Sleat, D. E., J. R. Donnelly, H. Lackland, G. C. Lin, I. Sohar, R. K. Pullarkat, P. Lobel.** Association of mutations in a lysosomal protein with classical late-infantile neuronal ceroid lipofuscinosis. – Science, **277**, 1997, 1802-1805.
33. **Wesley, U. V., A. P. Albino, S. Tiwari, A. N. Houghton.** A role for dipeptidyl peptidase IV in suppressing the malignant phenotype of melanocytic cells. – J. Exp. Med., **190**, 1999, 311-322.
34. **Wesley, U. V., S. Tiwari, A. N. Houghton.** Role for dipeptidyl peptidase IV in tumor suppression of human non-small cell lung carcinoma cells. – Int. J. Cancer, **109**, 2004, 855-866.
35. **Wickstroem, M., R. Larsson, P. Nygren, J. Gullbo.** Aminopeptidase N (CD13) as a target for cancer chemotherapy. – Cancer Sci., **102**, 2011, 501-508.
36. **Yana, I., M. Seiki.** MT-MMPs play pivotal roles in cancer dissemination. – Clin. Exp. Metastasis, **19**, 2002, 209-215.
37. **Yu, D. M. T., T.-W. Yao, S. Chowdhury, N. A. Nadvi, B. Osborne, W. B. Church, G. W. McCaughan, M. D. Gorrell.** The dipeptidyl peptidase IV family in cancer and cell biology. – FEBS Journal, **277**, 2010, 1126-1144.

Institute of Experimental Morphology, Pathology and Anthropology with Museum
Bulgarian Anatomical Society

Acta morphologica et anthropologica, 23
Sofia ● 2016

Down Syndrome – Anthropological Point of View: Review

A. Dimitrova

Institute of Experimental Morphology, Pathology and Anthropology with Museum, Bulgarian Academy of Sciences

In the recent years the interest to the morphological changes in the anthropological status in a number of diseases and their use as an additional diagnostic tool considerably increased. The disease with characteristic morphological manifestation is Down syndrome (DS) – most common genetic abnormalities. The individuals with DS are characterized with: short stature, microcephalia or brachicephalia, short extremities, wide hands and short fingers, clinodactyly, syndactyly, etc. The youths with DS demonstrate a great prevalence of overweight and obesity during the puberty. Nowadays anthropological characteristics of children with DS are subject of research in many countries. Knowledge of body composition in children with DS is of interest to clinicians and scientists because components of the body often provide more useful information than the measurements of weight, height or body mass index. To prepare and use DS specific growth charts is important for diagnosis, because growth in children with DS differ from that of their healthy peers.

Key words: Down syndrome, growth charts, short stature, obesity, anthropometry.

In the recent years the interest in the morphological changes in the anthropological status in a number of diseases and their use as an additional diagnostic tool considerably increased. Such disease characterized with morphological manifestation is Down syndrome.

Trisomy 21 is the most common genetic abnormalities, caused by non-disjunction of gametes in the first meiotic division. It occurs in 1 of 700 live births in all ethnic groups and one of the few aneuploidies compatible with postnatal survival. In Bulgaria each year about 100 children with DS are born. Characteristic manifestations of DS are: learning disability, early-onset Alzheimer disease, childhood leukaemia, congenital heart disease, duodenal stenosis, imperforate anus, Hirschprung disease, muscle hypotonia, immune system deficiencies [10]. The most phenotypic features vary among the patients. The individuals with DS are characterized with following morphological features: short stature, microcephalia or brachicephalia, short extremities, wide hands and short fingers, clinodactyly and syndactyly etc. Cytogenetic studies showed that extra chromosome 21 is transmitted through the maternal chromosome in 95% of cases [3]. It is widely assumed that the DS complex phenotype results from the imbalance of the genes located on D21S55 region [9].

Down syndrome is a disease which has existed since ancient times. Evidence can be found at many paintings from Antiquity. In "Madonna and Child" by A. Mantegna (15th c.); "The Peasant and the Satyr" by J. Jordanes (1635-40); "Woman with child" by Jacob Jordaens (1616); "Lady Cockburn and her Children" (1773) by Joshua Reynolds the subjects appear to show the stigmata of Down syndrome. These children which are illustrated at the above mentioned paintings, show different features typical for trisomy 21: prominent tongue, a small nose, an open mouth and slanted eyes.

The archeological data from different parts of the world indicates about cases of burials of individuals with trisomy 21. During excavations on the island of Santa Rosa, CA, a skeleton of a woman approximately around 5200 BC was found. The skull had the typical signs of the disease: flat face, low and wide nasal apertures. It is assumed that it is the oldest finding of an individual with trisomy 21 detected so far. A detailed description of the skull of an individual with Down syndrome found in Leicestershire, England was published in 1960. The rarity of ancient Down syndrome skeletons was unsurprising because of the smaller populations with a younger age structure and higher infant mortality than in modern times [22].

In 1938 the French doctor Escirol for the first time described a child with trisomy 21. The name of disease comes from the name of the British physician John Langdon Down. In the hospital where he worked, he observed a group of individuals with specific phenotype characteristics and mental retardation. For 10 years of work he was able to introduce its rehabilitation training models [10]. Even then it became clear that good medical care, the adequate training and socialization of the patients have a good impact on their health and quality of life.

Down syndrome is a chromosome disorder, well studied in genetic aspect all over the world. From the anthropological point of view, most of studies from 90 years of 20th century and today have been held in the USA. Nowadays anthropological characteristic of children with DS is a subject of research in many countries and specific growth charts for height and weight have been made [7, 26, 1, 19, 16, 23, 24, 25, 18, 11]. The conclusion which can be drawn is that: the preparation of such charts for each country separately, will provide a more reliable assessment of physical development and health of patients with DS.

Height, weight and head circumference are basic measurements used in medical practice and physical anthropology. During the childhood there are important diagnostic signs for the health status, and any deviation from the standard norms indicates the presence of disease. The human stature is genetically determined and has age, sexual, racial and territorial specificity, and it also could be influenced by the environmental factors. Problems associated with growth are common in children. As low growth can be defined the growth with 2 or more standard deviations (SD) below the average rate for age and gender. DS is one of the diseases manifested by variations in basis anthropometric measurements – short stature, microcephaly, low birth weight and risk of overweight and obesity mainly in puberty. Children and adolescents with DS have a set of health, anatomical, physiological and cognitive attributes predisposing them to limitations on their physical activity capacities.

A detailed analysis of the morphological status of children with DS was made in Poland and it determined a tendency to reduce the height and length indexes of the upper limb (arm and forearm lengths). Reports of the measurements of the newborns with DS showed shorter gestation periods (176.5 days), lower birth weights (1.5SD) and birth length reduced by 2SD from the mean of control study [5]. Head circumference showed 1.5 SD from the health controls of the same age. There are no significant sex differences in the patients with DS in this earliest period of physical development [12].

Childhood and adolescence are stages of human life associated with the dynamic growth and development processes in the body. They are the periods of greatest accumulation of muscle, fat and bone mass density (BMD). High levels of BMD are a key determinant for adult skeletal health [20, 21]. The children and adolescent with DS have low BMD and BMDH (BMD/height), compared with non-DS peers [4, 15]. This is the main reason of osteoporotic problems in adulthood in population with DS [2]. The hip region, especially the femoral neck is very important area to be studied, because there is a high risk of bone fracture [14]. Effort to develop physical activity programs, which may enhance bone mass should be considered.

Some authors indicate that the youth with DS demonstrate a great prevalence of overweight and obesity, during the puberty after 10 years of age. In healthy individuals puberty occurs around 10-11 years of age in female and about 12-13 years of age in male and ends in 17th in both sexes. In different investigations of growth and physical development of children with DS found that the puberty begins and ends earlier than their peers. The final height in boys and girls with DS reached 163.4 cm and 151.8 cm respectively [5, 6, 24].

According to some authors there is a relationship between somatotipological characteristics (somatotype) of the patients with DS and some musculoskeletal deformities. Somatotype gets important biometric data that defines the shape and proportionality of human body. It depends on inheritance, the geografical and socio-economical factors. The patients with DS have a great prevalence of endomorph component which determines the presence of overweight and obesity and leads to increased risk of cardiovascular disease, hypertension, diabetes. Therefore annual monitoring of nutritional status in patients with DS is necessary. Endomorphy somatotype is in high correlation with musculoskeletal deformities such as flat foot, forward abdomen and lumbar lordosis, in adolescents with trisomy 21 [8].

Knowledge of body composition in children with DS is of interest to clinicians, and scientists because the components of the body often provide more useful information than the measurements of weight, height or body mass index (BMI). Children with DS have a genetic predisposition to become overweight. Bioelectrical impedance can be a useful technique for body composition analysis in healthy individuals and in those with a number of chronic conditions such as diabetes mellitus, dialysis patients, and patients at risk of obesity. Most studies on body composition of children with DS include height, weight and BMI, but only in few of them is used the bioelectrical impedance analysis (BIA) [13]. Another method, used to study the body composition in healthy individuals and in patients with DS is dual-energy X-ray absorptiometry (DXA). It can be used to more accurately determine adiposity in population with DS. Percentage body fat (PBF) determined by DXA correlated well with PBF determined by BIA in both sexes [17].

In Bulgaria anthropological investigations of individuals with trisomy 21 are very rare and mainly associated with dermatoglyphic features and psycho-physical characteristics [27, 28, 29]. The finger papillar patterns are genetic determinated and very variable in form and size, and may be classified in: loops (L), arches (A) and whorls (W). One of the important quantitative features is the finger ridge count. It consists of the number of ridges, which cut or touch a straight line running from the triradius to the core or center of the pattern. Patients with DS have a great prevalence of loops of the distal phalanges of the fingers, centrally located axial triradius-t and significantly lower finger ridge count on fingers and palmar areas. Normally there are three major flexion creases on the palmar surface of the hand. It may be found in 12 weeks embryos. Abnormal flexion creases can be found in different genetically diseases, like DS. As it is known in 20% of cases of DS there is an additional IV abnormal flexion crease [29].

Morphological investigation of children with mental retardation is known from distant 1972 year [28]. The study included psycho-physical characteristics of children, as 102 of them have a DS. The author established a delay of physical development and stepwise reduction of the height and length of the upper and lower limbs.

Plenty of researches of the anthropological status of the children with DS all over the world and only few in Bulgaria suggest that detailed anthropological characteristics of Bulgarian children and adolescents with DS and specific growth tables and curves need to be developed. This will provide the possibility of monitoring of physical development of individuals with DS and to established deviations from the norms in every age period. This is important for prevention of early occurred complications, related to their physical development.

References

1. **Aburawi, E. H., N. Nagelkerke, A. Deeb, S. Abdulla, Y. M. Abdulrazzaq.** National Growth Charts for United Arab Emirates Children with Down syndrome from birth to 15 years of age. – J. Epidemiol., **25**(1), 2015, 20-29.
2. **Angelopoulou, N., V. Souftas, A. Sakadamis , K. Mandroukas.** Bone mineral density in adults with down syndrome. – Eur. Radiol., **9**, 1999, 648-651.
3. **Antonarakis, S. E., R. Lyle, R. Chrast, H. S. Scott.** Differential gene expression study to explore molecular pathophysiology of Down syndrome. – Brain Res. Rev., **36**, 2001, 265-274.
4. **Baptista, F., A. Varela, L. B. Sardinha.** Bone mineral mass in males and females with and without Down syndrome. – Osteoporos. Int., **16**, 2005, 380-388.
5. **Buday, J.** Growth and physique in Down syndrome children and adults. – Humanbiol. Budapest, 1990, 1-117.
6. **Cannalire, G., M. Bellini, G. Biasucci.** The importance of knowing growth and pubertal development in Down syndrome. – J. Clin. Case Rep., 5:640, 2015, doi: 10.4172/2165-7920.1000640
7. **Cronk, C., A. C. Crocker, S. M. Pueschel, A. M. Shea, E. Zackai, G. Pickens, R. B. Reed.** Growth charts for children with Down syndrome: 1 month to 18 years of age. – Pediatrics, **81**, 1988, 102-110.
8. **Dehghani, L., M. Hashemi, R. Saboonchi, A. Hematfar, A. Roonasi.** Relationship between somatotype and some of musculoskeletal deformities of girl students with Down syndrome. – European Journal of Experimental Biology, **2**(4), 2012, 1209-1213.
9. **Delabar, J. M., D. Theophile, Z. Rahmani, Z. Chettouh, J. L. Blouin, M. Prieur, B. Noel, P. M. Sinet.** Molecular mapping of twenty- four features of Down syndrome on chromosome 21. – Eur. J. Hum. Genet., **1**(2), 1993, 114-124.
10. **Epstein, C. J., J. R. Korenberg, J. Anneren, S. E. Antonarakis, S. Ayme, E. Courchesne, L. B. Epstein, A. Fowler, Y. Groner, J. L. Huret, et al.** Protocols to establish genotype- phenotype correlations in Down syndrome. – Am. J. Hum. Genet., **49**, 1991, 207-235.
11. **Fernandes, A., A. P. Mourato, M. J. Xavier, D. Andrade, C. Fernandes, M. Palha.** Characterisation of the somatic evolution of Portuguese children with Trisomy 21-Preliminary results. – Down syndrome Research and Practice, **6**(3), 2001, 134-138.
12. **Horvath, L., J. Buday.** Birth data of patients with Down syndrome. – Anthrop. Kozl., **30**, 1986, 93-96.
13. **Grammatikopoulou, M. G., A. Manai, M. Tsigga, A. Tsiliqiroqlou-Fachantidou, A. Galli-Tsinopoulou, A. Zacas.** Nutritient intake and anthropometry in children and adolescents with Down syndrome. – Developmental Neurorehabilitation, **11**(4), 2008, 260-267.
14. **Guijarro, M., C. Vabro, B. Paule, M. J. Gonzales, J. A. Riancho.** Bone mass in young adults with Down syndrome. – J. Intellect Disabil., Res., **52**, 2008, 182-189.
15. **Kao, C. H., C. C. Chen, S. T. Wang, S. H. Yeh.** Bone mineral density in children with Down's syndrome detected by dual photon absorptiometry. – Nucl. Med. Commun., **13**, 1992, 773-775.
16. **Lopes, T. S., D. M. Ferreira, R. A. Pereira, G. V. da Veiga, V. M. R. de Marins.** Assessment of

anthropometric indexes of children and adolescents with Down syndrome. – Journal de Pediatria (Rio J), **84**(4), 2008, 350-356.
17. **Loveday, S. J., John M. D. Thompson, E. A. Mitchell.** Bioelectrical impedance for measuring percentage body fat in young persons with Down syndrome: Validation with dual- energy absorptiometry. – Acta Pediatrica, **101**, 2012, pp.e491-e495.
18. **Myrelid, A., J. Gustafsson, B. Ollars, G. Anneren.** Growth charts for Down`s syndrome from birth to 18 years of age. – Arch Dis Child, **87**, 2002, 97-103.
19. **Raja, C. G., C. Parkash, B. V. Bhat, R. K. Ramachandra, B. Rajesh.** Anthropometric measurements in Down's syndrome children during preschool period. – Curr. Pediatr. Res., **11**(1& 2), 2007, 17-20.
20. **Rizzoli, R., J. P. Bonjour.** Determinants of peak bone mass and mechanisms of bone loss. – Osteoporos. Int ., **9** (2), 1999, 17-23.
21. **Rizzoli, R., M. L. Bianchi, M. Garabedian, E. A. McKay, L. A. Moreno.** Maximizing bone mineral mass gain during growth for the prevention of fractures in the adolescents and the elderly. – Bone, **46**, 2010, 294-305.
22. **Starbuck, J. M.** On Anticity of Trisomy 21: Moving towards a quantitative diagnosis of Down syndrome in historic material culture. – Journal of contemporary anthropology, Vol. II, Iss.1, 2011, 21-32.
23. **Styles, M. E., T. J. Cole, J. Dennis, M. A. Preece.** New cross sectional stature, weight, and head circumference references for Down's syndrome in the UK and Republic of Ireland. – Arch. Dis. Child, **87**, 2002, 104-108.
24. **Tuysuz, B., N. T. Goknar, B. Ozturk.** Growth charts of Turkish children with Down syndrome. – An. J. Med. Genet. A., **158A**(11), 2012, 2656-64.
25. **Van Gameren-Oosterom, H. B., P. Van Dommelen, A. M. Oudesluys-Murphy, S. E. Buitendijk, S. van Buuren, J. P. van Wouwe.** Healthy growth in children with Down syndrome. – Plos One, **7**, 2012, e31079.
26. **Zemel, B. S., M. Pipan, V. A . Stalling, W. Hall, K. Schadt, D. S. Freedman, P. Thorpe.** Growth Charts for children with Down syndrome in the United States. – Pediatrics, **136**(5), 2015, e1204-e1211.
27. **Елазарова, Л. Д.** Дерматоглифски проучвания при деца с вродени малформации и техните родители. Автореферат на дис. София, Труд, 1983.
28. **Мутафов, С.** Психо-физически особености на децата с аномалии. София, Медицина и физкултура, 1981.
29. **Торньова-Ранделова, С.** Дерматоглифика при здрави деца и деца със зрителна, слухова и интелектуална недостатъчност. Автореферат на дис. труд. София, 1986.

Institute of Experimental Morphology, Pathology and Anthropology with Museum
Bulgarian Anatomical Society

Acta morphologica et anthropologica, 23
Sofia ● 2016

Transferrin Receptors and Hematopoiesis: Review

Y. Gluhcheva

Institute of Experimental Morphology, Pathology and Anthropology with Museum – BAS

The effectiveness of hematopoiesis depends on hematopoietic cell activity as well as on the presence of iron. Iron uptake is regulated by some of the members of the transferrin family of iron-containing proteins – transferrin and its receptors which assigns them a key regulatory role in hematopoiesis. Transferrins are expressed mainly in the liver, but small amounts arise also in the bone marrow, pancreas, testes, brain, spleen and kidneys. Experimental data show three types of transferrin receptors – transferrin receptor 1 (TfR1), transferrin receptor 2 (TfR2) and soluble transferrin receptor (sTfR). The expression of TfR1 and TfR2 is tissue- and cell cycle specific and is regulated by different control mechanisms, suggesting that they have different roles in iron metabolism. Cell surface TfR expression and concentration reflect iron requirements of the cells and they may be a useful marker for quantitative evaluation of the erythroid lineage, erythropoiesis and iron deficiency.

Key words: transferrin, transferrin receptor 1 (TfR1), transferrin receptor 2 (TfR2), soluble transferrin receptor (sTfR).

Introduction

Transferrin receptor is a cell membrane glycoprotein regulating cellular iron uptake by transferrin (Tf), a plasma protein which binds and transports iron [13]. Cell surface TfR concentration reflects iron requirements of the cell. Normally, about 60-70% of total body iron is incorporated in hemoglobin. Myoglobin, cytochromes and other iron-containing enzymes comprise 10% and the remaining 20-30% is stored in ferritin. Although iron bound to transferrin is less than 0.1% of the total body iron, it is the most important iron pool with the highest rate of turnover [13]. The transferrin binding site is situated on the extracellular domain of the receptor and each receptor subunit binds one transferrin molecule. Iron chelation by transferrin serves three main purposes: a) maintains Fe^{3+} in a soluble form under physiologic conditions, b) facilitates regulated iron transport and cellular uptake, and c) maintains Fe^{3+} in a redox-inert state, preventing the generation of toxic free radicals. Tf has an indirect defensive role against systemic infections by depriving the potential pathogens of extracellular iron, which is essential for their growth [4]. Under normal conditions, approximately 30% of the Tf iron-binding sites are saturated. In humans, values of Tf saturation <15% indicate iron deficiency, whereas >45% are consistent with iron overload [4].

According to the scientific data there are three types of transferrin receptors – transferrin receptor 1 (TfR1), transferrin receptor 2 (TfR2), and soluble transferrin receptor (sTfR).

1.Transferrin receptor 1 (TfR1)

Transferrin receptor (TfR) also known as CD71 is ubiquitously expressed at low levels on normal cells and at greater levels on cells with a high proliferation rate such as cells of the basal epidermis, intestinal epithelium, activated peripheral blood mononuclear cells, on cells that require large amounts of iron such as placental trophoblasts and maturing erythroid cells that require iron for heme synthesis. Mature erythroid cells do not express TfR. TfR expression has also been observed on nonproliferating cells such as the vascular endothelium of the brain capillaries, endocrine pancreas, seminiferous tubules of the testes, cells of the pituitary gland, luminal membranes of the breast, hepatocytes, Kupffer cells in the liver and tubules of the kidney [2, 5, 7]. Elevated levels of expression of the TfR are reported on cancer cells when compared to the normal cells [2]. Liu et al. demonstrate that during cell development from myeloid dysplasia to apparent leukemic cells, both CD71 and CD34 gradually increase and suggest that these molecules may be useful tools for understanding clonal development in leukemia [9]. According to Marsee et al. CD71 is a highly effective marker for the detection of cells of the erythroid lineage in bone marrow biopsy specimens as its immunoreactivity is restricted to erythroid precursors and exhibits a membranous and cytoplasmic staining pattern [10].

In humans, the TfR1 gene is located on human chromosome 3q29. TfR1 is the primary target of transferrin in the iron transport system and is expressed as a type II transmembrane glycoprotein composed of a disulfide-bonded homodimer on the surface of nearly every cell type. Each monomer (760 amino acids, molecular weight 90-95 kDa) contains a large extracellular C-terminal domain (671 amino acids) known as the ectodomain that contains the Tf-binding site, a single-pass transmembrane domain (28 amino acids), and a short intracellular N-terminal domain (61 amino acids). The ectodomain contains 3 N-linked glycosylation sites and one O-linked glycosylation site. Glycosylation at these sites is required for adequate function of the receptor [2]. TfR expression is primarily regulated at the post-transcriptional level in response to intracellular iron levels. The 3' untranslated region of the TfR transcript is large and plays an important role in the regulation of mRNA stability. This region contains 5 iron response elements (IRE) that consist of approximately 30 nucleotides each that form loop structures and are involved in the post-transcriptional regulation of TfR expression. These IRE are recognized by two RNA-binding iron regulatory proteins (IRP) [2]. Once Tf binds to the extracellular domain of the TfR on the plasma membrane, it changes its conformation and dimerizes. The Tf-TfR complex enters the endocytic pathway via endocytosis mediated by clathrin-coated pits and is transported to early endosomes. TfR1-mediated endocytosis is the only route for iron delivery to erythroid precursors [4]. Ablation of the TfR1 gene impairs erythropoiesis and neurologic development in mice and leads to embryonic lethality [8]. The Tf/TfR1 route is also essential for iron transport to the central nervous system (CNS) which is separated from the circulation by the blood brain barrier [4]. Astrocytes play a crucial role in providing iron to neurons, exporting the metal via ferroportin. Exported iron can bind to brain Tf, which is locally produced by the choroid plexus. Brain Tf delivers iron to TfR1-expressing cells, such as developing oligodendrocytes and neurons [4].

2.Transferrin receptor 2 (TfR2)

Transferrin receptor 2 (TfR2) is a 105 kDa type II transmembrane glycoprotein, member of the TfR family and homologous to TfR1. The TfR2's extracellular domain is

approximately 45% identical and 66% similar to the TfR1 ectodomain [2]. TfR2 binds to Tf with a 25-fold lower affinity and cannot substitute for TfR1, even though it is expressed in the erythroid compartment [12]. The gene for human TfR2 is located on human chromosome 7q22 [7]. The expression of TfR2 is restricted to hepatocytes, enterocytes of the small intestine and erythroid precursors and is not regulated by iron regulatory proteins (IRP) [2, 16]. Surface expression of TfR2 was also found on a wide variety of human cell lines derived from solid tumors and selected B and myeloid cell lines [2]. Expression of TfR2 increased in the liver during embryo development, whereas expression of TfR1 decreased. In the spleen, expression of TfR1 increased while the levels of TfR2 were constant during development [6]. Low expression of TfR transcripts was also found in lungs, testis, heart, duodenum, brain and kidneys [6]. In human bone marrow TfR2 protein staining was detected on erythroblasts but not on more differentiated erythroid cells. There was also staining on megakaryocytes, but not myeloid cells [6].

Forejtnikova et al. show that TfR2 and the receptor for erythropoietin (EpoR) are synchronously coexpressed during the differentiation of erythroid progenitors. TfR2 associates with EpoR in the endoplasmic reticulum and is required for the efficient transport of this receptor to the cell surface. Erythroid progenitors from TfR2-/- knockout mice show a decreased sensitivity to Epo and increased circulating levels of erythropoietin (Epo) [3]. According to Nai et al. by modulating the Epo sensitivity of the erythroid precursors, TfR2 may act as a control system of red blood cells count to maintain a correct balance between their production and the available iron [11]. Erythroid TfR2 restricts Epo sensitivity to limit excessive erythropoiesis [12]. Wallace et al. suggest a possible regulatory role of TfR2 in Epo production by the kidney [18].

TfR2 and TfR1 differ in their expression during erythroid differentiation. TfR2 was reduced while TfR1 levels increased with differentiation in MEL cells and in human erythroid cells having the highest TfR2 expression in erythroblasts [6]. TfR2 mRNA expression is cell cycle dependent. In MG63 osteosarcoma cells, there was no expression in the G_0/G_1 phase and expression reached its highest level in the late G_1 phase, with a lower level of expression continuing through the remaining stages of the cell cycle. In contrast, TfR1 expression peaked at both late G_1 and G_2/M stages [17]. Inactivation of TfR2 leads to the development of hemochromatosis due to inappropriate hepcidin levels relative to body iron [14]. The authors show in a model of anemic mice that the absence of hematopoietic TfR2 delays erythroid differentiation and immature polychromatic erythroblasts accumulate in the spleen and bone marrow of anemic mice. The results demonstrate that erythroid TfR2 is essential for an appropriate erythropoietic response in iron-deficient anemia [14]. Along with hemojuvelin and HFE, TfR2 is regarded as an upstream regulator of of iron signaling to hepcidin [12]. TfR2 is stabilized in response to high Tf saturation. Hepatic TfR2 promotes iron signaling to hepcidin to inhibit further iron fluxes to the bloodstream. Experimental data reveal that mice lacking TMPRSS6 and TfR2 have splenomegaly and extramedullary hematopoiesis in the spleen [18]. The authors observe altered red-white pulp architecture, infiltration of red pulp with nucleated red cells and variable megakaryocyte infiltration. Flow cytometric analysis revealed increased proportions of cells in the immature erythroblast subpopulations I, II and III compared to wild type (control) mice and reduction in subpopulation IV, corresponding to mature erythrocytes, suggesting that TfR2 is required for terminal erythroblast differentiation [18]. Rishi et al. demonstrate that mice with similar knockout alleles fed an iron deficient diet significantly accumulated nucleated erythroid cells in their liver. The authors also show a significantly increased extramedullary hematopoiesis in the liver and spleen as compared to the control mice on the same diet [14]. The results suggest a key regulatory role of TfR2 in erythropoiesis.

3. Soluble transferrin receptor (sTfR)

TfRs are also present in the circulation and the circulating serum TfR (sTfR) level reflects total body TfR concentration [15]. Under normal conditions erythroid precursors – the erythroblasts are the main source of sTfR. Serum sTfR levels average 5.0 ± 1.0 mg/l in normal subjects. The most important determinant of sTfR levels is the bone marrow erythropoietic activity which can cause variations up to 8 times below and up to 20 times above average normal values [1]. Disorders of the bone marrow with reduced erythroid precursors are associated with low sTfR levels. The sTfR concentration begins to rise early in iron deficiency with the onset of iron-deficient erythropoiesis. It is also increased in patients with expanded erythropoiesis, including hemolytic anemias, myelodysplastic syndromes and use of erythropoietic stimulating agents [15]. sTfR level is decreased in cases of decreased erythropoiesis, bone marrow ablation with stem cell transplantation, aplastic anemia, pure red cell aplasia, etc. [15]. Measurements of sTfR are very helpful to investigate the pathophysiology of anemia, quantitatively evaluating the absolute rate of erythropoiesis and the adequacy of bone marrow proliferative capacity for any degree of anemia and to monitor the erythropoietic response to various forms of therapy, in particular allowing to predict response early when changes in hemoglobin are not yet apparent. With the exception of chronic lymphocytic leukemia (CLL) and high-grade non-Hodgkin's lymphoma and possibly hepatocellular carcinoma, sTfR levels are not increased in patients with malignancies [1].

Hematopoiesis depends on bone marrow hematopoietic cells' proliferative activity as well as on the effectiveness of iron uptake. Iron uptake is regulated by transferrin which binds to a transferrin receptor. Alterations in this receptor impair erythropoiesis and development in mice. In light of the current experimental data one can say that despite of the high homology between TfR1 and TfR2, both receptors exhibit tissue and cell cycle specific expression and regulate hematopoiesis, each in a different way. Ablation in one of the receptors cannot be compensated by the other which suggests that each one regulates the process in a unique way. TfR expression and cell surface concentration may be a useful marker for quantitative evaluation of the erythroid lineage, inefficient erythropoiesis and iron deficiency. Measurement of serum TfR will allow adequate evaluation of erythropoiesis, body iron demands as well the response to therapy in cases of hematological disorders.

References

1. **Beguin, Y.** Soluble transferrin receptor for the evaluation of erythropoiesis and iron status. – Clin. Chim. Acta, **329**, 2003, 9-22.
2. **Daniels, T. R., T. Delgado, J. A. Rodriguez, G. Helguera, M. L. Penichet.** The transferrin receptor part I: Biology and targeting with cytotoxic antibodies for the treatment of cancer. – Clin. Immunol., **121**, 2006, 144-158.
3. **Forejtnikova, H., M. Vieillevoye, Y. Zermati, M. Lambert, R. M. Pellegrino, S. Guihard, M. Gaudry, C. Camaschella, C. Lacombe, A. Roetto, P. Mayeux, F. Verdier.** Transferrin receptor 2 is a component of the erythropoietin receptor complex and is required for efficient erythropoiesis. – Blood, **116**, 2010, 5357-536.
4. **Gkouvatsos, K., G. Papanikolaou, K. Pantopoulos.** Regulation of iron transport and the role of transferrin. – Biochimica et Biophysica Acta, **1820**, 2012, 188-202.
5. **Harms, K., T. Kaiser.** Beyond soluble transferrin receptor: old challenges and new horizons. – Best Pract. Res. Clin. Endocrinol. Metab., **29**, 2015, 799-810.
6. **Kawabata, H., R. S. Germain, T. Ikezoe, X. Tong, E. M. Green, A. F. Gombart, H. P. Koeffler.** Regulation of expression of murine transferrin receptor 2. – Blood, **98**, 2001, 1949-1954.

7. **Lambert, L.** Molecular evolution of the transferrin family and associated receptors. – Biochimica et Biophysica Acta, **1820**, 2012, 244-255.
8. **Levy, J. E., O. Jin, Y. Fujiwara, F. Kuo, N. C. Andrews.** Transferrin receptor is necessary for development of erythrocytes and the nervous system. – Nat Genet., **21**, 1999, 396-399.
9. **Liu, Q., M. Wang, Y. Hu, H. Xing, X. Chen, Y. Zhang, P. Zhu.** Significance of CD71 expression by flow cytometry in diagnosis of acute leukemia. – Leuk. Lymphoma, **55**, 2014, 892-898.
10. **Marsee, D. K., G. S. Pinkus, H. Yu.** CD71 (Transferrin Receptor). An effective marker for erythroid precursors in bone marrow biopsy specimens. – Am. J. Clin. Pathol., **134**, 2010, 429-435.
11. **Nai, A., M. R. Lidonnici, M. Rausa, G. Mandelli, A. Pagani, L. Silvestri, G. Ferrari, C. Camaschella.** The second transferrin receptor regulates red blood cell production. – Blood, **125**, 2015, 1170-1179.
12. **Pantopoulos, K.** TfR2 links iron metabolism and erythropoiesis. – Blood, **125**, 2015, 1055-1056.
13. **Ponka, P., C. N. Lok.** The transferrin receptor: role in health and disease. – Int. J. Biochem. Cell. Biol., **31**, 1999, 1111-1137.
14. **Rishi, G., E. S. Secondes, D. F. Wallace, V. N. Subramaniam.** Hematopoietic deletion of transferrin receptor 2 in mice leads to a block in erythroid differentiation during iron-deficient anemia. – Am. J. Hematol., **91**, 2016, 812-818.
15. **Skikne, B.** Serum transferrin receptor. – Am. J. Hematol., **83**, 2008, 872-875.
16. **Silvestri, L., A. Nai, A. Pagani, C. Camaschella.** The extrahepatic role of TfR2 in iron homeostasis. – Front. Pharmacol., **5**, 2014, 1-6.
17. **Trinder, D., E. Baker.** Transferrin receptor 2: a new molecule in iron metabolism. – Int. J. Biochem. Cell. Biol., **35**, 2003, 292-296.
18. **Wallace, D. F., E. S. Secondes, G. Rishi, L. Ostini, C. J. McDonald, S. W. Lane, T. Vu, J. D. Hooper, G. Velasco, A. J. Ramsay, C. Lopez-Otin, V. N. Subramaniam.** A critical role for murine transferrin receptor 2 in erythropoiesis during iron restriction. – Br. J. Haematol., **168**, 2015, 891-901.

Institute of Experimental Morphology, Pathology and Anthropology with Museum
Bulgarian Anatomical Society

Acta morphologica et anthropologica, 23
Sofia ● 2016

Rearrangements of Oocyte Cytoskeleton during Mammalian Oogenesis: Review

M. Markova, V. Hadzhinesheva, R. Zhivkova, V. Nikolova, I. Chakarova, S. Delimitreva

Department of Biology, Medical Faculty, Medical University of Sofia, Bulgaria

Primary oocytes lose their centrosomes at pachytene stage. Chromosome movements during oocyte meiotic maturation are mediated by a barrel-shaped acentrosomal spindle, a unique situation for animal cells. Spindle poles are assembled from numerous small microtubule organizing centers. Microfilaments initially accumulate in the subplasmalemmal and perinuclear regions, then surround the spindle and form an actin cap. They mediate spindle migration and anchoring to the cell cortex, spindle rotation and the highly asymmetric cytokinesis. Cytokeratins and vimentin have also been shown to be present in mammalian oocytes and to undergo redistribution during oogenesis, though their precise functions are still to be clarified.

Key words: meiosis, oocyte maturation, microtubules, microfilaments, intermediate filaments.

Mammalian germ cells differentiate early in prenatal development in extraembryonic tissues and then migrate to the embryo proper, settle in gonadal ridges and proliferate by mitosis. During this process, they resemble undifferentiated somatic cells [15]. In female embryos, with the development of gonadal ridges into ovaries, primordial germ cells differentiate to oogonia. At this stage, their tubulin cytoskeleton is characterized by a typical juxtanuclear centrosome with a pair of centrioles and dense pericentriolar material rich at gamma tubulin which nucleates microtubules [11]. Microtubules are needed for the formation of Balbiani body, a transient complex of organelles that forms in oogonia and is the first lineage-specific morphological feature of female germ cells [5]. Microfilaments are located in the peripheral layer of cytoplasm, beneath the plasma membrane [11]. This cortex of fibrillar actin will persist throughout oogenesis and after fertilization [14].

During later prenatal development, oogonia differentiate into primary oocytes and start meiosis. It is arrested upon reaching diplotene. At the same stage, centrosomes degenerate, presumably to prevent parthenogenetic development. Centrioles are disassembled. The gamma tubulin from the pericentriolar material is included into two multivesicular aggregates. These structures, however, do not take over the function of centrosomes as microtubule organizing centers and do not nucleate microtubules, suggesting that gamma tubulin in them is inactive [6].

The third cytoskeletal system composed of cytoplasmic intermediate filaments is still poorly studied in female germ cells. Some authors, however, report the presence of keratins in fetal oocytes in the form of a perinuclear aggregate, showing that intermediate filaments are already present in early prophase I [10].

After the onset of puberty, with each estrous/menstrual cycle a group of oocytes resume meiosis. One or more of them, depending on the species, completes the first meiotic division, extrudes the first polar body, starts the second meiotic division and reaches its metaphase, where it is arrested until fertilization. This sequence from arrested prophase I to metaphase II, called oocyte meiotic maturation, requires major rearrangements of cytoskeletal structures. The tubulin cytoskeleton is organized without centrosomes, a situation quite atypical for animal cells. With the resumption of meiosis, the oocyte in prophase I, now often referred to as germinal vesicle stage, disassembles its multivesicular aggregates. Its gamma tubulin is transferred to multiple small microtubule organizing centers located in the vicinity of the nucleus [6]. Actually, researchers of oogenesis often use the term "microtubule organizing center" specifically to designate these small accumulations of gamma tubulin, excluding the centrosome. Microfilaments at germinal vesicle stage are found in subplasmalemmal and perinuclear position [1, 7]. The same regions are positive for cytokeratins and vimentin [7, 8] (**Fig. 1A**). The role of cytoplasmic intermediate filament proteins in oocytes is still to be clarified. Vimentin has been reported to facilitate pronuclear positioning in the zygote [9]. The distribution of keratins shows very similar patterns in maturing oocytes of different vertebrate classes, suggesting some important though yet unknown function [8].

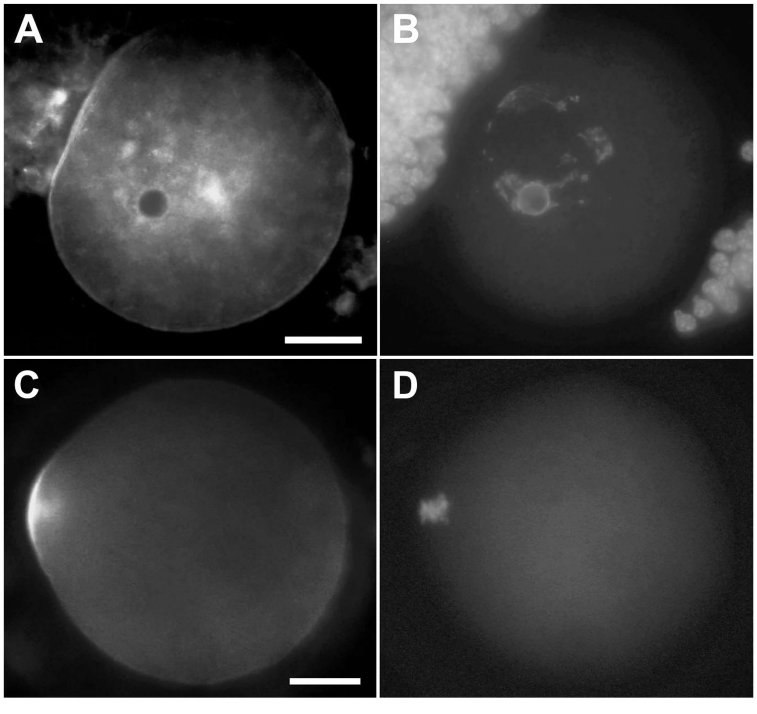

Fig. 1. Immunofluorescent localization of cytokeratins 1, 5, 6 and 8 in mouse oocytes, performed as described in [8]: **A** – germinal vesicle stage (surrounded by cumulus); **C** – metaphase I; **B** and **D** show DNA in the same cells, visualized by Hoechst 33258. Bars = 20 μm

Meiotic resumption is triggered by the cyclin-dependent kinase MPF. Its activity soon causes disassembly of the nuclear envelope during a brief stage called germinal vesicle breakdown. Chromosomes now have free contact with cytoplasmic components and this allows them to drive the meiotic spindle formation. A protein component of chromatin (particularly of centromeric chromatin) known as RCC1 activates a soluble GTPase called Ran, which in turn activates the microtubule organizing centers at close distance. This leads to formation of small asters in the vicinity of chromosomes and subsequent binding of the (+) ends of their microtubules to kinetochores. Microtubules stabilized this way elongate and eventually form a barrel-shaped bipolar spindle [12]. The process is mediated by microtubule associated proteins such as NuMA, kinesins (notably Kif11) and dyneins that "focus" the (–) ends of microtubules, binding them together into spindle poles [6]. Meanwhile, microfilaments that have been in perinuclear position now encircle the chromosomes and the microtubules, forming a larger spindle-shaped actin cage around the tubulin spindle [2].

Once formed, the meiotic spindle carries out the process of chromosome congression and arranges the bivalents at the equatorial plane. The oocyte is now in metaphase I. At this stage, fibrillar actin is localized in the cortex and around the meiotic spindle. Cytokeratins and vimentin are found in the same regions and also associated with the chromosomes [7, 8] (**Fig. 1C**).

Initially, the metaphase I spindle has central localization. Then microfilaments connect one of its poles to the cortex, pull it to peripheral position and anchor it under the cell membrane, a process called spindle migration [1]. This is a prerequisite for the subsequent asymmetric division. The migration is regulated by the microfilament nucleator protein formin-2 [2]. Upon reaching the cortex, the spindle causes its modification. Microfilaments accumulate above the spindle and form an actin cap devoid of microvilli. It will take part in anchoring the spindle to subplasmalemmal position and in cytokinesis. Cap formation is caused by Ran GTPase activated locally by the chromosomes [3]. The thickening of the cap is accompanied by reduction of other parts of actin cortex, most likely to make it more dynamic and to reflect the disconnection from cumulus cells. Similar changes affect the distribution of intermediate filament proteins that colocalize with actin [7] (**Fig. 1C**).

After the metaphase plate is properly arranged, anaphase I and telophase I follow quickly and chromosomes are segregated into two haploid sets. Microfilaments from the actin cap form a contractile ring and extrude the 1st polar body. The transition from meiosis I to II in animal oocytes is brief, with chromosomes remaining condensed [4]. It is sometimes referred to as "metaphase I – metaphase II transition". The actin cap and the meiotic spindle undergo fast reorganization and the oocyte reaches metaphase II. The spindle is parallel to the cell membrane and remains anchored beneath it until fertilization [13]. The distribution of actin and intermediate filament proteins in metaphase II is the same as in metaphase I [7, 8]. At this stage, the oocyte is ready to be fertilized and undergoes ovulation.

At the beginning of fertilization, the contact with the sperm cell activates the oocyte and triggers microfilament-mediated rotation of its spindle to make it perpendicular to the cell surface, a prerequisite for cytokinesis. Spindle rotation is followed by anaphase II, telophase II and second polar body extrusion. Experiments with cytoskeletal inhibitors show that damage to microtubules arrests meiosis in metaphase while damage to microfilaments prevents spindle migration, rotation and polar body extrusion [16]. Carrying out telophase II is the last function of the acentrosomal meiotic spindle of the oocyte. After gamete fusion, sperm centrioles organize a dominant microtubule organizing center by recruiting dispersed oocyte centrosomal proteins; this new centrosome forms an aster responsible for pronuclear migration. An exception are rodents, in which sperm centrioles degenerate and centrosomes are formed *de novo* during cleavage [6].

It can be concluded that the action of cytoskeletal structures mediates the mechanical aspects of oogenesis, with microtubules being responsible for chromosome congression and segregation and microfilaments for spindle positioning and cytokinesis. Knowledge of cytoskeletal reorganizations during oogenesis is crucial for understanding the physiology and pathology of the oocyte and for the success of assisted reproductive technologies.

References

1. **Almonacid, M., M. É. Terret, M. H. Verlhac.** Actin-based spindle positioning: new insights from female gametes. – J. Cell Sci., **127**, 2014, 477-483.
2. **Azoury, J., K. W. Lee, V. Georget, P. Rassinier, B. Leader, M. H. Verlhac.** Spindle positioning in mouse oocytes relies on a dynamic meshwork of actin filaments. – Curr. Biol., **18**, 2008, 1514-1519.
3. **Dehapiot, B., G. Halet.** Ran GTPase promotes oocyte polarization by regulating ERM (Ezrin/Radixin/Moesin) inactivation. – Cell Cycle, **12**, 2013, 1672-1678.
4. **George, O., M. A. Johnston, C. B. Shuster.** Aurora B kinase maintains chromatin organization during the MI to MII transition in surf clam oocytes. – Cell Cycle, **5**, 2006, 2648-2656.
5. **Lei, L., A. C. Spradling.** Mouse oocytes differentiate through organelle enrichment from sister cyst germ cells. – Science, **352**, 2016, 95-99.
6. **Manandhar, G., H. Schatten, P. Sutovsky.** Centrosome reduction during gametogenesis and its significance. – Biol. Reprod., **72**, 2005, 2-13.
7. **Markova, M. D., V. P. Nikolova, I. V. Chakarova, R. S. Zhivkova, R. K. Dimitrov, S. M. Delimitreva.** Intermediate filament distribution patterns in maturing mouse oocytes and cumulus cells. – Biocell, **39**, 2015, 1-7.
8. **Nikolova, V. P., S. M. Delimitreva, R. S. Zhivkova, I. V. Chakarova, V. P. Hadzhinesheva, M. D. Markova.** Immunocytochemical Study of Mouse Oocytes Suggests Conserved Keratin Organisation in Tetrapod Oogenesis. – Acta Zool. Bulg., **68**, 2016, 35-38.
9. **Payne, C., V. Rawe, J. Ramalho-Santos, C. Simerly, G. Schatten.** Preferentially localized dynein and perinuclear dynactin associate with nuclear pore complex proteins to mediate genomic union during mammalian fertilization. – J. Cell Sci., **116**, 2003, 4727-4738.
10. **Santini, D., C. Ceccarelli, G. Mazzoleni, G. Pasquinelli, V. M. Jasonni, G. N. Martinelli.** Demonstration of cytokeratin intermediate filaments in oocytes of the developing and adult human ovary. – Histochemistry, **99**, 1993, 311-319.
11. **Sathananthan, A. H., K. Selvaraj, A. Trounson.** Fine structure of human oogonia in the foetal ovary. – Mol. Cell. Endocrinol., **161**, 2000, 3-8.
12. **Schuh, M., J. Ellenberg.** Self-organization of MTOCs replaces centrosome function during acentrosomal spindle assembly in live mouse oocytes. – Cell, **130**, 2007, 484-498
13. **Sun, Q. Y, H. Schatten.** Regulation of dynamic events by microfilaments during oocyte maturation and fertilization. – Reproduction, **131**, 2006, 193-205.
14. **Wang, W. H., L. R. Abeydeera, R. S. Prather, B. N. Day.** Polymerization of nonfilamentous actin into microfilaments is an important process for porcine oocyte maturation and early embryo development. – Biol. Reprod., **62**, 2000, 1177-1183.
15. **Wear, H. M., M. J. McPike, K. H. Watanabe.** From primordial germ cells to primordial follicles: a review and visual representation of early ovarian development in mice. – J. Ovarian Res., **9**, 2016, 36.
16. **Zhu, Z. Y., D. Y. Chen, J. S. Li, L. Lian, L. Lei, Z. M. Han, Q. Y. Sun.** Rotation of meiotic spindle is controlled by microfilaments in mouse oocytes. – Biol. Reprod., **68**, 2003, 943-946.

Corresponding author:
Maya Markova
Department of Biology, Medical Faculty
Medical University of Sofia
1 Sv. Georgi Sofiiski Street,
BG-1431 Sofia, Bulgaria
e-mail: mayamarkov@gmail.com

Institute of Experimental Morphology, Pathology and Anthropology with Museum
Bulgarian Anatomical Society

Acta morphologica et anthropologica, 23
Sofia ● 2016

In Memoriam

Professor Jürgen Koebke (1945-2012)

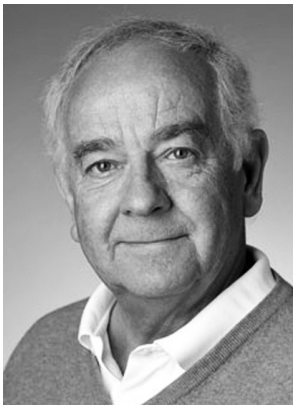

Professor Koebke

Professor Dr. rer. nat. Jürgen Koebke is a distinguished German anatomist, long-standing director of the Medical Faculty of the University of Cologne which is one of the well-organized anatomical institutes in Germany. He is an honorary member of the Bulgarian Anatomical Society and a great friend of the Medical University of Varna. He died suddenly on February 23, 2012 at the age of 66.

The students qualify him as a lovely teacher with unique sense of humor and great personality. A lot of physician generations and more than 200 postgraduates remember him with honor and respect. Innovative and very important activities organized and conducted by Prof. Koebke were the practical human cadaver courses for physicians from the surgical training, attended also by Bulgarian colleagues.

The scientific interests of Prof. Koebke were in the field of the topographic and clinical anatomy, the functional anatomy and biomechanics of the locomotor system, where he generated fundamental achievements of great importance for clinical practice. He was the first scientist-anatomist who developed the morphological aspects of the implantology and endoprosthesis techniques.

Professor Koebke with his students

Professor Koebke worked very actively for development of the cooperation with the Bulgarian anatomists and numerous Bulgarian colleagues have worked at his Institute. His collaboration with the University of Varna was impressive leading to the participation of numerous anatomists and orthopedists from Cologne in the 6th, 7th , 8th and 9th Symposia on Clinical Anatomy.

Professor Koebke in the dissecting hall

Professor Koebke at Koprivshtitsa Morphological Days

Professor Koebke significantly contributed to the affirmation of the Koprivshtitsa Morphological Days as an international event organized by the Institute of Experimental Morphology and Anthropology with Museum of the Bulgarian Academy of Sciences and the Bulgarian Anatomical Society, as well. His contribution to the Bulgarian anatomical science was greatly appreciated and he was awarded the title "Honorary Member of the Bulgarian Anatomical Society" in 2006. In honour of Prof. Koebke, one of the Dissecting Halls of the Department of Anatomy in Medical University Varna was renamed Koebke's Hall.

The decease of Professor Jürgen Koebke is a heavy loss for the Bulgarian Anatomical Society. We lost a very distinguished, worthy and unforgettable Person, Teacher, Scientist and a great Friend of Bulgaria.

Prof. Dr. V. Vassilev,
Prof. Dr. M. Davidoff

ISSN 1311-8773

AIMS AND SCOPE

Acta morphologica et anthropologica publishes original and review articles in the following sections:

Section A – Morphology:

1. Neurobiology; 2. Structure and Metabolism of the Cells;
3. Cell Differentiation and Kinetics; 4. Cellular Immunology;
5. Experimental Cytology; 6. New Methods.

Section B – Anthropology and Anatomy:

1. Physical Development; 2. Somatotype and Body Composition;
3. Population Genetics and Medical Anthropology;
4. Paleoanthropology and Paleopathology; 5. Anatomy.